MAINLINE

MAINtenance, renewal and Improvement of rail transport iNfrastructure to reduce Economic and environmental impacts

Collaborative project (Small or medium-scale focused research project)

Theme SST.2011.5.2-6.: Cost-effective improvement of rail transport infrastructure

Deliverable 2.4:
Field-validated Performance Profiles

Grant Agreement number: 285121 SST.2011.5.2-6.

Start date of project: 1 October 2011 Duration: 36 months

Lead beneficiary of this deliverable: Jacobs/SKM

Due date of deliverable: 31/03/2014 Actual submission date: 29/09/2014

Release: Final

Project co-funded by the European Commission within the 7th Framework Programme		
Dissemination Level		
PU	Public	x
PP	Restricted to other programme participants (including the Commission Services)	
RE	Restricted to a group specified by the consortium (including the Commission Services)	
CO	Confidential, only for members of the consortium (including the Commission Services)	

Abstract of the MAINLINE Project

Growth in demand for rail transportation across Europe is predicted to continue. Much of this growth will have to be accommodated on existing lines that contain old infrastructure. This demand will increase both the rate of deterioration of these elderly assets and the need for shorter line closures for maintenance or renewal interventions. The impact of these interventions must be minimized and will also need to take into account the need for lower economic and environmental impacts. New interventions will need to be developed along with additional tools to inform decision makers about the economic and environmental consequences of different intervention options being considered.

MAINLINE proposes to address all these issues through a series of linked work packages that will target at least €300m per year savings across Europe with a reduced environmental footprint in terms of embodied carbon and other environmental benefits. It will:

- Apply new technologies to extend the life of elderly infrastructure
- Improve degradation and structural models to develop more realistic life cycle cost and safety models
- Investigate new construction methods for the replacement of obsolete infrastructure
- Investigate monitoring techniques to complement or replace existing examination techniques
- Develop management tools to assess whole life environmental and economic impact.

The consortium includes leading railways, contractors, consultants and researchers from across Europe, including from both Eastern Europe and the emerging economies. Partners also bring experience on approaches used in other industry sectors which have relevance to the rail sector. Project benefits will come from keeping existing infrastructure in service through the application of technologies and interventions based on life cycle considerations. Although MAINLINE will focus on certain asset types, the management tools developed will be applicable across a broader asset base.

Partners in the MAINLINE Project

UIC, FR; Network Rail Infrastructure Limited, UK; COWI, DK; SKM, UK; University of Surrey, UK; TWI, UK; University of Minho, PT; Luleå tekniska universitet, SE; Deutsche Bahn, DE; MÁV Magyar Államvasutak Zrt, HU; Universitat Politècnica de Catalunya, ES; Graz University of Technology, AT; TCDD, TR; Damill AB, SE; COMSA EMTE, ES; Trafikverket, SE; Cerema (ex SETRA), FR; ARTTIC, FR; Skanska a.s., CZ.

WP2 in the MAINLINE project

The main objectives for WP2 are:

- To identify and model important degradation phenomena and processes for selected railway assets for the purpose of LCC and LCA
- To quantify the influence of intervention strategies on degradation time profiles
- To develop performance time profiles for selected asset types
- To validate the developed degradation and performance profiles through case studies.

Table of Contents

Table of Figures

Table of Tables

Glossary

Abbreviation / acronym	Description
BA	Burrowing Assessment
CAA	Construction Activity Assessment
DA	Drainage Assessment
FLS	Fatigue Limit States
ITZ	Interfacial Transition Zone
LCA	Life Cycle Analysis
LCAT	Life Cycle Assessment Tool
LCC	Life-Cycle Cost
LSE	Exposed Longitudinal Secondary beams/girders
LSI	Inner Longitudinal Secondary beams/girders
MA	Movement Assessment
MGE	Exposed Longitudinal Main beams/girders
MGI	Inner Longitudinal Main beams/girders
NR	Network Rail [company]
OeBB	Austrian Federal Railways [company]
O&M	Operations & Maintenance
PRA	Previous Remediation Assessment
RBI	Risk-Based Inspection
SKM	Sinclair Knight Merz [company]
SKMA	SKM Algorithm
SRV	Slope Risk Value
SSHI	Soil Slope Hazard Index
SWA	Surface Water Assessment
ULS	Ultimate Limit States
VA	Vegetation Assessment
VBA	Visual Basic Applications in Excel
WP	Work Package
XGE	End Transverse beams/girders
XGI	Inner Transverse beams/girders

1. Executive Summary

The consensus from current railway asset management practice is that available deterioration and degradation models have been based on limited and scarce real data and/or that assumptions and idealisations have sometimes been transferred from other industry sectors without the possibility of full validation.

The MAINLINE project aims to improve available degradation and structural models in order to develop more realistic life cycle cost and safety estimates for asset management purposes. As part of this effort, the present work focuses on the validation of the performance-time profiles that have been developed in previous tasks of this work package for a diverse group of railway assets, namely track, soil cuttings, metallic bridges and concrete lined tunnels.

The methodologies for validating performance-time profiles are mainly based on case studies and statistical analysis and their results are presented in this report. In this task, typical performance profiles have been compared with a sample of assets for which detailed inspections, refined assessments, structural health monitoring programmes and other interventions have been undertaken.

The aim of this work is to scrutinize the methods adopted in previous tasks, compare theoretical profiles with real data and establish the level of confidence that can be placed on the model predictions.

Different validation exercises have been undertaken for the four asset types due to the inherent differences in the types of assets being studied. The outputs from this work will be made available to the Life Cycle Assessment Tool which is being developed in Work Package WP5.

2. Acknowledgements

This report has been prepared within Work Package WP2 of the MAINLINE project by the following team of contractors, with Jacobs/SKM acting as deliverable co-ordinator and the University of Surrey acting as WP leader:

- Cerema (ex SETRA) – Concrete tunnels
- Jacobs/SKM – Soil cuttings
- TU Graz – Track
- University of Surrey – Metallic bridges

Detailed discussions and feedback with all the MAINLINE partners are gratefully acknowledged, in particular COWI who have contributed significantly to the Bridges and Tunnels sections. Also, particular thanks go to the Internal Reviewers Dr. Polyvios Polyviou (TWI), Brian Bell (UIC) and the members of the Project Advisory Committee Dr. Rosemarie Helmerich (BAM) and Dr. Livia Pardi (Autostrade) who have undertaken the technical review of the present deliverable.

3. Introduction

3.1 Scope of the Report

The project 'MAINtenance, renewaL and Improvement of rail transport iNfrastructure to reduce Economic and environmental impacts' (in short MAINLINE) is an integrated project within the 7th Framework Programme. It has been financed on the basis of the contract SST.2011.5.2-6 between the European Community represented by the Commission of the European Communities and International Union of Railways (UIC) acting as coordinator of the project.

The main objectives of the project are to:

- apply new technologies to extend the life of elderly infrastructure
- improve degradation and structural models to develop more realistic life cycle cost and safety models
- investigate new construction methods for the replacement of obsolete infrastructure
- investigate monitoring techniques to complement or replace existing examination techniques
- develop management tools to assess whole life environmental and economic impact

The present report D2.4 - Field validated performance profiles has been prepared within Work Package WP2 (from month M18 to month M30) of the MAINLINE project, named 'Degradation and structural models to develop realistic life cycle cost and safety models', one of the eight work packages WP1 to WP8 dealing with relevant tasks for maintenance, renewal and improvement of rail transport infrastructure to reduce economic and environmental impacts.

WP2 interacts with WP1, WP4 and WP5. The interaction with WP1 consists of inputs for degradation and performance models that will be developed within WP1 and will also be utilised within WP2. The two-way interaction with WP4 is focused on identifying model parameters for the degradation and structural models that would benefit (in terms of the confidence with which they can be specified in models) through monitoring and examination. The main outputs from WP2 being time-dependent performance profiles will be passed on to WP5.

An overview of the general organisation of the project is presented below together with the list of all the partners in WP2.

General organisation of the project

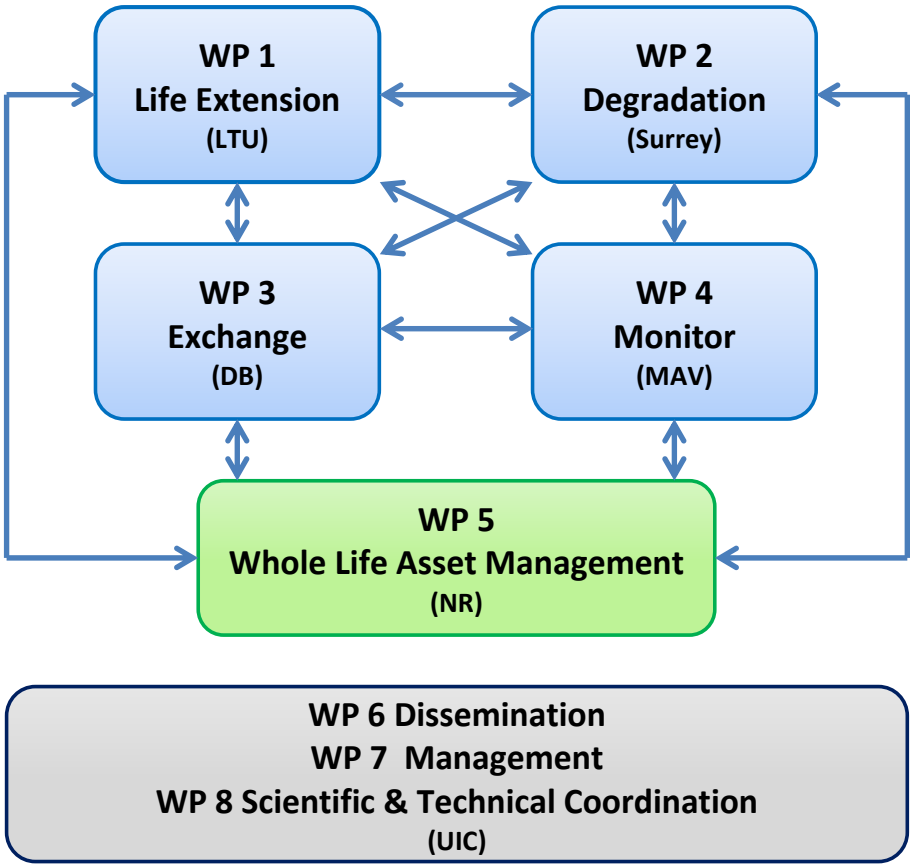

Figure 3-1 General organisation of the project.

UIC, Surrey, MAV and NR are listed below. DB is Deutche Bahn AG (Germany) and LTU is Lulea Tekniska Universitet (Sweden).

Table 1.1: WP2 Partners

Part n°	WP2 Partners	Country
1	UNION INTERNATIONALE DES CHEMINS DE FER - UIC	FR
2	NETWORK RAIL INFRASTRUCTURE LTD	UK
3	COWI A/S	DK
5	UNIVERSITY OF SURREY	UK
6	TWI LIMITED	UK
10	MAV MAGYAR ALLAMVASUTAK ZARTKORUEN MUKODO RT	HU
12	TECHNISCHE UNIVERSITAET GRAZ	AT
17	SERVICE D'ETUDES SUR LES TRANSPORTS, LES ROUTES ET LEURS AMENAGEMENTS	FR
20	SINCLAIR KNIGHT MERZ/JACOBS	UK

This Deliverable D2.4 is derived from Task 2.5 within WP2 of the MAINLINE project.

The scope of Task 2.5 from the MAINLINE Description of Work document is as follows:

- **Task T2.5: Validation of deterioration and performance profiles through case studies and development of best-practice guide**

  In this task, typical outputs from Tasks T2.3 and T2.4 will be compared with a sample of assets for which refined assessments, detailed inspections and/or structural health monitoring programmes, and other interventions have been undertaken. The aim of this work is to scrutinise the methods adopted in previous tasks, compare theoretical profiles to real data and, hence, to ascertain the level of confidence that can be associated with model predictions.

The scope of Deliverable 2.4 from the MAINLINE Description of Work document is as follows:

- **D2.4: Field-validated performance profiles**

  Report with comparisons between predicted performance profiles and actual profiles based on field data. Commentary on observed differences and recommendations on potential improvement.

This document should be read in conjunction with the following previous deliverables from the MAINLINE project:

- Deliverable 2.1 – Degradation and performance specification for selected assets
- Deliverable 2.2 – Degradation and intervention modelling techniques
- Deliverable 2.3 – Time-variant Performance Profiles for Life-Cycle Cost and Life-Cycle Analysis

This task involves the validation of performance profiles previously developed for the asset types Track, Soil Cuttings, Metallic Bridges and Concrete Tunnels under D2.3. In practice, these performance profiles were generated in a variety of ways:

- Bridges – Theoretical models with empirical constants from other studies
- Cuttings – Analysis of Network Rail Data
- Track – Analysis of Austrian Federal Railways (OeBB) Data
- Tunnels – Theoretical models with empirical constants from other studies

So for Cuttings and Track: field data has been used to generate the profiles in the first instance, so within this task we have investigated new ways to validate these performance profiles, including sample assets and alternative sources of field data.

Within previous WP2 deliverables the majority of information was obtained from various organisations across the UK and Austria. As such this task has been conducted on the basis that comparative data from outside the UK or Austria would be preferable for the purpose of validation.

3.2 Structure of Report

It has been agreed, amongst the MAINLINE partners that the validation of deterioration performance profiles is aimed at those assets for which a Life Cycle Assessment Tool (LCAT) has been developed.

Life Cycle Assessment Tools (LCAT) for soil cuttings, metallic bridges and plain track are being developed under task 5.5. These asset types represent a good variety of structural, track and geotechnical asset types as described in D2.3. The method of modelling within each of these LCATS is bespoke and quite detailed; the LCATs have been individually custom-designed based on the engineering behaviour of the asset types.

Despite the best efforts of the MAINLINE partners, the required data has not been discovered for tunnels, which has necessarily prevented the development of wide deterioration profiles and thus the development of a fully functional LCAT. Therefore, the performance validation for soil cuttings, metallic bridges and plain track are explained in the main text of that report. Additional work that has been undertaken for tunnels has been included in the appendixes.

4. Track (TU Graz)

4.1 Outline of D2.3 Performance Profiles for Plain Line Track

Track service life in a cyclic track renewal regime is defined by the end of life of one of the major track components, rails, sleepers and ballast. As rails are situated at the top of the track construction, they can be easily changed even though this measure of course is quite costly. However sleepers have a complex interface with the ballast bed which is sensitive to contact conditions, which should be as continuous as possible taking into consideration that at least five sleepers are engaged in distributing the wheel loads to the ballast bed. Due to this fact, single sleeper exchange cannot deliver the quality that is needed for this task, even though if it is technically possible. Hence worn out sleepers generally lead to a total track renewal - and are therefore one of the factors limiting track service life. The third main track component is the ballast bed. As load distribution only works if the ballast bed performs as an elastic layer, any disturbance of this elasticity is critical for the track system. The elastic behaviour of ballast is achieved with a defined grain size distribution. If too much fine material moves this distribution curve, the elasticity is lost. Additional fine material within a ballast bed can arise from crushed or abraded ballast; soil from the formation being drawn up into the ballast bed by the pumping action of sleepers moving vertically under the weight of passing trains or contamination from material like coal dropped from passing trains. In such a situation there are only two options left; ballast cleaning or ballast replacement, both of which are very costly. In most cases the need for major work to the ballast bed is, economically, the best point in time to replace the entire track superstructure (rails, sleepers and the ballast bed) particularly as this returns the track to a high overall quality. Thus it is very important to keep the ballast bed at a good quality level, not provoking excessive wear due to high impact forces cause by low track geometry conditions.

Taking these assumptions, the service life of track is either limited to the lifetime of sleepers or to the need to change or clean the ballast bed. Under a proper maintenance regime, wooden sleepers can reach 25 to 35 years or even some 50 years in case of concrete sleepers. Consequently, where high volumes of traffic are carried track service life is limited by the ballast condition. This fact has been proven by intensive bottom-up track analyses in several countries as Switzerland, Austria, and Croatia.

Track quality can therefore be described by track geometry as measured by a track recoding car. Generally, the vertical track alignment is taken as the main indicator for the overall behaviour of track. As track is a longitudinal engineering construction, the vertical geometry is described by the standard deviation of the vertical failures over a predefined length of 200 m as required due to EN 13848-6. This standard deviation, σh, is used at least in Europe and is doubtlessly a good approach as long as the track under consideration does not contain radii less than 400 m. Smaller radii show a different behaviour. Thus either the standard devation for the horizontal failure or a quality figure taking all track failures into account should be implemented. The MDZ-figure used at Graz, University of Technology consists of all three measurements and moreover covers the speed level, as track quality can be objectified only by referring it to a riding quality. MDZ is a German abbreviation of the tamping unit, as this quality figure highlights the demand of tamping.

However, one dataset can never tell everything about track behaviour and the track recording car data must be analysed as a time sequence.

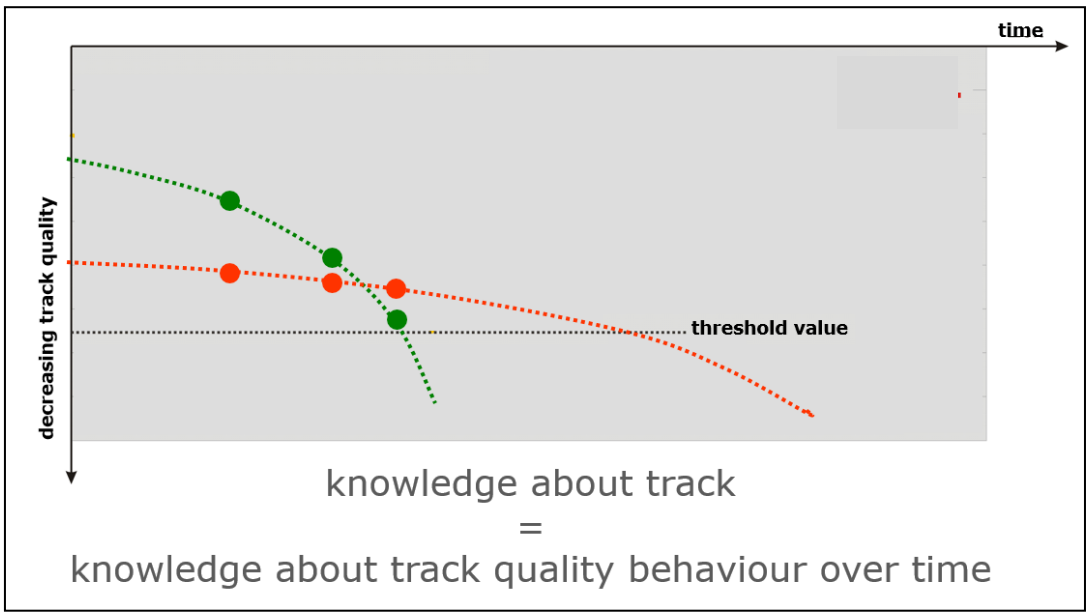

Figure 4-1: Track behaviour over time

Figure 4.1 shows that the first measuring point of the track section given in green colour is better than the one from the section given in red colour. Nevertheless the behaviour of the two track sections over time shows that the green section is deteriorating more rapidly and hence requires more attention.

The MAINLINE mathematical approach, a non-linear, e-functional regression curve that is described in Deliverable D2.3 (Mainline.2.3-2013) is equally valid for both vertical standard deviation and MDZ-figure data.

The regression specifies that the track quality index deteriorates on the basis of the following exponential function:

$$Q_t = Q_n \times e^{b \times t} \qquad (1)$$

The starting value for Q is either the initial quality (Q_0) after track relaying or the quality Q_n after tamping. This initial quality value is artificial as it is calculated to time 0 with a regression function using measured or calculated quality over time. Therefore Q_n signifies the actual, initial quality after tamping, including the initial settlement.

The exponent b (the deterioration rate) of the exponential function reflects the speed of the deterioration process over time (t) under different influences.

The Q and the b-values are calculated for all relevant different boundary conditions using a nonlinear regression model considering a time series of track recording car geometry data..

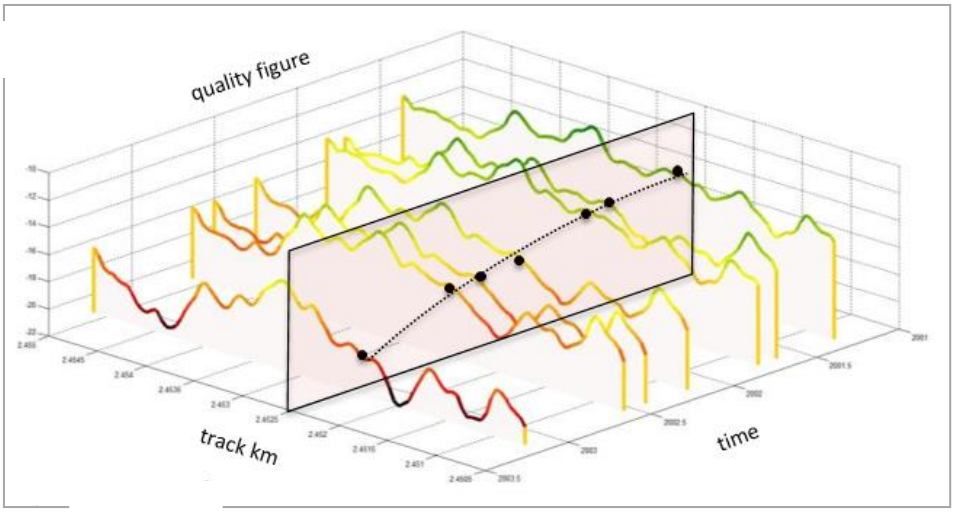

Figure 4-2: Track deterioration analysis

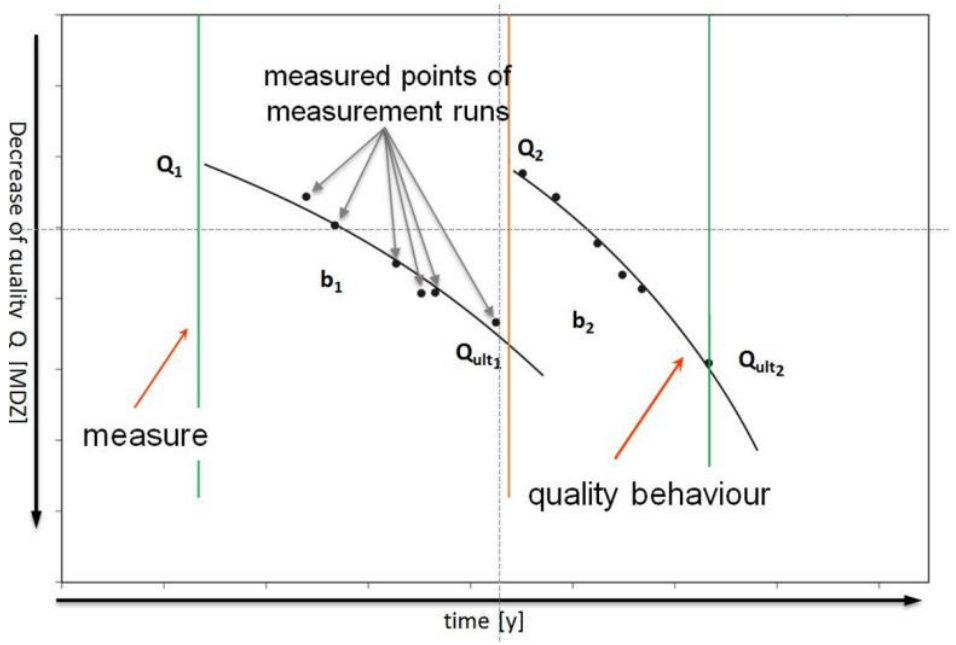

Figure 4-3: Track deterioration function (Veit, 2013)

These data (example in figure 4.3) permit the calculation of the track quality behaviour over time using a nonlinear regression, as the information from different recording car runs create a time sequence. However creating this time sequence can be time consuming as all information within a given time sequence must describe exactly the same point in the track. For example, the Austrian track recording car delivers a full data set every 25 cm but the automatic positioning of the recording car is not precise enough to ensure that a given time sequence actually represents a single point on the track. This is because position is measured by dGPS and based on the wheel circumference, which due to wheel slippage, can be slightly inaccurate. Therefore the data needs repositioning using the precisely known location of peaks in the data (e.g. frog of turnouts) and stretching or compressing the data set to these precise positions. As the quality function shows only two variables, Q and b, theoretically two measuring results of the track recording car would permit the calculation of

the function. However in reality the function becomes stable using data of four to five recording car runs.

It is important to realise that the depicted description of track quality can be used for predicting track service life only by attaching additional information about the other components' actual status. The calculated service life in the LCAT therefore is a maximum achievable service life, presuming that maintenance is executed properly for the other components. The following example should highlight the importance of this pre-condition.

Track deterioration is a result of lots of different aspects. It is obvious that the wear of single track components influences the general performance of track, whilst the wear of the individual components are influenced by the boundary conditions under which they are operating. One of the most relevant influencing parameters is the track alignment. Taking sharp curves as an example, rails and their specific wear get into focus: the outer rail is subject to excessive side wear of the rail head as the wheel flange comes into contact with the rail due to inadequate super-elevation (cant). On the inner rail high dynamic effects lead to a deformation of the rail surface – corrugation waves. While the first effect can be dealt with grinding (re-profiling) and mainly with rail exchange, the corrugation waves have to be ground frequently. Neglecting this maintenance task could lead overstressed superstructure and thus crushed ballast under the sleeper and finally to a system fall out followed by a necessary track renewal.

Figure 4-4: Consequences of neglected grinding of corrugation waves in sharp curves from corrugation waves (left-hand picture) to crushed ballast under the sleepers (middle picture) leading to a system fall out (right-handed picture)

But not only this aspect could cut down track service life significantly. Due to the applied lateral forces in small radius curves the rail pads suffer significant one-sided wear. Failing to change the worn out rail pads could lead to failure of concrete sleepers due to spalling of concrete at the rail fastenings as rails more and more lose their inclination. This process can be monitored taking the rail inclination signal of recording cars. Again, if maintenance, in this case rail pad exchange, is not executed properly and in time, the possible track service life cannot be reached due to the breakdown of one component, the sleepers.

Another example is shown in figure 4.5. Accepting fines in the ballast bed will increase the stiffness of the system track, the loads cannot be spread to more sleepers, the components including the rails and fastener will be overloaded resulting in reduced service life of several components.

Figure 4-5: Ballast bed with a high degree of fines

A safety critical situation can appear when the rail surface is not maintained properly by grinding or milling and Rolling Contact Fatigue (RCF) increase.

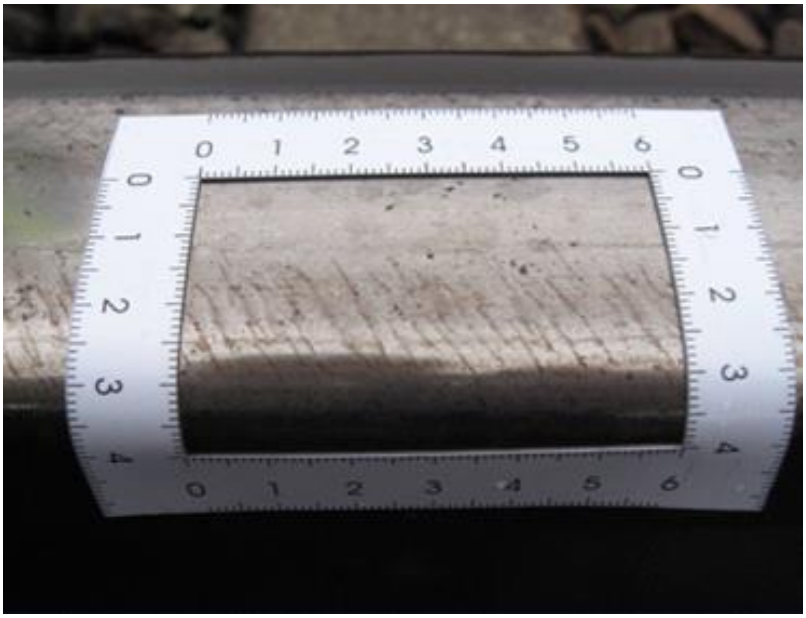

Figure 4-6: Head checks on rails

Anyhow, it must be emphasised again, that track quality cannot be described without reference to different boundary conditions.

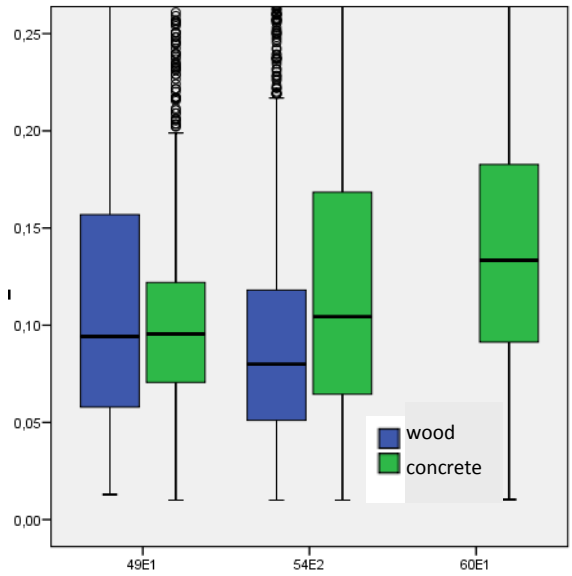

Figure 4-7: Analysis of different types of superstructure without taking the boundary condition into account

Figure 4.7 shows box-plots of the deterioration rate b for the entire Austrian core railway network specified for different types of superstructures (rail 49E1, 54E2, 60E1, wooden and concrete sleepers). It clearly shows that the heaviest type of superstructure (60E1 on concrete sleepers) deteriorates the most. This result is understandable as heavy superstructure is used on heavy loaded lines while light superstructure is used in low loaded branch lines. So the result does not tell anything about track behaviour but tells that all different boundary conditions must be taken into account.

It is necessary to know the constraints to be able to assess a given quality level. Next to numerous effects, the five most relevant influencing parameters are track alignment, transport volume, sleeper type, the drainage system, and subsoil condition. The latter is the most critical one, as insufficient subsoil quality leads to exploding maintenance demands and significant service life losses, both relevant aspects of total life cycle cost of track. Research activities [1,8] on track quality behaviour covered and still cover many of these boundary conditions, having led to different generalised results. These results were used in the LCAT to cope with as many boundary conditions as possible.

Within the MAINLINE project, the following deterioration profiles were analysed in detail:

- Three types of sleepers
- Two different transport loadings
- Two different track alignments
- Two types of drainage situation
- Two types of sub-layer quality

The three base cases are formulated for boundary conditions of a good sub-layer quality and sufficient drainage facilities. Other boundary conditions are not covered within the base cases but are considered within an extrapolation process for quality values, deterioration rates, and threshold values, based on the research results mentioned above.

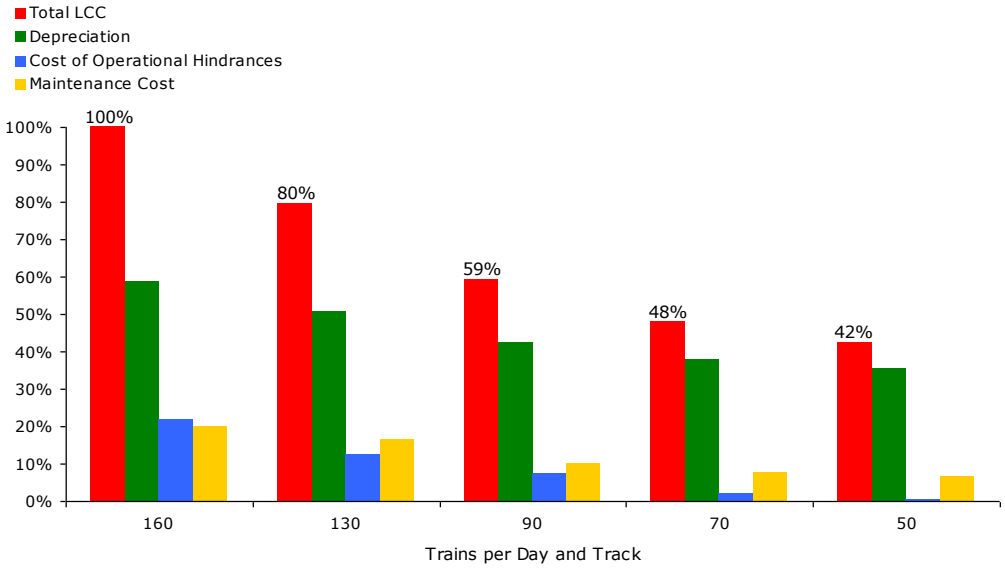

Figure 4-8: Annual average costs and the importance of depreciation for life cycle costs (Marschnig and Veit, 2011)

The prototype LCAT-track will cover only investment and tamping, being the most relevant maintenance actions for track. These two track works form the main portions of life cycle costs. Costs of operational hindrances can be added. However, some portions of the maintenance costs (yellow bar in figure 4.8) cannot be taken into account as track maintenance is executed in various ways in different railways regarding the type of maintenance actions and mainly their frequency. Hence LCAT-track is focusing on the theoretical possible service life assuming that maintenance is executed at an appropriate frequency and to a high standard. The following examples show the influence of quality and maintenance decisions for the service life of track. In figures 4.9 and 4.10 track quality behaviour is given over the service life in years as calculated in several case studies executed for Austrian Federal Railways (ÖBB).

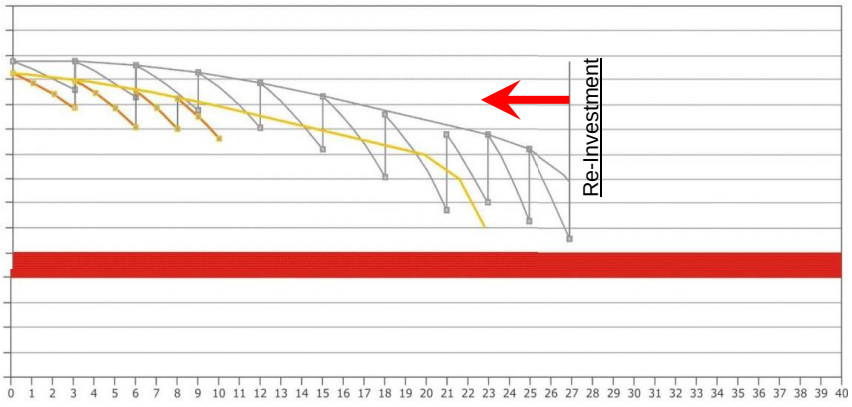

Figure 4-9: Reduction of service life by choosing incorrect components (quality over service life; the red bar indicates the intervention level)

This effect is covered by LCAT-track in taking quality levels and deterioration values into account which are specific for different types of superstructure and traffic load.

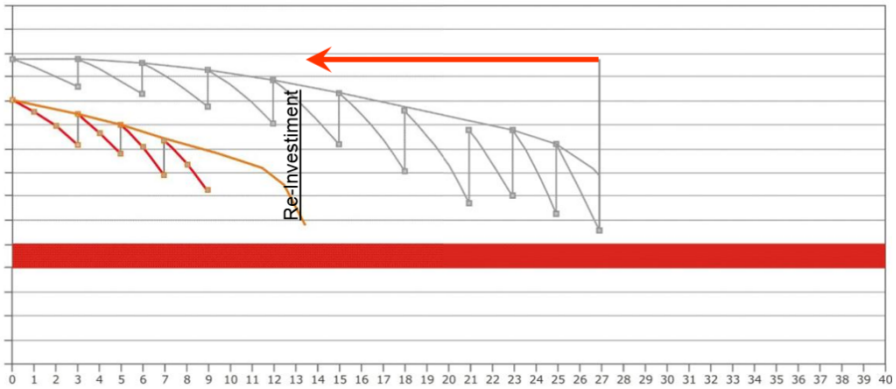

Figure 4-10: Reduction of service life by neglecting sub-layer rehabilitation and drainage maintenance (quality over service life; the red bar indicates the intervention level)

This effect is covered by LCAT-track in taking quality levels and deterioration values into account which are specific for different types of sub-layer quality and drainage situations.

Consequently the following three profiles were provided as base case examples in the table below.

Traffic loading				<15.000 [t/d]
				<30.000 [t/d]
		x		<45.000 [t/d]
	x		x	<65.000 [t/d]
				<100.000 [t/d]
track age				[a]
operating speed	130	130	130	[km/h]
ballast				hard, [basalt, hq granite, siliceous material], LA<16
	x	x	x	medium, [granite, diabase, dolomite], LA<23
				soft, [limestone], LA>23
sleeper	x	x		concrete
			x	concrete with under sleeper pads
				wooden
radii				<250m
				<400m
				<600m
	x	x	x	>600m
sublayer condition	x	x	x	good
				bad
drainage condition	x	x	x	good
				bad
avg. tamping cycle	3	3	4	[a]
After Relaying				
Q0	-7	-5	-6	
	0-10 a	0-15 a	0-10 a	
bn	0.2	0.11	0.12	
Qn	-8	-5	-7.5	
Qult	-12	-7	-12	
	10-25 a	15-25 a	10-20 a	
bn	0.15	0.11	0.09	
Qn	-10	-9	-8	
Qult	-15	-13	-15	
	25-30 a	25-30 a	20-30 a	
bn	0.19	0.12	0.11	
Qn	-14	-11	-12	
Qult	-20	-15	-20	
	N/A	30 ongoing	30-40 a	
bn	-	0.12	0.12	
Qn	-	-11	-15	
Qult	-	-15	-25	
	N/A	40 +	40-50 a	
bn	-	-	0.13	
Qn	-	-	-18	
Qult	-	-20	-25	
	30+	30+ 2 Tamp	50+	
bn	0.19	0.12	0.13	
Subsequent reduction,	0.02	-0.005	-0.01	
Qn	-20	-11	-20	
Subsequent reduction,	0.5	-0.5	-0.5	
Qult	-25	-15	-25	
	N/A	30+ 3 Tamp	N/A	
bn	-	0.12	-	
Subsequent reduction,	-	-0.005	-	
Qn	-	-11	-	
Subsequent reduction,	-	-0.5	-	
Qult	-	-17	-	
Resulting service life	-> 36 yrs	-> 45 yrs	-> 56 yrs	

Figure 4-11: Track performance profiles

Further variations of boundary conditions are covered by extrapolation from the given base cases.

This leads to the following input-parameter into LCAT-track.

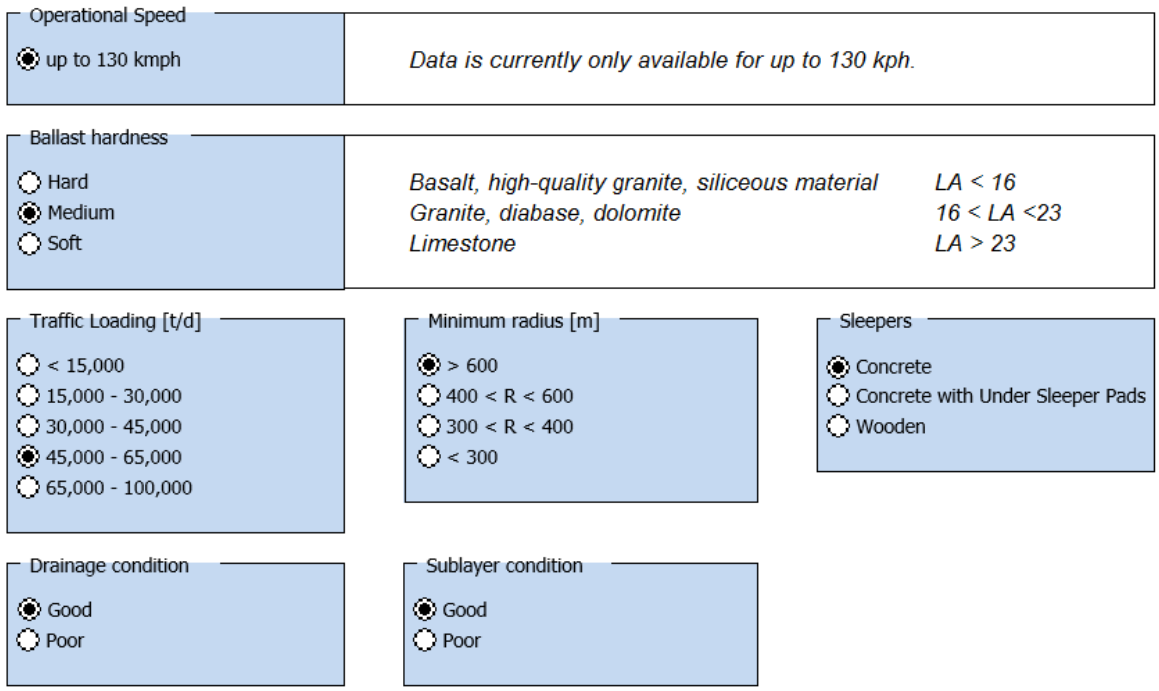

Figure 4-12: Input parameters forming the data set for estimating the potential service life of track

This input mask takes the importance of parameters regarding track deterioration into account. Research [1,2,3] depicted the ranking of cost drivers as mentioned below:

1. Initial track quality, depending on the type of superstructure (ballast status, sub-soil quality, functionality of the drainage system)
2. Alignment (radii)
3. Costs of operational hindrances
4. Traffic density
5. Length of track work section
6. Type and quality of rolling stock.

Numbers 1 to 4 are taken into account by LCAT-track, showing these boundary conditions input parameters. Costs of operation hindrances [9] are calculated covering the financial costs of infrastructure companies and train operators. Macroeconomic costs are not taken into account.

Optimising the length of track work sections is country specific and has little impact on track service life and is thus not taken into account. Cost driver number 6 is showing the cost potential of track friendly bogies (track cost reduction up to 10% in the network of Austria) but optimising rail wheel interaction is not part of MAINLINE.

4.2 Field Validation of Performance Profiles for Track

4.2.1 Scope of Validation

It has been agreed, amongst the MAINLINE partners, that the validation of performance profiles for tack will employ the developed Life Cycle Assessment Tool (LCAT). Relevant case studies will be fed into the model and a detailed analysis of the results will be undertaken and commented upon. Therefore, this validation exercise is directly linked with ensuring the correct operation of the LCAT tool, as opposed to the underlying modelling assumptions, and will be covered in more detail in the WP5 deliverables.

In this report, the reader can find a high level plan of this exercise, but detailed analysis will form part of the D5.5 deliverable in WP5.

4.2.2 Fundamentals

Previous projects carried out by the Institute of Railway Engineering and Transport Economy together with the infrastructure departments of the railways in Austria, Switzerland, Croatia and Norway have shown a significant correlation between boundary conditions like subsoil condition, ballast quality etc. and the resulting service life of railway tracks. Furthermore different boundary conditions lead obviously to different maintenance efforts. As an example, poor ballast quality leads to an increase of tamping actions as well as to a dramatic reduction of track service life. The track geometry as a possible indicator for this correlation has been analysed for various parameter sets over the whole service life of the asset. The results were extrapolated for other parameter sets as described in MAINLINE report on WP5. In summary, the deterioration of track geometry provides a useful measure to estimate the service life of the track considering various differing parameters. Thus the analyses provide essential input data for the prognosis model of LCAT.

4.2.3 Validation Process

It is necessary to validate the MAINLINE LCAT model by using experiences from different infrastructure managers as boundary conditions vary from country to country. The validation process is divided into two main parts. Both parts are independent of each other and can be described as follows:

Part 1:

Infrastructure managers have detailed average descriptions of maintenance cycles dealing with a significant number of different boundary conditions existing within their entire networks. These maintenance cycles, gained from general experience, have formed a solid base for different company strategies based on the calculation of life cycle costs. The Institute for Railway Engineering and Transport Economy (TUGraz) has built up strategies together with IMs in several countries. These general strategies, or better the input data for these strategies, are used to validate the generalised deterioration process.

General track strategies, seen from the point of view of life-cycle-costing, must contain both investment and maintenance elements. Basic input data for the identification and evaluation of track strategies are the track service life and the maintenance regime, which are closely linked as a poor maintenance regime will lead to a shorter service life. This forms a general

working cycle between one re-investment and the next. The working cycles used in the MAINLINE LCAT cover the one strategy leading to the lowest life cycle cost, which can differ from country to country due to different cost structures.

Apart from that, the working cycles reflect different boundary conditions. The combination of always one characteristic of these boundary conditions is named standard kilometre. The boundary conditions covered are:

1. traffic load
2. track alignment
3. superstructure type
   a. rail profile
   b. steel grade
   c. sleeper type
   d. further information such as rail pad type, fastener
4. subsoil quality and status of the dewatering system
5. number of tracks

In figure 4.13 the boundary conditions taken into account to form specific standard elements is shown. Note that sub-layer and subsoil together are subsumed under the term “substructure” as the capability of carrying the traffic load is the only important information for track behaviour. In practice a sub-layer needs to be inserted if the subsoil would be overstressed.

transport volume [GBT/day, track]	ballast	sleeper	radius [m]	sub-layer subsoil	drainage
65,000 - 100,000	Hard	concrete	> 600 m	Good	Good
45,000 - 65,000	Medium	wooden	400 m - 600 m	Poor	Poor
30,000 – 45,000	Soft	concrete with USP	250 m - 400 m		
15,000 – 30,000			< 250 m		
< 15,000					

Figure 4-13: Input values forming the parameter set for estimating the potential service life of track

In reality just some of the possible parameter combinations are relevant. It is possible to describe frequent track situations with about 50 to 80 standard elements.

For all these standard kilometres working cycles are generated, describing maintenance needs for all the specific situations and thereby defining basic strategies called reference strategies. Furthermore cost figures must be identified to make use of these standard kilometres and their working cycles within an economic evaluation.

For each standard element it is possible to sum up all necessary maintenance actions over the whole life cycle. Additionally an estimation of the amount of unplanned maintenance work is added in based on the experience of the different infrastructure managers.

As examples some standard elements for different ballast types, substructure qualities and functionality of the drainage system, radius and sleeper types are listed in following figures. There are three types of ballast, two types of sub-layer quality, two types of status of

drainage, two different radii and two sleeper types forming these eleven examples chosen out of many more possibilities (highlighted in red).

example	traffic load [GT/d]	rail profile	radius [m]	sleeper	ballast	substructure	drainage
1.1	30.000-45.000	60E1	R>600	Concrete	Hard	Good	Good
1.2	30.000-45.000	60E1	R>600	Concrete	Medium	Good	Good
1.3	30.000-45.000	60E1	R>600	Concrete	Soft	Good	Good
2.1	15.000-30.000	60E1	R>600	Wooden	Medium	Good	Good
2.2	15.000-30.000	60E1	R>600	Wooden	Medium	Good	Poor
2.3	15.000-30.000	60E1	R>600	Wooden	Medium	Poor	Good
2.4	15.000-30.000	60E1	R>600	Wooden	Medium	Poor	Poor
3.1	45.000-65.000	60E1	400<R<600	Concrete	Hard	Good	Good
3.2	45.000-65.000	60E1	300<R<400	Concrete	Hard	Good	Good
4.1	65.000-100.000	60E1	R>600	Concrete	Medium	Good	Good
4.2	65.000-100.000	60E1	R>600	Concrete with USP	Medium	Good	Good

Figure 4-14: Standard elements given as examples

The standard elements in figures 4.15 to 4.17 are based on different ballast qualities. All other parameters are the same within the standard elements 1.1 to1.3. All ballast has a good particle-size distribution.

The standard element 1.1 is valid for an excellent ballast quality (“hard ballast”).

1.1							
traffic load [Gt/d]	rail profile	steel grade	radius	sleeper	ballast	substructure	drainage
30.000 - 45.000	60E1	R260	R>600m	concrete	hard	good	good

service life in years	50,0	0	1	2	3	4	5	6	7	8	9	10	11	12	13	14	15	16	17	18	19	20	21	22	23	24	25	26	27	28	29	30	31	32	33	34	35	36	37	38	39	40	41	42	43	44	45	46	47	48	49
Relaying	1,0	1																																																		
Levelling-Lining-Tamping	8,0	1						1						1						1								1						1						1						1					
Rail Grinding	8,0	1						1						1						1								1						1						1						1					
Rail Exchange	0,0																																																		
Joint Maintenance	0,0																																																		
Rail Pad Exchange	0,0																																																		
Spot Repair	50,0	0,5	0,5	0,5	0,5	0,5	0,5	0,5	0,5	0,5	0,5	0,5	0,5	0,5	0,5	0,5	0,5	0,5	0,5	1	1	1	1	1	1	1	1	1	1	1	1	1	1	1	1,5	1,5	1,5	1,5	1,5	1,5	1,5	1,5	1,5	1,5	1,5	1,5	1,5	1,5	1,5	1,5

Figure 4-15: Standard element 1.1

The standard element 1.2 is based on a good ballast quality (“medium ballast”).

1.2							
traffic load [Gt/d]	rail profile	steel grade	radius	sleeper	ballast	substructure	drainage
30.000 - 45.000	60E1	R260	R>600m	concrete	medium	good	good

service life in years	36,0	0	1	2	3	4	5	6	7	8	9	10	11	12	13	14	15	16	17	18	19	20	21	22	23	24	25	26	27	28	29	30	31	32	33	34	35
Relaying	1,0	1																																				
Levelling-Lining-Tamping	6,0	1						1						1						1					1						1						
Rail Grinding	4,0	1									1									1								1									
Rail Exchange	0,0																																				
Joint Maintenance	0,0																																				
Rail Pad Exchange	0,0																																				
Spot Repair	36,0	0,5	0,5	0,5	0,5	0,5	0,5	0,5	0,5	0,5	0,5	0,5	0,5	1	1	1	1	1	1	1	1	1	1	1	1	1,5	1,5	1,5	1,5	1,5	1,5	1,5	1,5	1,5	1,5	1,5	1,5

Figure 4-16: Standard element 1.2

The standard element 1.3 describes the consequences of a poor ballast quality (“soft ballast”)

1.3																								
traffic load [Gt/d]	rail profile	steel grade			radius			sleeper			ballast			substructure			drainage							
30.000 - 45.000	60E1	R260			R>600m			concrete			soft			good			good							
service life in years	25,0	0	1	2	3	4	5	6	7	8	9	10	11	12	13	14	15	16	17	18	19	20	21	22	23	24
Relaying	1,0	1																								
Levelling-Lining-Tamping	12,0		1			1		1		1		1		1		1		1		1		1		1	1	
Rail Grinding	1,0		1																							
Rail Exchange	0,0																									
Joint Maintenance	0,0																									
Rail Pad Exchange	1,0															1										
Spot Repair	25,0	0,5	0,5	0,5	0,5	0,5	0,5	0,5	0,5	1	1	1	1	1	1	1	1	1	1,5	1,5	1,5	1,5	1,5	1,5	1,5	1,5
ballast cleaning	1,0															1										

Figure 4-17: Standard element 1.3

Example	traffic load [GT/d]	rail profile	radius [m]	sleeper	ballast	substructure	drainage	service life [years]	tamping cycle [years]
1.1	30.000-45.000	60E1	R>600	Concrete	Hard	Good	Good	50	> 6
1.2	30.000-45.000	60E1	R>600	Concrete	Medium	Good	Good	36	6
1.3	30.000-45.000	60E1	R>600	Concrete	Soft	Good	Good	25	2

Figure 4-18: Comparison of standard elements 1.1 to 1.3

Figure 4.18 gives a comparison of these three working cycles. The major difference between these standard elements is the service life, which can be calculated from track behaviour via its quality level and deterioration rate. As the deterioration rate keeps constant between two track measures the tamping cycle also needs to be taken into account. The examples show that taking into account the ballast hardness is vital for calculating the possible service life.

In the case of soft ballast there is also a requirement to ballast clean within the service life (figure 4.16) to ensure that the possible service life calculated with LCAT-track is achieved. If this maintenance work is not executed, for whatever reason r, the service life given by LCAT-track would not be achievable.

Therefore the user of LCAT-track has to take into consideration whether the tamping cycle resulting from LCAT-track is actually followed and if the condition of all the track components is adequate to permit the predicted service life of the track to be reached. For instance, in the case of track with soft ballast inspection could show a polluted ballast bed, which would either reduce track service life significantly or require cleaning of the ballast bed. However, the output from LCAT-track gives the possible maximum service life and thus delivers guidance on the optimum track strategy.

In figures 4.19 to 4.22 the standard elements show different substructure and drainage conditions.

The standard element 2.1 describes a situation with a proper substructure and a good dewatering system.

2.1								
traffic load [Gt/d]	rail profile	steel grade	radius	sleeper	ballast	substructure	drainage	
15.000 - 30.000	60E1	R260	R>600m	wood	medium	good	good	

service life in years	40,0	0	1	2	3	4	5	6	7	8	9	10	11	12	13	14	15	16	17	18	19	20	21	22	23	24	25	26	27	28	29	30	31	32	33	34	35	36	37	38	39
Relaying	1,0	1																																								
Levelling-Lining-Tamping	5,0	1								1								1								1								1								
Rail Grinding	4,0	1												1												1													1			
Rail Exchange	0,0																																								
Joint Maintenance	0,0																																								
Rail Pad Exchange	0,0																																								
Spot Repair	40,0	0,5	0,5	0,5	0,5	0,5	0,5	0,5	0,5	0,5	0,5	0,5	0,5	1	1	1	1	1	1	1	1	1	1	1	1	1	1	1	1,5	1,5	1,5	1,5	1,5	1,5	1,5	1,5	1,5	1,5	1,5	1,5

Figure 4-19: Standard element 2.1

The standard element 2.2 is based on proper substructure but a poor drainage conditions.

2.2								
traffic load [Gt/d]	rail profile	steel grade	radius	sleeper	ballast	substructure	drainage	
15.000 - 30.000	60E1	R260	R>600m	wood	medium	good	poor	

service life in years	40,0	0	1	2	3	4	5	6	7	8	9	10	11	12	13	14	15	16	17	18	19	20	21	22	23	24	25	26	27	28	29	30	31	32	33	34	35	36	37	38	39
Relaying	1,0	1																																								
Levelling-Lining-Tamping	7,0	1						1						1						1						1						1						1			
Rail Grinding	4,0	1												1												1												1			
Rail Exchange	0,0																																								
Joint Maintenance	0,0																																								
Rail Pad Exchange	0,0																																								
Spot Repair	40,0	0,5	0,5	0,5	0,5	0,5	0,5	0,5	0,5	0,5	0,5	0,5	0,5	1	1	1	1	1	1	1	1	1	1	1	1	1	1	1	1,5	1,5	1,5	1,5	1,5	1,5	1,5	1,5	1,5	1,5	1,5	1,5

Figure 4-20: Standard element 2.2

Facing a situation with a substructure which is overloaded substructure but a proper working dewatering system is described in the standard element 2.3.

2.3								
traffic load [Gt/d]	rail profile	steel grade	radius	sleeper	ballast	substructure	drainage	
15.000 - 30.000	60E1	R260	R>600m	wood	medium	poor	good	

service life in years	40,0	0	1	2	3	4	5	6	7	8	9	10	11	12	13	14	15	16	17	18	19	20	21	22	23	24	25	26	27	28	29	30	31	32	33	34	35	36	37	38	39
Relaying	1,0	1																																								
Levelling-Lining-Tamping	10,0	1				1				1				1				1				1				1				1				1				1			
Rail Grinding	4,0	1												1												1												1			
Rail Exchange	0,0																																								
Joint Maintenance	0,0																																								
Rail Pad Exchange	0,0																																								
Spot Repair	40,0	0,5	0,5	0,5	0,5	0,5	0,5	0,5	0,5	0,5	0,5	0,5	0,5	1	1	1	1	1	1	1	1	1	1	1	1	1	1	1	1,5	1,5	1,5	1,5	1,5	1,5	1,5	1,5	1,5	1,5	1,5	1,5

Figure 4-21: Standard element 2.3

Finally the worst case, overloaded substructure and drainage problems is described by the standard element 2.4

2.4								
traffic load [Gt/d]	rail profile	steel grade	radius	sleeper	ballast	substructure	drainage	
15.000 - 30.000	60E1	R260	R>600m	wood	medium	poor	poor	

service life in years	20,0	0	1	2	3	4	5	6	7	8	9	10	11	12	13	14	15	16	17	18	19
Relaying	1,0	1																			
Levelling-Lining-Tamping	5,0	1				1				1				1				1			
Rail Grinding	2,0	1												1							
Rail Exchange	0,0																				
Joint Maintenance	0,0																				
Rail Pad Exchange	0,0																				
Spot Repair	20,0	0,5	0,5	0,5	0,5	0,5	0,5	0,5	1	1	1	1	1	1	1,5	1,5	1,5	1,5	1,5	1,5	1,5

Figure 4-22: Standard element 2.4

example	traffic load [GT/d]	rail profile	radius [m]	sleeper	ballast	substructure	drainage	service life [years]	tamping cycle [years]
2.1	15.000-30.000	60E1	R>600	Wooden	Medium	Good	Good	40	8
2.2	15.000-30.000	60E1	R>600	Wooden	Medium	Good	Poor	40	6
2.3	15.000-30.000	60E1	R>600	Wooden	Medium	Poor	Good	40	4
2.4	15.000-30.000	60E1	R>600	Wooden	Medium	Poor	Poor	20	4

Figure 4-23: Comparison of standard elements 2.1 to 2.4

Figure 4.23 gives a comparison of these four working cycles. These standard elements differ in service life and tamping demand (the same tamping cycle in years within half of the service life means tamping after half of the transport load passed). Also spot repair including (spot tamping is increasing to a high degree which will lead to a large increase in costs.

In figures 4.24 and 4.26 the standard elements valid for different radii are presented.

The standard element 3.1 describes track behaviour in radii of 400 m to 600 m. Here there is some side wear.

3.1							
traffic load [Gt/d]	rail profile	steel grade	radius	sleeper	ballast	substructure	drainage
45.000 - 65.000	60E1	R350HT	400<R<600	concrete	hard	good	good

service life in years	42,0	0	1	2	3	4	5	6	7	8	9	10	11	12	13	14	15	16	17	18	19	20
Relaying	1,0	1																				
Levelling-Lining-Tamping	10,0	1					1					1					1					1
Rail Grinding	10,0	1					1					1					1					1
Rail Exchange	3,0											1										1
Joint Maintenance	0,0																					
Rail Pad Exchange	8,0						1					1					1					1
Spot Repair	42,0	0,5	0,5	0,5	0,5	0,5	0,5	0,5	0,5	0,5	0,5	0,5	0,5	0,5	0,5	1	1	1	1	1	1	1

service life in years	21	22	23	24	25	26	27	28	29	30	31	32	33	34	35	36	37	38	39	40	41
Relaying																					
Levelling-Lining-Tamping					1				1				1			1			1		
Rail Grinding					1				1				1			1			1		
Rail Exchange									1												
Joint Maintenance																					
Rail Pad Exchange					1				1					1				1			
Spot Repair	1	1	1	1	1	1	1	1,5	1,5	1,5	1,5	1,5	1,5	1,5	1,5	1,5	1,5	1,5	1,5	1,5	1,5

Figure 4-24: Standard element 3.1

The standard element 3.2 describes track behaviour in even smaller radii (300 m to 400 m). In that case more or less all standard types of rolling stock cause rail side wear on the outer rail and corrugation waves on the inner one.

3.2							
traffic load [Gt/d]	rail profile	steel grade	radius	sleeper	ballast	substructure	drainage
45.000 - 65.000	60E1	R350HT	300<R<400	concrete	hard	good	good

service life in years	39,0	0	1	2	3	4	5	6	7	8	9	10	11	12	13	14	15	16	17	18	19
Relaying	1,0	1																			
Levelling-Lining-Tamping	10,0	1					1					1					1				1
Rail Grinding	10,0	1					1					1					1				1
Rail Exchange	3,0											1									1
Joint Maintenance	0,0																				
Rail Pad Exchange	13,0			1		1			1			1				1			1		1
Spot Repair	39,0	0,5	0,5	0,5	0,5	0,5	0,5	0,5	0,5	0,5	0,5	0,5	0,5	0,5	1	1	1	1	1	1	1

service life in years	20	21	22	23	24	25	26	27	28	29	30	31	32	33	34	35	36	37	38
Relaying																			
Levelling-Lining-Tamping				1				1			1			1			1		
Rail Grinding				1				1			1			1			1		
Rail Exchange											1								
Joint Maintenance																			
Rail Pad Exchange			1			1			1		1			1			1		
Spot Repair	1	1	1	1	1	1	1,5	1,5	1,5	1,5	1,5	1,5	1,5	1,5	1,5	1,5	1,5	1,5	1,5

Figure 4-25: Standard element 3.2

example	traffic load [GT/d]	rail profile	radius [m]	sleeper	ballast	substructure	drainage	service life [years]	tamping cycle [years]
3.1	45.000-65.000	60E1	400<R<600	Concrete	Hard	Good	Good	42	> 4
3.2	45.000-65.000	60E1	300<R<400	Concrete	Hard	Good	Good	39	< 4

Figure 4-26: Comparison of standard elements 3.1 and 3.2

Figure 4.25 shows the effects of different radii. The influence is not that big for the service life. However the demand on rail exchange and rail pad exchange increases in a big scale (though in both cases head hardened rails are assumed) or would – if not executed – reduce the service life of track much more.

In figure 4.27 and 4.28 the standard elements valid for sleeper types are presented.

The standard element 4.1 describes track behaviour with standard concrete sleepers.

4.1																														
traffic load [Gt/d]	rail profile	steel grade			radius			sleeper			ballast			substructure			drainage													
65.000 - 100.000	60E1	R260			R>600m			concrete			medium			good			good													
service life in years	26,0	0	1	2	3	4	5	6	7	8	9	10	11	12	13	14	15	16	17	18	19	20	21	22	23	24	25			
Relaying	1,0	1																												
Levelling-Lining-Tamping	10,0	1			1			1			1			1		1			1			1		1		1				
Rail Grinding	7,0	1			1				1				1				1				1				1					
Rail Exchange	0,0																													
Joint Maintenance	0,0																													
Rail Pad Exchange	0,0																													
Spot Repair	26,0	0,5	0,5	0,5	0,5	0,5	0,5	0,5	0,5	0,5	1	1	1	1	1	1	1	1	1,5	1,5	1,5	1,5	1,5	1,5	1,5	1,5	1,5			

Figure 4-27: Standard element 4.1

The standard element 4.2 describes track behaviour using concrete sleepers with under sleeper pads [4,6].

4.2																																
traffic load [Gt/d]	rail profile	steel grade			radius			sleeper					ballast			substructure			drainage													
65.000 - 100.000	60E1	R260			R>600m			concrete with USP					medium			good			good													
service life in years	36,0	0	1	2	3	4	5	6	7	8	9	10	11	12	13	14	15	16	17	18	19	20	21	22	23	24	25	26	27	28	29	30	31	32	33	34	35
Relaying	1,0	1																																			
Levelling-Lining-Tamping	5,0	1							1							1							1							1							
Rail Grinding	10,0	1			1				1				1			1				1				1				1		1				1			
Rail Exchange	0,0																																				
Joint Maintenance	0,0																																				
Rail Pad Exchange	0,0																																				
Spot Repair	36,0	0,5	0,5	0,5	0,5	0,5	0,5	0,5	0,5	0,5	0,5	0,5	0,5	1	1	1	1	1	1	1	1	1	1	1	1,5	1,5	1,5	1,5	1,5	1,5	1,5	1,5	1,5	1,5	1,5	1,5	1,5

Figure 4-28: Standard element 4.2

example	traffic load [GT/d]	rail profile	radius [m]	sleeper	ballast	substructure	drainage	service life [years]	tamping cycle [years]
4.1	65.000-100.000	60E1	R>600	Concrete	Medium	Good	Good	26	3 - 4
4.2	65.000-100.000	60E1	R>600	Concrete with USP	Medium	Good	Good	36	> 7

Figure 4-29: Comparison of standard elements 2.1 to 2.4

Figure 4.29 shows the positive effect of using under sleeper pads.

These standard elements presented here are just examples for the data source in the background for validating LCAT.

The resulting service life and the maintenance effort are simply based on the behaviour of the track. This means that standard elements generally describe the deterioration of a track but are neither able to consider all influencing parameters nor describe every situation in detail. It must be stressed that standard elements exist for all possible combinations of boundary conditions. As the quality values and the b rates derived from a nonlinear regression of track recording car data specific to all relevant combinations of boundary conditions form the model within LCAT-track, the standard elements are a proper data set for validation of the base cases of LCAT-track and all subsequent extrapolations to deal with the different combinations of the various boundary conditions.

Whilst these track strategies were developed for different countries a comparison between the results of the LCAT focusing on the Croatian, Austrian and Swiss railways will establish a validation of the model itself. In contrast to the sleepers, rails, vehicle collectives (traffic) and various subsoil conditions the ballast conditions in these countries are completely different. The comparison between the three countries shows the influence of excellent, quite good and poor ballast condition, on the resulting tamping cycle and service life. This comparison

mainly focuses on the standard elements of the three countries and the economic evaluation and, although the cost levels in the three countries are different, this will not influence the result of the technical validation process.

Part 2:

In the second step the results of LCAT are compared with several renewal projects which will be executed over the next few years by the Austrian Federal Railways. These renewal projects are part of research projects mainly carried out in cooperation with the Austrian Federal Railways and were monitored in a technical as well as economic way.

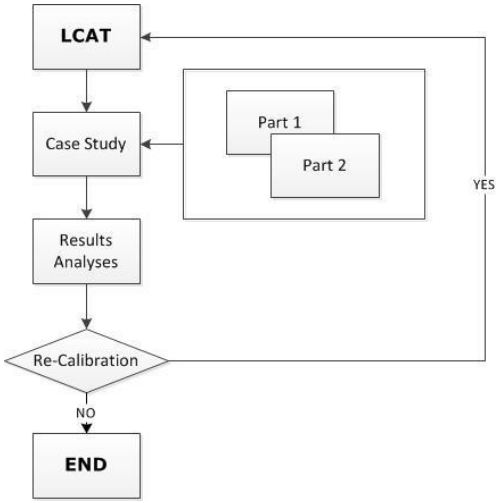

Figure 4-30: Flow diagram of the validation process

4.2.4 Conclusion

The main target of the whole validation process is to compare the calculated service life out of the LCAT model with the resulting service life of the three different described data sources.

It would not be possible in the time available to evaluate every possible combination of the boundary conditions shown in the figure below. However, it is necessary to evaluate a substantial sample, which is the methodology followed for this validation process. This sample should at least cover the most commonly applied combinations and should demonstrate the logical and technical consistency of the whole model. Any possible deviation of the calculated values must be technically discussed to understand the implications. Possible reasons for such deviations will be listed and where necessary potential options for recalibration of the model will be given.

Traffic loading		<15.000 [t/d]		
		<30.000 [t/d]		
		<45.000 [t/d]		
	x	<65.000 [t/d]		
		<100.000 [t/d]		
track age		[a]		
operating speed	130	[km/h]		
ballast		hard	[basalt, good granite]	LA<16
	x	medium	[granite,diabase]	LA<23
		soft	[limestone]	LA>23
sleeper	x	concrete		
		concrete with under sleeper pads		
		wooden		
radii		<250m		
		<400m		
		<600m		
	x	>600m		
sublayer condition	x	good		
		bad		
drainage condition	x	good		
		bad		
avg. tamping cycle	3,5	[a]		

Figure 4-31: Possible boundary conditions in LCAT

4.3 References

[1] Landgraf, M., Marschnig, S., Veit, P. (2013), FJORD - Further Juxtaposition of Cost Optimisation, On Track towards LifeCycleManagement, (internal report)

[2] Veit, P. (2013), Handbuch Eisenbahninfrastruktur. - in: Handbuch Eisenbahninfrastruktur. , S. 1009 – 1054

[3] Marschnig, S.; Hansmann, F.; Veit, P., ÖBB LCM – MDZEingriff, (internal report)

[4] Marschnig, S.; Veit, P. (2011), Towards a more sustainable track. - in: Railway gazette international January, S. 42 – 44

[5] Marschnig, S.; Veit, P. (2011), Making a case for under-sleeper pads. - in: International railway journal, S. 27 – 29

[6] Marschnig, S.; Veit, P.; Berghold, A. (2010), WINS - Wirtschaftlicher Nutzen von Schwellenbesohlungen, (internal report)

[7] Veit, P. (2009), Life Cycle Costing in Practice in Europe. - in: Guidelines to Best Practices for Heavy Haul Railway Operations, S. 2-22 - 2-34

[8] Veit, P.; Marschnig, S. (2009),Technische und wirtschaftliche Aspekte zum Thema Schwellenbesohlung. - in: ZEVrail 11-12 2009, S. 436 - 443

[9] Marschnig, S.; Veit, P. (2008), Baustellenlogistik Sperrpausenoptimierung, (internal report)

5. Soil Cuttings (Jacobs/SKM, NR)

5.1 Outline of D2.3 Performance Profiles for Soil Cuttings

This chapter has built upon work done to date within other MAINLINE Work Packages and deliverables and therefore a summary of the key findings related to the validation of deterioration performance profiles is provided here first.

As part of D2.2 [5] and D2.3 [6] reports, Jacobs/SKM has collected and analysed eight years of historical data of soil cuttings examinations. This comprises the Soil Slope Hazard Index (SSHI) data. This tool was developed by Network Rail and Babtie Group to facilitate the rapid and repeatable inspection of rail earthworks and is meant to enable a consistent and impartial assessment of their condition from Network Rail (NR) in UK.

Based on that analysis and the geotechnical expertise of SKM, a prototype soil cuttings scoring system, which is known as the SKM Algorithm (SKMA), has been developed and deterioration and degradation performance profiles derived [1].

The final SKMA combines three fixed and six changeable factors (assessments) in a particular way (further details can be found in D2.2 [5]), classifies the asset by soil type and calculates a risk score for every slope. These factors are summarised in the tables below.

Table 5.1: SKMA changeable factors

SKMA changeable factors	
Movement Assessment	MA
Vegetation Assessment	VA
Surface Water Assessment	SWA
Drainage Assessment	DA
Burrowing Assessment	BA
Construction Activity Assessment	CAA

Table 5.2: SKMA fixed factors

SKMA fixed factors	
Slope Angle Factor	SAF
Slope Height Factor	SHF
Adjacent Landform Factor	ALF

Table 5.3: SKMA soil type

Soil type
Cohesive
Granular
Inter-bedded

Using the revised SKMA system, the eight years' worth of Network Rail's SSHI's data was converted to the SKMA format. This allowed the derivation of degradation performance profiles based on a quantitative analysis which is explained in full detail in D2.3 [6]. Additionally, the reader should be mindful that these deterioration rates that were derived are entirely based on historical information from NR and include no theoretical forecasting of deterioration mechanisms.

The tables below show the SKMA deterioration performance profiles as they appear in D2.3 [6]. In particular, starting values of each of the six factors (Input scores) and the expected values of the change in score after five years are presented. The changes for cohesive, granular and inter-bedded soils are classified and shown separately.

Input scores						Cohesive						Granular						Inter-bedded					
MA	VA	SW	DA	BA	CA	MA	VA	SW	DA	BA	CA	MA	VA	SW	DA	BA	CA	MA	VA	SW	DA	BA	CA
Movement Assessment	Vegetation Assessment	Surface Water Assessment	Drainage Assessment	Burrowing Assessment	Construction Activity Assessment	Movement Assessment	Vegetation Assessment	Surface Water Assessment	Drainage Assessment	Burrowing Assessment	Construction Activity Assessment	Movement Assessment	Vegetation Assessment	Surface Water Assessment	Drainage Assessment	Burrowing Assessment	Construction Activity Assessment	Movement Assessment	Vegetation Assessment	Surface Water Assessment	Drainage Assessment	Burrowing Assessment	Construction Activity Assessment
0.0	0.0	0.0	-1.0	0.0	0.0	0.00	0.48	0.69	1.04	0.57	0.05	0.00	0.32	0.27	0.94	0.49	0.05	0.00	0.73	0.71	1.89	0.47	0.10
1.0	0.2	1.0	0.0	1.0	1.0	1.27	0.49	0.64	0.35	0.42	0.00	0.45	0.27	0.55	0.16	0.39	0.03	0.93	0.50	0.71	0.41	0.53	0.04
1.5	0.3	1.5	0.5	2.0	2.0	1.68	0.79	0.63	0.16	0.00	0.00	1.15	0.57	0.62	0.23	0.00	0.00	1.54	1.25	0.78	0.34	0.00	0.00
2.0	0.5	2.0	1.5	-	-	0.62	0.81	0.79	0.00			0.13	0.30	0.32	0.00			0.49	1.56	0.99	0.00		
2.5	1.0	2.5	-	-	-	0.22	0.03	0.22				0.08	0.03	0.12				0.15	0.05	0.15			
4.0	1.5	3.0	-	-	-	0.00	0.00	0.00				0.00	0.00	0.00				0.28	0.00	0.00			
5.0	-	-	-	-	-	0.00						0.00						0.00					

Figure 5-1: SKMA deterioration performance profiles

5.2 Field Validation of Performance Profiles for Soil Cuttings - Introduction

This chapter reports on the development of a validation exercise to test the derived deterioration performance profiles as well as the revised SKM Algorithm (SKMA). The aim of this work in general is to scrutinise the methods adopted in previous tasks, compare theoretical profiles to real data as well as to validate the SKMA Algorithm with other tools and, hence, to establish the level of confidence that can be associated with model predictions.

That said, the purpose of the field validation of performance profiles for soil cuttings is two-fold:

- To validate the SKM Algorithm through sensitivity and statistical analyses and comparison with other tools such as the SSHI Algorithm.
- To compare deterioration performance profiles to real data and case studies to verify the validity of the degradation modelling approach.

Therefore, this chapter splits in two parts: The first part gives the details of the comparison of SKMA and SSHI through sensitivity and statistical analyses and outlines conclusions on the results. The second part continues with the validation of the deterioration profiles through comparison with real data, discusses the final conclusions and outlines the limitations of the modelling approach.

5.3 Source Data

As discussed above, historical data from Network Rail (NR) in the UK was used to derive the deterioration profiles in D2.3. This is the only known available source of extensive, numerical, and historical data regarding condition of soil cuttings from which trends can be derived. The NR soil cutting scoring system is known as the Soil Slope Hazard Index (SSHI) and the data includes details of the location and date of each examination but also crucially describes the critical features and condition of the soil slopes in terms of predefined characteristics with alpha-numeric scores.

In order to make the condition criteria more general and usable by other infrastructure managers the scoring system has been simplified from SSHI for use in the LCAT. The revised scoring system derived by SKM is known in the context of this project as the SKM Algorithm (SKMA). The conversion process and the development of SKMA have been described in the D2.2 report.

5.4 The SKM Algorithm

5.4.1 Adjustments to the SKM Algorithm since D2.2

Within the D2.4 report, the SKM Algorithm (SKMA) has been further refined and enhanced to increase functionality and transparency. The scope of this section is to outline what changes have been made to the SKM Algorithm since D2.2 and comment on any observed differences in the function of the tool.

SKM Algorithm as is in D2.2

In the D2.2 report, the tool was based on two blocks of parameters that can be independently defined and then inter-related through their relative impact on cutting stability. The identified building blocks are:

1) Base Values (Slope geology and geometry)

- Soil type
- Slope angle factor (SAF)
- Slope height factor (SHF)
- Adjacent landform factor (ALF)

The Base Value (BV) is calculated by summating the scores for Slope Angle, Slope Height and Adjacent Landform

$$C_{BV} = SAF + SHF + ALF \quad (5.1)$$

2) Assessment Values

- Movement assessment (MA)
- Surface water assessment (SWA)
- Drainage assessment (DA)
- Vegetation assessment (VA)
- Burrowing assessment (BA)
- Construction activity assessment (CAA)
- Previous Remediation assessment (PRA)

The Slope Assessment Value (SAV) calculation is as follows:

$$SAV = [MA\ or\ VA] + [SWA\ or\ DA] + CAA + BA + PRA \quad (5.2)$$

Slope Risk Value (SRV)

It can be sensibly argued that the overall assessment of a slope should be primarily based on the assessment values. However, when considering the long term liability that any given slope presents to the operator, consideration should be given to the original condition. In line with this philosophy and to account for both the observed state of the slope (AV) and its original projected tendency to show signs of instability (BV), the Slope Risk Value (SRV) is calculated from a combination of the two parameters as follows:

$$SRV = SAV \times (1 + \frac{C_{BV}}{10}) \quad (5.3)$$

5.4.2 The Final SKM Algorithm

As discussed above, SKM has further developed and modified the SKM Algorithm for soil cuttings. The most important features of the current version are described below:

The final SKMA is based on a suite of similar input parameters, but with a number of slight modifications:

1) Base Values (Slope geology and geometry)

- Soil type
- Slope angle & height factor (SAHF)
- Adjacent landform factor (ALF)

The Base Value (BV) calculation has remained the same as that in D2.2:

$$C_{BV} = SAHF + +ALF \quad (5.4)$$

2) Assessment Values

- Movement assessment (MA)
- Surface water assessment (SWA)
- Drainage assessment (DA)
- Vegetation assessment (VA)
- Burrowing assessment (BA)
- Construction activity assessment (CAA)

The Slope Assessment Value (SAV) calculation has been slightly modified and does not incorporate the PRA factor now:

$$SAV = MAX(MA, VA) + MAX(SWA, DA) + CAA + BA \quad (5.5)$$

Slope Risk Value (SRV)

Slope Risk Value calculation is the same:

$$SRV = SAV \times (1 + \frac{C_{BV}}{10}) \quad (5.6)$$

5.4.3 Forensic Comparison of SKM Algorithm

To conclude, there have also been some minor modifications of the SKM Algorithm which do not affect the results of the model. All the algorithm's weights, formulae and calculations have remained the same.

Nonetheless, some non-critical modifications have been applied to simplify the structure of the parameters' matrices (see items 3-8 below), remove redundant parameters such as PRA (see item 2) and simplify the calculations (see item 1) of the risk score.

A full list with all the SKMA modifications can be seen below:

Table 5.4: SKMA forensic comparison

Item	Source	Difference	Description	Critical to results of SKMA
1	D2.2	Function of SKMA	D2.2 calculates the BV by summating the scores of SAF, SHF and ALF	**No**
	D5.5	Function of SKMA	D2.4 calculates the BV by summating the SAHF and ALF (having previously and separately summate the SAF and SHF into the combined SAHF)	**No**
2	D2.2	Function of SKMA	D2.2 estimates SRV by adding Previous Remediation Assessment	**No**
	D5.5	Function of SKMA	Previous Remediation Assessment has been removed in D5.5	**No**
3	Forensic comparison (internal spreadsheet)	Structure of matrices	D2.2 scores' matrices are one dimensional, having "n/a features" in the other side of the diagonal, whereas D5.5 matrices reflect the scores in a symmetric way	**No**

Item	Source	Difference	Description	Critical to results of SKMA
4	Forensic comparison (internal spreadsheet)	MA	D2.4 Movement Assessment (MA) matric incorporates a "none features" option which is equal to the diagonal of the original matric in D2.2	**No**
5	Forensic comparison (internal spreadsheet)	SWA	D2.4 Surface Water Assessment (SWA) matric incorporates a "none features" option which is equal to the diagonal of the original matric in D2.2	**No**
6	Forensic comparison (internal spreadsheet)	VA	D2.4 Vegetation Assessment (VA) matric has become symmetric, incorporating the "slope cracked" feature in both dimensions	**No**
7	Forensic comparison (internal spreadsheet)	BA	D2.4 Burrowing Assessment (BA) matric incorporates a "none features" option which is implied to be equal to zero	**No**
8	Forensic comparison (internal spreadsheet)	CAA	D2.4 Construction Activity Assessment (CAA) matric incorporates a "none features" option which is implied to be equal to zero	**No**

5.5 Part I: Sensitivity Analysis of SKM Algorithm

5.5.1 Introduction and Objectives of Sensitivity Analysis

Sensitivity analysis is a technique used to study how the uncertainty in the output of a mathematical model or system (numerical or otherwise) can be apportioned to different sources of uncertainty in its input values. In other words, sensitivity analysis allows the decision maker to determine which inputs (parameters) are the key drivers of a model's results. Subsequently, sensitivity analysis can be useful for testing the SKM Algorithm which is the basis for the MAINLINE Life Cycle Assessment Tool (LCAT) in a range of scenarios, including [8]:

- Testing the robustness of the output.
- Enforced understanding of the relationships between input and output.
- Reduced variation by identifying the most critical model inputs that cause significant variation in the output and should therefore be the focus of attention.
- Searching for errors in the model (by encountering unexpected or unintended relationships between inputs and outputs).

- Model simplification – identifying model inputs that have no effect on the output, so that redundant parts of the decision process may be removed.
- Finding regions in the space of input variables for which the output is either maximum or minimum or meets some optimum criterion (optimization procedures).

Before the LCAT response can be thoroughly appreciated, it is important to understand the way that this associated algorithm works and contributes to the final output.

Settings and constraints

The choice of the method of sensitivity analysis of the LCAT is restricted by a number of problem constraints, which include the following main challenges:

- **Computational complexity:** Sensitivity analysis is almost always performed by running the model a large number of times (i.e. sampling-based approach in probabilistic theory). This can be a major constraint when,
  - A single run of the model takes a significant amount of time.
  - The solution space is vast. Sensitivity analysis is essentially the exploration of the multidimensional solution space, which grows exponentially in size with the number of inputs.

In our case, the solution space of the LCAT algorithm, which comprises all the potential combinations of input values, is quite large. More specifically, LCAT is loaded with 8 initial factors, the combinations of which create more than 29×10^9 different scenarios. Therefore, a systematic and comprehensive approach should be adopted in order to reduce the computational complexity of this problem. Alternatively, some more sophisticated methods of reducing computational complexity include the use of emulators (meta-models), and the screening methods (for reducing the dimensionality of the problem).

- **Correlated inputs:** Many sensitivity analysis methods assume independence between model inputs, but sometimes inputs can be strongly correlated, which means that interactions occur when the perturbation of two or more inputs simultaneously causes variation in the output greater than that of varying each of the inputs alone. Such interactions are presented in any model that is non-additive, and this is still an immature field of research where definitive methods have yet to be conclusively established. The LCAT algorithm is not an additive model, thus there are potentially some correlations between the factors which pose considerable obstacles in this analysis.

5.5.2 Background – Overview of SKM Algorithm

The SKMA is intended to provide an indication of the geotechnical condition of an earthwork (i.e. soil cuttings). In short, the user sets the characteristics of the asset (a soil cutting) by selecting the values of 16 initial factors (e.g. slope height), and the algorithm assigns appropriate scores to these specific characteristics and returns a risk value associated with this particular asset.

More specifically, the mechanism behind the LCAT algorithm combines the initial 16 factors and returns 8 interim ones, of which 6 are changeable over time (e.g. drainage condition) and 2 are assumed to be static or constant over time within the LCAT model (e.g. height of cutting).

The formula that combines the final 8 factors and returns back a risk value is as follows:

$$Slope\ Risk\ Value = [(MAX(Movement\ assessment, Vegetation\ assessment) + MAX(Surface\ water\ assessment, Drainage\ assessment) + Burrowing\ assessment + Construction\ activity\ assessment)\ ] \times\ [(Slope\ angle\ \&height + Adjacent\ land) \times 0.1 + 1)] \quad (5.7)$$

It is clear that the formula above creates a complex and non- additive model, where **correlations between the factors** might play a role and affect the ultimate score.

5.5.3 Sensitivity Analysis Techniques

There are several different ways of undertaking sensitivity analysis, each of which is briefly discussed in more detail below.

One- way sensitivity analysis

The most straightforward form of sensitivity analysis is to simply vary one input variable by a given amount, and examine the impact that the change has on the model's results. For each parameter change, the researcher might record the percentage impact on the model's main outcome, which can be shown graphically in the form of a **tornado diagram**. Despite its simplicity however, this approach does not fully explore the input space, since it does not take into account the simultaneous variation of input variables. This means that the one- way approach cannot detect the presence of interactions between input variables [2].

Multi-way sensitivity analysis

While one-way sensitivity analysis is useful in demonstrating the impact of *one* factor varying in the model it might be necessary to examine the relationship of two or more different factors changing simultaneously. One method that is sometimes used to assess this, especially in computationally intensive problems, is to undertake **extreme** sensitivity analysis, by varying *all except one* of the parameters in a model to their 'best', 'average' and 'worst' case while simultaneously changing that one in its corresponding 'best', 'average' and 'worst' value [2].

Other approaches

Last but not least, further sensitivity analysis approaches that might be considered include numerous of different techniques, from which, the most significant are the following:

- Partial derivatives
- Regression analysis
- Scatter plots
- Meta- models
- Variance- based methods
- What-if analysis and Solver in Excel

A two- stages methodology

In our context, the sensitivity analysis of the LCAT has been undertaken in a two-stage approach: In the first stage an initial one-way sensitivity analysis of the intermediate 8 factors was conducted and its results were compared to that of a more comprehensive multi-ways approach, where the value of one factor simultaneously changed against the values of all the other remaining factors. These two sensitivity analysis approaches were implemented in Visual Basic for Applications (VBA) in Excel.

Note that this sensitivity analysis has assessed the algorithm in isolation: no consideration is made of which input parameters are likely to occur (or not) in real life.

5.5.4 Stage 1: One-Way Sensitivity Analysis

Methodology

In the first instance, an initial one-at-a-time approach was undertaken. As discussed previously, this analysis involves the following process:

- Moving one input variable to its highest value, keeping others at their baseline (lowest) values, then,

- Returning the variable to its baseline value and then repeating for each of the other inputs individually in the same way.

For the purposes of this one-way sensitivity analysis, it has been assumed that the baseline value is the minimum possible value that a factor can take, and every time a factor moves it does so from its baseline (minimum) value to its maximum one. In this way the sole effect of every input factor on the model's output can be examined and recorded. Furthermore for the sake of this analysis and due to the structure of the formula (the changeable factors are multiplied by the static ones), it has been assumed that the static variables always take their maximum values.

The figure below contains all the discrete values that every factor within the SKM algorithm can take. So, for instance the range of the second factor (Vegetation Assessment) is (0, 1.5), although the *allowable values* are: *0, 0.1, 0.2, 0.3, 0.5, 1, and 1.5*. It is worth to mentioning that all the factors have a baseline (minimum) value of *0.00* expect for Drainage Assessment which has a minimum value of *-1.00*.

	Code	Assessment	*Min.*	Value	Value	Value	Value	Value	Value	*Max.*
Changeable factors	MA	Movement assessment	0.0	1.0	1.5	2.0	2.5	3.0	4.0	5.0
	VA	Vegetation Assessment	0.0	0.1	0.2	0.3	0.5	1.0		1.5
	SW	Surface Water Assessment	0.0	0.5	1.0	1.5	2.0	2.5		3.0
	DA	Drainage Assessment	-1.0	0.0	0.5	1.0				1.5
	BA	Burrowing Assessment	0.0	1.0						2.0
	CA	Construction Activity Assessment	0.0	1.0						2.0
Static factors	SHF	Slope Angle & Height Factor	0.0	1.0	2.0	3.0				4.0
	ALF	Adjacent Land Factor	0.0	1.0	1.5					2.0

Figure 5-2: SKMA input variables ranges

Results

Having applied Visual Basic in Excel and after running the one-way sensitivity analysis for every factor, we recorded the sole impact of every factor on the model's main outcome, which can be shown graphically in the form of a **tornado diagram**.

Figure 5-3: Results of one-way SKMA sensitivity analysis

Looking at this summary figure, it can be deduced that the factor with the highest sole impact on the output (taking no correlation effects into account) is Movement Assessment, followed by Surface Water Assessment. Construction Activity Assessment and Burrowing Assessment feature in third place, and Drainage and Vegetation Assessments have the lowest effect on the model's output. Finally, it is noticeable that because of the structure of the formula (multiplication of static and changeable variables) the impact of the two static variables is zero in this analysis.

5.5.5 Stage 2: Two-Way Sensitivity Analysis

Methodology

As previously discussed, the main limitation of the one-way sensitivity analysis is that it overlooks the potential correlations of the input factors and this might lead to misleading conclusions. Given that correlations between factors might seem very possible from the formula of LCAT algorithm (Section 5.5.2), a potential method that sometimes is used to account for correlations is to undertake **extreme two-way sensitivity analysis**, by varying *all except one* of the factors in the model to their 'best', 'average' and 'worst' case while simultaneously changing that one across its corresponding 'best', 'average' and 'worst' value.

To be more specific, since the higher the risk value the worse the situation for an asset, it has been assumed that the minimum value of a factor corresponds to the 'best' case, whereas that of maximum to the 'worst' (riskier) one.

Also, a comparison of all factors 'average' level, matrix 'midway' and 'median' has been done, which can be seen in Figure 5.4, where the last column contains the chosen 'average' value of every factor that will be needed in the second stage of the sensitivity analysis.

	Code	Assessment	Min.	Value	Value	Value	Value	Value	Value	Max.	Average	Midway	Median	Chosen
Changeable factors	MA	Movement assessment	0.0	1.0	1.5	2.0	2.5	3.0	4.0	5.0	2.4	2.5	2.25	2.5
	VA	Vegetation Assessment	0.0	0.1	0.2	0.3	0.5	1.0		1.5	0.5	0.75	0.3	0.5
	SW	Surface Water Assessment	0.0	0.5	1.0	1.5	2.0	2.5		3.0	1.5	1.5	1.5	1.5
	DA	Drainage Assessment	-1.0	0.0	0.5	1.0				1.5	0	1.25	0.5	0
	BA	Burrowing Assessment	0.0	1.0						2.0	0.75	1	1	1
	CA	Construction Activity Assessment	0.0	1.0						2.0	1.11	1	1	1
Static factors	SHF	Slope Angle & Height Factor	0.0	1.0	2.0	3.0				4.0	2	2	2	2
	ALF	Adjacent Land Factor	0.0	1.0	1.5					2.0	1	1	1.25	1

Figure 5-4: SKMA input variables ranges and statistics

Results

The number of potential different scenarios of the 8 interim factors which can be varied from their 'low' to 'average' and finally to their 'high' value while all the other remaining factors can be changed similarly are $8 \times 9 = 72$ (i.e. 9 scenarios for every of the 8 factors). This was designed and run in VBA.

If VBA were to be run in Excel to calculate the output of *all* the different potential combinations of the 8 factors which can take 'low', 'average' and 'high' values - this would be a huge solution space, with: $3^8 = 6{,}561$ scenarios. If VBA needs 0.5 seconds to calculate one scenario, it creates 120 scenarios per minute or it needs almost one hour to search the whole solution space. This computational time is not affordable for this small problem, therefore, by doing this extreme two-way sensitivity analysis, we significantly reduce the computational complexity of the problem from 6,561 different scenarios to a selection of 72 representative ones. The tables below contain the outputs of all these 72 scenarios.

Table 5.5: Results of multi-way sensitivity analysis

No.	Code	Adjusted Variable	Adjusted Variable Setting	Other Variables	Slope Risk Value	Differnce	Differnce	Effect of Variable	Final Effect
1	MA	Movement Assessment	Low	Low	0.00	2.50		5.00	5.48
2	MA	Movement Assessment	Medium	Low	2.50		2.50		
3	MA	Movement Assessment	High	Low	5.00				
4	MA	Movement Assessment	Low	Medium	5.20	2.60		5.85	
5	MA	Movement Assessment	Medium	Medium	7.80		3.25		
6	MA	Movement Assessment	High	Medium	11.05				
7	MA	Movement Assessment	Low	High	13.60	1.60		5.60	
8	MA	Movement Assessment	Medium	High	15.20		4.00		
9	MA	Movement Assessment	High	High	19.20				
10	VA	Vegetation Assessment	Low	Low	0.00	0.50		1.50	0.50
11	VA	Vegetation Assessment	Medium	Low	0.50		1.00		
12	VA	Vegetation Assessment	High	Low	1.50				
13	VA	Vegetation Assessment	Low	Medium	7.80	0.00		0.00	
14	VA	Vegetation Assessment	Medium	Medium	7.80		0.00		
15	VA	Vegetation Assessment	High	Medium	7.80				
16	VA	Vegetation Assessment	Low	High	19.20	0.00		0.00	
17	VA	Vegetation Assessment	Medium	High	19.20		0.00		
18	VA	Vegetation Assessment	High	High	19.20				
19	SW	Surface Water Assessment	Low	Low	0.00	1.50		3.00	3.10
20	SW	Surface Water Assessment	Medium	Low	1.50		1.50		
21	SW	Surface Water Assessment	High	Low	3.00				
22	SW	Surface Water Assessment	Low	Medium	5.85	1.95		3.90	
23	SW	Surface Water Assessment	Medium	Medium	7.80		1.95		
24	SW	Surface Water Assessment	High	Medium	9.75				
25	SW	Surface Water Assessment	Low	High	16.80	0.00		2.40	
26	SW	Surface Water Assessment	Medium	High	16.80		2.40		
27	SW	Surface Water Assessment	High	High	19.20				
28	DA	Drainage Assessment	Low	Low	0.00	0.00		1.50	0.50
29	DA	Drainage Assessment	Medium	Low	0.00		1.50		
30	DA	Drainage Assessment	High	Low	1.50				
31	DA	Drainage Assessment	Low	Medium	7.80	0.00		0.00	
32	DA	Drainage Assessment	Medium	Medium	7.80		0.00		
33	DA	Drainage Assessment	High	Medium	7.80				
34	DA	Drainage Assessment	Low	High	19.20	0.00		0.00	
35	DA	Drainage Assessment	Medium	High	19.20		0.00		
36	DA	Drainage Assessment	High	High	19.20				

Table 5.5: Results of multi-way sensitivity analysis (continued)

No.	Code	Adjusted Variable	Adjusted Variable Setting	Other Variables	Slope Risk Value	Differnce	Differnce	Effect of Variable	Final Effect
37	BA	Burrowing Assessment	Low	Low	0.00	1.00		2.00	2.60
38	BA	Burrowing Assessment	Medium	Low	1.00		1.00		
39	BA	Burrowing Assessment	High	Low	2.00				
40	BA	Burrowing Assessment	Low	Medium	6.50	1.30		2.60	
41	BA	Burrowing Assessment	Medium	Medium	7.80		1.30		
42	BA	Burrowing Assessment	High	Medium	9.10				
43	BA	Burrowing Assessment	Low	High	16.00	1.60		3.20	
44	BA	Burrowing Assessment	Medium	High	17.60		1.60		
45	BA	Burrowing Assessment	High	High	19.20				
46	CA	Construction Activity Assessment	Low	Low	0.00	1.00		2.00	2.60
47	CA	Construction Activity Assessment	Medium	Low	1.00		1.00		
48	CA	Construction Activity Assessment	High	Low	2.00				
49	CA	Construction Activity Assessment	Low	Medium	6.50	1.30		2.60	
50	CA	Construction Activity Assessment	Medium	Medium	7.80		1.30		
51	CA	Construction Activity Assessment	High	Medium	9.10				
52	CA	Construction Activity Assessment	Low	High	16.00	1.60		3.20	
53	CA	Construction Activity Assessment	Medium	High	17.60		1.60		
54	CA	Construction Activity Assessment	High	High	19.20				
55	SHF	Slope Angle & Height Factor	Low	Low	0.00	0.00		0.00	2.40
56	SHF	Slope Angle & Height Factor	Medium	Low	0.00		0.00		
57	SHF	Slope Angle & Height Factor	High	Low	0.00				
58	SHF	Slope Angle & Height Factor	Low	Medium	6.60	1.20		2.40	
59	SHF	Slope Angle & Height Factor	Medium	Medium	7.80		1.20		
60	SHF	Slope Angle & Height Factor	High	Medium	9.00				
61	SHF	Slope Angle & Height Factor	Low	High	14.40	2.40		4.80	
62	SHF	Slope Angle & Height Factor	Medium	High	16.80		2.40		
63	SHF	Slope Angle & Height Factor	High	High	19.20				
64	ALF	Adjacent Land Factor	Low	Low	0.00	0.00		0.00	1.20
65	ALF	Adjacent Land Factor	Medium	Low	0.00		0.00		
66	ALF	Adjacent Land Factor	High	Low	0.00				
67	ALF	Adjacent Land Factor	Low	Medium	7.20	0.60		1.20	
68	ALF	Adjacent Land Factor	Medium	Medium	7.80		0.60		
69	ALF	Adjacent Land Factor	High	Medium	8.40				
70	ALF	Adjacent Land Factor	Low	High	16.80	1.20		2.40	
71	ALF	Adjacent Land Factor	Medium	High	18.00		1.20		
72	ALF	Adjacent Land Factor	High	High	19.20				

Some noteworthy comments with respect to this table are the following:

- The table above presents all the scenarios that every factor can take based on the two-way sensitivity analysis and their corresponding risk value.
- The purpose of this table is to somehow quantify and simultaneously simplify the number of risk values of these factors. Initially each factor can take around 820 different risk values, and by doing this analysis the number is reduced to 9 (the sixth column of

table 5.5) and finally to 1 main risk value (the last column of table 5.5) which is taken as representative of the sensitivity of every factor.

- Columns 7 and 8 estimate the differences in the effect of every factor, step by step. Hence, it is possible to break down any potential interesting findings to its original source.
- The ninth column in table 5.5 depicts the way that the initial 9 risk values are simplified to the final one for every factor. Essentially, column 9 contains the main effect that a factor contributes to the model's output moving from the 'low' to the 'high' case, given that all the other factors are stable. Thus, the 9 scores are reduced to 3.
- Column 10, which contains the final score representing every factor, shows the average of the 3 previous scores from column 9.

5.5.6 Comparison of Stage 1 and Stage 2 Sensitivity Analysis Results

This section is devoted to a comparison of the results and a discussion of the findings provided by the "two-stage" sensitivity analysis methodology. Figure 5.5 compares the results of the two methods and summarizes the key features of this comparison.

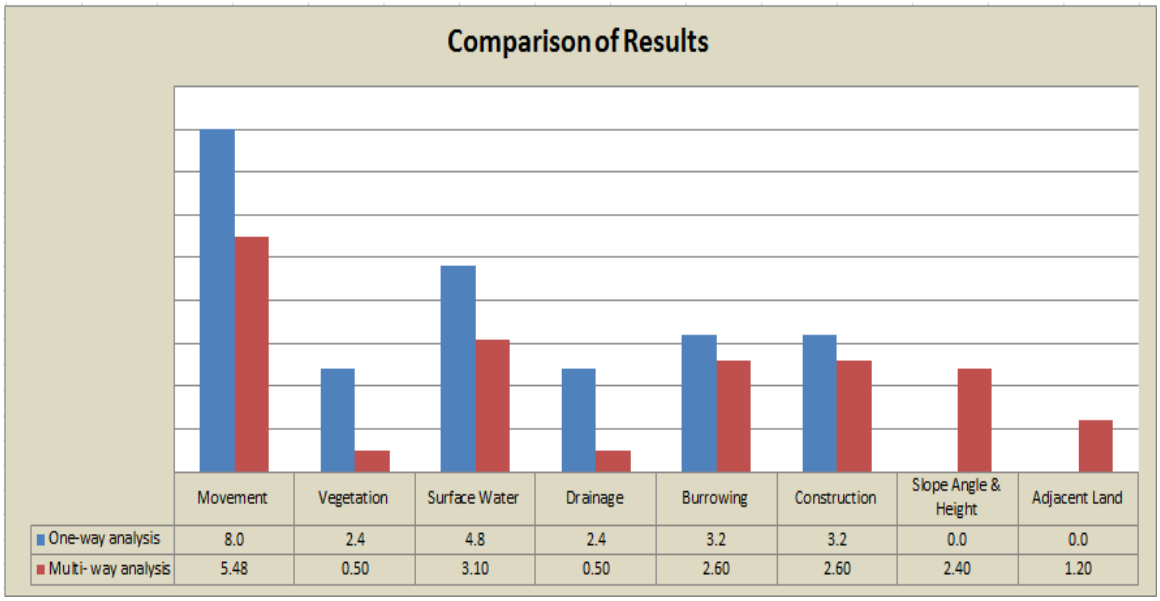

Figure 5-5: Comparison of two sensitivity analysis approaches

Various conclusions can be deduced from this figure and Table 5.5: The list below attempts to capture all of them:

***Key comments**:*

- First of all, looking at the results of the two analyses it can be concluded that the relative importance of every factor **remains stable**. That means that neither the relative impact of every factor on the final output nor the relative ranking among them changed. In other words, the two sensitivity analyses result in the **same trend** in terms of the sensitivity of the input factors.

- The proposing ranking of the factors in terms of their impact on the final output is as follows:

    1) Movement Assessment
    2) Surface Water Assessment
    3) Burrowing Assessment and Construction Activity Assessment
    4) Slope Angle & Height Factor
    5) Adjacent Land Factor
    6) Vegetation Assessment and Drainage Assessment

***Changeable factors**:*

- **Movement Assessment** seems to be the most sensitive factor with the highest impact in the model's output. Moreover, its impact on the final output is quite similar in all the three levels (Table 5.5).
- **Surface Water Assessment** is the second most sensitive factor; however it seems to be more important when all the others are at the 'average' level (Table 5.5).
- **Burrowing Assessment** and **Construction Activity Assessment** seem to be identical in their effect on the model's output. They have exactly the same contribution in all the levels of the analysis. Additionally, their effect is identically incremental from 'low' to 'high' level (Table 5.5).
- **Vegetation Assessment** and **Drainage Assessment** have the lowest impact on the current model. Furthermore, they seem to be almost identical, in terms of their impact. More specifically, their impact in the output is the same in all the scenarios except from one: Vegetation has a slightly negative impact when is moved from 'low' to 'average' value and the rest of the factors remain in the 'low' section; while drainage's impact remains as zero (Table 5.5).
- **Drainage Assessment** is the only factor which has a minimum value of *-1.00* whereas the majority have a minimum score of *0.00*. From Table 5.5, it is clear that the 'low' scenarios of drainage assessment have no different effect than that of the 'average' scenarios which deliberately have been assigned the value of *0.00*. Consequently, it is suggested that a replacement of the weighting of *-1.00* with *0.00* for Drainage Assessment – Low can be done without any risk of losing any information from the model. This is a logical statement coming from the structure of the formula that is applied in the algorithm; due to the max() function in the formula and the fact that the other variables take *0.00* as a minimum value, Drainage assessment's minimum value would never be activated.

***Static factors**:*

- **Slope Angle & Height Factor** and **Adjacent Land Factor** have no impact when all the other factors are in 'low' level. Again, this happens due to the structure of the formula which multiples the static variables with the changeable ones. However, they negatively contribute to the output in the 'average' and 'high' levels (Table 5.5).
- Lastly, **Slope Angle & Height Factor** compared to **Adjacent Land Factor** seems to have double impact in the model's output (Figure 5.4). This is again driven by the algorithm formula, where the score weightings for **Slope Angle & Height Factor** are twice those of the **Adjacent Land Factor.**

5.5.7 SKMA Sensitivity Analysis Conclusions

Summary of task process and objectives

- The scope of this task was to undertake a sensitivity analysis of the LCAT algorithm and ultimately provide an insight into the key drivers of LCAT's output. Initially, a one-way sensitivity analysis was implemented and the sole impact of every factor was recorded. In the second part, a more comprehensive two-ways sensitivity analysis was undertaken in order to examine potential correlated effects among the factors.

- The comparison and the findings of this two-stage approach show that both the two analyses return comparable results and follow the same trends and patterns. Accordingly, their proposed rankings, in terms of the impact of every factor, are the same, and this allows us to make substantive conclusions regarding the sensitivity of every factor.

Limitations and further improvements

- Further work might more thoroughly investigate the effects of the **correlated inputs**. Due to the high computational complexity of the problem, our two-stage analysis focused on changing one factor every time against the changes of all the other remaining ones. That means that although two parameters are changed every time, the way this takes place makes the difference, since one parameter is changed against the changes of all the others together. Thus, it could be beneficial if other sensitivity analysis approaches such as What-If analysis in Excel or Regression analysis are undertaken in multiple ways in order to examine these interconnections more holistically.

- Lastly, one final note has to do with the range of one static factor which seems not to be totally stable. Specifically, the Slope Angle & Height Factor has a **dynamic upper limit**, depending on the asset's specifications in terms of Geology. In fact, the maximum value of Slope Angle & Height Factor can utilise three values (3.0, 4.0, and 5.0) depending on the type of soil (Granular, Cohesive or Inter-bedded). Although, the sensitivity analysis was undertaken only for the Cohesive type (the middle one) slightly different results would be found if the analysis is done for the other two types of soil. However, we expect that the relative importance of the input variables would remain the same as outlined above.

5.6 Part I: Sensitivity analysis of SSHI Algorithm

5.6.1 Introduction and Objectives of Sensitivity Analysis

As previously discussed, sensitivity analysis allows the decision maker to determine which inputs (parameters) are the key drivers of a model's results. Sensitivity analysis can be useful for testing the Soil Slope Hazard Index (SSHI) algorithm in a range of scenarios, including:

- Testing the robustness of the output.
- Enforced understanding of the relationships between input and output.

- Reduced variation by identifying the most critical model inputs that cause significant variation in the output and should therefore be the focus of attention.
- Searching for errors in the model (by encountering unexpected or unintended relationships between inputs and outputs).
- Model simplification – identifying model inputs that have no effect on the output, so that redundant parts of the decision process may be removed.
- Finding regions in the space of input variables for which the output is either maximum or minimum or meets some optimum criterion (optimization procedures).

5.6.2 Background – Overview of SSHI Algorithm

The SSHI algorithm has been developed for Network Rail [1] to facilitate the rapid and repeatable inspection of rail earthworks (embankments and soil cuttings) and enables an impartial assessment of their condition. In other words, SSHI gives an indication of the geotechnical condition of an earthwork and its likelihood of failure.

Within Network Rail's cuttings SSHI algorithm there are thirty "Stability Index Parameters", each measuring a separate characteristic of slope in question. Each Stability Index Parameter features a number of sub- options called "Observed/ Measured Values", hereafter referred to as 'Input Parameters' (see the 179 parameters values and their scores in Appendix A of this document).

Each Input Parameter either features or does not feature for a particular slope, and when a slope undergoes a condition exam the presence or absence of every Input Parameter is assessed across all Stability Index Parameters.

The SSHI algorithm contains weighted scores for each Input Parameter in terms of the level of risk they are thought to contribute to each of the five defined failure modes Rotational, Translational, Earthflow, Washout and Burrowing. These collected Input Parameter scores are processed in a particular way to obtain a SSHI score for each failure mode; being a numeric score that sits between 2 and 16 corresponding to a high-level risk indicator for that failure mode.

With respect to the design of the SSHI algorithm, the objective was to assign appropriate scores to each of the Input Parameters and combine them in such a way to generate representative SSHI scores in order to inform the associated earthwork overall condition classification.

Briefly, the logic behind the SSHI algorithm is the following: the various Input Parameters are broken down into those that indicate actual failure, those that indicate potential future failure and those factors that could influence the magnitude of a slope failure (i.e. slope height).

The Soil Slope Hazard Index (SSHI) is derived **for each failure mode** by combining the two failure factors and the earthwork height in the following way:

$$(Actual\ failure\ score + Potential\ failure\ score) \times Height\ factor \qquad (5.8)$$

The earthworks' overall condition classification will be based on the failure mode producing the **highest** SSHI score. The highest (worst) SSHI score of the five failure modes is taken forward as the slope's overall score, and this is used to define the earthwork's overall condition classification, i.e. 'Poor', 'Marginal' or 'Serviceable'. For example, a 'Poor' overall

condition will result if at least one of the five major failure modes is present in the poor range of scores.

Notice that the multiplication effect of Height Factor creates a multiplicative (non-additive) model where **correlations between factors** play a role, and non-additively affect the final SSHI score.

The Actual failure factor and Potential failure factor are determined for each of the five failure modes by summing the scores for the relevant Input Parameters. The scores for each are then ranked as High, Medium or Low on the following basis:

Table 5.6: SSHI band scores for failure modes

Actual Failure Score	Ranking	Potential Failure Score
<30	Low	<45
30 – 69	Medium	45 – 69
>69	High	>69

The Earthworks Factor is determined based on the slope height as follows:

Table 5.7: SSHI Slope height and earthworks factor

Slope Height	Earthworks Factor
< 3 metres	Low
3 – 10 metres	Medium
> 10 metres	High

Based on the ranking of the three factors as High, Medium or Low, the following operation is carried out:

Table 5.8: SSHI failure modes bands and scores

Factor	High	Medium	Low	
Actual Failure Factor	6	3	1	**+**
Potential Failure Factor	4	2	1	
Earthworks Height Factor	1.6	1.3	1	**x**
				=SSHI

The two failure factors (actual and potential) are added together to obtain a score between 2 and 10. The greater weighting given to actual failure indicators reflects their greater importance compared to potential failure indicators. This sum is then *multiplied* by the Earthwork Factor to produce a Soil Slope Hazard Index (SSHI) ranging from 2 to 16. Limits have been set that define the earthwork condition as ‘Poor’, ‘Marginal’ or ‘Serviceable’, based on the outputs from these logic gates.

Settings and constraints

The choice of method of sensitivity analysis of the SSHI algorithm is restricted by a number of constraints, which includes the following main challenges:

- **Computational complexity:** Sensitivity analysis is almost always performed by running the model a large number of times (i.e. sampling-based approach in probabilistic theory). This can be a major constraint when:
  - A single run of the model takes a significant amount of time.
  - The solution space is vast. Sensitivity analysis is essentially the exploration of the multidimensional solution space, which grows exponentially in size with the number of inputs.

In our case, the solution space of the SSHI algorithm, (all the potential combinations of input values), is extremely large. More specifically, SSHI is loaded with 30 different initial factors categories, having 179 input parameters in total, and the combinations of all of them create a massive solution space of greater than 4.827×10^{21} different scenarios. Therefore, exploring the solution space is computationally extremely hard or impossible.

- **Correlated inputs:** Many sensitivity analysis methods assume independence between model inputs, but sometimes inputs can be strongly correlated, which means that interactions occur when the perturbation of two or more inputs simultaneously causes variation in the output greater than that of varying each of the inputs alone. Such interactions are presented in any model that is non-additive, however this is still an immature field of research where definitive methods have yet to be conclusively established. The SSHI algorithm is not an additive model, thus there are potentially some correlations between the factors which pose considerable obstacles in this analysis.

5.6.3 Stage 1 – Sensitivity Analysis of Input Parameters

Methodology

Despite the high computational complexity of the problem that severely inhibits us for examining the effect of all scenarios, the weighted score of every Input Parameter is known (see Appendix A), allowing us to analyse and compare them under different approaches.

In particular, from the formula 5.8 it can be deduced that the effect of every parameter in the SSHI is **additive** if the multiplicative effect of height factor is excluded.

As such, if the correlated effects of the parameters are not considered then the sensitivity analysis can be considered ‘additive’, where every factor contributes a specific, pre-defined score to the model’s output. Three different sensitivity analysis methods have been applied to compare this impact of every Input Parameter:

Accumulative method

The most straightforward form of sensitivity analysis is to sum the scores of all the 179 input parameters across all failure modes and compare them with the summation of the effect of the average of all the parameters. Thus, a relative impact ratio is created and a comparison of the sensitivity of input parameters can be undertaken.

Maximum method

Due to the fact that the final SSHI is derived by taking the highest SSHI score of the five failure mechanisms, an alternative approach is to calculate the maximum impact of all Input Parameters across the five failure modes and compare these scores with the average of the maximum scores across all parameters.

Proportional method

The last and most sophisticated approach transforms the score of every Input Parameter into a ratio relative to the threshold score of 'Medium' and 'High' Failure Factor bands, for actual and potential failure modes (Table 5.6).

More specifically, the deterioration score of every input factor is divided by the threshold value of each band and the subsequent ratio informs us about the "seniority" of this factor inside that particular band. Finally, a summation of these ratios across the five failure modes, having weighted by the bands by their Failure Factor Scores (Table 5.8), returns a cumulative relative score of importance of this factor across all failure modes and bands.

For instance, if an input parameter has a deterioration score of 60 for the burrowing actual failure mode, this will be assigned to a ratio of 60 / 30 = 200% for the 'Medium' band (as 30 is the cut-off for an Actual Failure Factor of 'Medium') and 60 / 70= 85.7% for the 'High' band (as 70 is the cut-off for an Actual Failure Factor of 'High'). This means that this parameter in that failure mode has a deterioration value which is 200% higher than the threshold value for the 'Medium' band and slightly less (85.7%) than the threshold value of the 'High' band. Then, these two scores are weighted by the corresponding band scores (in this case the deterioration scores belongs to the actual failure modes, so the weights would be 3 and 6 respectively; see Table 5.8) and the final relative score is produced in the following way:

$$200\% \times 3 + 85.7\% \times 6 = 1{,}114.2\%$$

The main advantage of this method is that every deterioration score is broken down to its component parts, and the following are accounted for:

- The likelihood that an Input Parameter will push a failure mode factor over a boundary to a higher score
- The relative importance (weightings) of each of the various actual and potential failure mode factors

Finally, note that this sensitivity analysis has assessed the algorithm in isolation: no consideration is made of which input parameters are likely to occur (or not) in real life.

Results

This section is devoted to an analysis of the findings and a discussion of the results provided by the different approaches. There are two major parts in this section.

Firstly, the results of the main sensitivity analysis of the input parameters are introduced, analysed and categorized, and in the second part details about a high level sensitivity analysis of the five failure modes is presented.

A classification of the 179 input parameters has been implemented with respect to their sensitivity level and their corresponding impact on the model's output. Depending on their sensitivity, the input parameters have been split in four separate categories: 'highly

sensitive', 'sensitive', 'moderately sensitive' and 'low sensitive', creating a 4-tier analysis. Below, an explanation of the corresponding selection criteria is presented:

Tier 1: Highly sensitive input parameters

This first category comprises the most sensitive and significant input parameters that have the highest deterioration impact on the model's output. The selection criterion for this band is as follows:

Table 5.9: SSHI highly sensitive selection criterion

Sensitivity analysis method	Cut-off ratio	Selection criterion
Accumulative method's score	> 150%	Fulfilled ***all*** cut-off ratios
Maximum method's score	> 150%	
Proportional method's score	> 750%	

Consequently, all input parameters whose score met all the three cut-off ratios have been categorized as 'highly sensitive'.

Tier 2: Sensitive input parameters

The second category includes slightly lower sensitive factors (compared with tier-1) in terms of their effect on the model's output, but still very important. The selection criterion for this band is as follows:

Table 5.10: SSHI sensitive selection criterion

Sensitivity analysis method	Cut-off ratio	Selection criterion
Accumulative method's score	> 150%	Fulfilled ***any 2 of the 3*** cut-off ratios
Maximum method's score	> 150%	
Proportional method's score	> 750%	

Accordingly, all the input parameters that their score fulfilled any two of the previous three cut-off ratios have been classified as 'sensitive' parameters.

Tier 3: Moderately sensitive input parameters

This third input parameters category contains the moderately significant input parameters that in general have a medium deterioration impact on the model's output. The selection criterion for this band is as follows:

Table 5.11: SSHI moderately sensitive selection criterion

Sensitivity analysis method	Cut-off ratio	Selection criterion
Accumulative method's score	> 150%	Fulfilled ***any 1 of the 3*** cut-off ratios
Maximum method's score	> 150%	
Proportional method's score	> 750%	

Similarly, the input parameters whose scores met only one of the three cut-of values have been categorized as 'moderately sensitive'.

Tier 4: Low sensitive input parameters

The last category comprises all the remaining input parameters which do not meet any of the previous three criteria and can be characterized as 'low sensitive' or even insignificant (have zero effect on model's output) for the sensitivity analysis's purposes.

The figures below illustrate the 4-tier analysis of the input parameters and their corresponding sensitivity levels. For the sake of simplicity, only the first three categories are presented, since they are of most interest.

Tier 1: Highly sensitive input parameters

The below two figures inform us that based on these three analyses, 15 input parameters meet the minimum requirements of the 'highly sensitive' category and seem to play the most determinant role in the model's output (Figure 5.6). The parent categories of these factors are: *Slope Angle and Slope Height, Retaining Walls, Slope erosion, Slope form, Track Movements, Cracking, History of Instability, Burrows.*

Row	Code	Accumulative method's score	Accumulative method's ratio	Maximum method's score	Maximum method's	Proportional method's ratio	Cut-off value 1	Cut-off value 2	Cut-off value 3
4	A4	145	496.80%	50	339.59%	**1473.02%**	TRUE	TRUE	TRUE
8	A8	145	496.80%	50	339.59%	**1473.02%**	TRUE	TRUE	TRUE
12	A12	145	496.80%	50	339.59%	**1473.02%**	TRUE	TRUE	TRUE
21	C5	70	188.11%	35	207.71%	**1300.00%**	TRUE	TRUE	TRUE
22	C6	70	188.11%	35	207.71%	**1300.00%**	TRUE	TRUE	TRUE
116	S1	70	188.11%	70	515.42%	**1300.00%**	TRUE	TRUE	TRUE
131	U6	75	208.69%	30	163.75%	**1392.86%**	TRUE	TRUE	TRUE
135	W1	140	476.22%	70	515.42%	**2600.00%**	TRUE	TRUE	TRUE
151	Y6	75	208.69%	40	251.67%	**1392.86%**	TRUE	TRUE	TRUE
152	Y7	80	229.27%	45	295.63%	**1485.71%**	TRUE	TRUE	TRUE
153	Y8	100	311.59%	50	339.59%	**1857.14%**	TRUE	TRUE	TRUE
161	AA2	70	188.11%	35	207.71%	**1300.00%**	TRUE	TRUE	TRUE
162	AA3	300	1134.77%	70	515.42%	**5571.43%**	TRUE	TRUE	TRUE
171	CC4	75	208.69%	55	383.55%	**1224.60%**	TRUE	TRUE	TRUE
172	CC5	90	270.43%	60	427.50%	**1419.05%**	TRUE	TRUE	TRUE

Figure 5-6: SSHI highly sensitive parameters

Row	Code	Input parameter description	Input parameter description	Parent category
4	A4	>35 degrees, <3m High	Slope Angle and Slope Height	Slope Geometry
8	A8	>35 degrees, 3m to <10m High		
12	A12	>35 degrees, >10m High		
21	C5	Cracking / evidence of lateral displacements	Retaining walls 1m high or greater	
22	C6	Evidence of Repairs		
116	S1	Multiple – well defined	Slope erosion	Associated Drainage
131	U6	Stepped Crest	Slope form of Earthwork	Movement Indicators (Overall Failure)
135	W1	Track Heave	Track Movements (vis. to naked eye)	
151	Y6	10 to 50 >30	Cracking	
152	Y7	>50 <30		
153	Y8	>50 >30		
161	AA2	No Remediation - Presence of piezometers, slip indicator tubes / inclinometers	History of instability	
162	AA3	Regular maintenance required		
171	CC4	Frequent Rabbit (>10 burrow holes /20m2)	Burrows	Animal Activity
172	CC5	Frequent Fox / Badger (>3 burrow holes /50m2)		

Figure 5-7: SSHI highly sensitive parent categories

Tier 2: Sensitive input parameters

With respect to Tier-2, the two figures below tell us that 9 input parameters meet the minimum requirements of the 'sensitive' factors. These factors can be assumed to have a medium impact on the SSHI score. It is worth mentioning that most of these parent categories (Figure 5.9) are similar to those in tier-1 (Figure 5.7), although the observed / measured values which correspond to the actual Input Parameters are different.

Row	Code	Accumulative method's score	Accumulative method's ratio	Maximum method's score	Maximum method's	Proportional method's ratio	Cut-off value 1	Cut-off value 2	Cut-off value 3
3	A3	75	208.69%	25	119.79%	**761.90%**	TRUE	FALSE	TRUE
7	A7	75	208.69%	25	119.79%	**761.90%**	TRUE	FALSE	TRUE
11	A11	75	208.69%	25	119.79%	**761.90%**	TRUE	FALSE	TRUE
129	U4	65	167.53%	25	119.79%	**1207.14%**	TRUE	FALSE	TRUE
149	Y4	50	105.79%	30	163.75%	**928.57%**	FALSE	TRUE	TRUE
150	Y5	55	126.37%	30	163.75%	**1021.43%**	FALSE	TRUE	TRUE
158	Z5	60	146.95%	60	427.50%	**1114.29%**	FALSE	TRUE	TRUE
159	Z6	60	146.95%	60	427.50%	**1114.29%**	FALSE	TRUE	TRUE
170	CC3	50	105.79%	30	163.75%	**760.32%**	FALSE	TRUE	TRUE

Figure 5-8: SSHI sensitive parameters

Row	Code	Input parameter description	Input parameter description	Parent category
3	A3	25 to <35 degrees, <3m High	Slope Angle and Slope Height	Slope Geometry
7	A7	25 to <35 degrees, 3m to <10m High		
11	A11	25 to <35 degrees, >10m High		
129	U4	Toe bulging	Slope form of Earthwork	Movement Indicators (Overall Failure)
149	Y4	<10 >30	Cracking	
150	Y5	10 to 50 <30		
158	Z5	Translational Failure	Mass movements	
159	Z6	Rotational failure		
170	CC3	Occasional Fox / Badger (<3 burrow holes /50m2)	Burrows	Animal Activity

Figure 5-9: SSHI sensitive parent categories

Tier 3: Low sensitive input parameters

Similarly, Figures 5.10 and 5.11 tell us that 9 Input Parameters meet the minimum requirements of the 'Low sensitive' factors. These factors can be seen as some of the least significant in terms of their impact on the output of SSHI.

Row	Code	Accumulative method's score	Accumulative method's ratio	Maximum method's score	Maximum method's	Proportional method's ratio	Cut-off value 1	Cut-off value 2	Cut-off value 3
75	J5	66	171.65%	24	111.00%	**670.48%**	TRUE	FALSE	FALSE
76	J6	62	155.19%	20	75.83%	**629.84%**	TRUE	FALSE	FALSE
57	H3	51	109.91%	30	163.75%	**518.10%**	FALSE	TRUE	FALSE
65	I3	51	109.91%	30	163.75%	**518.10%**	FALSE	TRUE	FALSE
117	S2	30	23.48%	30	163.75%	**557.14%**	FALSE	TRUE	FALSE
118	S3	30	23.48%	30	163.75%	**557.14%**	FALSE	TRUE	FALSE
132	V1	60	146.95%	30	163.75%	**609.52%**	FALSE	TRUE	FALSE
155	Z2	37	52.29%	30	163.75%	**687.14%**	FALSE	TRUE	FALSE
157	Z4	40	64.64%	30	163.75%	**742.86%**	FALSE	TRUE	FALSE

Figure 5-10: SSHI low sensitive parameters

Row	Code	Input parameter description	Input parameter description	Parent category
75	J5	Surface issues on lower slope	Slope face drainage conditions	Associated Drainage
76	J6	Surface issues on upper slope		
57	H3	Fine granular / Ash	Predominant Material Type	Slope Composition at Crest
65	I3	Fine granular / Ash		
117	S2	Multiple – poorly defined	Slope erosion	Associated Drainage
118	S3	Single – well defined		
132	V1	Deep-seated landslips	Geomorphology of Adjacent Land	Movement Indicators (Overall Failure)
155	Z2	Slope wash	Mass movements	
157	Z4	Local slumping at slope face		

Figure 5-11: SSHI low sensitive parent categories

Chart

The last segment of the results section plots all the data in a graph, in order to facilitate the visualisation of the significance of every factor discussed in Section 5.6.3.

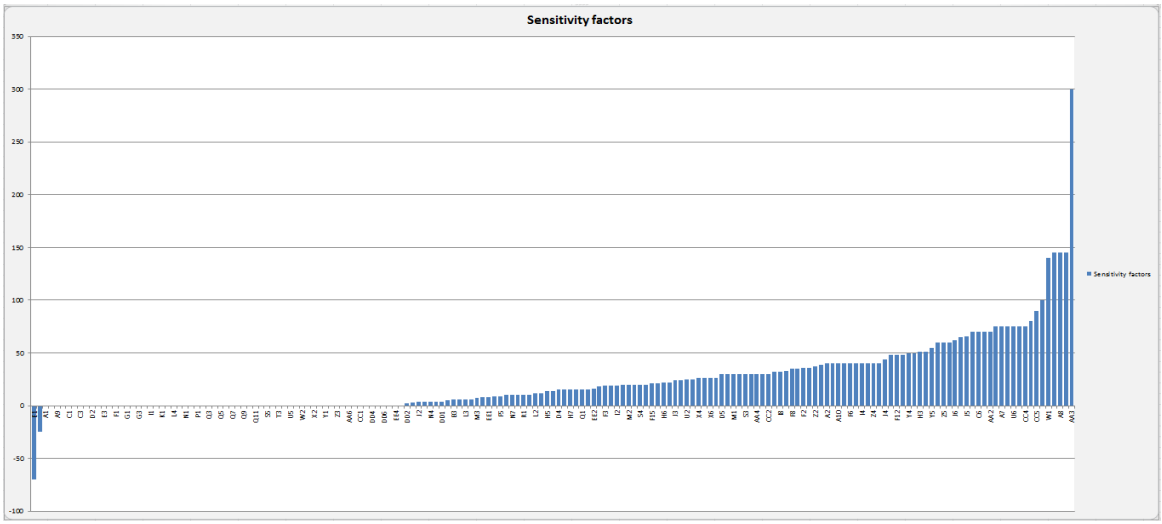

Figure 5-12: SSHI ranking of input parameters scores

In short, Figure 5.12 illustrates a ranking of all the 179 input parameters, beginning from those with the least negative impact (less significant) on the model's output, to those with the worst effect on score (most significant).

The method applied in order to create this chart was to allocate the **higher** (worse) of the accumulative and maximum method's scores to every input parameter; hence every input parameter was characterized by one score:

$$MAX\ (Accummulative\ mothd's\ score, Maximum\ method's\ score) \quad (5.9)$$

Looking at this chart, there are some noteworthy observations:

- There are two factors with **positive** scores (E1, E2). That means that instead of indicating increased risk for the condition of an asset, these factors actually help in lowering the Soil Slope Hazard Index (SSHI) of the asset.
- There are 62 factors (i.e. almost 1/3 of the total) that have no impact on the model's output. More precisely, they have a zero contribution to an asset's condition. Accordingly, there are 5 factors with very high negative effect and 1 factor that seems a clear **outlier** with an extremely huge negative impact. These frequencies distributions can be seen on the Table 5.12 and Figure 5.13, below:

Table 5.12: SSHI distribution of risk scores

Risk Score	Frequencies
<0	2
0	62
0-50	86
50-100	23
100-150	5
>150	1
Total	**179**

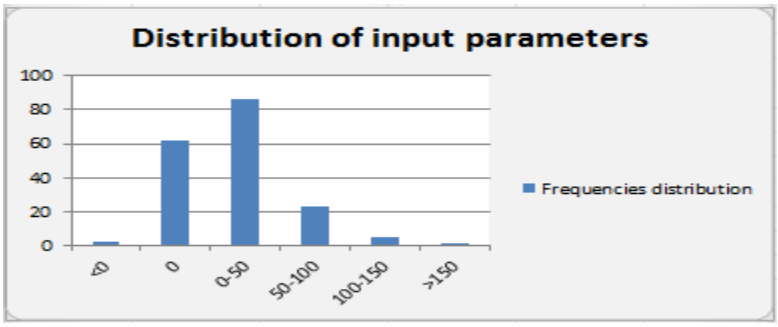

Figure 5-13: SSHI distribution of risk scores

5.6.4 Stage 2 – Sensitivity Analysis of Failure Modes

This section contains a generic sensitivity analysis of the 5 failure modes of the SSHI Algorithm. The approach that was adopted was to sum the deterioration scores of all the 179 Input Factors across the 5 failure modes, including separation of their Actual/ Potential effects. Some notable findings can be seen in the table below:

Table 5.13: SSHI total deterioration of failure modes

	ACTUAL FAILURE					POTENTIAL FAILURE				
	ROTATIONAL	TRANSLATIONAL	EARTHFLOW	WASHOUT	BURROWING	ROTATIONAL	TRANSLATIONAL	EARTHFLOW	WASHOUT	BURROWING
TOTAL DETERIORATION	649	589	261	260	90	587	621	455	479	263
TOTALS	1,849					2,405				
PERCENTAGES	35%	32%	14%	14%	5%	24%	26%	19%	20%	11%

Figure 5.14 demonstrates that in general the potential failure mode is more significant to the model's output (as 2,405 represents 57% of the total scores for actual and potential combined) than the actual (as 1,849 represents 43% of the total scores for actual and potential combined).

This is particularly interesting as it demonstrates this algorithm has a slight movement towards future performance.

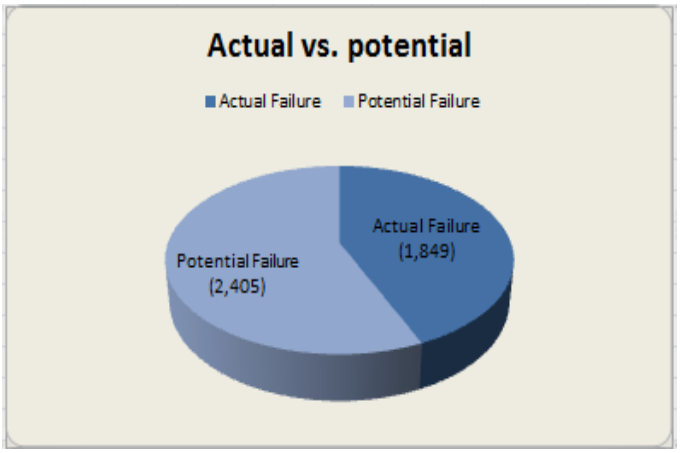

Figure 5-14: SSHI actual vs. potential failure modes

Figures 5.15 and 5.16 break down the total deterioration scores per failure category. Figure 5.15 contains the absolute values of the contribution scores of every failure mode and Figure 5.16 their corresponding percentages.

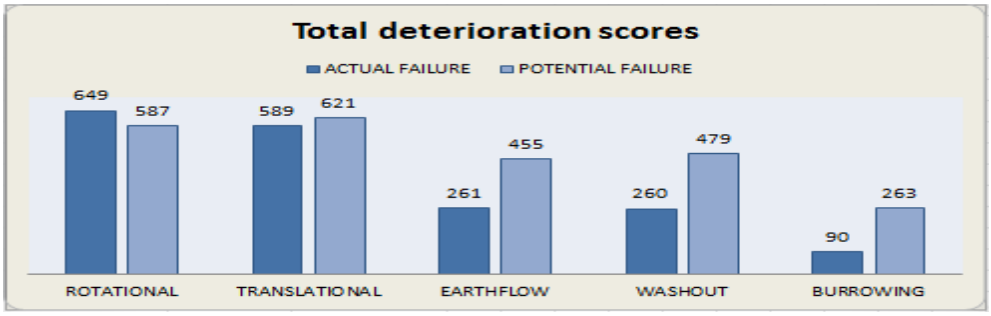

Figure 5-15: SSHI actual vs. potential total deterioration

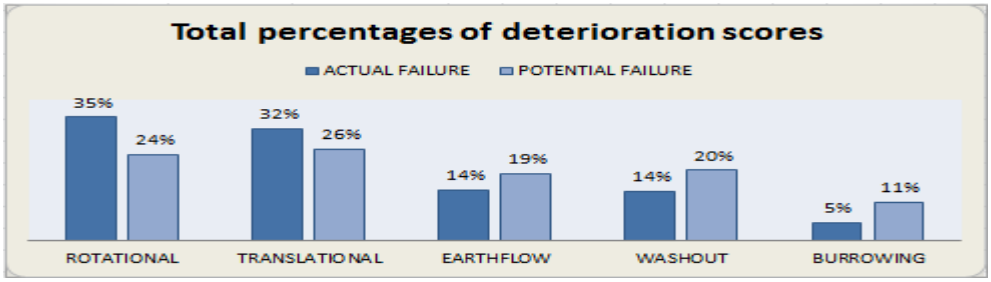

Figure 5-16: SSHI actual vs. potential percentages

In summary, some general comments about the sensitivity analysis of the failure modes are:

- Potential failure is higher scoring than actual failure (Figure 5.14).
- Under every analysis, burrowing seems to be the least important failure category.
- With respect to the Actual failure type, there is a clear order across the 5 failure categories: Rotational (35%) and Translational (32%) are in the first place, followed by Earthflow (14%) and Washout (14%) and Burrowing (5%) is in the last place (Table 5.13).
- Regarding the potential mode, there is not such a strict difference across the modes (expect for Burrowing), perhaps because these refer to the chance of failures in the future and there is a lot of more uncertainty compared to the present (Table 5.13).

5.6.5 Stage 3 – Sensitivity Analysis of Height Factor

The purpose of this section is to illustrate the high impact of Input Parameters describing slope height, since our earlier sensitivity analysis did not account for this multiplicative effect in order to simplify the SSHI score formula and create an additive model.

This “outstanding” impact of height factor can be demonstrated by the following table, where, the ‘best’ and ‘worst’ case SSHI score of every height factor has been calculated. More specifically, Table 5.14 contains all 12 height input parameters (i.e. A1 - A12), their multiplicative effect in the score (i.e. earthwork factor column) and the corresponding ‘best’ and ‘worst’ SSHI scores given the combinations of the remaining Stability Index Parameters. A ‘best’ SSHI score for one input parameter has been defined if only its presence score is switched on and nothing else, whereas a ‘worst’ case SSHI score has been defined where all the remaining Input Parameters are also switched on (maximum effect).

Table 5.14: SSHI height factor impact

STABILITY INDICATORS FOR SOIL CUTTINGS	STABILITY INDEX PARAMETER	OBSERVED/MEASURED VALUE	REF CUT	EARTHWORKS FACTOR	EARTHWORKS EFFECT	BEST CASE SSHI SCORE	WORST CASE SSHI SCORE
Slope Geometry	Slope Angle and Slope Height	<15 degrees, <3m High	A1	L	1	*2.00*	*10.00*
		15 to <25 degrees, <3m High	A2	L	1	*2.00*	*10.00*
		25 to <35 degrees, <3m High	A3	L	1	*2.00*	*10.00*
		>35 degrees, <3m High	A4	L	1	*3.00*	*10.00*
		<15 degrees, 3m to <10m High	A5	M	1.3	*2.60*	*13.00*
		15 to <25 degrees 3m to <10m High	A6	M	1.3	*2.60*	*13.00*
		25 to <35 degrees, 3m to <10m High	A7	M	1.3	*2.60*	*13.00*
		>35 degrees, 3m to <10m High	A8	M	1.3	*3.90*	*13.00*
		<15 degrees, >10m High	A9	H	1.6	*3.20*	*16.00*
		15 to <25 degrees, >10m High	A10	H	1.6	*3.20*	*16.00*
		25 to <35 degrees, >10m High	A11	H	1.6	*3.20*	*16.00*
		>35 degrees, >10m High	A12	H	1.6	*4.80*	*16.00*

We can see from this that the Slope Angle and Height Input Factor, specifically the component of height, is highly critical in generating the overall SSHI Score. For example a low slope (<3m) can never go above a score of 10, and a high slope (<10m) can never go below a score of 3.2.

5.6.6 SSHI Sensitivity Analysis Conclusions

Summary of task process and objectives

The scope of this task was to undertake a sensitivity analysis of the SSHI algorithm and ultimately provide an insight of the key drivers of SSHI's output.

Initially, due to the high computational complexity of the problem, the idea of running the model multiple times was excluded as a feasible approach and a simplification of the algorithm's formula (5.8) was attempted in order to "dismiss" the multiplicative effects of the height factor creating an additive model, where **no correlated effects** in the input parameters are included. Correlated effects exist when the perturbation of two or more inputs simultaneously causes variation in the output greater than that of varying each of the inputs alone.

Consequently, this modification allows us to exclude these unpredictable multiplicative effects and come up with comparable results which demonstrate that *Slope Angle and Slope Height, Retaining Walls, Slope erosion, Slope form, Track Movements, Cracking, History of*

Instability and Burrows are the most sensitive parent factors of SSHI Algorithm (Section 5.6.3).

Limitations and further improvements

Further work might identify more efficient ways of handling the huge computational complexity of the problem, more thoroughly investigating the impact of **correlated inputs** and more specifically the multiplicative effects of height factor.

Possible ideas might include the application of a deliberate **screening method** (in order to reduce the huge solution space) and a running of multiple extreme scenarios with fewer parameters; in this way height factor can be incorporated in the model, or the employment of meta-models.

Notwithstanding that, it seems unlikely from the results that this would change the conclusions of this sensitivity analysis substantially, since it has been already identified that height factor plays a fundamental and conclusive role in the model's output.

5.7 Part I: Comparison of Results of SKMA and SSHI Sensitivity Analyses

This section reflects on the sensitivity analysis of SKMA and SSHI, discusses its major findings and attempts to shed light on the mutual and different characteristics of these two algorithms.

First of all, due to the special nature of the algorithms, different sensitivity analysis methods have been applied, making the direct comparison of the results impossible. Nonetheless, the findings and the methodologies are still relatively comparable to each other and the most critical conclusions can be listed below:

- SSHI is a more detailed, holistic, geographically specific (in the UK) algorithm that aims to quantify a huge amount of information captured by 179 parameters in an exhaustive way. The effort to collect such a level of information can be considerably demanding and expensive as well as the way that the information is stored and analysed can dramatically increase the complexity of the tool.
- SKMA is intended to serve the broader audience of rail infrastructure managers across Europe. It was designed to incorporate a subset of the SSHI input parameters, more specifically 47 out of the 179 factors, but it was intentionally kept as simple and comprehensive as possible. Also, in terms of the model's practicality and usefulness, it is much easier for rail infrastructure managers to collect data for 8 rather than 30 different attributes.

Therefore, these two algorithms are not the same; even though there is a clear connection and overlapping, their mechanisms and scope are significantly different. This is underpinned by the results of the sensitivity analysis which are not perfectly lined up. Below, is the list of the most critical attributes of these tools, as identified by the sensitivity analysis:

Level of significance	SKMA Input Parameters	SSHI Input Parameters
1	Movement Assessment	Slope Angle & Height Factor
2	Surface Water Assessment	Retaining Walls > 1m
3	Burrowing Assessment	Associate Drainage
4	Construction Activity Assessment	Movement Indicators
5	Slope Angle & Height Factor	Burrows
6	Adjacent Land Factor	Material Type
7	Vegetation Assessment	-

Figure 5-17: SSHI and SKMA comparison of sensitivity analyses results

As can be demonstrated by the above mentioned table, the order of significance of the key factors of these two algorithms varies significantly. For example, SSHI gives extra attention to the static characteristics of the slope such as the Slope Angle & Height, whereas, SKMA outweighs changeable factors such as the Movement assessments.

Moreover, there are critical factors that appear only in one of the two lists or that are similar but not exactly identical such as the retaining walls in SSHI or the adjacent land factor in SKMA.

To sum up, the sensitivity analyses highly recommend that although there are some commonalities between SSHI and SKMA, they are essentially different by nature, having different mechanisms and weighting of factors.

5.8 Part I: Validation of SKMA Algorithm as a Tool for scoring Risk

5.8.1 Method of SKM Algorithm Validation

It can be sensibly argued that since the SKMA condition scoring system for soil cuttings is intended to operate on a very similar basis as Network Rail's SSHI algorithm (coupled with the fact that it is in many ways a simplified version of SSHI) a validation process can be undertaken by processing SSHI examination data, producing SKMA-equivalent scores and assessing their correlation between SKMA scores and SSHI scores via statistical analysis.

This has been done, and the following two sections demonstrate the two steps of this correlation exercise:

a) Conversion of SSHI examination data to SKMA scores
b) Correlation of results through statistical analysis (regression analysis)

5.8.2 Conversion of SSHI to SKMA scores

Scope of the process:

The first step of this correlation exercise is to convert the SSHI data to SKMA scores. This process involves a transformation of the SSHI data (from “text” to “binary” format) and a mapping exercise to line up that data to create SKMA equivalent scores.

The entire conversion process has been conducted in a Microsoft Access 2007 database via a series of around 100 queries which reference the eight years of Network Rail SSHI data.

However, the detailed field transformations have not been described here (the information is too extensive) but these have been tabulated and are available from the MAINLINE partners if required. Nonetheless, a high level description is given below and specific details of the conversion steps are provided in Appendix A of this report.

Data transformation process

From the latest inspections of earthworks condition in 2012, NR was able to provide data for 68,108 sections of soil cutting slopes, each approximately a 100-metre (5-chain) section of the side of a cutting being a separate slope record.

This information has been stored in what NR calls “065 databases”. More specifically, information about the SSHI parameters was found in three different places in the 065 database. The main source of data has been kept in a “parent” table, and that data is coupled with some more detailed information about movement factors which have been stored in “child” tables.

The transformation process is made complex by the structure of the SSHI data (information in different tables), nonetheless assumptions and processing steps can be put in place to overcome such problems. The following section is a high level description of the steps that were followed:

Step 1: Process of data that exists only in the parent table

- Queries were run to Group by the fields of all SSHI input parameters and all the unique combinations were summarised.
- For each SSHI parameter, summary tables were created from these.
- Queries were run to combine the summary tables with the parent one, transforming the SSHI input parameters from text format into binary format.
- Finally, all these queries were put together to bring results into one table.

Step 2: Process of data that exist in the parent and child tables

- Likewise, Group By queries were run to summarise the fields of all SSHI movement parameters and get all the unique combinations in one place.
- For each of the four SSHI movement indicators, summary tables were created.
- Queries were run to consolidate the “Items” and “Observed” values of the tables. A maximum criterion assumption was applied to ensure that information is not missed. The initial four tables were then consolidated

- Then, a UNION query was run to combine the results from the last two summary tables.
- Finally, a series of UPDATE queries were run to replace nulls with zero in the parent and children tables.

Step 3: Data integration

- Having processed all the SSHI parameters, queries were run to put the scores from the parent and child tables together.

Step 4: Data cleansing

In order to ensure that the data that would be carried forward to the statistical analysis was correct, accurate and complete, some potentially suspicious records had to be removed by a series of queries. Some of the reasons for dropping out records are the following:

- Duplicate IDs
- Incomplete and inaccurate data
  - "Not inspected" features in the SSHI input parameters
  - "Not inspected" features in the failure modes
  - "Bulk populated" data which have not feasible SSHI scores
- Inconsistent data
  - Data that exists in the parent table but not in the child ones.
  - Data that is not present in the parent but exists in the child tables.

Table 5.15 summarises how many records were removed from each of the data cleansing queries:

Table 5.15: Conversion of SSHI to SKMA data

	Number of records
Number of starting records	**68,108**
Duplicate IDs	36
"Not inspected" features in the SSHI A parameter	13,591
"Bulk populated" data with no feasible SSHI scores	14,990
"Not inspected" features in the failure modes	47,569
"Not inspected" features in the rest of SSHI input parameters	51,000
Data that exist in all tables	44,781
Total number of clean records	**40,451**

5.8.3 Statistical Analysis of Results

Introduction

Having transformed, cleansed and mapped the historical data of the SSHI algorithm into SKMA scores, a correlation exercise has been undertaken to validate the SKMA algorithm with real data and ascertain the level of confidence that can be associated with the model predictions from a statistical point of view.

SSHI and SKMA scores were compared and analysed using statistical analysis methodologies and their results were visualized by employing data visualisation techniques.

This section consists of two main parts. In the first place a correlation coefficient was applied in the two data sets, followed by a more comprehensive linear regression model. Lastly, data visualisation techniques were employed to illustrate the results.

Correlation coefficient

In statistics, the Pearson correlation coefficient (r or ρ) is a measure of the strength of the relationship between pairs of variables. It gives the linear correlation (dependence) between two variables *X* and *Y*, giving a value between +1 and −1 inclusive, where 1 is total positive correlation, 0 is no correlation, and −1 is total negative correlation. For a population, Pearson's correlation coefficient between two variables is defined as the covariance of the two variables divided by the product of their standard deviations [3].

$$\rho_{X,Y} = \frac{COV(X,Y)}{\sigma_X \sigma_Y} = \frac{E[(X-\mu_X)(Y-\mu_Y)}{\sigma_X \sigma_Y} \quad (5.10)$$

Where, COV is the covariance, σ_X is the standard deviation of X, μ_X is the mean of X, and E is the expected mean [3,7].

The correlation coefficient ranges from −1 to 1. A value of 1 implies that a linear equation describes the relationship between *X* and *Y* perfectly, with all data points lying on a line for which *Y* increases as *X* increases. A value of −1 implies that all data points lie on a line for which *Y* decreases as *X* increases. A value of 0 implies that there is no linear correlation between the variables. More generally, note that $(X_i - X)(Y_i - Y)$ is positive if and only if X_i and Y_i lie on the same side of their respective means. Thus the correlation coefficient is positive if X_i and Y_i tend to be simultaneously greater than, or simultaneously less than, their respective means. The correlation coefficient is negative if X_i and Y_i tend to lie on opposite sides of their respective means [3,7,8].

Subsequently, a correlation coefficient has been calculated in Microsoft Excel by applying the formula above and it was found that the correlation coefficient between SKMA and SSHI scores is 0.5.

$$\rho_{SSHI,SKMA} = 0.5 \quad (5.11)$$

In simple terms, that means that there is **a moderate positive linear relationship** between SKMA and SSHI scores. A scatter plot of the SKMA and SSHI scores and their relationship can be visualised below:

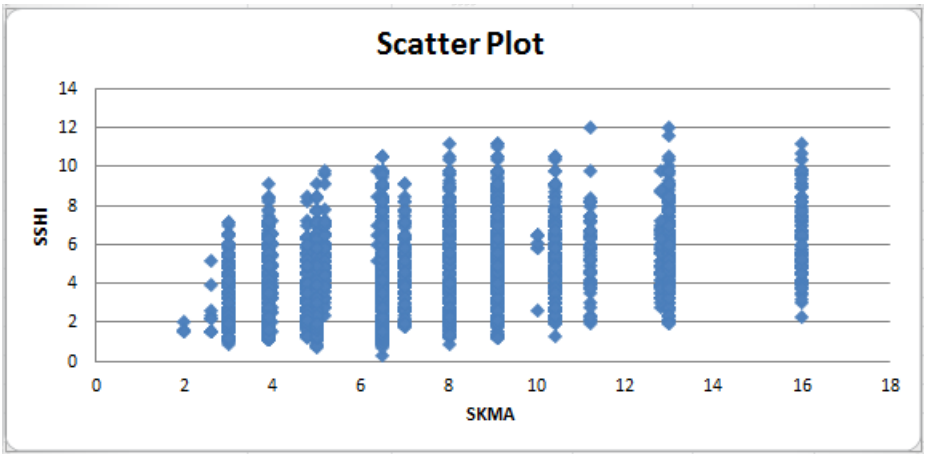

Figure 5-18: SKMA and SSHI scatter plot

Simple linear regression

In statistics, simple linear regression analysis is a multivariate technique that can be used to analyze the relationship between a single outcome (dependent, explained) variable and one predictor (independent, explanatory) variable (If we have two or more predictor variables then we have multiple regression). This functional relationship may then be formally stated as an equation, with associated statistical values that describe how well this equation fits the data. An example of this equation is presented below [3]:

$$Y = a + b * X + e \quad (5.12)$$

Where, Y is the output variable, X is the predictor, a is the constant term (intercept), b the regression coefficient and e is the error term (residual).

The method of the least squares is applied to estimate a dependent variable. In simple words, simple linear regression fits a straight line through a set of n points in such a way that makes the sum of squared residuals of the model (that is, vertical distances between the points of the data set and the fitted line) as small as possible [2].

The least squares principle leads to a formula for b:

$$b = \frac{\sum_1^n (x - \bar{x})(y - \overline{y})}{\sum_1^n (x - \bar{x})^2} \quad (5.13)$$

and for a:

$$a = \bar{y} - b * \bar{y} \quad (5.14)$$

Moreover, the regression model should follow some assumptions about the error term e [3,7]:

- It has a normal distribution with a mean of 0.
- The variance of the error term is constant across cases and independent of the variables in the model (homoscedasticity).
- The value of the error term for a given case is independent of the values of the variables in the model and of the values of the error term for other cases (white noise).

Finally, the relationship of measured phenomenon should be linear.

A linear regression model was built and run in Microsoft Excel and the key outputs are summarized below:

Table 5.16: SKMA linear regression statistics

Regression Statistics	
Multiple R	*0.5*
R Square	*25%*
Adjusted R Square	*25%*
Standard Error	*1.36*
Observations	*40,451*

Table 5.17: SKMA analysis of variance (ANOVA)

ANOVA	*df*	*SS*	*MS*	*F*	*Significance F*
Regression	1	24,926.92	24,926.92	13,481.90	0
Residual	40,449	74,786.85	1.85		
Total	40,450	99,713.77			

Table 5.18: SKMA regression coefficients

	Coefficients	*Standard Error*	*t Stat*	*P-value*	*Lower 95%*	*Upper 95%*
Intercept	1.14	0.02	57.02	0	1.11	1.18
X Variable	0.38	0	116.11	0	0.38	0.39

Looking at the summary output in Table 5.18, the regression equation would be as follows:

$$Y = 1.14 + 0.38X \quad (5.15)$$

Furthermore, a graph of the errors (residuals) and the regression's fitted line as well as how well this line fits to the real data are depicted below:

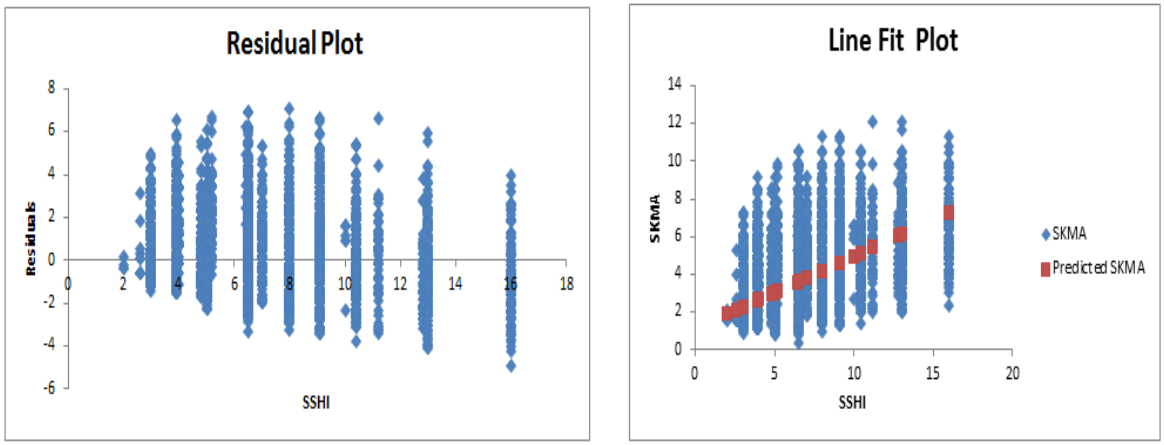

Figure 5-19: SKMA linear regression output

From a statistical standpoint [7], there are a lot of complex statistical issues that are worth mentioning, mainly about the underlying assumptions and the results. However, for the sake of simplicity, extensive reporting of all the regression's features has not been discussed in this deliverable. Hence, although there are different ways of assessing the success of this regression (ANOVA, R^2, b coefficient t-test, confidence intervals of coefficients) this report will focus only in the assessment of the coefficient of determination, R^2 [9].

In statistics [3,10], the coefficient of determination, R^2 measures the percentage of total variation that has been explained by the regression and it is a statistic that will give some information about the goodness of fit of a model. It measures how well the regression line approximates the real data points and in the case of a simple linear regression, the R^2 is simply the square of the correlation coefficient between the outcome and their predicted value that was calculated in the previous section.

In our example, the R^2 is 25%, which means *that 25% of the SKMA scores fall within the fitted regression line or that the model explains the 25% of the total variance of the SKMA scores*. Clearly, a coefficient of determination of 25% seems to tell us that the model is not well-fitted and captures only 25% of the total variability.

Nevertheless, from the summary output, the F statistic [2,3,10], which informs us about the statistical significance of the model, is very high (F= 13,481.90) meaning that the model is statistically valid, inefficient though to capture the variability of the dependant variable (SKMA scores). That might be due to a plethora of different reasons which mainly focus on the assumptions of the model. Some of them are listed below [3]:

- The relationship of the model might not be linear
- The error term might not follow a normal distribution with a mean of 0.
- The variance of the error term is not constant across cases and independent of the variables in the model (heteroscedasticity).
- The value of the error term for a given case is not totally independent of the values of the variables in the model and of the values of the error term for other cases (no white noise).

Taking into account the summary output and the correlation coefficient of the previous section, it can be concluded that all the previous assumptions are not met in our model. That indicates that there are patterns in the dataset that the fitted regression model cannot

capture, even though data transformation and rescaling techniques are applied (e.g. logarithm transformation of SKMA dataset) [3].

Once again, it should be stressed that this is not due to flaws in the model but due to the differences in inherent characteristics between SSHI and SKMA. Digging deeper in understanding why the correlation of SKMA and SSHI scores is not very high, we should remind ourselves that the SKM Algorithm was designed to encompass only a subset of the SSHI input parameters, intending to provide a simplified but sustainable tool to rail infrastructure operators around Europe, and that the form of the algorithm calculations are quite different.

5.8.4 Conclusion of Validation of SKM Algorithm

To conclude with, a validation of the SKM Algorithm was undertaken by statistically analysing the correlation of its output with that of the SSHI counterparts. From a statistical standpoint, the findings highly recommend that the correlation between SKMA and SSHI scores is moderately positive.

This is due to the fact that the two algorithms are quite different to each other. There are patterns in the SSHI dataset that the SKM Algorithm cannot incorporate since the former is an extensive, very detailed, geographically specific tool, whereas, the latter has been designed to be a more basic, high level analytical process for rail infrastructure managers across Europe.

5.8.5 Visualisation of Results

Data visualisation helps to communicate complex technical information clearly and effectively through graphical means. Hence, these techniques have been employed to convey the complex ideas and conclusions of the previous section to a non-technical audience and demonstrate in an intuitive way that the results of the validation of the SKM Algorithm through the SSHI dataset are moderately positive.

Heat map

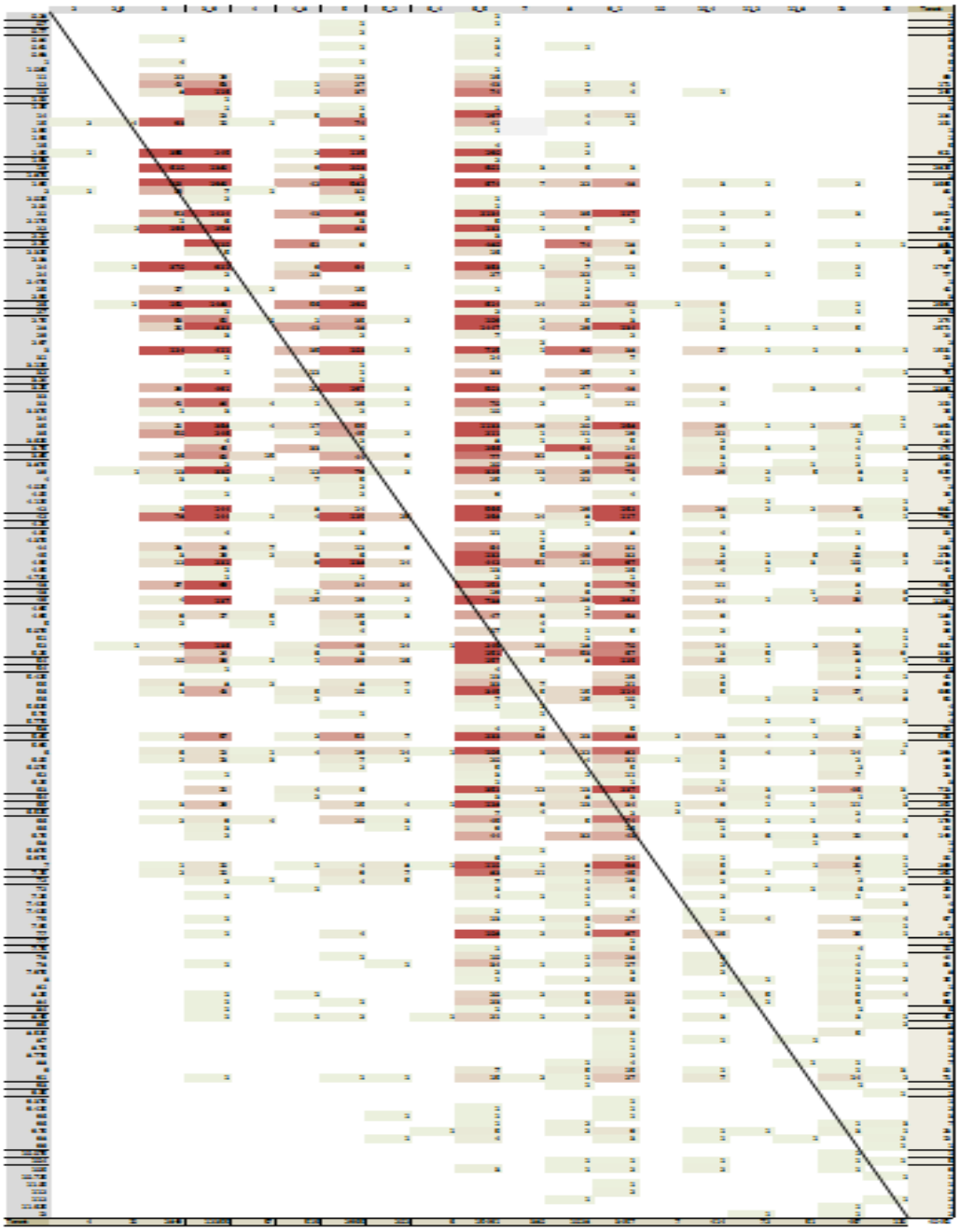

Figure 5-20: Visualisation of correlation results through heat map

The first visualisation technique employed is a heat map. The heat map is a summary table that restructures and aggregates data in a matrix format and helps the user to see the data from different perspectives.

The table headings show the range of the SSHI scores, whereas, their SKMA counterparts are in the rows. Inside the matrix, the count of the records for every possible pair of SSHI and SKMA scores are presented and their frequency is highlighted by colours.

Looking at this heat map, it can be concluded that there is not always a consistent, clear trend in the selection of the pairs of SSHI and SKMA scores. This indicates a moderate correlation between them. In other words, the spread of the combinations does not fall on the diagonal straight line (perfect correlation), but follows a more random path.

Bubble chart

An alternative way to visualize this conclusion is a bubble chart which displays three dimensions of data. In our example, the horizontal x axis represents the SSHI scores, the vertical y axis the corresponding SKMA ones and the size of the bubbles the frequency (magnitude) of every potential combination (pair) of scores.

Likewise in that bubble chart, there is not a clear trend and bubbles often do not fall within or close to the straight line (perfect correlation) which indicates perfect linear correlation.

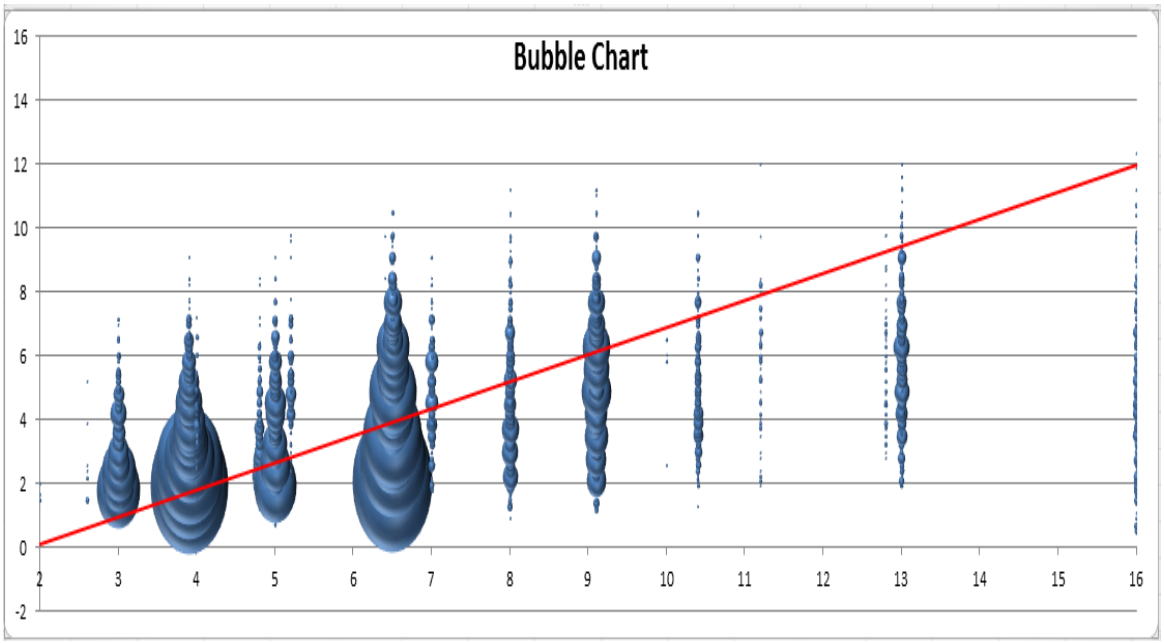

Figure 5-21: Visualisation of correlation results through bubble chart

5.9 Part II: Validation of Performance Profiles

5.9.1 Method

The second part of the validation exercise discusses the validation of the theoretical deterioration performance profiles through past data and case studies.

In this section, typical outputs of the Soil Cuttings LCAT (performance profiles) are compared with a sample of 30 real soil cuttings from NR for which detailed inspections have been undertaken in the past.

This process involves a thorough review and a qualitative analysis of the condition of these 31 sample assets against the deterioration profiles quantified in D2.3, if they are fed into the SKM Algorithm. It is worth mentioning that deterioration profiles have been produced for

every one of the six changeable factors (SKM Assessments) of the SKM Algorithm, so this analysis discusses their validity against real inspection data separately.

The next section provides the output of that qualitative analysis and conclusions regarding the validity of the D2.3 theoretical performance profiles.

5.9.2 Output from qualitative analysis and Conclusions

The conclusions of the SKM geotechnical review for the validation of the deterioration performance profiles through past data are split across each of the SKM Assessments changeable factor categories and are presented below:

Movement Assessment (MA)

Results are typically inconsistent with performance profiles.

- Properly documented remediation

These observations highlight a need for the proper documentation of improvements to cuttings, whereby the cutting condition should be reassessed at some time following the remediation works. The time against performance profile should be reset to zero years following the assessment of a remediated cutting.

- Development of movement

A track may heave or slump. In any case, the track is distorted. Typically, slumping of inter-bedded cuttings occurs due to washing out of fines, and heave of cohesive cuttings occurs due to a change in moisture conditions. The observations highlight a need to consider the mechanism causing the track misalignment, particularly when considering appropriate remediation strategies. In both inter-bedded and cohesive cuttings, erratic changes in MA were observed over the 5 years:

  - Inter-bedded cuttings: it is seen that the onset of movement can lead to a rapid decline in condition. This may be associated with inclement weather conditions.
  - Cohesive cuttings: it is seen that the change in MA coincides with a large increase in the Vegetation Assessment (VA) category. The trees are reported as having grown from saplings to mature trees, leading to greater slope loading and a change in moisture conditions.

This highlights a need to consider the interaction between elements affecting slope movements i.e. the observed onset of minor movements and presence of semi-mature trees at the crest or upper two-thirds of the slope face could be an indicator for a significant increase in MA over the 5 year period. The positioning of mature trees should be recorded [toe, lower third, upper two-thirds, crest], as they can have a stabilising and destabilising impact.

A significant decline in condition is not observed when considering granular cuttings. Only a minor increase in MA was observed at one location. This coincides with a change in recorded cutting geology from granular to inter-bedded.

- Frost

In regions prone to significant rainfall and freezing temperatures, freeze-thaw processes can result in greater rates of degradation of slopes or in track movements. The rainfall and temperature variation across regions may therefore need to be considered.

- Catastrophic events

The closure of railways due to cutting failure tends to be observed during and following catastrophic events, such as major rainfall events and seismic tremors. Catastrophic events cannot be accounted for during the assessment and will interrupt any attempt to predict cutting degradation.

Vegetation Assessment (VA)

Results are typically inconsistent with performance profiles, but some alignment is observed for granular and cohesive cuttings. Vegetation can have a stabilising and destabilising impact; this depends on various attributes, including root structure, position on the slope and forces applied to the slope.

Grasses and shrubs that grow upon slopes are considered to act favourably by restraining shallow particles, intercepting rainfall and drawing water out of the ground. Trees, on the other hands, can have a stabilising and destabilising impact. Destabilising forces arise from the self-weight of the trees and moment forces in the ground from wind acting at an unfavourable position on the slope i.e. above the bottom third of the slope face. It would therefore be appropriate to record the typical diameter and position of trees on slopes.

The performance profiles show a steep increase in VA over the first 10 years. This may be accurate in the case of saplings growing into mature trees upon the slope, but misleading if the vegetation is trees at the toe of the slope or a thick covering of grass and shrubbery.

Surface Water Assessment (SWA)

Results are typically inconsistent with performance profiles, but some alignment is observed for granular and inter-bedded embankments. Consider including ponding at crest and on the slope face.

Inter-bedded cuttings show gradual to erratic changes in surface water occurring over the 5 year period. The erratic changes are seen to coincide with significant changes in Burrowing Activity (BA).

Drainage Assessment (DA)

Results are typically inconsistent with performance profiles. Clarification needed on difference between DA1 and DA6.

Burrowing Assessment (BA)

Results are typically inconsistent with performance profiles.

Construction Activity Assessment (CA)

Results are inconsistent with performance profiles.

It is proposed that construction activity should not be modelled using the proposed approach. The likelihood of construction activity will increase with increasing MA and construction work will take place over a short period and will be of a finite extent. Moreover, the presence of construction activity is likely to be something that can be controlled by the infrastructure manager, rather than something that is likely to trigger at some point in the future due to “deterioration”.

5.10 Revised Performance Profiles

5.10.1 Requirement for Revised Performance Profiles

Part of the scope of D2.4 is to test and improve the deterioration performance profiles that were derived from soil cuttings data and described in documents D2.2 [5] and D2.3 [6].

By running and validating the LCAT soil cuttings model, some non-sensible deterioration performance scores for movement and drainage input parameters were noticed. As such, a revised deterioration analysis was undertaken to validate the accuracy of deterioration performance scores for these factors.

The following sections refer to the methodology of the revised performance profiles, demonstrate its results and conclude on the differences of probabilistic and deterministic degradation modelling approaches.

5.10.2 Method of Deriving Revised Performance Profiles

The deterioration rates that were derived here as well as in D2.3 [6] are entirely based on slope condition data from eight years of examinations by Network Rail (UK). Similar to the D2.3 conversion process [6], this condition data has been processed to provide the revised changes in the condition scores of the movement and drainage factors over a five-year period.

The entire revised conversion process has been conducted in a Microsoft Access 2007 database via a series of more than 100 queries and in Microsoft Excel spreadsheets via VBA code (see Appendix A) which reference the eight years of Network Rail SSHI data; identifying repeat examinations (paired examinations) and transforming their characteristics into SKMA scores.

The detailed field transformations within this data analysis have not been described here, since the information is too extensive; these have been tabulated and are available from the MAINLINE project team, if required. Nonetheless, a high level guide of the conversion method undertaken is presented below:

Conversion Steps of Revised Performance Profiles

1) **Base data:** SSHI condition data from the previous eight years was gathered and accumulated in one common place. Data cleansing techniques were employed to remove problematic records containing untrustworthy data such as duplicates or null values and formulate the base data for the analysis.

2) **Paired examinations:** Base data was checked for paired examinations over the past eight years. The change in the deterioration scores of movement and drainage indicators were processed and calculated. Slopes without at least one paired examination in the previous eight years were discarded from the analysis.

3) **Gap analysis:** The paired examinations were typically separated by a time interval of between about one and five years. The change in scores over this interval in each case was calculated and then linearly extrapolated to the change in 5 years (normalization of data based on a five-year period). Paired examinations that had negative score movements (i.e. showing improvement rather than deterioration) or changes in an interval less than six months were discarded from the analysis.

4) **Starting score:** This data was stratified by the initial score from which is started, so that typically for each possible initial score value a number of projected scores after five years were established.

5) **Soil type:** This data was stratified by soil type. The soil type of each slope was categorized as granular, cohesive or inter-bedded. In some cases the same slope was recorded as a different soil type in different examinations; in these cases the soil type was assumed to be inter-bedded. This classification resulted in 2,058 granular, 2,270 cohesive and 15,997 inter-bedded slopes.

6) **Mean score:** The resulting dataset gave the weighted mean change in score, classified by:

a. soil type (three possible types)
b. starting score (2 to 7 depending on the variable)
c. Score variable (movement or drainage)

7) **Gap analysis:** The final step of this process was to implement some final substitutions of results (gap filling), where this revised analysis found data to be missing, or where the results looked non sensible.

5.10.3 Results – Revised Performance Profiles

The tables below show the results of the revised deterioration analysis. Yellow indicates where a revision of the scores was implemented.

Starting values of each of the six scores (Inputs) and the expected values for the change in score after five years are presented. The changes in scores are classified by soil type; cohesive, granular and inter-bedded and shown separately (3 tables). The first table sets out all the starting scores.

Inputs					
MA	VA	SW	DA	BA	CA
Movement Assessment	Vegetation Assessment	Surface Water Assessment	Drainage Assessment	Burrowing Assessment	Construction Activity Assessment
0.0	0.0	0.0	-1.0	0.0	0.0
1.0	0.2	1.0	0.0	1.0	1.0
1.5	0.3	1.5	0.5	2.0	2.0
2.0	0.5	2.0	1.5	-	-
2.5	1.0	2.5	-	-	-
4.0	1.5	3.0	-	-	-
5.0	-	-	-	-	-

1 Cohesive					
MA	VA	SW	DA	BA	CA
Movement Assessment	Vegetation Assessment	Surface Water Assessment	Drainage Assessment	Burrowing Assessment	Construction Activity Assessment
0.11	0.48	0.69	0.12	0.57	0.05
0.88	0.49	0.64	0.12	0.42	0.00
1.09	0.79	0.63	0.08	0.00	0.00
0.91	0.81	0.79	0.00		
0.04	0.03	0.22			
0.04	0.00	0.00			
0.00					

2 Granular					
MA	VA	SW	DA	BA	CA
Movement Assessment	Vegetation Assessment	Surface Water Assessment	Drainage Assessment	Burrowing Assessment	Construction Activity Assessment
0.07	0.32	0.27	0.12	0.49	0.05
1.02	0.27	0.55	0.12	0.39	0.03
1.15	0.57	0.62	0.12	0.00	0.00
0.20	0.30	0.32	0.00		
0.08	0.03	0.12			
0.08	0.00	0.00			
0.00					

3 Inter-bedded					
MA	VA	SW	DA	BA	CA
Movement Assessment	Vegetation Assessment	Surface Water Assessment	Drainage Assessment	Burrowing Assessment	Construction Activity Assessment
0.20	0.73	0.71	0.22	0.47	0.10
1.74	0.50	0.71	0.22	0.53	0.04
0.98	1.25	0.78	0.13	0.00	0.00
1.08	1.56	0.99	0.00		
0.12	0.05	0.15			
0.12	0.00	0.00			
0.00					

Figure 5-22: Revised deterioration performance profiles

5.10.4 Conclusions Regarding Assumptions and Uncertainty

Probabilistic and Deterministic Modelling Approaches

Once a condition scoring system (i.e. SKMA) has been built, it is possible to undertake deterioration modelling by observing and predicting how the defined condition scores change over time (LCAT models). The modelling approach adopted might be deterministic or probabilistic.

A deterministic approach will always lead to the same outcome given the same set of inputs; having full knowledge of the inputs, it will say with 100% certainty what the outcome will be. Alternatively, a probabilistic process incorporates uncertainty in the inputs which lead to a set of possible outcomes occurring; instead of one definitive answer.

There are benefits and limitations to each of these deterioration modelling approaches, which pose a challenge in selecting the most appropriate technique. Intuitively, it would be better to describe everything in a deterministic way as knowing the outcome with 100% certainty is more practical and useful than simply knowing a set of probabilities. However, in practice many of the processes that are important in the subject of asset management involve risk and it is usually difficult to inform completely and accurately describe them with a deterministic forecast without taking into account the inherent uncertainty of the behaviour of the assets. Earthworks are a good example of assets that – though they can look very similar, and feature the same combinations of input parameters – they can behave very differently over time, due to detailed differences that are hard to identify from a basic data collection process (for example a condition scoring based on slope features like SSHI and SKMA).

Limitations of the Deterioration Modelling Approach

This section refers to some limitations of the deterioration modelling approach used. Even though the probabilistic deterioration modelling approach would deal with risk and the complexities surrounding the processes involved, due to some limitations of the project (e.g.

simplicity of the LCAT model and ease of output interpretation) a deterministic approach has been chosen; for more information the reader is encouraged to reference the D2.2 final report [5].

As discussed above, the main assumption of the modelling approach is that it ignores stochasticity; it assumes single values for the input parameters (deterioration profiles) instead of a range of probabilities. It attempts to forecast how the overall condition score will change over a defined period of time, based on one definite set of input parameters rather than a range of parameters.

The histogram below illustrates the limitations of this assumption and demonstrates the importance of stochasticity in an earthworks model, based on the SSHI examination data received from Network Rail and used to generate the revised MA and DA deterioration rates presented here.

This frequency distribution shows the observed score change between pairs of exams. More specifically, the distribution demonstrates the changes between pairs of exams for the movement (MA) variable that start from a score of one on their first exam. That variance in the distribution indicates that the change in the movement score can take different values (uncertainty) and averaging them might be a severe assumption.

MA_Change	CountOfPair
-1.0	2641
0.0	627
0.5	15
1.0	252
1.5	30
2.0	143
4.0	1

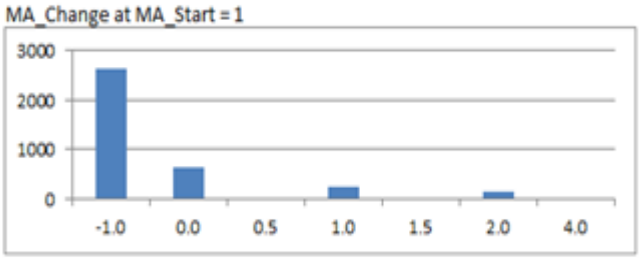

Figure 5-23: Limitations of a deterministic deterioration modelling approach (1)

Furthermore, the matrix above supports the previous comment about the variability of the scores: There are 627 observed cases that movement score remained unchanged during the 5 years period, 15 cases that the movement score deteriorates from 1.0 goes to 1.5 (by 0.5) and so on.

It is worth noticing that there is a large number of occurrences that are negative (2,641 cases); these represent assets that are improving over time. It might be expected there to be some of these (Network Rail are spending some money doing maintenance work to improve condition of the assets), but there is a huge number of cases that make the data a bit untrustworthy. Consequently, the analysis of the scores did not incorporate that negative changes.

Instead of getting a weighted average as the input variable of the model, a probabilistic model would get a set of probabilities and give back a range of possible input values such as the following matrix:

Table 5.19: A matrix from probabilistic deterioration modelling approach

MA_Change	CountOfPair	Probability of occurrence
-1.0	2,641	71.2%
0.0	627	16.9%
0.5	15	0.4%
1.0	252	6.8%
1.5	30	0.8%
2.0	143	3.9%
4.0	1	0.0%
Total	3,709	-

Likewise, the next histogram exhibits the distributions of the changes of the drainage variable starting from zero score. That variance in the distribution indicates that the change in the score of drainage can be a wide range of different numbers, and that averaging them might be a severe assumption.

DA_Change	CountOfPair
0	5,207
1	660
1	697

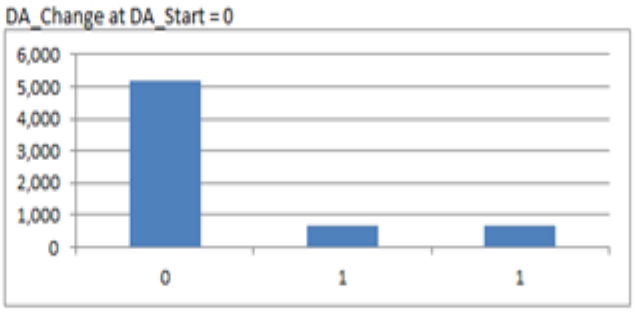

Figure 5-24: Limitations of deterministic modelling approach (2)

In conclusion, taking the above into consideration it is clear that there is a lot of uncertainty surrounding the input values for deterioration; simply taking a single weighted average is a big assumption that might lead to a wrong decision making process.

Therefore, intervention plans and financial outputs of the soil cuttings LCAT model should be treated only as indicative of a general cuttings life cycle cost in the future, and not as definitely valid results for a particular asset.

5.11 Conclusions

This chapter discussed the development of a validation exercise to test the derived deterioration performance profiles as well as the developed SKM Algorithm (SKMA). The purpose of this work was to scrutinise the methods adopted in previous tasks, compare theoretical profiles to real data as well as to validate the SKMA Algorithm with other tools and, hence, to ascertain the level of confidence that can be associated with model predictions.

The chapter splits in two parts: The first part provided the details of the comparison of SKMA and SSHI through sensitivity and statistical analyses and concludes that SKMA has a

moderate *correlation* with SSHI, mainly because it was deliberately designed to do so. The second part continued with the validation of the deterioration profiles through comparison with real data and a geotechnical desk study and concluded that deterioration performance profiles are in most of the cases **inconsistent** with real data.

5.12 References

[1] Babtie Group (2003), Development of the Soil Slope Hazard Index and Associated Algorithm, Network Rail

[2] Bechhofer, R.E., T. J. Santner and D. Goldsman (1995), "*Design and Analysis of Experiments for Statistical Selection, Screening and Multiple Comparisons*". John Wiley & Sons, New York.

[3] Daniel and Terrell (1995), Business Statistics for Management and Economics, 7th Edition, Houghton Miffilin.

[4] MAINLINE (2012), Deliverable 2.1 – Degradation and performance specification for selected assets

[5] MAINLINE (2012), Deliverable 2.2 – Degradation and intervention modelling techniques

[6] MAINLINE (2013), Deliverable 2.3 – Time-variant performance profiles for LCC and LCA

[7] Çetinkaya-Rundel M. (2014), Data Analysis and Statistical Inference, [PowerPoint slides], Retrieved from: < https://my.coursera.org>, Duke University, [Accessed 22 March 2014]

[8] Saltelli, A., Terry, A., et al. (2008), Global Sensitivity Analysis: Sensitivity Analysis in Practise, Willey

[9] Zhang, W. (2012), Business Statistics, [PowerPoint slides], Retrieved from: < https://my.wbs.ac.uk>, Warwick Business School, [Accessed 18 February 2014]

[10] Zhang, W. (2013), Advanced Data Analysis, [PowerPoint slides], Retrieved from: < https://my.wbs.ac.uk>, Warwick Business School, [Accessed 11 March 2014]

6. Metallic Bridges (Surrey, COWI, NR, Jacobs/SKM)

6.1 Outline of D2.3 Performance Profiles for Metallic Bridges

D2.3 [9] presented the methodology for determining performance profiles of metallic railway bridges subject to deterioration and degradation due to corrosion. This methodology combines coating and corrosion damage, presented in D2.2 [8], with structural behaviour and methods of analysis.

Coating deterioration and steel corrosion (following the loss of protection provided by the coating) are time-dependent processes, with their rates being determined by the exposure conditions experienced by the bridge. Furthermore, D2.3 [9] classifies outdoor corrosivity categories C1, C2, C3, C4, C5, CX and coating systems M27.4, M21 (as per Network Rail's standard classifications).

Based on academic research [8,9], it was concluded that the atmospheric corrosion model follows the relationship:

$$C(t) = At^B \qquad (6.1)$$

Where $C(t)$ is the uniform (measured as average over relatively small specimen surface areas) thickness loss (mm) after an exposure period of t years and coefficients A (mm/year) and B are empirical constants, obtained using regression analysis on physical test results grouped according to different atmospheric exposure conditions.

The time-dependent coating performance is modelled using information available in Network Rail standards where a range of expected life (T_L) values are provided for a number of coatings used in the UK [9].

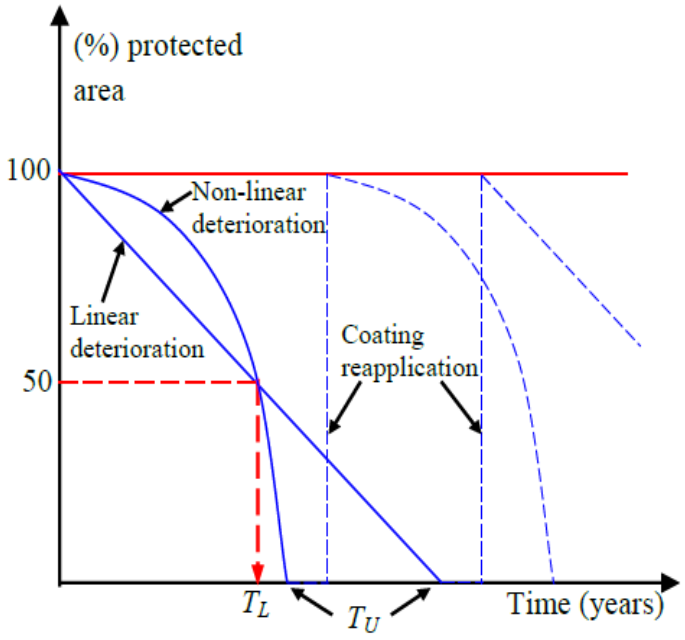

Figure 6-1: Deterioration model for coating system

A simple polynomial model (Equation 6.1) is developed, based on the assumption that 50% of the coated steel area will become unprotected at time T_L,

$$\frac{A_{pr}(t)}{A_{pr0}} = 1 - \left(\frac{0.6t^2}{T_L^2} - \frac{0.1t}{T_L}\right) \qquad (6.2)$$

Where $A_{pr}(t)$ and A_{pr0} are the residual and initial protected area (mm^2), respectively and t is the time in years.

These have been combined to develop coating / thickness loss models. which have been coupled with structural resistance models to obtain performance ratios for different element types.

The last element of the bridges' section in D2.3 [9] illustrates a case study where performance profiles were presented for a typical short-span railway bridge. Various Analysis cases tested are shown in the table below:

Table 6.1: Analysis cases for the external main girder of the examined bridge

Name	Yield Str (MPa)	Coating		Corrosion model	
		Coating type	Service life, TL (yrs)	Coefficient A (mm)	Coefficient B
EGC2NCu	300	No coating	-	0.025	0.575
EGC2M274u	300	M27.4	7	0.025	0.575

EGC2M21u	300	M21	22	0.025	0.575
EGC5NCu	300	No coating	-	0.2	0.575
EGC5M274u	300	M27.4	5	0.2	0.575
EGC5M21u	300	M21	18	0.2	0.575

6.2 Field Validation of Performance Profiles for Metallic Bridges through case studies

6.2.1 General

Estimation of a number of variables is needed when establishing or validating performance profiles for coated metallic bridges. Many of these parameters are needed regardless if it is an existing bridge or a new bridge.

Because of the variety in surface preparation, coating systems, exposure etc. it is generally recommended not to establish performance profiles as a desk study only. Inspection based performance profiles are required in order to obtain confident projections of future performance and hence maintenance works. Generally when establishing a performance profile, the level of uncertainty increases as the bridge age increases. This is due to the fact that important information is often lost over time such as surface preparation, type of coating system, time of repair and possible repainting etc.

The following input is required in order to estimate a performance profile using the methodology of ML D2.3 [9]:

Table 6.2: Bridges performance profiles

Input	**Output**
• Coating age • Coating type • Atmospheric corrosivity category in accordance with EN ISO 12944-2 [1] (together with EN ISO 9223 [3], 9224 [4], 9226 [5]) • Structural capacities (ULS, FLS) • Possible inspection results	=> Thickness loss *C(t)* => Service life T_L (and remaining service life) => Critical details => Adjustment of theoretical *C(t)* and T_L and critical details

6.2.2 Service life

Infrastructure Managers (IMs) may have individual approaches to re-painting interventions. Some IMs use a limit state definition where a touch up intervention is performed when the degree of rusting reaches a certain level. Touch-up will be repeated as many times as possible and maybe supplemented with a total new topcoat before abrasive blasting and repainting of the entire surface are needed. This approach is possible if the budget and other operational constraints allow for regular maintenance keeping the current coating in a good shape. Other IMs use a limit state where the coating system can degrade until a large loss of

coating area is reached. Then abrasive blasting and repainting of the entire surface are performed. Essentially both limit states need to be addressed in order to find the optimal maintenance strategy,

In ML D2.3 [9] it is assumed that the end of the service life of Network Rail coating systems is when 50% of the coated area becomes unprotected. This assumption seems uneconomic and difficult to manage due to the following reasons:

- It is difficult to estimate the unprotected area ratio. Periodic inspections of coating are usually performed by visual inspection only where the degree of blistering, cracking, rusting and flaking is estimated based on ISO 4628 [2]. Normally, the degree of rusting (Ri 0 to Ri 5) is governing for maintenance planning. Also, the degree of rusting is linked to the durability of new coatings specified according to EN ISO 12944 [1] (low = 2 to 5 years, medium = 5 to15 years, high more than 15 years). Durability according to EN 12944 [1] is defined as time to rusting degree, Ri 3, which corresponds to 1% rusted area. Furthermore, it is defined in EN 12944 [1] that when Ri 3 is reached major maintenance is required. Generally, it seems more appropriate to use Ri 3 (1% rusted area) as a definition of service life. It seems reasonable to use a power function for the degree of rusting, see Figure 6.2. This relationship should be updated based on inspections.

- Normally, if 50% of the coated area is lost, the only possible intervention is abrasive blasting of the entire surface and application of a total new coating system. This calls for expensive protective measures and extensive preparation and application. Generally, touch-ups or spot repairs that prolong coating life are economic and environmentally feasible (has the lowest Life Cycle Costs and Environmental impact because of postponement of major maintenance and favourable discounting). Sometimes touch-ups or spot repairs are followed by application of a total new top coat. These considerations also suggest that Ri 3 may be a better definition of service life.

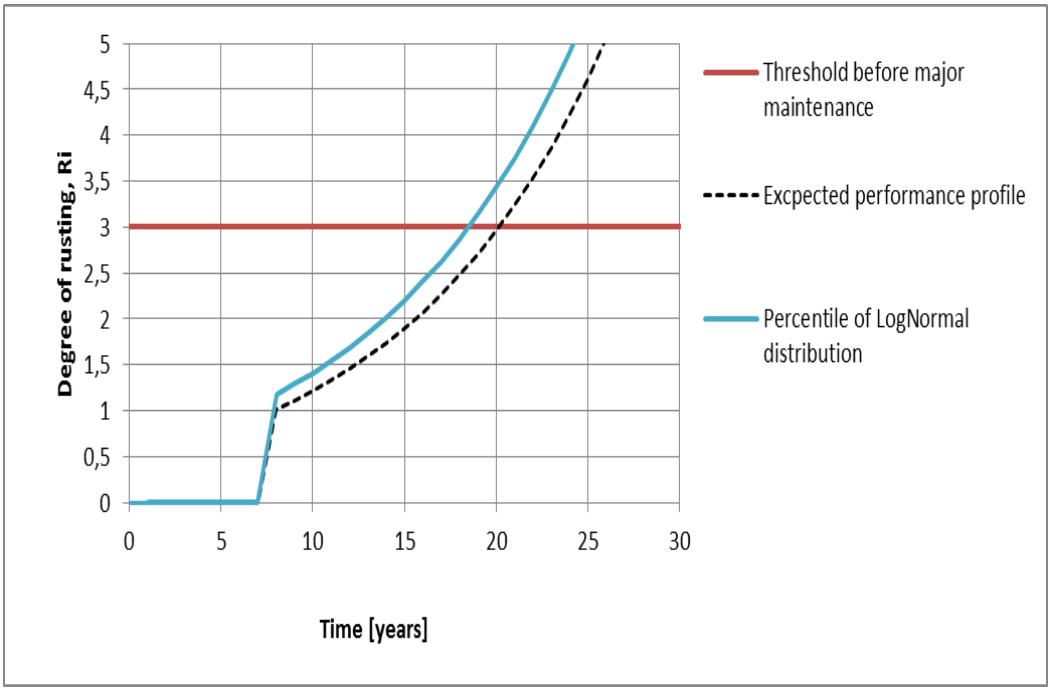

Figure 6-2: Possible performance profile related to degree of rusting

6.2.3 Correlation between critical details and corrosion

Often corrosion is not uniformly distributed. Poor detailing of bridges allows for collection of dirt and moisture which accelerates corrosion. EN 12944-3 [1] shows design features which may be used to avoid deposits accumulating or water being trapped. These examples may be used as a comparison to existing drawings indicating possible design features that attract corrosion. Please refer to ML D.2.2 [8] on this subject.

Also to be noted is that poor detailing may be difficult or impossible to recoat in a good way. Such detailing may cause crevice corrosion. For some of these details no guarantee from the contractor will be provided during recoating.

A special record should be made for each individual bridge where results of inspections on these “poor detailing items” should be listed. These items will define special future maintenance actions for the bridge. Poor details that behave differently to the remaining bridge, the latter as illustrated in Figure 6.2 should be given special attention when establishing a performance profile (a separate performance profile may be suggested).

Besides critical details related to corrosion progress, a detailed desk study should be performed in order to highlight details that are critical in relation to safety governed by the ultimate limit states (ULS) as well as fatigue limit states (FLS).

A desk study should be supplemented by inspections. These inspections will provide information on performance related to coating condition as well as structural safety, e.g. loose rivets and cracking of paint may indicate a FLS related safety issue.

Furthermore, the desk study should pay special attention to details that are hidden, i.e. where performance cannot be assessed during visual inspection.

In order to capture the real performance of a coated metallic bridge, analysis of several scenarios may be required. These scenarios should try to correlate coating performance and critical details with respect to ULS and FLS capacity. The Life Cycle Assessment Tool (LCAT) should be used for each scenario in order to show which maintenance intervention should govern future bridge performance and show the economic and environmental impact associated with it.

6.2.4 Source of data

As discussed above, the performance profiles in D2.3 were derived using a physical modelling approach for corrosion loss based on ISO standards, with supporting information on the interpretation of coating life from Network Rail’s (NR) guidance on maintenance. In order to validate these performance profiles two different approaches (and source of data) have been chosen:

- Comparison of performance profiles with inspection data from two Danish bridges (incl. sensitivity, studies section 6.5).
- Statistical analysis of inspection data (defect records) from Network Rail (NR) in the UK, section **Error! Reference source not found.**).

6.3 Condition versus capacity based maintenance

The LCAT will be tested and validated as part of WP5. One of the important issues that the WP5 validation should address is the cost and environmental implications if maintenance work is driven by capacity based performance instead of condition based performance.

In the case of a robust operation and maintenance budget infrastructural managers aim at condition based maintenance when it comes to coating of metallic bridges. This is generally considered as being cost optimal. On the other hand consideration of capacity based maintenance is required for some of the old metallic bridges (typically riveted bridges built within the period 1900-1940) where fatigue life is limited.

The case studies in chapter 6.5 will address both condition and capacity based performance for riveted metallic bridges in Denmark and may feed directly into the WP5 validation and testing of the LCAT.

6.4 Typical Danish coating systems for steel bridges

6.4.1 Coating on existing bridge

Traditionally, old metallic bridges were coated using lead based paint systems. Lead was added to paint to speed up drying, increase durability, maintain a fresh appearance, and resist moisture that causes corrosion. Later, lead based paint systems were replaced with paint systems based on chlorinated rubber or alkyd which was again replaced with epoxy, polyurethane and acrylic paint systems.

Many of the Danish riveted bridges still have the original lead based paint system underneath more recent layers of top coats, i.e. only touch up and reapplication of the top coat have been performed.

It is impossible to predict coating performance of old metallic bridges without inspections. This is partly because these bridges have several layers of coating and that distribution of corrosion is uneven. One of the major bridges in Denmark (Little Belt Bridge which is a riveted railway and roadway steel truss bridge) has 7 layers of coating. The touch up cycle beneath track/roadway is at present 5 yearly partly due to poor detailing whereas the paint repair cycle above track/roadway is more in the range of 20 years.

Furthermore, inspections are often supplemented by compatibility tests, i.e. adhesion and effect of solvents needs to be tested by professionals in order to stipulate possible maintenance scenarios.

6.4.2 Coating system on new bridge or coating for rehabilitation

When specifying coating systems on new metallic bridges or a complete new coating system for existing metallic bridges a C4 or a C5 coating system according to EN 12944-5 [1] is cost optimal when considering whole life costs. The cost of paint is marginal when compared to other construction costs for a new bridge and cost of preparatory works incl. measures for protection of people and environment for existing bridges.

C5 paint systems according to EN 12944-5 [1] are typically between 300-500 µm Mean Dry Film Thickness - MDFT (2-6 layers), primed by a Epoxy-, Polyurethane- or Ethyl-silicate binder and intermediate and top coats with a Epoxy-, Polyurethane- or Acrylic- binder.

Compatibility with the existing system, cost, environmental protection and track possession periods are key elements when Rail Net Denmark chooses one of the above mentioned systems. Often a system with high durability according to EN 12944-1 [1] is chosen because it ensures no major maintenance is required over the next 15 years if preparation and application is done properly.

Rail Net Denmark has used AC Antiox (Acrylic, water dispersed) coating with approximately 350µm MDFT on a number of recent repair projects. AC Antiox is environmental friendly (MAL-code 00-1).

6.5 Case studies

The aim of this section is to present field-validated performance profiles for metallic bridges. The performance profiles have been determined using the methodologies presented in D2.3 [9]. Field data from Danish railway bridges has been used for the validation presented in the following.

Out of 31 Danish short or medium span riveted railway bridges of various ages a few have been chosen for case studies. Case studies have been selected from among these bridges where ULS and FLS capacities and critical details are known (approximately 12 out of 31). All bridges have been subjected to periodic inspections.

Two bridges are chosen: Ermelundsvej and Jernbane Alle. The latter have railway and cross girders enclosed by concrete which will be disregarded in the following.

In the following sections, input, performance profiles, sensitivity studies and updating through inspections are detailed.

6.5.1 Input

Figure 6.3 and Figure 6.4 show the two bridges. Key input provided from drawings and inspections are listed in Table 6.3.

Figure 6-3: Bridge over Ermelundsvej

Figure 6-4: Bridge over Jernbane Alle

Table 6.3: Input. ULS and FLS utility is calculated in 1996.

**(Corrosivity class C3 is urban and industrial atmospheres, moderate sulphur dioxide pollution and coast areas with low salinity.
*Earlier inspection and maintenance performed is not known to us)**

Input	**Ermelundsvej**	**Jernbane Allé**
Year of construction	1914	1941
Length	16.2 m	20.5 m
Span	15.0 m	19.35 m
Width	7.76 m (two tracks)	4 m (single track)
Year of inspection*	1983/1984/1987/1990/1999/2006/2010 /2011	1984/1987/1990/2000/2006/2010
Condition rate (see next page for explanation)	1974 Repainted 1984 (rated 2 out of 5) 1990 Remaining coating life 10 years 1998 Remaining coating life 3 year 1999 (rated 3 out of 5) 2006 (rated 3 out of 5) 2011 (rated 3 out of 5)	1984 (rated 3 out of 5) 1984 55 µm horizontal surfaces, 35 µm vertical surfaces 1987 Partial repainted 1990 Remaining coating life 10 years 1998 Remaining coating life 10 years 2000 (rated 1 out of 5) 2006 (rated 3 out of 5) 2010 (rated 3 out of 5)
Possible repair works*	2011 (no structural or coating impact)	2009 (no structural or coating impact)
Coating type	Areas below track, blast cleaned areas (SA 2½): Primer: Calcium Plumbate (Epoxy based), 1 layer Intermediate: Coal Tar Epoxy, 1 layer Top coat: Coal Tar Epoxy, 1 layer MDFT: 200 my Areas below track, hand tool cleaned areas: Primer: Oil based paint with iron oxides, 2 layers Intermediate: Oil based paint with iron oxides, 1 layer Top coat: Oil based paint with iron oxides, 2 layer MDFT: 200 my	Delaminated and rusted areas, blast cleaned (SA 2½): Primer: Zinc-rich, 1 layer Intermediate: Acrylic, 2 layers Top coat: Acrylic, 1 layer MDFT: 230 my Intact areas after water-cleaning: Primer (spot repair): Zinc-rich, 1 layer Intermediate: Acrylic, 2 layers Top coat: Acrylic, 1 layer MDFT (spot repair): 230 my
Coating age (in 2014)	40 years	27 years
Corrosivity class (EN 12944-2, [1])	C3	C3
Steel quality	st. 37	st. 37

Input	Ermelundsvej	Jernbane Allé
ULS utility	Main girder: 0,4 (bending), 0,3 (shear) Cross girder: 0,5 (bending), 0,4 (shear) Railway girder: 0,4 (bending), 0,7 (shear)	Main girder: 0,6 (bending), 0,7 (shear) End cross girder: 0,6 (bending), 0,7 (shear) Cross girder: 0,5 (bending), 0,4 (shear)
FLS capacities	Year 2038 based on the following details: Main girder: Bottom flange (mid-span) Cross girder: Bottom flange, inner girder (mid-span) Railway girder: Bottom flange between 4th and 5th cross girder (mid-span) Connection between 5th cross girder and main girder (shear) Connection between railway girder and cross girder (shear)	Year 2038 based on the following details: Main girder: Bottom flange (mid-span) Cross girder: Bottom flange, inner girder (mid-span) End cross girder: Bottom flange (mid-span) Connection between 5th cross girder and main girder (shear) Connection between end cross girder and main girder (shear)

It is to be noted from the above table that condition rate 3 equals “deterioration has developed to an extent where there is a risk that the element may experience functional failure within a short time span, i.e. remedial actions are required within a few years”.

In 2010 the inspector estimated coating repair works to be performed in 2014 at a cost of 64,000 Euro for Ermelundsvej bridge. In 2010 the inspector estimated coating repair works to be performed in 2010 at a cost of 2,730 Euro for Jernbane Allé bridge.

Photographs and drawings including identification of critical sections are shown in Section 9 (Appendix B).

6.5.2 Performance profiles

As seen from Table 6.3 the service life of the new coating system on Ermelundvej is 40 years whereas the service life of the replacement system on Jernbane Alle is 27 years.

These service lives seem to be significantly above the minimum service life of coating systems specified according to ISO 12944 [1] (15 years for high durability systems). Whether or not this statement is true depends on the level of degradation that has been observed for the two bridges. For Ermelundsvej the percentage of rusting is closer to RI 4 (8% rusted area) instead of RI 3 (1% rusted area). For Jernbane Alle the percentage of rusting is below 1% (1% corresponds to Ri 3). For illustrative purposes 1% rusting for Jernbane Allé Bridge has been assumed in the following.

The actual normalised coating performance for the two bridges is shown below together with the normalised coating performance when assuming that service life is related to 50% area loss (assumption of D2.3). The latter represents a conservative boundary when estimating possible degradation scenarios.

The two “actual coating performances” are based on 8% rusted area at year 40, viz. anticipated year of repair at Ermelundsvej and 1% rusted area at year 27, viz. anticipated year of repair at Jernbane Alle. It has been assumed that the rusted area is equal to the

coating area loss. The actual coating performances have been generated by calibrating a constant at the anticipated year of repair using equation (6.5). This constant has been applied to eq. (6.5) with a constraint that eq. (6.5) should only estimate values between 0 and 1.

$$\frac{A_{pr}(t)}{A_{pr0}} = 1 - \left(\frac{0.6t^2}{T_L^2} - \frac{0.1t}{T_L}\right) \qquad (6.5)$$

Where $A_{pr}(t)$ and A_{pr0} are the residual and initial protected area, respectively and t is the time in years.

Figure 6.5 shows actual and conservative (50% at time equal to service life) loss of protected area as function of time for the two bridges Ermelundsvej and Jernbane Alle.

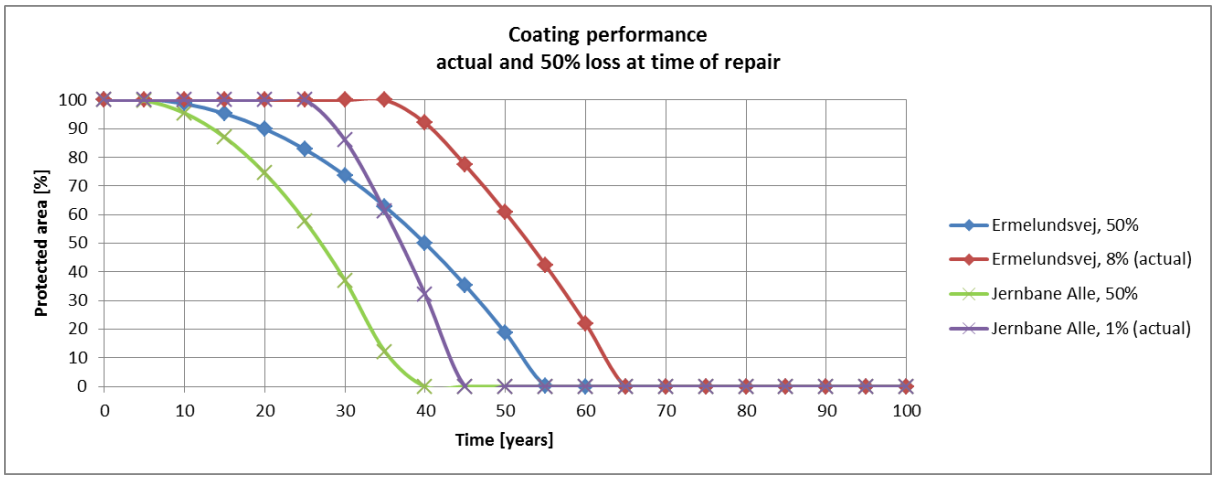

Figure 6-5: Actual and conservative loss of protected area

(50% at time equal to service life - as function of time for the two bridges Ermelundsvej and Jernbane Alle. Environment exposure according to corrosion category C3 has been assumed at both locations)

When comparing the different scenarios it is seen that a significant difference in coating performance is obtained dependent on the threshold defining coating service life. At Ermelundsvej the coating performance is shifted by approximately 10-20 years. At Jernbane Alle the coating performance is shifted by 5-15 years. This highlights the need for inspection-based performance profiles.

Also, when comparing the two coating systems (that are also different in age) the coating performance is quite different.

The above two observations suggest that various sensitivity studies are mandatory when predicting (long term) future coating performance.

The difference in coating performance will map into flange and web thickness predictions and then again into bending and shear capacity predictions (fatigue is treated separately later in this section).

The following thickness loss profiles may be benchmarked based on inspection results when such information is available. In this study only the above coating performance has been calibrated to the field data.

It has been assumed that thickness loss is happening on all sides of the steel member. Furthermore, the following performance profiles assume an average thickness loss. If a certain ratio of the more degraded area is local (i.e. within the capacity limiting cross section) the following “average” performance profiles are no longer valid.

Flange thickness performance is shown in Figure 6.6, for the cross girder in which the bending utility ratio is at its maximum.

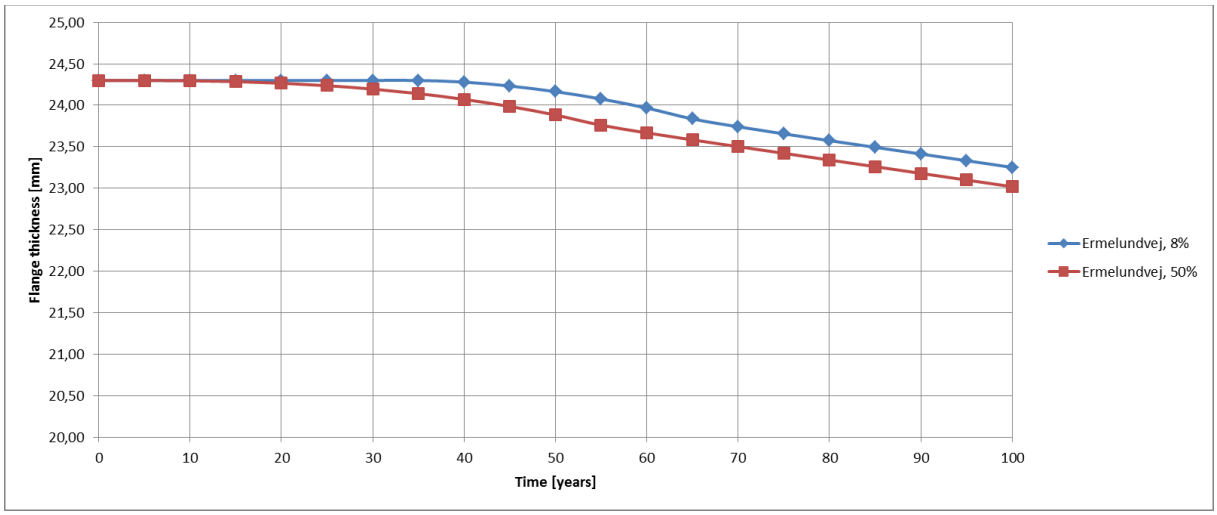

Figure 6-6: Cross girder (INP 450) flange thickness performance at Ermelundsvej bridge.

(Environment exposure according to corrosion category C3 has been assumed)

Web thickness performance is shown in Figure 6.7, for the railway girder in which the shear utility ratio is at maximum.

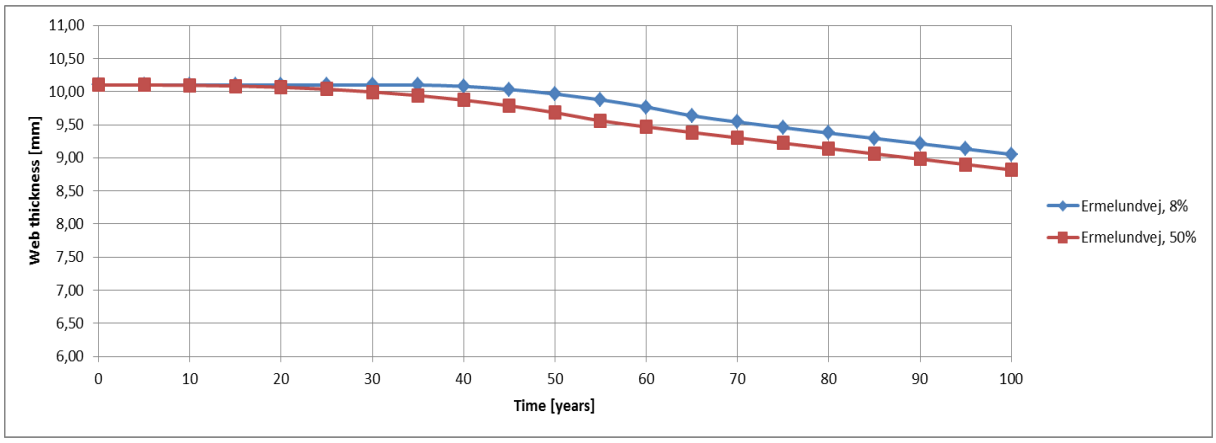

Figure 6-7: Railway girder (INP 250) web thickness performance at Ermelundsvej bridge.

(Environment exposure according to corrosion category C3 has been assumed)

Figure 6.8 shows the bending performance of the cross girder at Ermelundsvej bridge and Figure 6.9 shows the shear performance of the railway girder at Ermelundsvej bridge.

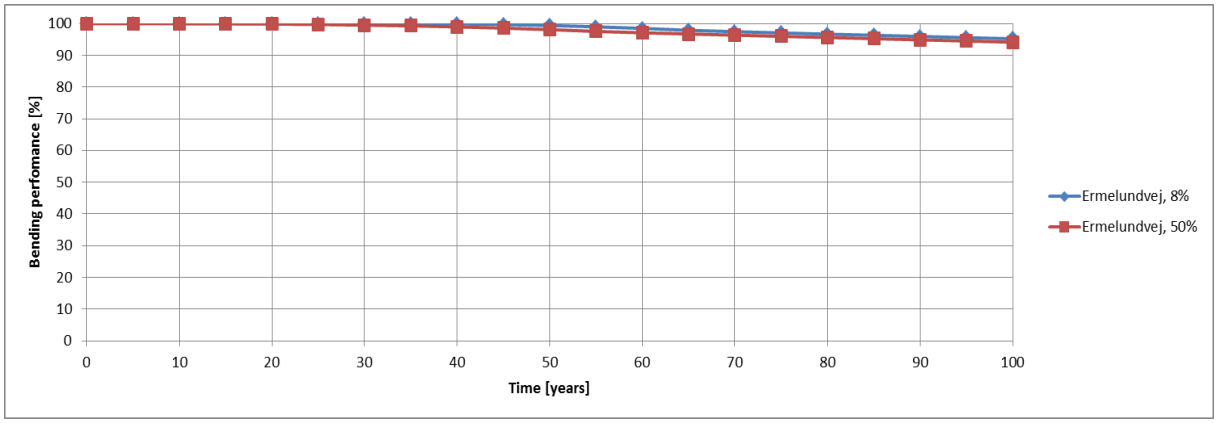

Figure 6-8: Cross girder (INP 450) bending performance at Ermelundsvej bridge.

(Environment exposure according to corrosion category C3 has been assumed)

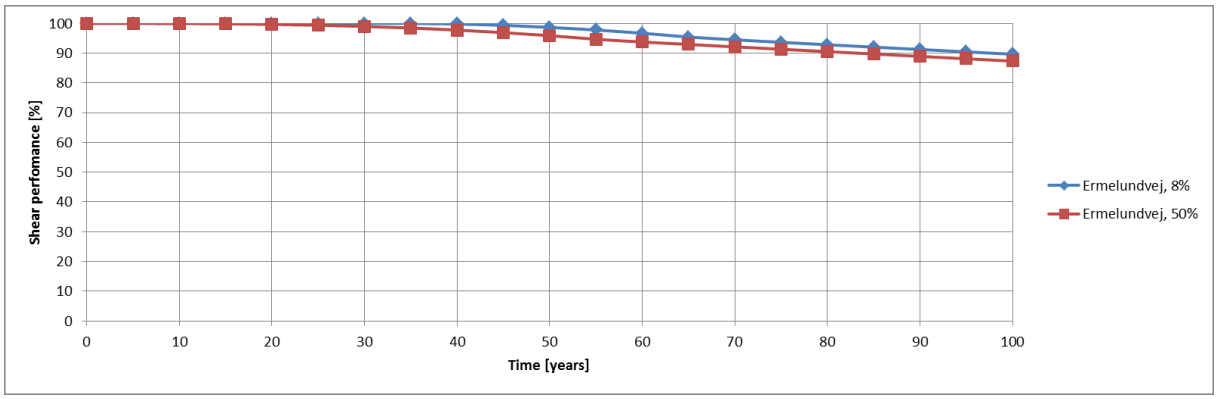

Figure 6-9: Railway girder (INP 250) shear performance at Ermelundsvej bridge.

(Environment exposure according to corrosion category C3 has been assumed)

It is seen that the performance prediction for the coating system under these environmental conditions is robust (little difference for very long predictions). As argued in previous chapters it can however not be concluded that the economic and environmental performance for both assumptions are similar. This will be demonstrated as part of the LCAT testing.

Performance profiles for the Jernbane Alle Bridge with performance profiles similar to Ermelundsvej bridge are given In Appendix B.

The marginal influence on bending and shear performance has to be compared to the actual limit state capacity. For the two brides in question they both have an ultimate limit state reserve in excess of 30%, hence load capacity loss due to corrosion under the given circumstances is not critical. Assuming a scenario where Rail Net Denmark wants to increase speed or axle on the bridge the above conclusion is no longer relevant.

For the two bridges in question it will be the fatigue life that governs the performance threshold. According to fatigue analyses year 2038 will roughly be the threshold for both bridges. When comparing that to the performance profiles of Figure 6.6 to Figure 6.9 it corresponds to year 2038-1974 = 64 for Emelundsvej bridge and year 2038-1987 = 51 for Jernbane Alle bridge (the latter when compared to figures in Appendix B).

In addition to the fatigue life (performance threshold) establishment of performance profiles for corroding metallic bridges needs to verify that the level of corrosion and the area where this will happen will not change the basis for performing the fatigue evaluation. The rough surfaces due to corrosion and pitting corrosion in particular act as notches which can cause crack initiation. However, fatigue life will not be influenced in the same way if the corrosion damage is located at the compression flange rather than the tension flange. Especially corrosion near rivets increases the local stress level which lead to low fatigue endurance.

6.5.3 Sensitivity study

The fact that performance profiles are relatively constant within the timeframe and environment considered should be demonstrated by the sensitivity study.

Two simple sensitivity studies have been performed for the Ermelundsvej Bridge as an example.

First, the environment changes from corrosion category C3 (actual) to C4 (Industrial areas and coastal areas with moderate salinity). In Figure 6.10 the railway girder web thickness for the actual coating performance is compared for C3 and C4 corrosion categories. It is seen that during a 100 year period the difference between the web thicknesses of two environments is in the order of 0.7 mm.

In Figure 6.11 the railway girder shear performance for the actual coating performance is compared for C3 and C4 corrosion categories. It is seen that during a 100 year period the difference between the shear performances is in the order of 10%.

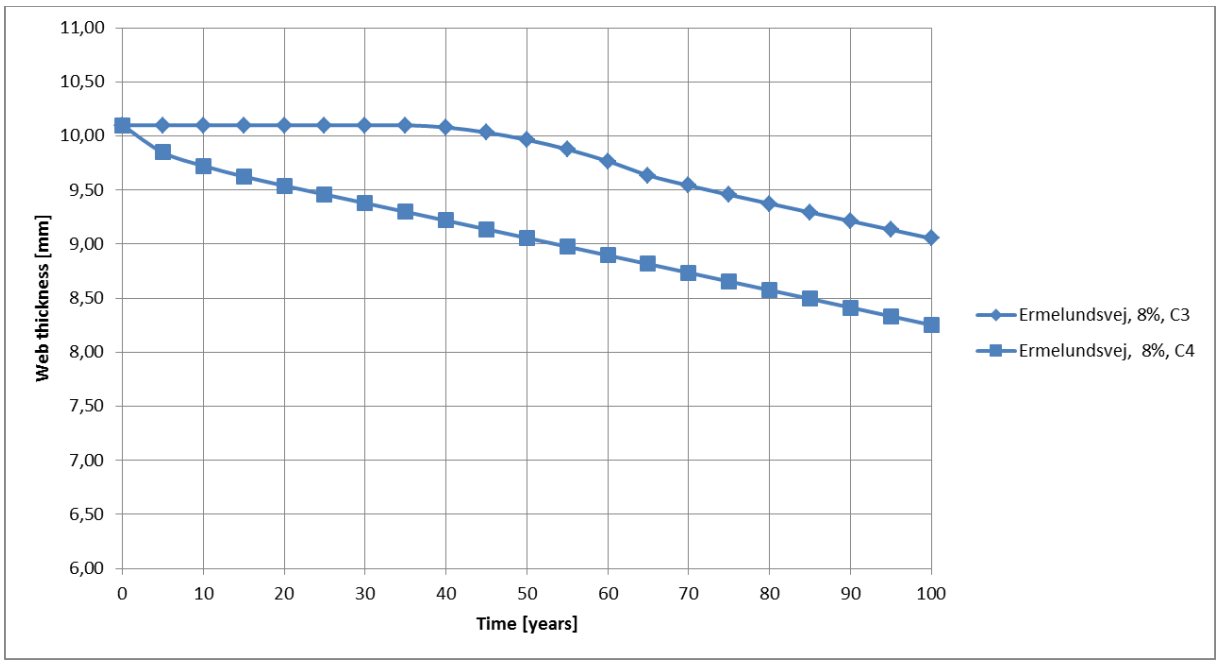

Figure 6-10: Railway girder (INP 250) web thickness performance at Ermelundsvej bridge

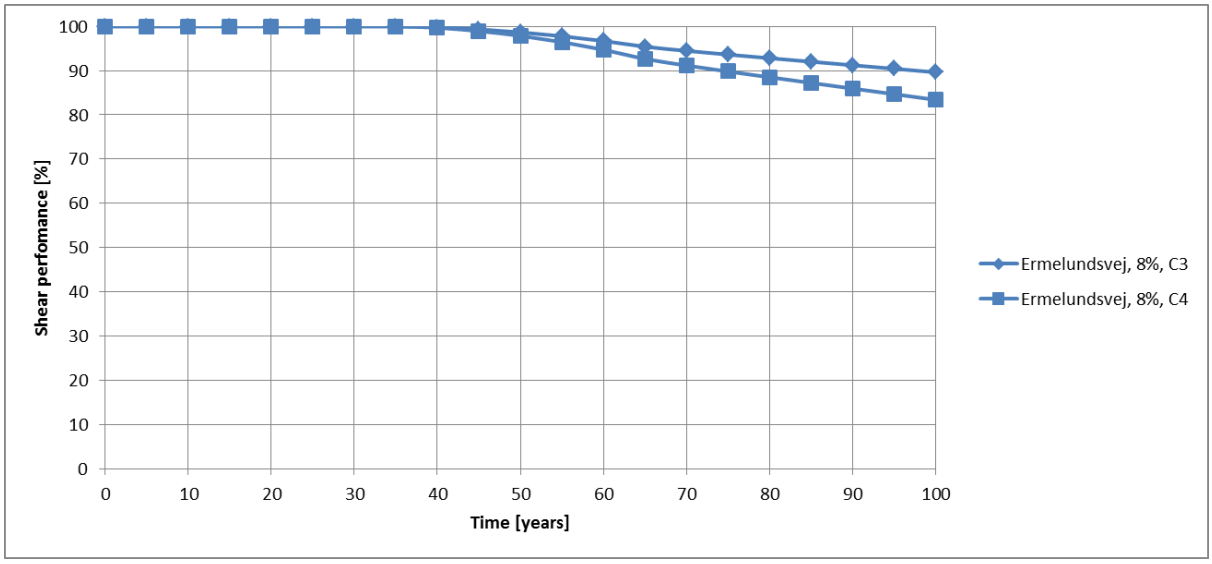

Figure 6-11: Railway girder (INP 250) shear performance at Ermelundsvej bridge

Secondly, coated (actual) versus the uncoated condition is compared for corrosion category C3 (actual). In Figure 6.12 the railway girder web thickness for the actual coating performance is compared for coated (actual) and uncoated situation. It is seen that during a 100 year period the difference between the web thicknesses is in the order of 0.8 mm.

In Figure 6.13 the railway girder shear performance for the actual coating performance is compared for the coated (actual) and uncoated situation. It is seen that during a 100 year period the difference between the shear performances is in the order of 10%.

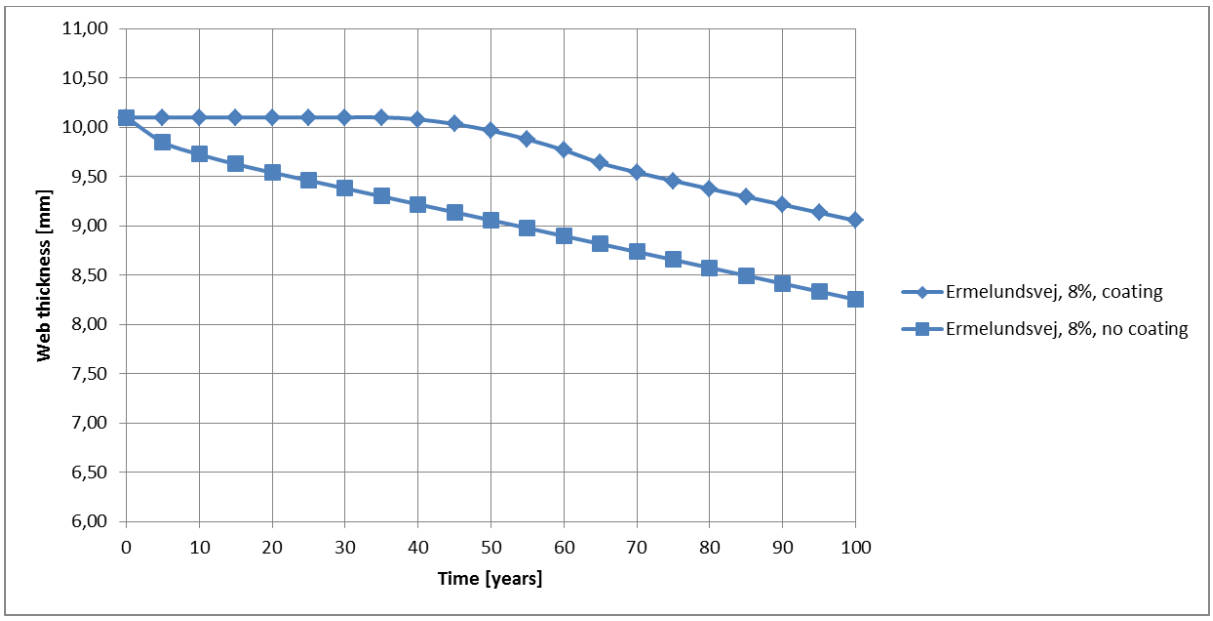

Figure 6-12 Railway girder (INP 250) web thickness performance at Ermelundsvej bridge

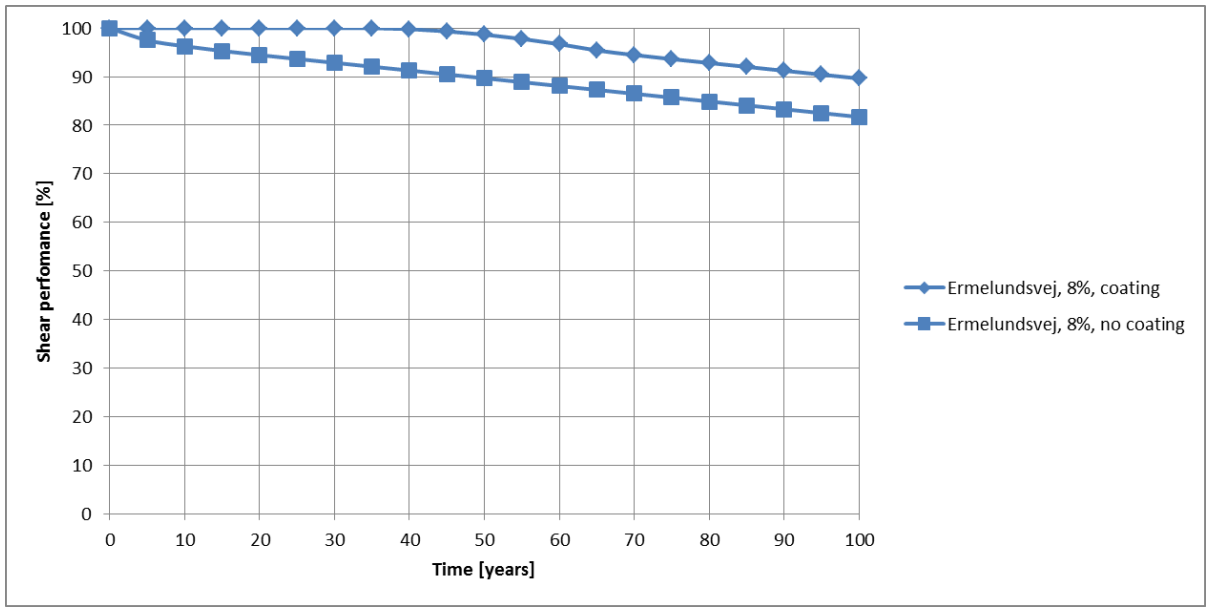

Figure 6-13 Railway girder (INP 250) shear performance at Ermelundsvej bridge.

The above studies suggest that designing with a corrosion allowance of say 1-2 mm is superior to coating. However this is typically not the case. The reasoning for this is related to aesthetics/appearance, public opinion, uncertainty related to inspections of corroded elements etc.

6.5.4 Updating through inspections

A large portion of the Operations and Maintenance O&M budget is associated with keeping the coating system fit for purpose, i.e. it is desirable to have optimal O&M plans.

Visual inspection of the coating system is the only relevant detection method. Risk-Based Inspection (RBI) may be relevant. The actual registered coating condition may be utilized for calculating time for the next necessary inspection possibly based on reliability based principles.

If it is identified that areas degrade differently, they may be treated separately in the RBI plan, if it is beneficial from an economical point of view.

Pull off Adhesion Tests (EN ISO 4624) [6] and Cross-cut tests (EN ISO 2409) [7] together with reporting and acceptance criteria related to significant damages (major crevice corrosion, loose rivets, impact from traffic etc.) are outside the scope of this report.

The RBI plan depends on a number of important assumptions. These assumptions are:

- The mean value of the Coating Condition, CC_{mean}, is equal to the degradation rate as estimated based on inspection, see Figure 6-14.
- A percentile of e.g. a lognormal distribution determines when the next RBI based inspection is performed.
- A constant Coefficient of Variation may be used for coating degradation. This parameter may be updated based on actual inspection results using Bayes statistics (using conditional probabilities). This has not been included in the present report.

The threshold value is an acceptance criteria determining how degraded the coating can be before maintenance is considered. The threshold value may be adjusted due to Life Cycle Cost Study or other circumstances. It is important that the coating supplier verify all the above assumptions.

Degradation of coating is illustrated in Figure 6-14 together with possible inspection results during the first 16 years. RBI based inspection is to be performed at year 24 possibly together with a paint touch-up if cost optimal.

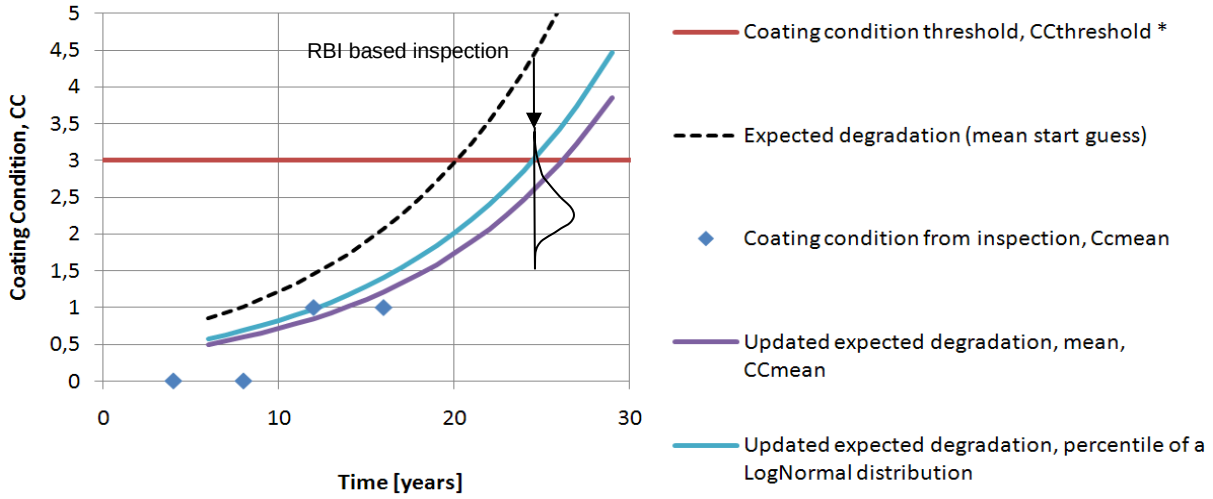

Figure 6-14 Degradation of coating

(incl. updating based on inspection results)

Figure 6-14 shows how inspection based updating may postpone the time for inspection.

6.6 Analysis of inspection data

6.6.1 Introduction

The main focus of this section of the report is the validation of the degradation models for metallic bridge elements, as presented in deliverable D2.3 [9], using field collected bridge condition data provided by Network Rail (UK). The key features of this database, the procedures used during data collection as well as the criteria for data filtering used in this study are discussed in subsequent sections of this report. This database is used to examine some of the assumptions made in the coating and corrosion loss model development presented in D2.3 [9], by considering the following points:

a) Develop an understanding of the defect population related to coating degradation and corrosion loss within a large stock of metallic bridges, based on the results of visual inspections over a number of years.
b) Appreciate the differences in coating deterioration and thickness reduction between different types of elements in metallic bridges (e.g. girders, stiffeners, etc.)
c) Examine the influence of an element's location within a bridge (i.e. external vs. internal elements) in relation to the observed severity and extent of degradation.
d) Investigate the temporal and spatial characteristics of corrosion damage observed in metallic railway bridges (e.g. local and/or general corrosion).

6.6.2 Background

The condition assessment of metallic bridges is based on Part 2C of the Handbook for the examination of structures [10], which provides guidance for the examination and condition marking of bridges. Based on the classification framework used therein, the individual elements of a bridge are broadly classified as major or minor elements. Major elements are the deck and the intermediate/end supports of the bridge. In [10], a bridge is a structural system consisting of several types of minor elements including, among others, exposed and inner longitudinal main beams/girders (denoted using MGE and MGI codes, respectively), exposed and inner longitudinal secondary beams/girders (denoted using LSE and LSI codes) and end and inner transverse beams/girders (denoted using XGE and XGI codes).

Several other types of minor elements which are included in the database, such as abutment (ABT), bearings (BGL), bracing (BRG), etc. are not considered in this study. A summary list of minor elements along with their description can be found in Tables 2C.2 and 2C.3 in [2]. The same document provides guidance for the condition marking of minor elements based on the type of material (i.e. metal, masonry, reinforced concrete and timber) and the protective system (i.e. coating to metal).

The condition rating is described by an alphanumeric score (e.g. A1, B2, etc.) with the letter and the number denoting the defect severity and extent, respectively; the relevant definitions are summarised in Tables 6.4 and 6.5 for *metal* condition and in Tables 6.6 and 6.7 for *coating to metal* condition. In this report, the aforementioned minor elements (i.e. MGE, MGI, LSE, LSI, XGE and XGI) are studied in relation to both.

Table 6.4: Severity ratings for metal condition

(extracted from [10])

Severity rating	Definition
A	No visible defects to metal
B	Corrosion/loss of section < 1mm deep
C	Corrosion/loss of section 1mm up to 5mm
D	Corrosion/loss of section > 5mm up to 10mm deep
E	Corrosion/loss of section > 10mm but not through section
F	Corrosion/loss of section to full thickness of section
G	**Choose most extensive from:** Tears, fracture, cracked welds Buckling, permanent distortion or displacement

Table 6.5: Extent ratings for metal condition

(extracted from [10])

Extent	Definition	
1	No visible defects	
2	Localised defect due to local circumstances (such as isolated damage caused by a single bridge strike or isolated water leakage)	
3	Percentage of surface of the element occupied by defect	< 5%
4		5% up to 10%
5		> 10% up to 50%
6		> 50%

Table 6.6: Severity ratings for coating to metal condition

(extracted from [10])

Severity rating	Definition
A	All coating intact, no visible defects or no coating applied
I	All coating intact, surface defects/abrasion (no corrosion of underlying metal)
J	Flaking or blistering of top coat (no corrosion of underlying metal)
K	Corrosion spots showing through coating
L	Complete loss of coating to parent metal

Table 6.7: Extent ratings for coating to metal condition

(extracted from [10])

Extent	Definition	
1	No visible defects or no coating applied	
2	Localised defect due to local circumstances (such as an isolated waterproofing failure or the effect of an isolated drainage point in the bridge)	
3	Percentage of surface of the element occupied by defect	< 5%
4		5% up to 10%
5		> 10% up to 50%
6		> 50%

The elements of each bridge are periodically inspected (typically every 6 years) and their condition is marked using the rating codes of Tables 6.4-6.7. Thus, the database contains visual inspection results in terms of alphanumeric condition ratings of 92,210 metal elements for the period 1999 to 2014. Table 6.8 provides an overview of the database entries for metal elements which are including cast iron, wrought iron, early steel, carbon steel and Corten steel elements (these are all grouped as metal in the severity extent ratings). The vast majority of the metallic bridge population falls under the wrought iron, early steel and carbon steel types. It can be seen that the total number of examinations in about 1.35 million from which 22.8% (306,917) are metal element records.

The number of examination records with good defect codes for metal elements is 292,668 (i.e. metal elements with incomplete/inconsistent database entries are excluded) while the number of elements with good defects codes and more than one examination is 200,193. Following discussions with SKM, and bearing in mind the objectives of this investigation outlined above, metal elements with good defect codes and more than one examination result are used. Each examination record contains two condition ratings for metal and two condition ratings for coating to metal. The first condition rating corresponds to the worst defect observed on the element in terms of severity and extent while the second condition rating is determined by the second worst defect on the element. The rating A1 is given for the second defect in the case that no second defect is observed [10].

Table 6.8: Overview of database entries for metal elements

	Number of exam records
All element types	1,347,268
Metal elements	306,917
Metal Elements with good Defect Codes	292,668
Metal Elements with good Defect Codes and more than 1 exam	200,193

Figure 6.15 shows the annual number of examination records for all minor element types during the period 1999-2013. As it can be seen in this figure, the periodical inspection programme exhibits a gradual increase in the annual number of records obtained during the period 1999-2002. Beyond 2002 the annual number of records stabilises to around 15000, with the exception of 2012 where the number of records is double the average figure.

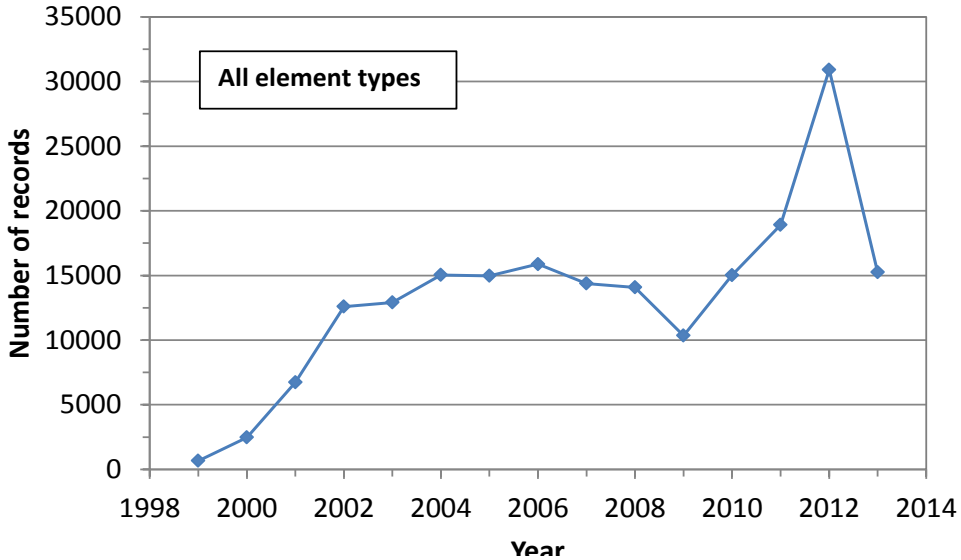

Figure 6-15: Number of examination records

(per year for the period 1999-2013. Data for 2014 is incomplete and hence not included in this figure)

Table 6.9 summarises the number of records for each of the metal elements considered in this study. It should be noted that during inspection element types MGE and MGI are marked individually, element types XGE and XGI are marked collectively, whereas element types LSE and LSI are marked individually and collectively, respectively. In this respect, it is not possible to use the numbers in Table 6.9 to determine the relative frequency of individual element types within the metallic bridge population (with the exception of MGI and MGE).

Table 6.9: Number of records for individual element types

Element type	Number of records
Exposed longitudinal main beams/girders (MGE)	37,265
Inner longitudinal main beams/girders (MGI)	48,153
Exposed longitudinal secondary beams/girders (LSE)	4,220
Inner longitudinal secondary beams/girders (LSI)	4,431
End transverse beams/girders (XGE)	8,868
Inner transverse beams/girders (XGI)	13,269
Total	116,206

6.6.3 Preliminary Analysis

The processing of the data is carried out using filters in Microsoft Excel. Initially, the data for the different minor element types (i.e. MGE/MGI, LSE/LSI and XGE/XGI, see Table 6.9) are extracted from the bulk data and inserted into different worksheets. For each element type, internal and external elements are treated separately, i.e. two groups are established to separate the data for external/end and internal elements.

The first issue to be addressed pertained to the possible use of the entire database as opposed to a fraction that corresponds to the interval between two successive inspections (typically 6 years). Use of the latter is more appropriate in capturing a 'snapshot' of the population at a particular inspection cycle, whereas the former would provide a richer sample. However, the issue of sample homogeneity would have to be considered, i.e. whether there are significant changes to the element conditions over longer time periods. Figure 6.16 shows that in terms of the average corrosion loss (see section 6.6.4.3 for the definition of this indicator) in MGI elements there is no noticeable difference in the statistical distributions.

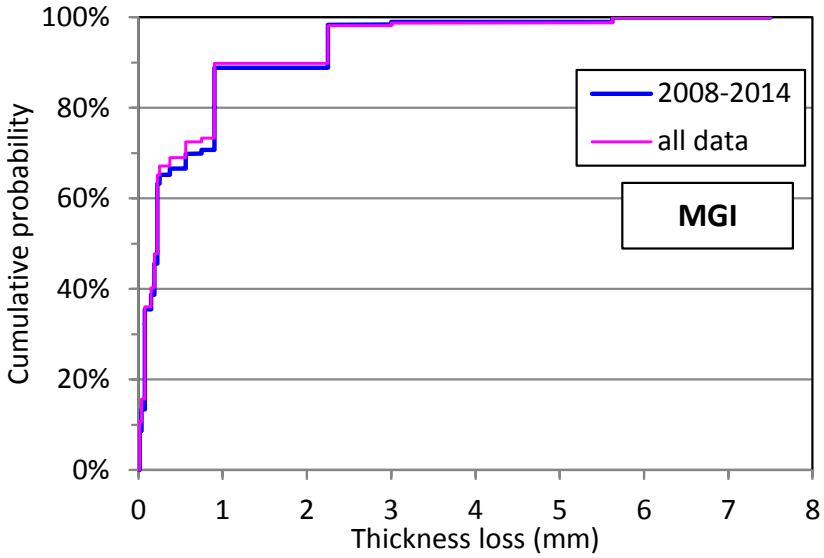

Figure 6-16: Comparison of empirical cumulative distribution functions for MGI

[using all the data (1999-2014) and using the last 6 years (2008-2014) of the available data.]

In fact, the corresponding mean and standard deviations for the two distributions are very similar, namely:

- Period 1999-2014: Mean loss = 0.543mm, Standard deviation = 0.884mm.
- Period 2008-2014: Mean loss = 0.568mm, Standard deviation = 0.864mm.

Similar results were obtained for the MGE elements. It was, therefore, decided that the data analysis for the selected element groups will be undertaken by using the entire database.

6.6.4 Main Analysis

Comparisons between internal and external elements

In this section, the inspection data is used to examine the influence of the location of an element within the bridge (i.e. external/end vs. internal elements) on the severity and extent of the observed deterioration. This is done by considering separately the cumulative number of inspection results in terms of severity and extent ratings for each of element types examined. Figures 17a and 17b show a comparison between the cumulative number of exam records for MGI and MGE elements in relation to increasing severity and extent ratings, respectively, for their 1st (most severe) metal defect.

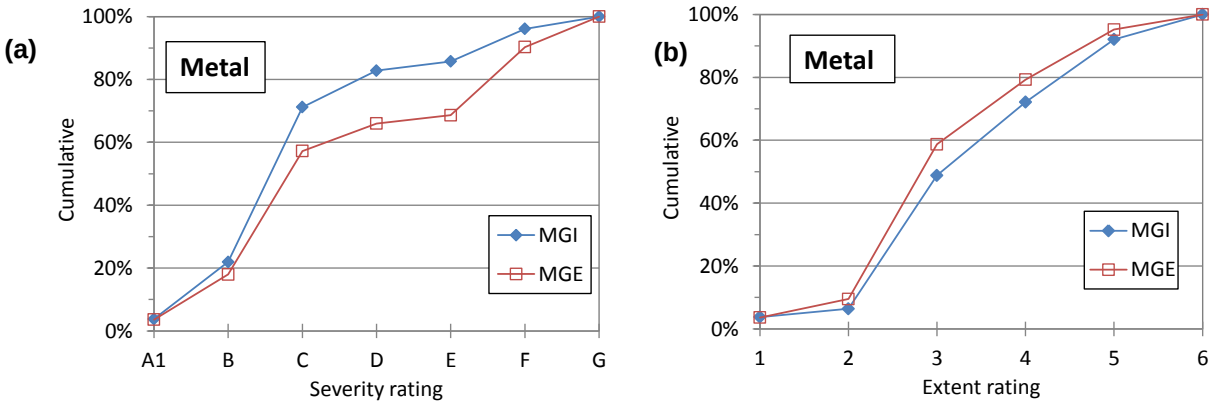

Figure 6-17: Cumulative distributions of 1st metal defect for MGI/MGE

[(a) severity and (b)extent]

The results in Figure 6.17a indicate that there are insignificant differences between the percentages of MGI and MGE elements where no deterioration is observed (i.e. % of A1 ratings), while small differences are observed between MGI and MGE for severity rating B.

As the severity rating increases, it can be seen that a larger percentage of MGE elements are associated with higher severity ratings indicating more advanced deterioration in comparison with MGI elements.

For example, about 65% of MGE elements have defects of rating D or better, whereas the corresponding percentage for MGI is more than 80% (conversely: less than 20% of MGI have defects with severity worse than D, whereas the same is true for 35% of MGE).

When looking at Figure 6.17b, small differences are observed between the percentage of MGI and MGE elements in extent rating categories 1 (no visible defects) and 2 (extent rating 2 is associated with localised defects due to local circumstances, see Table 6.5).

The results in this figure indicate that as the extent rating increases, a slightly larger percentage of MGI (internal elements) are associated with higher extent ratings. Figures 6.18a and 6.18b show a comparison between the cumulative number of exam records for MGI and MGE elements in relation to increasing severity and extent ratings, respectively, for their 2nd metal defect.

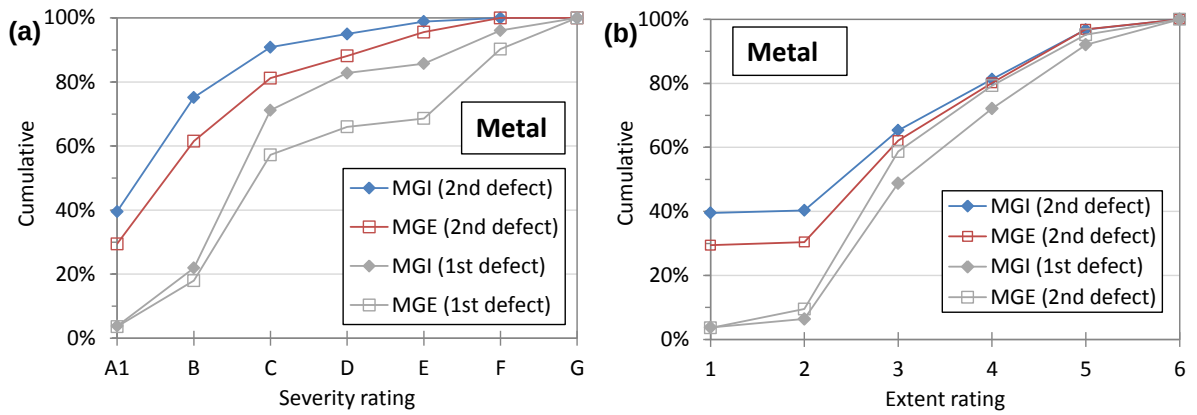

Figure 6-18: Cumulative distribution of 1st and 2nd metal defect for MGI/MGE

[(a) severity (b) extent]

MGE are associated with lower values of severity and extent compared to the 1st defect (also shown in these figures). It can also be seen in Figure 6.18a that the 2nd metal defect of MGE is associated with higher severity rating values compared to MGI, which indicates more advanced deterioration. A similar but less strong trend is observed in Figure 6.18b, although the differences become insignificant beyond the middle part of the extent rating scale.

Figures 6.19a and 6.19b show a similar comparison for MGI and MGE elements in relation to increasing severity and extent ratings, respectively, for their 1st coating to metal defect. The results indicate that there are insignificant differences between MGI and MGE in terms of the cumulative numbers of recorded severity and extent ratings for the coating to metal defects.

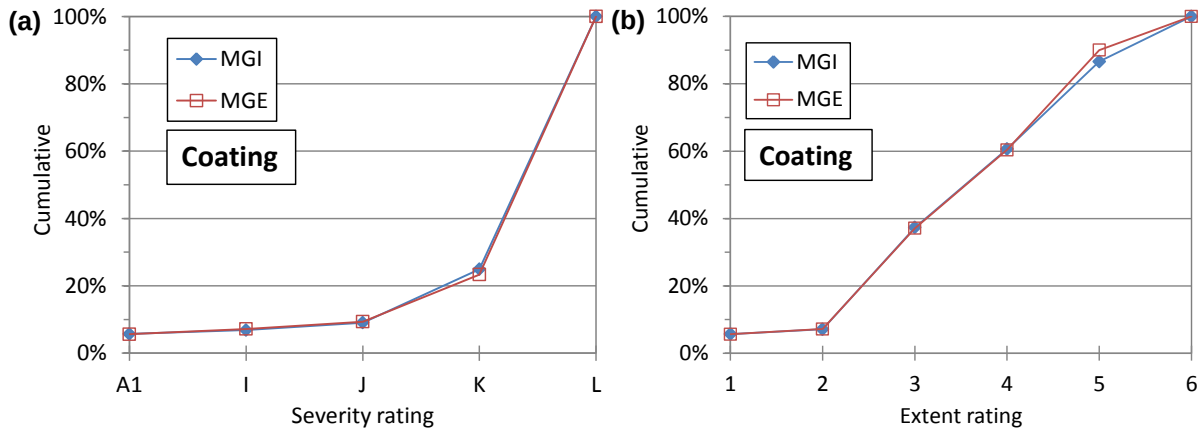

Figure 6-19: Cumulative distribution of 1st coating to metal defect for MGI/MGE

[(a) severity and (b) extent]

It is interesting to note that Figure 6.19a indicates that the majority of severity ratings for both MGI and MGE are associated with complete loss of coating to parent metal (see definition of category L in Table 6.6). This supports the assumption that, in general, coating reapplication would take place after a significant fraction of the element's surface area had been affected.

Figures 6.20a and 6.20b show a comparison between the cumulative number of exam records for MGI and MGE elements in relation to increasing severity and extent ratings, respectively, for their 2nd coating to metal defect.

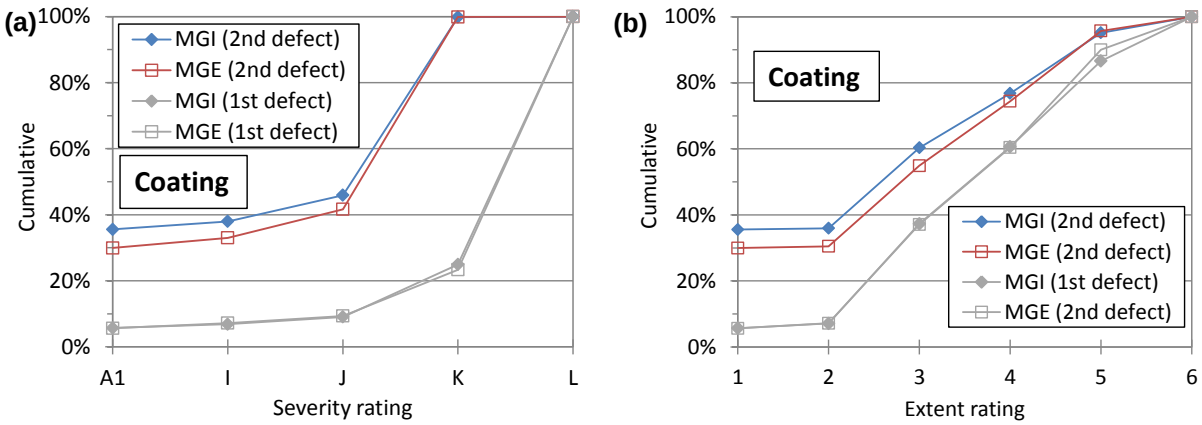

Figure 6-20: Cumulative distribution of 2nd coating to metal defect for MGI/MGE

[(a) severity and (b) extent]

Figure 6.20a shows that the 2nd coating to metal defect of MGE is associated with slightly lower values of severity rating values compared to MGI for severity categories A, I and J. Based on the definitions in Tables 6.5 and 6.6, these categories are associated with no damage (cat. A1) or superficial coating damage (cat. I and J) where no corrosion is observed (the metal beneath the coating is still protected against corrosion). However, overall the differences are relatively small.

Figures 6.21a and 6.21b show similar comparisons for LSI and LSE elements in relation to increasing severity and extent ratings, respectively, for their 1st metal defect. The results in Figure 21a indicate that the differences are insignificant. Moreover, it is interesting to note that more than 65% of severity ratings for both LSI and LSE fall within severity categories A to C (see Table 6.4). The results in Figure 6.21b indicate that there are insignificant differences between the percentages of LSI and LSE elements where no deterioration is observed (i.e. % of A1 ratings), while small differences are observed between LSI and LSE for extent rating 2. As the extent rating increases, it can be seen that a larger percentage of LSE elements is associated with the higher extent ratings 5 and 6, indicating that deterioration affects a larger portion of the elements' surface in comparison with LSI elements.

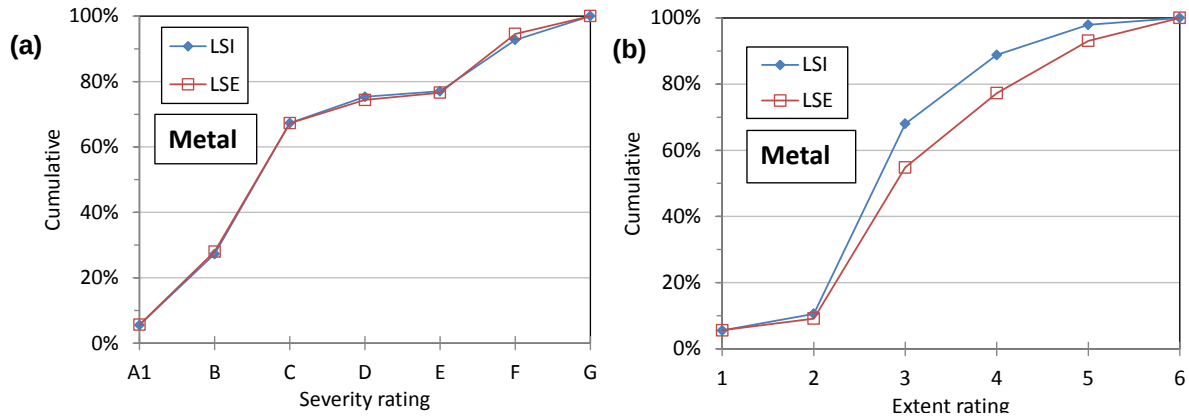

Figure 6-21: Cumulative distribution of 1st metal defect for LSI/LSE

[(a) severity and (b) extent]

Figures 6.22a and 6.22b show a comparison between the cumulative number of exam records for LSI and LSE elements in relation to increasing severity and extent ratings, respectively, for their 1st coating to metal defect.

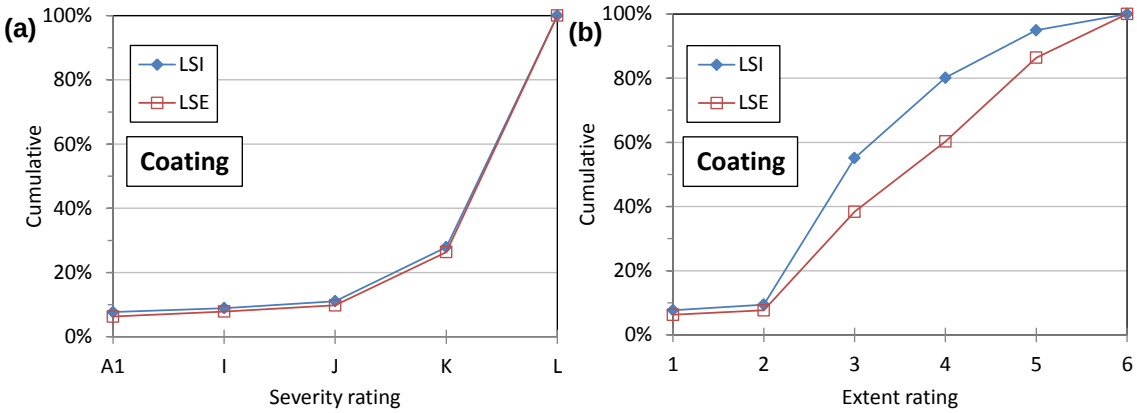

Figure 6-22: Cumulative distribution of 1st coating to metal defect for LSI/LSE

[(a) severity and (b) extent]

The results in Figure 6.22a indicate that there are minor differences between LSI and LSE in terms of the severity rating distribution for the coating to metal defects. Similarly to the corresponding diagrams for MGI/MGE, the results in Figure 6.22a indicate that the majority of severity ratings for both LSI and LSE are associated with complete loss of coating to parent metal (see cat. L in Table 6.6). Looking at Figure 6.22b, the results indicate that there are minor differences between the percentages of LSI and LSE elements where no deterioration is observed (i.e. % of A1 ratings). As the extent rating increases, it can be seen that larger % of LSE elements are associated with higher extent ratings; this indicates that coating deterioration/loss affects a larger portion of the elements' surface in comparison with LSI elements.

Further comparisons between the cumulative number of exam records for XGI and XGE elements in relation to increasing severity and extent ratings, respectively, for their 1st metal defect, revealed that there are insignificant differences between them, with a slightly larger percentage of XGE elements being associated with higher severity rating compared to XGI (almost identical cumulative curves are obtained for XGI and XGE for the extent rating). A similar situation is observed when comparing their cumulative numbers of exam records of XGI-XGE for increasing severity and extent rating of the 1st defect in coating to metal.

The overarching conclusion from the above investigations seems to be that for a large metallic bridge population, the assumption that external elements are more likely to suffer from coating deterioration and corrosion loss is generally valid. More detailed analysis, involving the paired comparison of external and internal elements for specific bridges in different climatic/pollution environments would be needed in order to quantify this conclusion at a deeper level. For such an analysis it would be necessary to distinguish between external and internal elements (e.g. MGE and MGI) within specific bridge environments, which in turn would require an assessment of the bridge's geographical and environmental location.

Spatial-temporal analysis of deterioration

In this section, the inspection corrosion data for the most severe defect (i.e. 1st metal defect) are used to examine the spatial-temporal characteristics of deterioration. Starting with the categories shown in tables 6.4 and 6.5, a classification was developed to categorise the corrosion damage in terms of its temporal (emerging to advanced) and spatial (local to general) characteristics. This is shown in Table 6.10, where the contents of each cell are presented in relation to the alphanumeric codes resulting from the application of condition marking using tables 6.4 and 6.5.

Table 6.10: Spatial-temporal staging matrix

	No corrosion	**Emerging**	**Developing**	**Advanced**
No corrosion	A1	-	-	-
Local	-	B2, B3, C2	D2, D3	E2, E3, F2, F3
Spreading	-	B4, C3	C4, D4, C5	E4, F4
General	-	B5, B6	C6, D5, D6	E5, E6, F5, F6

Table 6.11 shows the spatial-temporal matrices developed using the proposed staging matrix of Table 6.10 by calculating the percentage of exam records corresponding to each cell. It should be noted that category G (tears, fracture, cracked welds, etc., see Table 6.4) is not considered in this section, since it refers to defects with a distinctly different characteristic compared to thickness loss due to corrosion.

As might be expected, within an ageing and diverse asset population subject to adverse, potentially worsening, environmental exposure/conditions, the most common categories are found to be in the intermediate stages, i.e. emerging/developing corrosion which is spreading spatially. However, it is interesting to note that at an advanced stage, local attack is much more prevalent than general. This tends to support the validity of the assumption made in developing the D2.3 [9] models that, in moving from condition to capacity based assessment, it is reasonable to carry out performance checks using sectional analysis at critical locations along an element's length.

Table 6.11: Spatial-temporal staging matrix for different minor metal elements

MGI	**No visible defects**	**Emerging**	**Developing**	**Advanced**
No visible defects	3.93%	-	-	-
Local	-	10.22%	6.34%	10.38%
Spreading	-	21.28%	31.33%	2.05%
General	-	5.16%	7.92%	1.39%

MGI	No visible defects	Emerging	Developing	Advanced

MGE	No visible defects	Emerging	Developing	Advanced
No visible defects	4.01%	-	-	-
Local	-	9.04%	5.76%	21.68%
Spreading	-	19.64%	26.16%	3.64%
General	-	4.00%	4.49%	1.58%

LSI	No visible defects	Emerging	Developing	Advanced
No visible defects	5.99%	-	-	-
Local	-	16.26%	5.91%	14.02%
Spreading	-	29.81%	19.13%	3.38%
General	-	2.41%	1.73%	1.36%

LSE	No visible defects	Emerging	Developing	Advanced
No visible defects	5.96%	-	-	-
Local	-	11.23%	4.26%	15.13%
Spreading	-	23.65%	22.35%	3.73%
General	-	7.34%	3.86%	2.48%

XGI	No visible defects	Emerging	Developing	Advanced
No visible defects	6.55%	-	-	-
Local	-	12.37%	5.42%	11.89%
Spreading	-	26.35%	24.21%	2.51%
General	-	3.80%	4.62%	2.28%

XGE	No visible defects	Emerging	Developing	Advanced
No visible	6.55%	-	-	-

MGI	No visible defects	Emerging	Developing	Advanced
defects				
Local	-	10.76%	6.93%	14.93%
Spreading	-	24.11%	23.47%	3.00%
General	-	3.34%	4.72%	2.17%

A test of independence using the chi-square test is performed to test the difference of spatial-temporal characteristics of deterioration between internal and external/end elements using the element pairs and the 10 possible categories for in which an element might be. Initially, Table 6.11 is converted to frequencies by multiplying the percentages by the total number of exam records for each element type and the expected values were calculated for each pair of internal-external/end elements. As previously mentioned, in all cases G defects codes are excluded from the analysis. Finally, chi-square values are calculated and comparisons are made with the table values of χ^2 distribution for the appropriate number of degrees of freedom at p = 0.01 level of significance. The results, which are summarised in Table 6.12, reveal that in all cases there is statistically significant difference at a high confidence level in the spatial-temporal patterns between internal and external/end elements.

Table 6.12: Summary of results for test of independence using chi-square

Element Pair	Total no. of exams (Int./Ext. elements)	Degrees of freedom	Calculated χ^2	Table value of χ^2 at p = 0.01 significance	Comment
MGI/MGE	46265/33639	9	2479.27	21.67	In all cases there is significant difference in the spatial-temporal patterns of the internal and external/end elements.
LSI/LSE	4109/3991		237.40		
XGI/XGE	12654/8559		85.64		

Quantification of corrosion defect size

In this section, the data is used to quantify the corrosion defect size in terms of average thickness loss (mm) by substituting the alphanumeric code with a single numerical value. Table 6.13 provides a summary of the proposed interpretation of the severity and extent ratings (see also Tables 6.4 and 6.5). As can be seen, where possible, for both severity and extent a median value has been assigned in lieu of the original intervals. Table 6.14 provides a summary of the resulting rating codes and their corresponding computed thickness losses.

Table 6.13: Interpretation of severity and extent rating

Severity	**(mm)**
A	0
B	0.5
C	3
D	7.5
E	10
F	full thickness of section
G	tears, fracture, cracked welds, etc.
Extent	**%**
1	0
2	Localised
3	2.5%
4	7.5%
5	30.0%
6	75.00%

As gleaned from Table 6.14, only a subset of the data is considered in this part of the study. Specifically, all defect codes with extent rating 2, which are termed localised (i.e. localised defects due to local circumstances, see Table 6.5), are excluded from the analysis. Similarly, defect codes G are not considered since they seem to be associated with damage unrelated to corrosion (e.g. fracture, cracked welds, etc. - see Table 6.5). Defect code A1 (i.e. no visible defects to metal, see Table 6.4 and 6.5) is also excluded from the analysis. Finally, defect codes F are considered separately, since the section thickness of individual elements is not known.

Table 6.14: Values of average corrosion thickness loss

(see also Table 6.13)

Rating code	**Thickness lost (mm)**
B3	0.0125
B4	0.0375
B5	0.1500
B6	0.3750
C3	0.0750
C4	0.2250
C5	0.9000
C6	2.2500
D3	0.1875

D4	0.5625
D5	2.2500
D6	5.6250
E3	0.2500
E4	0.7500
E5	3.0000
E6	7.5000

Table 6.15 summarises the statistical characteristics of thickness loss in different types of minor elements. These values have been calculated using only the number of exam records corresponding to the defect codes of Table 6.14.

Table 6.15: Median, mean and standard deviation of thickness loss (mm)

[in different metal minor elements obtained using all data years (1999-2013) available (see also Table 6.14)]

Metal element type	Median (mm)	Mean (mm)	Standard deviation
MGI	0.225	0.543	0.884
MGE	0.188	0.452	0.754
LSI	0.075	0.250	0.551
LSE	0.150	0.408	0.841
XGI	0.150	0.400	0.755
XGE	0.188	0.413	0.742
Notes: Ratings codes A (No visible defects to metal), F and G (tears, fracture, cracked welds, buckling, etc.) as well as codes with extent rating 2 (localised defect due to local circumstances) are not considered for the derivation of this table.			

For all element types, the results in Table 6.15 reveal that the corrosion loss distributions are asymmetric with the mean value considerably higher than the median. The standard deviation in all cases is quite high, leading to coefficient of variations well over unity. Moreover, the results show that MGI elements are associated with a higher mean thickness loss (mm) as well as greater variability compared to thickness loss calculated for MGE elements. The reverse situation is observed in the results obtained for LSI and LSE elements, where LSE elements are associated with a much higher mean thickness loss and much greater variability compared to LSI elements. Finally, small differences are observed in the results obtained for XGI and XGE elements; that is, XGE elements have a slightly higher value of mean thickness loss while XGI are associated with a higher variability compared to XGE elements.

Further comparisons are made between the pair of elements MGI-MGE, LSI-LSE and XGI-XGE in relation to severity category F. A much greater percentage of the exam records (more than double) fall within severity rating F for the MGE elements compared to MGI

elements in relation to both the 1st and 2nd metal defects; this can be clearly seen in Figures 6.17a and 6.18a, respectively as well as in Table 6.11. This indicates that external main girders are more susceptible to advanced thickness loss due to corrosion (loss corresponding to the full thickness of section). Although a similar trend is observed for the other element pairs LSI-LSE and XGI-XGE, the differences in these pairs are much smaller compared to those observed between MGI and MGE.

It should be noted that the influence of exposure conditions on the observed spatial-temporal patterns (section 6.6.4.2) as well as the magnitude of corrosion loss in different element types discussed in this section (see Table 6.15) was not examined since no information was readily available regarding the location of individual bridge assets. This could be part of a future study in which a link could be established between the exposure conditions of the bridge and the observed deterioration.

6.6.5 Concluding remarks

A statistical analysis of the extensive NR database from visual examinations on metallic bridge elements over a period of fifteen years has been undertaken and the following conclusions can be drawn in relation to the deterioration models developed for use in the LCAT tool:

- The type and location of an element within a bridge is significant in determining the likely corrosion deterioration
- External versus internal main girders seem to exhibit the most significant differences, with the former being more susceptible than the latter.
- The situation is more complex for longitudinal stiffeners and cross girders, though with the above trend being discernible in the majority of cases.
- In cases where corrosion has developed, a localised form seems to be more prevalent; it is therefore appropriate for LCAT purposes to base performance indicators on sectional models.
- For the elements considered, average corrosion losses are small (less than 1mm) but the potential variability is high.
- Coating deterioration can often extend beyond localised areas, which implies that re-coatings tend to be applied after exposure of relatively large surfaces has taken place.

The absence of information on bridge geographical location prevents any conclusions with respect to the effect of the surrounding environment on the corrosion characteristics. If such information could be tagged to the existing data, there would be significant scope for a statistical analysis that could quantify this important factor which has been included in the LCAT models. Furthermore, the material type (e.g. wrought iron, early steel, carbon steel, etc.) and bridge form type (e.g. detailing, corrosion traps, etc.) are factors which may potentially affect the observed rate and patterns of deterioration. Finally, methods to explore the rate of deterioration by analysing element subsets with more than two inspection results can also be pursued. However, it is believed that this would yield potentially useful results only if the influence of the surrounding environment could be accounted for as well, otherwise the variability would be prohibitively high.

6.7 References

[1] ISO 12944 Paints and varnishes – Corrosion protection of steel structures by protective paint systems, 2000.

[2] ISO 4628 Paints and varnishes - Evaluation of degradation of coatings - Designation of quantity and size of defects, and of intensity of uniform changes in appearance, 2003.

[3] EN ISO 9223 Corrosion of metals and alloys - Corrosivity of atmospheres - Classification, determination and estimation, 2012.

[4] EN ISO 9224 Corrosion of metals and alloys - Corrosivity of atmospheres - Guiding values for the corrosivity categories, 2012.

[5] EN ISO 9226 Corrosion of metals and alloys - Corrosivity of atmospheres - Determination of corrosion rate of standard specimens for the evaluation of corrosivity, 2012.

[6] EN ISO 4624 Paints and varnishes - Pull-off test for adhesion, 2002.

[7] EN ISO 2409 Paints and varnishes - Cross-cut test, 2013.

[8] ML D2.2, MAINLINE Deliverable 2.2, Degradation and intervention modelling techniques, http://www.mainline-project.eu/Results,7.html

[9] ML D2.3, MAINLINE Deliverable 2.3, Time-variant Performance Profiles for Life-Cycle Cost and Life-Cycle Analysis, http://www.mainline-project.eu/Results,7.html

[10] NR. (2010), “Handbook for the examination of Structures Part 2C: Condition marking of Bridges”, NR/L3/CIV/006/2C, Network Rail, UK.

7. Conclusions

This report focuses on the methodology developed within the MAINLINE project for validating performance profiles having been built in previous tasks for a variety of assets. The aim of this work is to scrutinise the methods adopted in previous tasks and deliverables, check and compare the theoretical deterioration profiles with real data and, hence, to ascertain the level of confidence that can be associated with model predictions.

Methodologies have been presented for the validation of time-variant performance profiles for the following railway asset types:

- Track (plain line)
- Soil cuttings
- Tunnels with concrete lining
- Metallic bridges

The sections of this report for the different asset types provide different levels of detail. In the case of Track, the validation of deterioration rates has been agreed to employ the track LCAT and hence is directly linked with the operation of the LCAT tool, as opposed to the underlying modelling assumptions, and is extensively covered in the WP5 deliverables (D5.5 report).

The validation on soil cuttings includes two stages. Firstly, a comparison of the designed SKM Algorithm (SKMA) to Network Rail's SSHI algorithm is done by implementing sensitivity and statistical analysis. A linear regression model is formulated and its results show a moderate correlation between SKMA and SSHI. In the second stage, a geotechnical desk study is undertaken to compare thirty typical soil cuttings case studies provided by Network Rail to theoretical performance profiles. The main conclusion was that in most of the cases data from case studies are inconsistent when compared with their corresponding performance profiles.

For metallic bridges, a comparison of two metallic bridges case studies to coating and corrosion profiles and a subsequent statistical analysis of Network Rail's data are undertaken. Results in relation to the deterioration models developed for use in the LCAT tool are varied depending on the location and type of element. In general, it is concluded that external vs. internal main girders seem to exhibit the most significant differences, with the former being more susceptible than the latter; the situation is more complex for other types of elements.

Finally, with respect to tunnels deterioration profiles, case studies on deterioration models for concrete tunnels regarding carbonation and chloride ingress are analysed. These case studies are based on data from Danish infrastructure. Based on the two case studies regarding chloride ingress in concrete, it may be concluded that the approach proposed in the MAINLINE project for calculating the chloride diffusion coefficient is suitable as a first approximation, e.g. when little data on the concrete composition, binder type etc. is available. The main conclusion of this study is that the MAINLINE approach for prediction of carbonation of concrete overestimates the actual carbonation depth. Another model, i.e. the *fib* model, was used for comparison and was concluded that it underestimates the actual carbonation depth.

8. Appendices

8.1 Appendix A – Soil Cuttings

8.1.1 SSHI Inspection Sheet with Parameters Scores

STABILITY INDICATORS FOR SOIL CUTTINGS	STABILITY INDEX PARAMETER	OBSERVED/MEASURED VALUE	REF CUT	EARTHWORKS FACTOR	ROTATIONAL	TRANSLATIONAL	EARTHFLOW	WASHOUT	BURROWING
Slope Geometry	Slope Angle and Slope Height	<15 degrees, <3m High	A1	L	0	0	0	0	0
		15 to <25 degrees, <3m High	A2	L	5	10	5	5	5
		25 to <35 degrees, <3m High	A3	L	10	20	15	10	10
		>35 degrees, <3m High	A4	L	40	50	20	15	20
		<15 degrees, 3m to <10m High	A5	M	0	0	0	0	0
		15 to <25 degrees, 3m to <10m High	A6	M	5	10	5	5	5
		25 to <35 degrees, 3m to <10m High	A7	M	10	20	15	10	10
		>35 degrees, 3m to <10m High	A8	M	40	50	20	15	20
		<15 degrees, >10m High	A9	H	0	0	0	0	0
		15 to <25 degrees, >10m High	A10	H	5	10	5	5	5
		25 to <35 degrees, >10m High	A11	H	10	20	15	10	10
		>35 degrees, >10m High	A12	H	40	50	20	15	20
	Slope angle adjacent to earthwork (i.e. Sidelong Ground)	(-)ve	B1		0				
		(+)ve <5 degrees	B2		3				
		(+)ve 5 to 15 degrees	B3		6				
		(+)ve >15 degrees	B4		9				
	Retaining walls 1m high or greater	None	C1		**0**	**0**			
		<1m high but>20m length	C2		**0**	**0**			
		No evidence of distress	C3		**0**	**0**			
		Minor distress (spalling, pointing etc)	C4		**10**	**10**			
		Cracking / evidence of lateral	C5		**35**	**35**			
		Evidence of Repairs	C6		**35**	**35**			
	Construction activity	None	D1		0	0			
		Removal of material from crest	D2		0	0			
		Addition of fill <1m high	D3		0	0			
		Addition of fill between 1m & 5m high	D4		10	5			
		Addition of fill >5m high	D5		20	10			
		Removal of material from toe	D6		20	20			
Minimum slope to track separation	Distance between sleeper ends and toe of cutting	Cutting cess width >6m	E1						**-70***
		Cutting cess width 3-6m	E2						**-25***
		Cutting cess width 1-3m	E3						
		Cutting cess width<1m	E4						
Adjacent Geology	BGS Geological Strata Shown within 0.2km of Earthwork limits (if more than one of these is present, use the cumulative score)	No drift	F0						
		Boulder Clay	F1		3	3			
		Blown Sand	F2				10	10	15
		Alluvium	F3		6	3	6	6	15
		Terrace Deposits	F4				3	3	10
		Sand and Gravel	F5				3	3	10
		Peat	F6				3	3	0
		Head Deposits	F7		9	9	6	6	0
		Laminated Clay	F8		9	9			
		Landslip	F9		20	20			
		Made Ground	F10						
		Solid							
		Manchester Marl	F11		3	3			
		Mercia Mudstone	F12		3	3			
		Shale/Mudstone Carboniferous	F13						
		Other Competent	F20						
Slope Crest	Width	Crest to boundary <1.5m	G1						
		Crest to boundary 1.5-3m	G2						
		Crest to boundary >3m	G3						

STABILITY INDICATORS FOR SOIL CUTTINGS	STABILITY INDEX PARAMETER	OBSERVED / MEASURED VALUE	REF CUT	EARTHWORKS FACTOR	ROTATIONAL	TRANSLATIONAL	EARTHFLOW	WASHOUT	BURROWING
Slope Composition at Crest	Predominant Material Type	Very Weak or Weak Rock	H1		0	0	0	0	0
		Coarse granular	H2		0	0	5	4	10
		Fine granular	H3		3	0	10	8	30
		Mixed granular/cohesive	H4		6	5	5	4	20
		Cohesive (low - intermediate plasticity)	H5		9	5	0	0	0
		Cohesive (high – very high plasticity)	H6		12	10	0	0	0
		Unknown	H7		8	5	5	4	10
Slope Composition at Toe	Predominant Material Type	Very Weak or Weak Rock	I1		0	0	0	0	0
		Coarse granular	I2		0	0	5	4	10
		Fine granular	I3		3	0	10	8	30
		Mixed granular/cohesive	I4		6	5	5	4	20
		Cohesive (low - intermediate plasticity)	I5		9	5	0	0	0
		Cohesive (high - very high plasticity	I6		12	10	0	0	0
		Unknown	I7		8	5	5	4	10
Associated Drainage	Slope face drainage conditions	Face dry	J1		0	0	0	0	
		Functioning drainage	J2		0	0	4	0	
		Blocked drainage	J3		5	5	8	6	
		Marshy areas on slope	J4		10	10	12	12	
		Surface issues on lower slope	J5		15	15	24	12	
		Surface issues on upper slope	J6		15	15	20	12	
	Drainage of adjacent land	None	K1		0	0	0	0	
		Natural water course within 20m of slope crest	K2		10	10	8	8	
		Artificial water course within 20m of slope crest	K3		0	0	0	0	
	Adjacent catchment size	>50 Ha	L1		0	0	9	9	
		10 –50 Ha	L2		0	0	6	6	
		1-10 Ha	L3		0	0	3	3	
		< 1Ha	L4		0	0	0	0	
	Adjacent catchment gradient	> 25^{o}	M1		0	0	10	20	
		5-25^{o}	M2		0	0	5	15	
		< 5^{o}	M3		0	0	2	5	
		Slopes away from structure	M4		0	0	0	0	
	Catchment Surface	Rough Grass	N1				0	0	
		Grazed Pasture	N2				0	0	
		Ploughed	N3				2	2	
		Wooded/Large Scrub	N4				2	2	
		Other	N5				3	3	
		Residential	N6				5	5	
		Industrial/Hardstanding	N7				5	5	
	Catchment Geology	Permeable	P1				0	0	
		Impermeable	P2				5	5	
		Mixed	P3				2	2	

STABILITY INDICATORS FOR SOIL CUTTINGS	STABILITY INDEX PARAMETER	OBSERVED / MEASURED VALUE	REF CUT	EARTHWORKS FACTOR	ROTATIONAL	TRANSLATIONAL	EARTHFLOW	WASHOUT	BURROWING
Associated	Slope crest drainage	None Visible	Q1				5	10	
		French Drain	Q2				0	0	
		V Channel	Q3				0	0	
		U Channel	Q4				0	0	
		Size >0.25 m^2	Q5				0	0	
		Size 0.1m^2 to 0.25m^2	Q6				0	0	
		Size < 0.1m^2	Q7				0	0	
		Gradient <5^o	Q8				0	0	
		Gradient 5^0 to 15^0	Q9				0	0	
		Gradient >15^0	Q10				0	0	
		Free Draining	Q11				0	0	
		Partially blocked	Q12				5	10	
		Blocked	Q13				15	20	
	Slope Crest concentration features	Multiple Narrow – Well Defined	R1					10	
		Single Narrow – Well Defined	R2					20	
		Multiple - Shallow	R3					5	
		Single - Shallow	R4					10	
		None	R5					0	
	Slope erosion	Multiple – well defined	S1					**70**	
		Multiple – poorly defined	S2					**30**	
		Single – well defined	S3					**30**	
		Single – poorly defined	S4					**20**	
		None	S5					**0**	
	Cess Drainage	None	T1		3	3	3	3	
		Present clear running	T2		0	0	0	0	
		Present unknown condition	T3		0	0	0	0	
		Flooding apparent	T4		6	6	6	6	
		Blocked/Impaired	T5		10	10	10	10	
Movement Indicators (Overall Failure)	Slope form of Earthwork	Uniform toe	U1		**0**	**0**	**0**		
		Terracing in midslope	U2		**10**	**10**	**5**		
		Hummocky ground in midslope	U3		**10**	**10**	**5**		
		Toe bulging	U4		**25**	**25**	**15**		
		Uniform Crest	U5		**0**	**0**	**0**		
		Stepped Crest	U6		**30**	**30**	**15**		
	Geomorphology of Adjacent Land	Deep-seated landslips	V1		30	30			
		Hummocky Ground / Solifluction Lobes	V2		10	10			
		No Significant Features	V3		0	0			
	Track Movements (vis. to naked eye)	Track Heave	W1		**70**		**70**		
		No Significant Features	W2		**0**		**0**		
	Attitude of mature trees / fence lines / signals	Vertical	X1		**0**	**0**	**0**		
		Random	X2		**0**	**0**	**0**		
		Bent tree trunks (convex upslope)	X3		**0**	**0**	**0**		
		Bent tree trunks (convex downslope)	X4		**10**	**10**	**6**		
		Predominantly tilted downslope (<10 degrees off vertical)	X5		**10**	**10**	**6**		
		Predominantly tilted downslope (>10 degrees off vertical)	X6		**10**	**10**	**6**		
		Tilted upslope near cutting crest	X7		**10**	**10**	**6**		

STABILITY INDICATORS FOR SOIL CUTTINGS	STABILITY INDEX PARAMETER	OBSERVED / MEASURED VALUE		REF CUT	EARTHWORKS FACTOR	ROTATIONAL	TRANSLATIONAL	EARTHFLOW	WASHOUT	BURROWING
Movement Indicators (Overall Failure)	Cracking	None		Y1		**0**	**0**			
		Random orientation		Y2		**4**	**4**			
		Persistent and Parallel to slope crest								
		Width (mm)	Vertical							
		<10	<30	Y3		**15**	**15**			
		<10	>30	Y4		**30**	**20**			
		10 to 50	<30	Y5		**25**	**30**			
		10 to 50	>30	Y6		**40**	**35**			
		>50	<30	Y7		**35**	**45**			
		>50	>30	Y8		**50**	**50**			
	Mass movements	None		Z1			**0**	**0**	**0**	
		Slope wash		Z2			**0**	**7**	**30**	
		Soil creep movements		Z3			**0**	**0**	**0**	
		Local slumping at slope face		Z4			**10**	**30**	**0**	
		Transitional Failure		Z5			**60**	**0**	**0**	
		Rotational failure		Z6		**60**	**0**	**0**	**0**	
	History of instability	None		AA1		**0**	**0**	**0**	**0**	**0**
		Presence of piezometers, slip indicator tubes / inclinometers		AA2		**70**	**70**	**0**	**0**	**0**
		Regular maintenance required		AA3		**70**	**70**	**70**	**70**	**20**
		Counterfort Drains		AA4		**30**	**30**	**15**	**0**	**0**
		Previous failure		AA5		**25**	**25**	**10**	**10**	**0**
	Mining / Removal of Support	Known mining area		BB1		10	10			10
		No Significant Features		BB2		0	0			
Animal Activity	Burrows	None observed		CC1		0	0	0	0	**0**
		Occasional Rabbit (<10 burrow holes /20m^2)		CC2		4	4	0	2	**45**
		Occasional Fox / Badger (<3 burrow holes /50m^2)		CC3		8	8	0	4	**45**
		Frequent Rabbit (>10 burrow holes /20m^2)		CC4		8	8	0	4	**45**
		Frequent Fox / Badger (>3 burrow holes /50m^2)		CC5		12	12	0	6	**50**
Vegetation	Tree Cover	Absent		DD1					4	
		Saplings but no mature trees		DD2					2	
		Occasional mature trees (<10 trees /20m^2, on slope angles of <25degrees		DD3					0	
		Occasional mature trees (<10 trees /20m^2 on slope angles of >25degrees		DD4					0	
		Frequent mature trees (>10 trees /20m^2) on slope angles of <25degrees		DD5					0	
		Frequent mature trees (>10 trees /20m^2) on slope angles of >25degrees		DD6					0	
	Ground Cover	Bare areas		EE1				4	4	
		Hydrophilic		EE2				8	8	
		Sparse grass / bramble cover		EE3				0	0	
		Dense grass / bramble cover		EE4				0	0	
		Dense shrubs / bushes		EE5				0	0	

8.1.2 The RT065 SSHI > SKMA Conversion Process

The 61 individual steps applied to transform the SSHI scores to SKMA outputs are as follows:

Step	Query	Description
Note:	*The next queries are contained in Microsoft Access "140202 - SSHI to SKMA Inputs Conversion" database*	
1-18.	Qry_001_DataReturned (A) – Qry_018_DataReturned (EE)	Each of these queries processes a single SSHI input parameter. Its scope is to transforms the format of the SSHI input parameters (A-EE) from text to binary. Each of these queries combines the parent RT065_SSHI_Cutting_2012 table and ancillary summary ones. Note that in cases of type mismatch in the expression, auxiliary fields of the parent table were used to facilitate the process. Also, note that these 18 queries do not transform the format of the movement parameters since this information partially exists in the parent and child tables and thus special process is required. Finally, these 18 summary tables were exported to Microsoft Excel, filled with "0/1" depending if the feature exist or not and then reimported as the Breakout_name_of_parameter(x) tables.
19.	Qry_020_1st_Half_ParentTable	This query joints half of the derived 18 tables to combine the new binary format of the SSHI input parameters into one new table. MAPINFO_ID has been introduced as the unique identifier. Note that the process is done in two steps since it is too complex for Microsoft Access to process so many fields from sub-queries in one query. Finally, the tables of this query are joined with the lookup table of Query 51 (see below) to make sure that no duplicate IDs have been carried forward.
20.	Qry_021_2nd_Half_ParentTable	The second part of the previous process: Same logic is followed and this query joints the second half of the initial 18 queries. MAPINFO_ID was selected as the unique identifier of that query.
21.	Qry_030_Line_MI_Items	The next set of queries do the same process but for the SSHI movement parameters (U, W, Y, Z). This Group By query aggregates all the unique combinations of movement indicator items of the RT065_SSHI_Cutting_Movement_Indicator_2012_Lin

Step	Query	Description
		e table. The purpose of this query is to make summary tables having all the combinations of movement parameters that would later help us transforming that data. Again, similar process for summary tables is followed: The table is exported to Microsoft Excel, filled with "0/1" and reimported as the Breakout_Line_MI_Items table.
22.	Qry_031_Line_MI_Observed	Similarly, this Group By query aggregates all the unique combinations of observed movement factors of the RT065_SSHI_Cutting_Movement_Indicator_2012_Line table. The summary table is exported to Microsoft Excel, filled with "0/1" and then is reimported as the Breakout_Line_MI_Observed table.
23.	Qry_032_Point_MI_Items	In the same way, this Group By query aggregates all the unique combinations of movement indicator items of the RT065_SSHI_Cutting_Movement_Indicator_2012_Point table. The summary table is exported to Microsoft Excel, filled with "0/1" and then is reimported as the Breakout_Point_MI_Items table.
24.	Qry_033_Point_MI_Observed	Finally, this query aggregates all the unique combinations of observed movement indicators of the RT065_SSHI_Cutting_Movement_Indicator_2012_Point table. The summary table is exported to Microsoft Excel, filled with "0/1" and then is reimported as the Breakout_Point_MI_Observed table.
25.	Qry_040_Line_MI	This query combines the Breakout_Line_MI_Items table and the Breakout_Line_MI_Observed table and aligns their results. In the design of that, an IF statement ensures that for a record that information simultaneously exists in the Breakout_Line_MI_Items table and Breakout_Line_MI_Observed table, the worst (maximum) data is taken forward.
26.	Qry_041_Point_MI	Likewise, this query does the same but for the RT065_SSHI_Cutting_Movement_Indicator_2012_Point table.

Step	Query	Description
27.	Qry_042_LineAndPoint_MI_UnionAll	This UNION All query combines the result sets from Qry_040_Line_MI query and Qry_041_Point_MI query. Note that the RT065_SSHI_Cutting _Movement_ Indicator_2012_Line and RT065_SSHI_Cutting_ Movement_Indicator_2012_Point table have the same number of output fields, in the same order, and with the same or compatible data types. When the union query is run, data from each set of corresponding fields is combined into one output field, so that the query's output has the same number of fields as each of the select statements.
28.	Qry_043_LineAndPoint_MI_GroupBy	This aggregate query group by all the fields created by the previous UNION query, removing all the duplicate records. In the case of a duplicate, a max criterion is set up to ensure that the worst (maximum) data is kept.
29.	Qry_044_Bring_all_2nd_half	This query attempts to put all the binary information of the second half of the SSHI input parameters' process (including movement indicators) together. MAPINFO_ID has been used as the unique identifier and the tables are combined with the lookup Query 51 (see below) to make sure that no duplicate IDs are carried forward. **Note**: This table along with that of query 20 were imported into Microsoft Excel and the combined one is called SSHI_065_Data_Results table. Then, VBA code was designed and run to calculate and return back SKMA scores for every record. Those results were stored into the 'SSHI vs SRV table. Both were imported in the Microsoft Access 140205 SSHI Case studies results database (see below).
30.	Qry_051_IDs_Use	This query identifies all the doubtful IDs by checking three criteria: a) Duplicate IDs b) unfeasible SSHI scores c) Null values for the Slope and Height Factor (SHF) input parameter For details of the logic, see the accompanying Microsoft Access file.
31.	Qry_069 DataCleansing_MI_records present (Z)	The next bunch of queries focus on data cleansing of each SSHI movement parameters. Each of these queries deals with one movement parameter and identifies the records that contain information in the parent table but not in the child ones. These records

Step	Query	Description
		are assumed untrustworthy. This query combines the RT065_SSHI_Cutting_2012 table with the RT065_SSHI_Cutting_Movement_Indicator _2012_Line table, the RT065_SSHI_Cutting_Movement _Indicator_2012_Point table and the specific every time hidden xLUP_RT065_SSHI_Cutting-Validate_Mass_ Movement table. ID and AssociateID are employed as unique keys.
32.	Qry_070 DataCleansing_MI_records present (Y)	Similarly, this query does the same process but for the Y movement parameter. The hidden table is changed accordingly.
33.	Qry_071 DataCleansing_MI_records present (W2)	Similarly, but for the W2 movement parameter. The hidden table is changed accordingly.
34.	Qry_072 DataCleansing_MI_records present (U)	Same, but for U movement parameter. The hidden table is changed accordingly.
35.	Qry_075 DataCleansing_MI_records_UnionAll	This UNION All query combines the result sets of the 4 previous queries. Each SELECT statement within this UNION query has the same number of fields and similar data types.
36.	Qry_076 DataCleansing_MI_records_GroupBy	This aggregate query removes duplicate rows from the previous UNION All query.
37.	Qry_077 DataCleansing_MI_records_Present	This make a table query load the results of the previous query in two new table called Tbl_MI_Present table and tbl_IDs_OmitBasedOnMIs, respectively. Both are imported into the 140205 SSHI Case studies results database.
38.	Qry_080 DataCleansing_MI_records not present (Z)	The next set of queries focus on the other side of the data cleansing of the SSHI movement parameters. Each of these queries deals with one movement parameter and identifies the records that DO NOT contain information in the parent table but do contain in the child ones. It has been assumed that such records are untrustworthy. This query combines the RT065_SSHI_Cutting_2012 table with the RT065_SSHI_Cutting_Movement_Indicator _2012_Line table, the RT065_SSHI_Cutting_Movement _Indicator_2012_Point table and the specific hidden

Step	Query	Description
		xLUP_RT065_SSHI_Cutting-Validate_Mass_Movement table. ID and AssociateID have been employed as unique keys.
39.	Qry_081 DataCleansing_MI_records not present (Y)	Likewise, this query does the same process as above but for the Y movement parameter. The hidden table is changed accordingly.
40.	Qry_082 DataCleansing_MI_records not present (W2)	Similarly, but for the W2 movement parameter. The hidden table is changed accordingly.
41.	Qry_083 DataCleansing_MI_records not present (U)	Same, but for U movement parameter. The hidden table is changed accordingly.
42.	Qry_084 DataCleansing_MI_records not present_UnionAll	This UNION All query combines the results of the previous 4 queries. Each SELECT statement within this UNION query has the same number of fields and similar data types.
43.	Qry_085 DataCleansing_MI_records not present_GroupBy	This aggregate query removes duplicate rows from the previous UNION All query. The new table called tbl_IDs_NotPresent_MIs and is imported in the 140205 SSHI Case studies results database.
Note:	*The next queries are contained in the Microsoft Access "140205 SSHI Case studies results" database*	
44.	Qry_030 All Data	This query combines the SSHI 065 Data Results table and the 'SSHI vs SRV table. It put all the results from the previous database plus that of VBA in Excel together. MAPINFO_ID is employed as the unique identifier.
45-55.	Qry_040 DataCleansing (B) – Qry_050 DataCleansing (CC)	The next set of queries undertakes further data cleansing of untrustworthy items in the records. Each of these queries deals with one SSHI input parameters (excluding movement indicators) and identifies all the records that the particular SSHI input parameter is missing. The SSHI input parameters that were considered are the following: B, D, G, H, I, K, Q, S, T, U, V, W, Y, Z, BB, CC.
56.	Qry_051 DataCleansing ALL	This query combines the results of the previous 10 queries. MAPINFO_ID is used as the unique identifier.
57.	Qry_060 DataCleansing_MI_Present	This query combines the two tables created on step 37 with the results from Qry_030 All Data query in

Step	Query	Description
		order to align the information from the first part of the data cleansing of movement parameters with that of the main table from Qry_030 All Data query. MAPINFO_ID is used as the unique identifier.
58.	Qry_061 DataCleansing_MI_Not_Present	Similarly, this query combines the table created on step 43 with the results from Qry_030 All Data query in order to put the former together with the main information. MAPINFO_ID is used as the unique identifier.
59.	Qry_062 DataCleansing_MI_All	This UNION All query combines the results from the previous two queries.
60.	Qry_063 DataCleansing_MI_All_GroupBy	This aggregate query removes duplicate rows from the previous UNION All query.
61.	Qry_031 DataCleansing (failure modes)	This query makes sure that there is not any record without information about any of the five failure modes of the SSHI score.
62.	Qry_070_SSHI Data_All	This query consolidates all the information from the previous data cleansing processes. So, it combines the results from the main Qry_030 All Data query with that of steps 56 and 60. Having done this, the initial table of records has been updated containing only the trustworthy items. Finally, this table is exported to Microsoft Excel for further statistical analysis.

8.1.3 VBA in Microsoft Excel

The VBA code that was used for the iterative process of producing SKMA scores from the SSHI dataset can be seen below:

```
Sub SSHI_Case_Studies()


Application.ScreenUpdating = False
Sheets("SSHI Input (List)").Select

Dim i As Double

For i = 1 To 51035

    Sheets("SSHI Input (List)").Select
    Range("start").Offset(1, 0).Value = i

    Range("select").Select
    Selection.copy
    Sheets("Results").Select

    Range("results").Offset(i, 0).Select
    Selection.PasteSpecial Paste:=xlPasteValues, _
    Operation:=xlNone, _
    SkipBlanks:=False, _
    Transpose:=False

Next i

Sheets("Results").Select

End Sub
```

8.2 Appendix B. Metallic Bridges – Case Study

8.2.1 Bridge 13322 – Ermelundsvej

Bridge 13322 carries two S-train tracks from Hillerød to Copenhagen. The bridge is a riveted steel deck from 1914 with a span of 15 m.

Below is a collection of pictures from last inspection in 2011. Next inspection is in 2016.

Below is a sketch showing ULS and FLS critical details that have been assessed as part of the load capacity assessment.

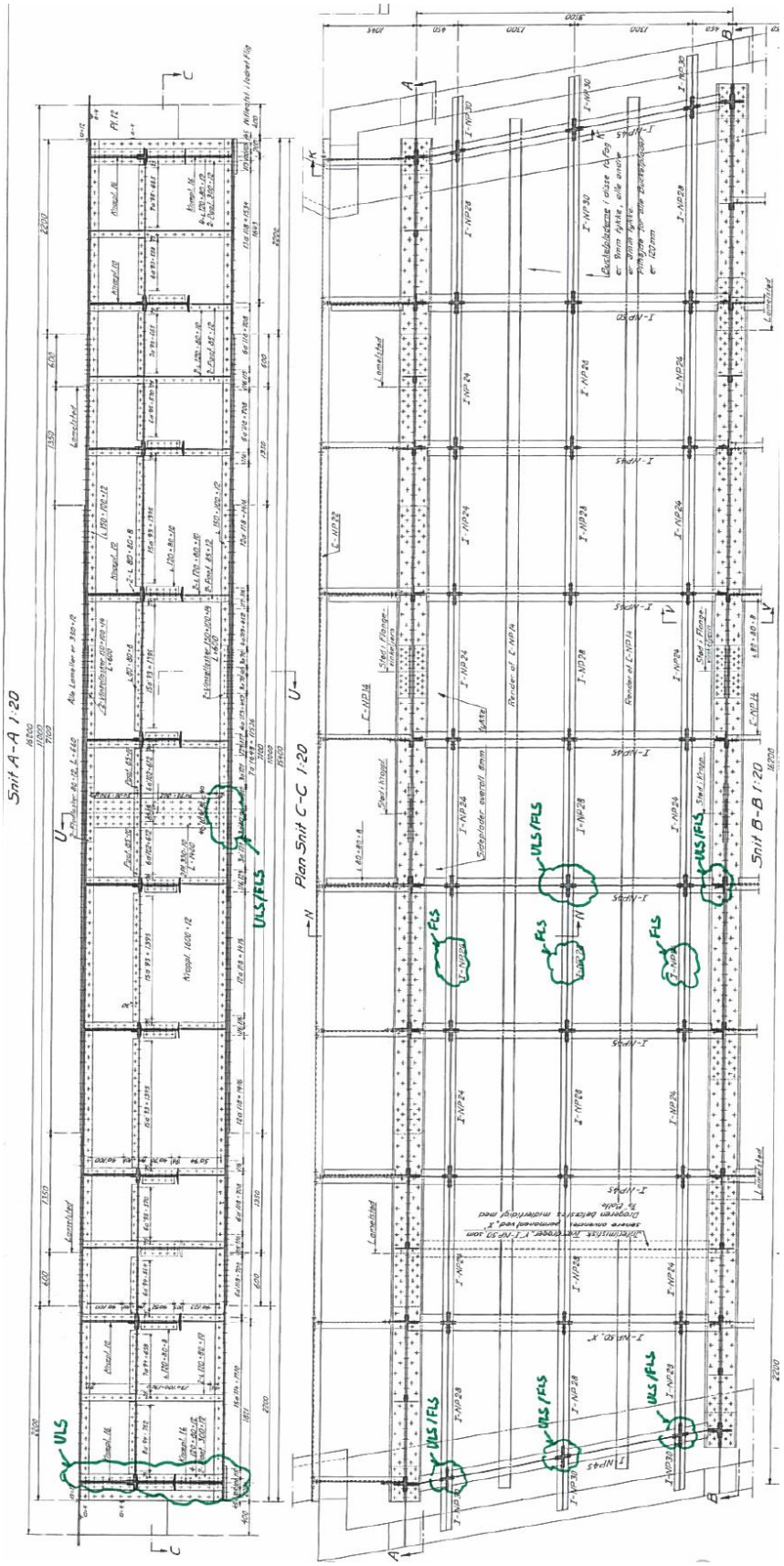

8.2.2 Bridge 11488.0.1 - Jernbane Alle

Bridge 11488 carries two S-train tracks from Frederiksund and Farum to Copenhagen. Bridge 11488.0.1 is the Northern of the two bridges. The bridge is a riveted steel deck from 1941 with a span of 19.35 m.

Below is a collection of pictures from 2014.

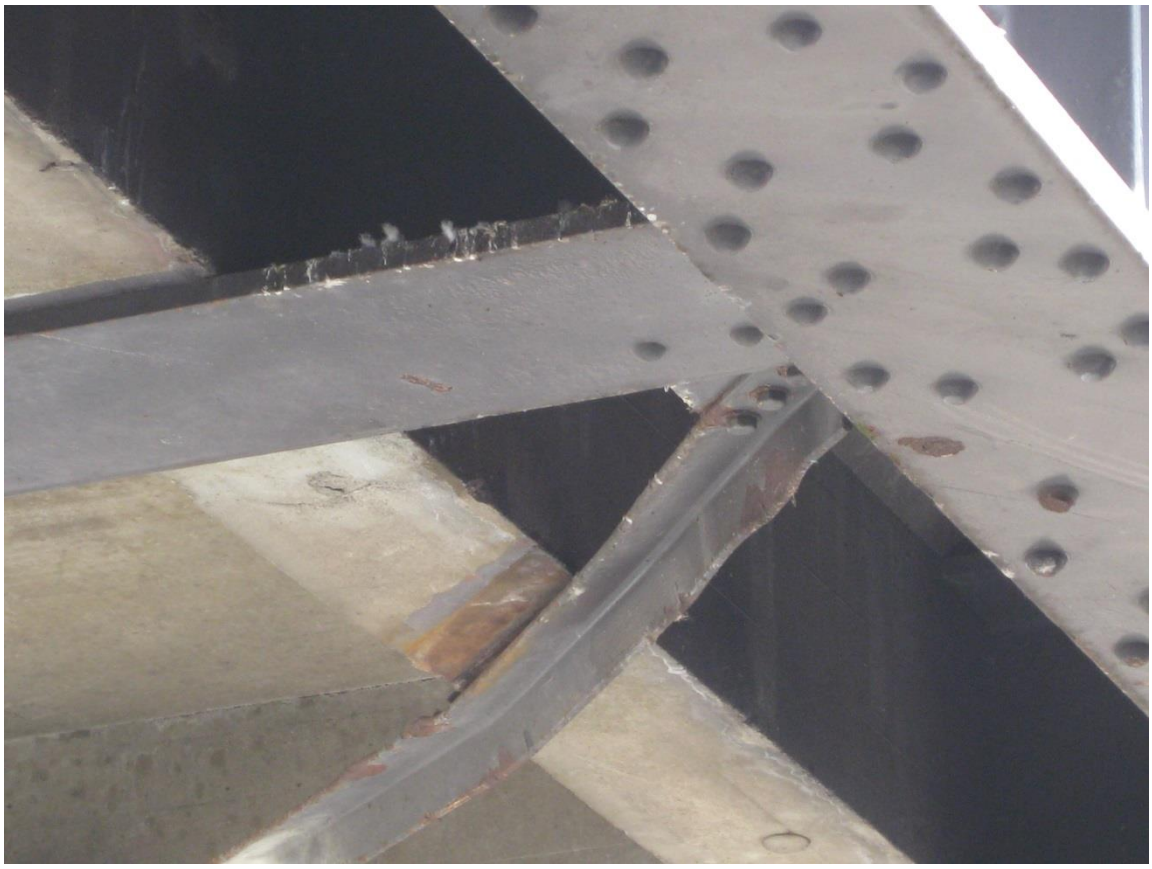

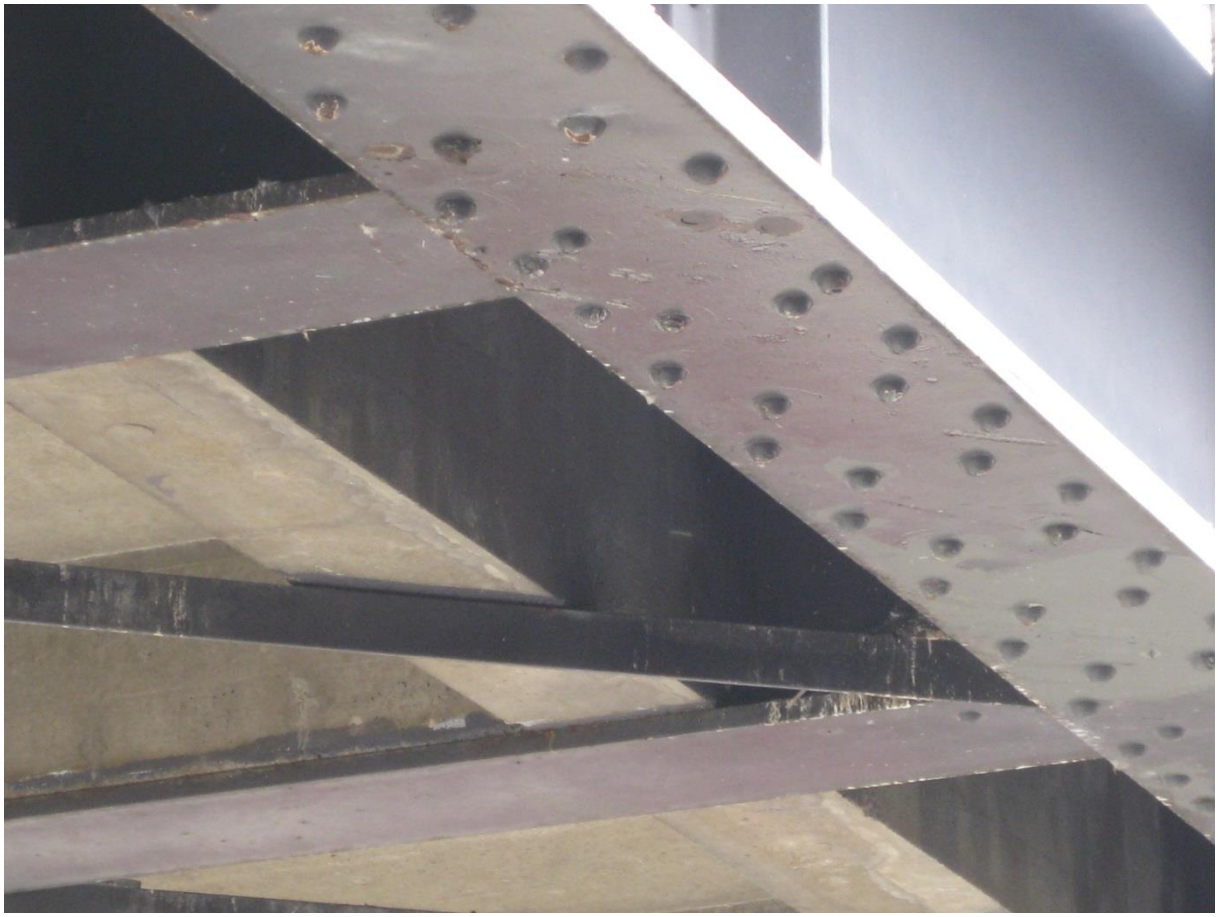

Below is a sketch showing ULS and FLS critical details that have been assessed as part of the load capacity assessment.

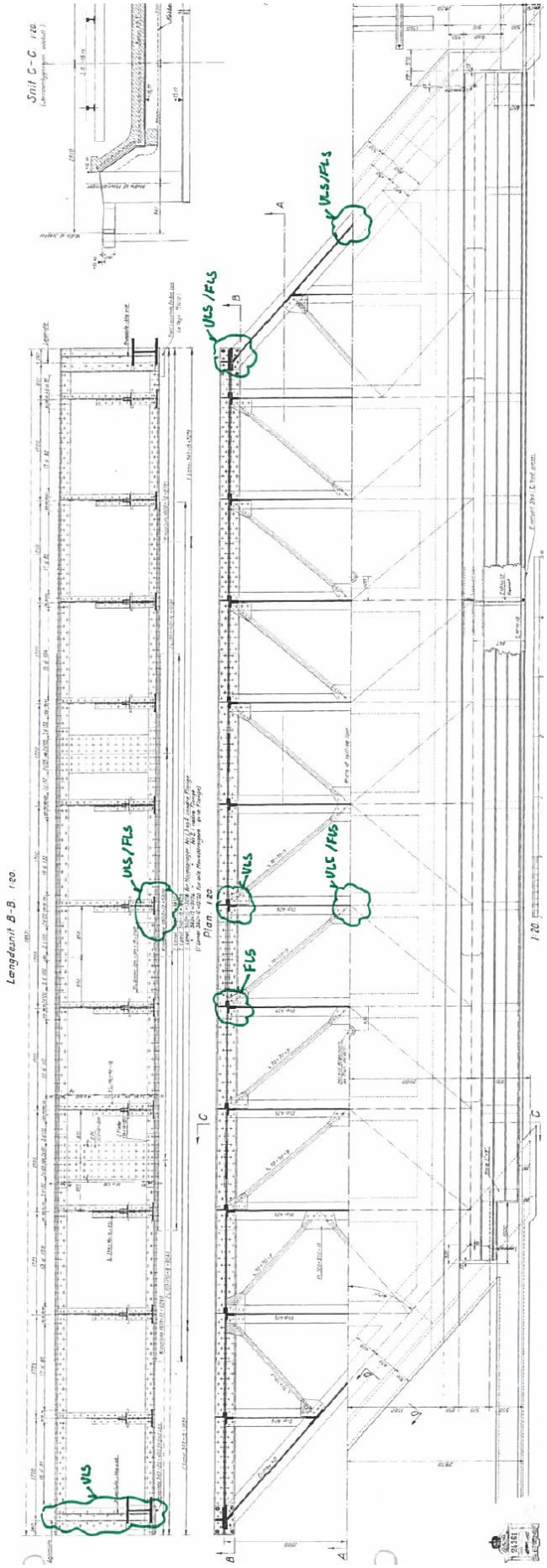
Snit C-C
ULS/FLS
ULS/FLS
ULS
ULS/FLS
ULS
ULC/FLS
FLS
ULS
Längsschnitt B-B
Plan

8.2.3 Performance profiles for Jernbane Alle

Below is a set of performance profiles for Jerbane Alle Bridge.

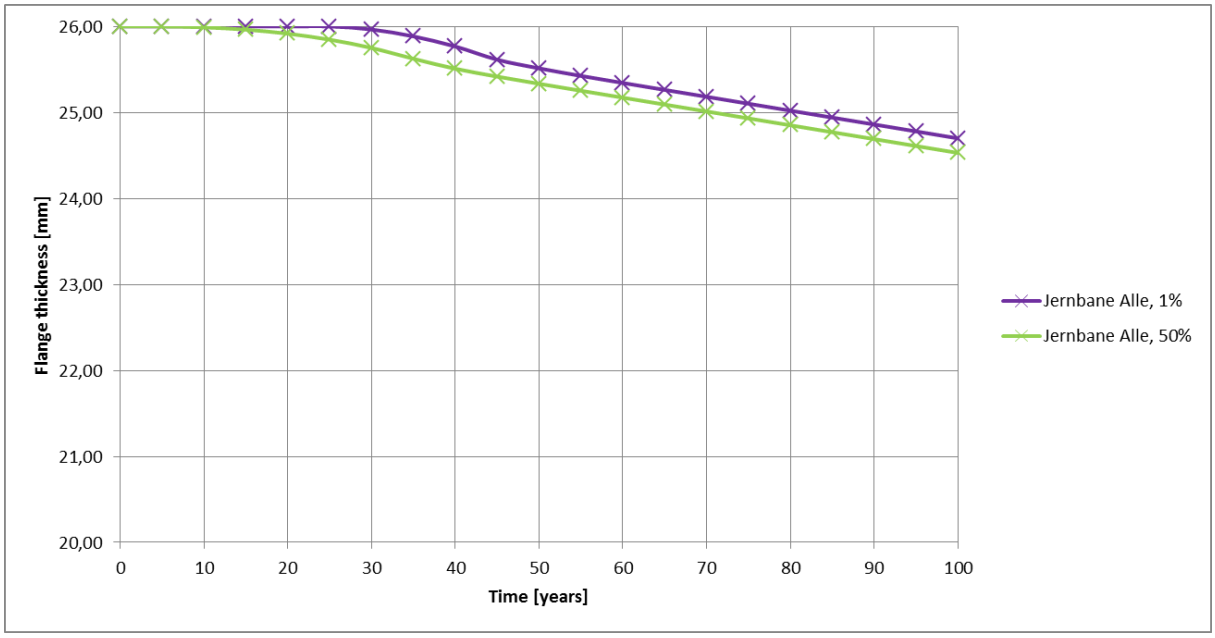

Cross girder (DIP 42½) flange thickness performance at Jernbane Alle bridge.

(Environment exposure according to corrosion category C3 has been assumed)

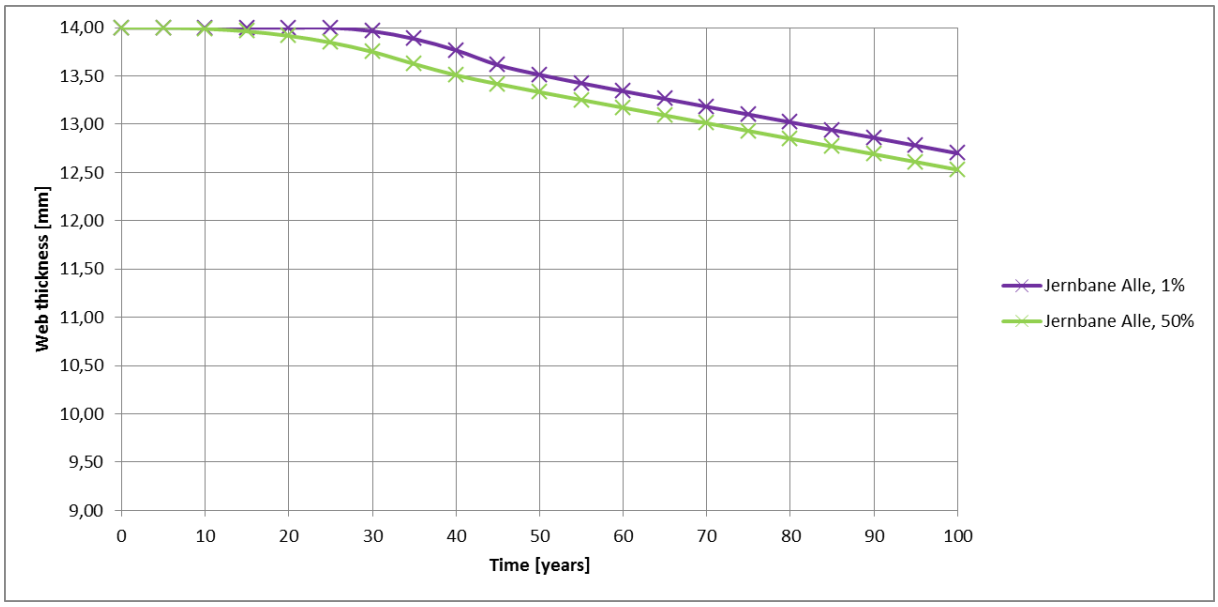

Railway girder (I DIP 42½) web thickness performance at Jernbane Alle bridge.

(Environment exposure according to corrosion category C3 has been assumed)

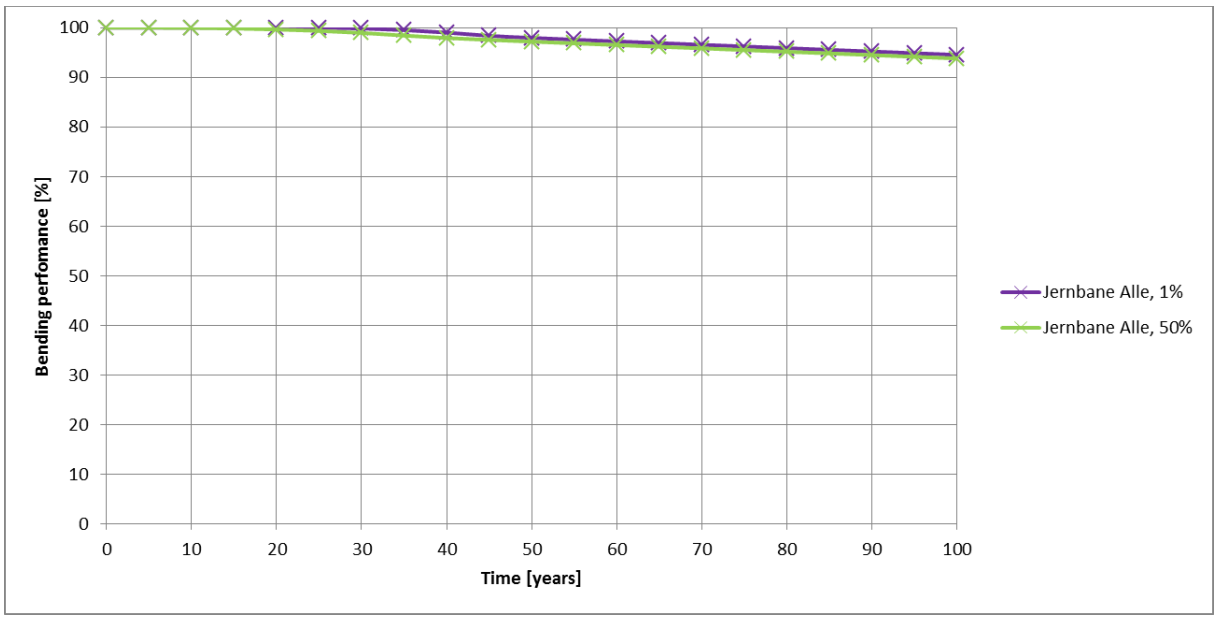

Cross girder (DIP 42½) bending performance at Jernbane Alle bridge.

(Environment exposure according to corrosion category C3 has been assumed)

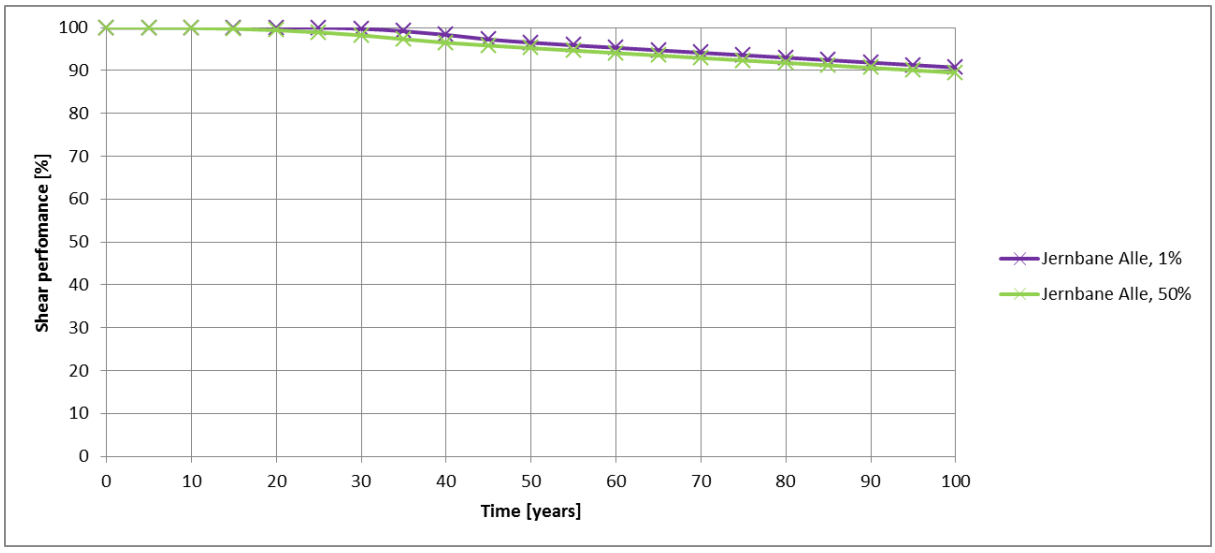

Railway girder (DIP 42½) shear performance at Jernbane Alle bridge.

(Environment exposure according to corrosion category C3 has been assumed)

8.3 Appendix C. Concrete Tunnels (SETRA, COWI, Surrey, NR)

8.3.1 Outline for D2.3 Performance Profiles for Concrete Tunnels

D2.3 (ML D2.3) presents the development of time-variant performance profiles concerning concrete lined tunnels based on time variable deterioration models.

Capacity performance over time is very complex to consider, therefore, only condition performance over time was addressed.

Tunnel concrete linings can undergo several types of degradation (steel reinforcement corrosion, swelling mechanisms, freeze-thaw attacks) which are now rather well known at least from a qualitative point of view (see descriptions in D2.2 (ML D2.2)).

Modelling the evolution with time of concrete remains a difficult task because of lack of simple time-variant performance models (i.e. not relying on heavy multi-chemo-physical numerical computations) for most of the mechanisms and the need for destructive tests for model calibration, which cannot be performed on a large number of assets.

As such, the present work focuses on the deterioration induced by the corrosion of steel reinforcements after introduction of aggressive agents such as carbon dioxide or chloride ions into the concrete cover.

The corrosion of reinforcing bars (rebars) can be separated into two phases:

- An initiation phase (Incubation)
  - The structure remains undamaged
  - Aggressive agents progressively penetrate into the concrete cover until the propagation front reaches the rebars (principally aggressive agents are carbon dioxide or chloride ions depending on the exposure conditions)
- A propagation phase starting once the aggressive agent front has reached the rebars
  - Leads to concrete cracking and spalling until a structural failure
  - This period can be divided in three sub-periods:
    - Time to corrosion induced cracking
    - Time to concrete spalling
    - Structural failure

Finally, for each phase and each deterioration mechanism, an analytical performance indicator has been proposed and several profiles could be drawn.

It remains difficult to quantify the effects of repair or protection on performance indicators unless the damaged rebars and concrete are completely replaced, which may allow raising the performance indicators to their initial maximum values, though partial recovery of performance may not be as simple to deal with.

8.3.2 Field Validation of Performance Profiles for Concrete Tunnels

Introduction

Following the reporting in D2.3 (ML D2.3) of simple models related to the deterioration of tunnel reinforced concrete linings due to the corrosion of steel rebars, the present chapter focuses on the preparation of performance profiles from real data. It should be noted that several performance profiles have been defined in D2.3 according to the fact that the corrosion phenomenon can be subdivided into successive phases: an initiation phase corresponding to the ingress of aggressive agents (carbon dioxide or chloride ion) into the concrete and a propagation phase, itself divided into a first phase leading to cracking, a second one leading to the end of the service limit state fulfilment, a third one leading to spalling and a last one leading to the structural failure (see Figure 8-1 of D2.3).

The present section of this chapter deals with the description of the methodology for performance profile construction including comments on the validity of the models proposed in D2.3 and information on data required to feed models to compare them to observations and measurements. It is worth recalling here that those models have not been selected according to arguments of physical precision and rigor, which would have required many chemo-physical parameters as well as heavy computation tools. Indeed, they have been chosen because of their simplicity of implementation into a spreadsheet and their dependence on a minimum set of parameters. This section also provides comments on the possible reasons of discrepancy between models and actual data. It concludes on the reasons of the difficulties encountered during the field data collection.

Performance profile for de-passivation due to carbonation

According to D2.3, carbonation occurs when carbon dioxide penetrates into the concrete cover and reacts with hydrates, especially portlandite. This acid-base reaction lowers the pH of concrete (initially around 13) and destroys the protective passive layer at the surface of the reinforcement when pH reaches 9 in the vicinity of the steel rebar. Corrosion products characterized by a molar volume greater than that of the consumed steel can then start propagating.

Recap of the models and comments on their validity

Many models of concrete carbonation have been proposed in the literature. A large review and references are presented in (AFGC 2007). The models are based on application of Fick's first law but differ from one another by the parameters taken into account (initial CSH (Calcium-Silicate-Hydrate) content, variable carbon dioxide diffusion coefficient, diffusion coefficient of water vapour, heat etc…), the simplifying assumptions concerning physicochemical mechanisms and the initial and boundary conditions. Table 8.1 (AFGC 2007) presents the parameters, hypotheses and limitations of different models.

The number of parameters and chemo-physical couplings increases with the complexity of the models. The most comprehensive ones aim at taking into account many chemo-physical phenomena and couplings at the microscopic scale as well as complex initial and boundary conditions but reaching a certain degree of sophistication requires resorting to numerical modelling. For example the LCPC-Carbo model (column 10 in Table 8.1) developed in (Thiery 2005a) takes into account porosity and saturation degree changes during carbonation, chemical kinetics (not instantaneous reactions) making the carbonation front non-stiff, material drying by Darcean transfer of the liquid phase and capillary effects. This model leads to a prediction of the pH field and thus the corrosion risk. Despite its very interesting capacities, this model cannot be selected for our purposes in MAINLINE since it

relies on a finite volume resolution which could not be implemented in the LCAT tool. Moreover some important parameters could be difficult to collect on actual structures (porosity fields before and after carbonation, saturation and pH initial fields, capillary pressure curves, kinetics parameters…).

Table 8.1: Models of carbonation with parameters

[hypotheses and limitations (AFGC 2007)]

Model	1 Ying-Yu	2 Papadakis	3 Miraghiotta	4 Al-Akchar	5 Bakker	6 Van Balen	7 Saetta	8 Sickert	9 LEO	10 LCPC-Carbo
Parameters taken into account										
-Chemical kinetics of $Ca(OH)_2$ carbonation				X		X	X	X		X
-Chemical kinetics of C-S-H carbonation										
-Diffusivity of CO_2	X	X	X	X	X	X	X	X	X	X
-Transport properties of water (water vapour, liquid water)					X	X	X			X
-Diffusivity of heat							X			
-Capillary pressure curve										X
Geometry										
-Monodirectional	X	X	X	X	X	X	X	X	X	X
-Bidirectional							X			
Couplings taken into account										
-Carbonation / Porosity			X					X		X
-Carbonation / Liquid water saturation										X
-Carbonation / Transport properties (CO_2, water)		X		X			X			X
-Carbonation / Microcracking										
-Relative humidity / Kinetics of $Ca(OH)_2$ carbonation						X	X	X	X	X
-Calcite formation / Kinetics of $Ca(OH)_2$ carbonation							X			X
-Carbonation / Hydration			X							
-Temperature / Carbonation						X	X			
Initial conditions										
-Initial $Ca(OH)_2$ content	X	X	X	X	X	X	X	X	X	X
-Initial C-S-H content		X	X							
-Initial C_3S content		X	X							
-Initial C_2S content		X	X							
-Degree of liquid water saturation (homogeneous)		X	X			X				
-Degree of saturation profile (non-homogeneous)							X			X
-Porosity (homogeneous)		X					X			X
-Porosity profile (non-homogeneous), allowance for skin concrete properties			X					X		
Boundary conditions										
-Variable relative humidity on outside					X		X			X
-Finite geometry (medium not necessarily semi-infinite)						X	X			X
-Temperature						X	X			
Model outputs										
-Stiff carbonation front	X	X	X		X			X	X	
-pH profile							X			X
-$Ca(OH)_2$ and $CaCO_3$ concentration profile				X		X	X			X
Domain of validity										
-Accelerated tests	X	X	X	X		X	X			X
-Natural carbonation (with wetting-drying cycles)					X		X	X	X	X

The model suggested in D2.3 was that of Papadakis (Papadakis 1991a, 1991b, 1991c). Its main hypotheses and limitations are the following:

- The model is one-dimensional. The penetration of carbon dioxide from two non-parallel boundary planes cannot be taken into account in this model.
- No carbon dioxide is present in concrete at initial time.
- The initial content of portlandite and other reactive materials is uniform.
- The concentration of carbon dioxide at the boundary is constant.
- Chemical reactions of carbonation are much faster than diffusion and are thus considered as instantaneous. This hypothesis leads to a sharp propagation front.
- The effective diffusion coefficient of carbon dioxide is uniform. As this property depends on the morphology of the porous phase as well as on the saturation degree, these parameters are implicitly also assumed uniform.
- The effective diffusion coefficient of carbon dioxide is constant over time. This means in particular that the progressive changes of the porous space due to calcium carbonate precipitation and the changes of the space left for gas diffusion due to water released by reacted hydrates are disregarded. It is only possible to consider that the constant diffusion coefficient is that resulting from the reduction of porosity after carbonation. However, such a choice would decrease the depth of the carbonation front compared to that obtained with the initial diffusion coefficient corresponding to higher porosity and would not therefore be conservative. This hypothesis also prevents from considering wetting-drying cycles although an adaptation can be found in Bakker's model (Bakker 1994).

Despite these limitations, this model is still being utilised in recent works (Thiery 2012) and engineering applications since it relies on a minimum number of physical parameters and simple analytical expressions. Indeed, for our purpose, it allows to express a performance indicator as a function of time *t*:

$$P_{dep}(t) = 1 - \frac{X_c(t)}{c_p} \text{ where } X_c(t) = K\sqrt{t} \qquad (8.1)$$

where $X_c(t)$ is the carbonation front depth and c_p is the thickness of the concrete cover (thickness between the external boundary, source of carbon dioxide, and the closest bed of steel rebars). The coefficient *K* is given by

$$K = \sqrt{\frac{2D_{CO_2}[CO_2]^0}{n^0_{Ca(OH)_2} + 3n^0_{CSH} + 3n^0_{C_3S} + 2n^0_{C_2S}}} \text{ often simplified in } \sqrt{\frac{2D_{CO_2}[CO_2]^0}{n^0_{Ca(OH)_2}}} \qquad (8.2)$$

where D_{CO_2} is the effective diffusion coefficient of carbon dioxide in the carbonated region (in m^2/s), $[CO_2]^0$ is the concentration of carbon dioxide in the outside air (i.e. at the boundary of the lining) per unit volume of the gas phase (in mol/m^3) and n^0_i is the apparent initial concentration of compound *i* (i.e. moles per unit volume of concrete in mol/m^3).

Comments about the effective diffusion coefficient

D_{CO_2} depends on the morphology of the porous phase as well as on the saturation degree (in relation with the relative humidity) and the temperature. As an initial approximation, (Papadakis 1991b) provides a simple expression:

$$D_{CO_2} = 1.64 \times 10^{-6} \times \phi_p^{c\,1.8} \times (1 - RH)^{2.2} \qquad (8.3)$$

where *RH* is the relative humidity and ϕ_p^c is the porosity of the carbonated paste (hydrated cement+water) in the concrete. The latter can be related to the porosity of carbonated concrete ϕ^c by means of the relationship (Papadakis 1991b):

$$\phi_p^c = \phi^c \left(1 + \frac{\frac{g\rho_c}{c\rho_g}}{1 + \frac{w\rho_c}{c\rho_w}} \right) \qquad (8.4)$$

with *g*, *c* and *w* respectively the weights of aggregates, cement and water per unit volume of concrete and ρ_g, ρ_c and ρ_w the corresponding respective densities. In a first approach, the porosity ϕ^c can be identified to the porosity of the sound concrete ϕ if the variation of porosity due to carbonation of the hydrates is neglected. To take the latter into account, (Papadakis 1991a) proposes the following relationship:

$$\phi^c = \phi - \left(n^0_{Ca(OH)_2} \times \Delta v_{Ca(OH)_2} + n^0_{CSH} \times \Delta v_{CSH} \right) \qquad (8.5)$$

where the variations in molar volumes due to respectively $Ca(OH)_2$ and CSH carbonations are given by

$$\Delta v_{Ca(OH)_2} = 3.85 \times 10^{-6} m^3.mol^{-1} \quad ; \quad \Delta v_{CSH} = 15.39 \times 10^{-6} m^3.mol^{-1} \qquad (8.6)$$

(8.5) relies on the hypothesis that all the initial contents of portlandite and CSH have been carbonated. As the initial CSH content should be very difficult to know in practice, the reduction of porosity predicted by (8.5) could be neglected. However, it remains important to mention it since the clogging effect due to the carbonation reaction products of molar volumes greater than those of the hydrates could affect the diffusion coefficient. Note that (8.5) is incomplete since other hydrates (ettringite, monosulfoaluminates, etc…) could also cause porosity variations. Moreover it has been recognized by several authors (Thiery 2005a, AFGC 2007) that the morphology of the porous domain, especially the distribution of pore sizes and throats, and consequently the transport properties were also affected by carbonation.

It should be emphasized here that (8.3) has been obtained in (Papadakis 1991b) following a regression analysis of experimental data of mortars and concretes with *w/c* ranging from 0.5

to 0.8, ϕ_p^c from 0.23 to 0.44, *RH* from 45% to 85% and *g/c*=0 or 3. The applicability of (8.3) to less porous concrete (*w/c*<0.5) is therefore not confirmed. From another regression analysis based on a subset of three concretes with *g/c*=3 from the same experimental data including sorption isotherm curves, the diffusion coefficient is expressed with respect to the concrete porosity ϕ^c and saturation level *S* in (Thiery 2005a):

$$D_{CO_2} = D_{CO_2}^0 \times \phi^{c\,2.74} \times (1-S)^{4.2} \text{ with } D_{CO_2}^0 = 1.6\times10^{-5} m^2 s^{-1} \text{ at T=25°C} \qquad (8)$$

The first comment arising from the expression (8.3) is that it depends on the porosity of hardened cement paste and therefore surprisingly not on the aggregate content (the relationship (8.4) introduces the latter but only in order to relate ϕ_p^c to ϕ^c). On the contrary, formula (8.7) provided by (Thiery 2005a) depends on the total porosity and therefore implicitly on the aggregate content, but it has apparently been calibrated only considering concretes with *g/c*=3 and not pure cement paste. Of course the presence of assumedly impermeable aggregates tends to increase the tortuosity (i.e. the path that particles have to cover across the gaseous phase of a porous concrete volume), so the effective diffusion would be expected to decrease with respect to the aggregate content and the relationship (8.3) could be questionable. Nevertheless it is argued in (Papadakis 1991b), from a reasoning based on concrete and mortar data with the same cement paste porosity, that the effect of aggregates can be more or less compensated by the presence of a high diffusive zone at the aggregate-paste interface called interfacial transition zone (ITZ). Indeed due to some wall effect, the porosity and then the local diffusion coefficient can be much higher in this zone of about tens of micrometres of thickness: see for example among many other references (Ollivier 1995) or (Sun 2011).

To illustrate quantitatively the argument of (Papadakis 1991b) on the role of the ITZ, an up-scaling calculation is proposed here. Let us first consider the dilute problem (see Figure 8.1) of an impermeable sphere of radius R_{agg}, surrounded by a thin layer of thickness e_{ITZ} and of diffusion coefficient D_{ITZ}, embedded in an infinite medium representing the cement paste matrix of diffusion coefficient D_{cp}. It is worth mentioning that the latter is itself an homogenized characteristic depending on the microstructure of the cement paste and the saturation degree. In order to estimate the effect of the "aggregate+ITZ" composite inclusion, remote boundary conditions represented as a macroscopic concentration gradient ***G*** are considered and the solution in terms of concentration gradient **grad***C* and diffusion flux **j** is calculated at any point of the domain. In particular, the average values of **grad***C* and **j** within the "aggregate+ITZ" composite write (Garboczi 1997):

$$<\mathbf{grad}C>_{agg+ITZ} = \frac{3(2\alpha+1)}{2(\alpha\beta+2\alpha-\beta+1)}\mathbf{G} \text{ and } <\mathbf{j}>_{agg+ITZ} = -D_{cp}\frac{3\beta(\alpha-1)}{\alpha\beta+2\alpha-\beta+1}\mathbf{G}$$

$$\text{with } \alpha = \left(1+\frac{e_{ITZ}}{R_{agg}}\right)^3 \text{ and } \beta = \frac{D_{ITZ}}{D_{cp}} \qquad (8.8)$$

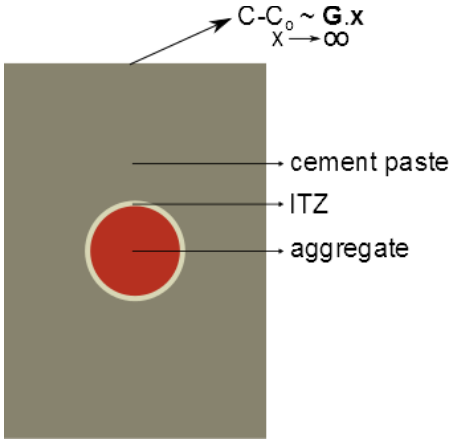

Figure 8-1: Dilute problem of the diffusion in an aggregate particle

(surrounded by an ITZ)

It is readily seen from (8.8) that the overall diffusive behaviour of the composite "aggregate+ITZ" boils down to that of the sole cement paste ($< \mathbf{j} >_{agg+ITZ} = -D_{cp} < \mathbf{grad} C >_{agg+ITZ} = -D_{cp}\mathbf{G}$) if and only if:

$$\beta = \frac{2\alpha + 1}{2(\alpha - 1)} \text{ i.e. } \frac{D_{ITZ}}{D_{cp}} = \frac{2\left(1 + \frac{e_{ITZ}}{R_{agg}}\right)^3 + 1}{2\left[\left(1 + \frac{e_{ITZ}}{R_{agg}}\right)^3 - 1\right]} \qquad (8.9)$$

Observing that the ITZ thickness is much smaller than the aggregate radius, α can be replaced by its Taylor expansion in (7.ITZ9) leading to

$$\frac{D_{ITZ}}{D_{cp}} \approx \frac{R_{agg}}{2e_{ITZ}} \qquad (8.10)$$

which is a result that can also be found in (Nguyen 2006a) or (Dormieux 2010) and allows to consider the ITZ as a two-dimensional domain of surface diffusion property $e_{ITZ}D_{ITZ}$. Taking for instance R_{agg}=5mm and e_{ITZ}=50µm, the ratio (8.10) becomes D_{ITZ}/D_{cp}=50. This order of magnitude may not be unrealistic considering the increase of porosity within the ITZ (Sun 2011).

If D_{ITZ} /D_{cp} does not exactly correspond to the ratio (8.9), the incorporation of a population of two-layer composite spheres "aggregate+ITZ" into a representative elementary volume of concrete (Figure 8.2) would lead to a decrease or increase of the effective diffusivity depending on the value of D_{ITZ} /D_{cp}. Homogenization schemes of random media can then be implemented.

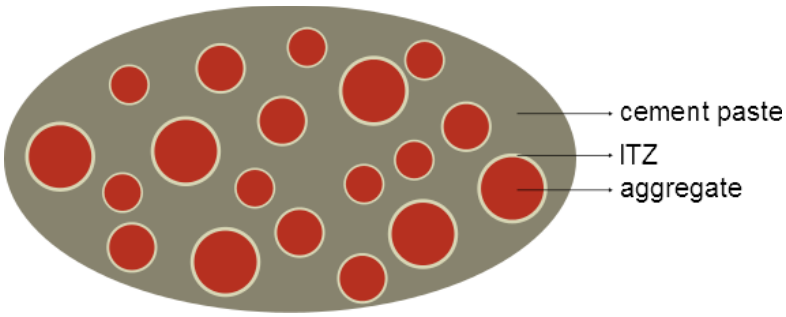

Figure 8-2: Representative volume element of concrete

For instance a Mori-Tanaka scheme is implemented in which the cement paste plays the role of the matrix embedding "aggregate+ITZ" composites (see details concerning such a scheme in (Dormieux 2006)). The calculation results in the following effective diffusion coefficient with respect to the coefficients α and β (8.8) and the aggregate volume fraction f_{agg}:

$$D^{\hom} = D_{cp}\frac{2\left[(2\alpha\beta-2\alpha-\beta-1)\alpha f_{agg}+\alpha\beta+2\alpha-\beta+1\right]}{(-2\alpha\beta+2\alpha+2\beta+1)\alpha f_{agg}+2(\alpha\beta+2\alpha-\beta+1)} \qquad (8.11)$$

It should be noted here that the same result would be obtained by implementing a generalized self-consistent scheme with a three-phase composite (aggregate, ITZ, cement paste) (Sun 2011), (Meshgin 2013).

Figure 8.3 plots the effective diffusion coefficient of concrete (8.14) (normalized by D_{cp}) versus the aggregate volume fraction for different values of D_{ITZ}/D_{cp} and R_{agg}/e_{ITZ}=100. As expected, the horizontal curve corresponds to the value obtained in (8.13), which is the case such that the presence of aggregates is exactly compensated by the increase of diffusion due to the ITZ. Figure 8.3 shows that D^{hom}/D_{cp} is rather sensitive to the ratio D_{ITZ}/D_{cp}. Therefore the hypothesis of equivalence between D^{hom} and D_{cp} from (Papadakis 1991b) relying on only one comparison between a mortar and a concrete may be questionable. Indeed some other experimental results in the framework of calcium leaching induced by diffusion (Nguyen 2008) confirmed by numerical models (Nguyen 2006b), show that the effect of large aggregates on the tortuosity may not be compensated by their ITZ although it could be the case for smaller inclusions as in mortars. This issue would probably deserve further investigations.

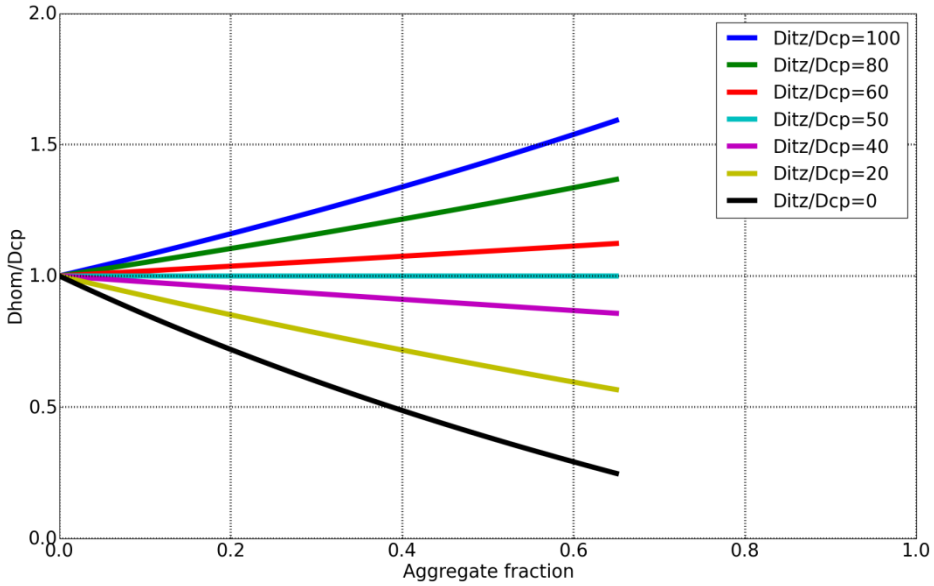

Figure 8-3: Normalized effective diffusion coefficient of a concrete vs aggregate fraction

[for different values of the diffusion coefficient of the ITZ]

Comments about the initial portlandite content

The initial portlandite content plays an important role in the carbonation process since it is considered as the main hydrate reacting with the carbon dioxide, which induces a pH decrease. This is why it appears in the expression (8.2). When no data can be obtained by means of sample analysis, (AFGC 2007) proposes an estimated calculation based on the mix design:

$$n^0_{Ca(OH)_2} = \sup(0\,;\, c \times f_{C_3S} \times \inf(1,(w/c)/0.418) \times 0.422 - s \times 0.617)/M_{Ca(OH)_2} \quad (8.12)$$

where c is the cement content per unit volume of concrete in kg.m^{-3}, f_{C3S} is the ratio of C_3S within the cement, w/c is the water-cement mass ratio, s is the silica fume or pozzolanic mineral addition content per unit volume of concrete in kg.m^{-3} and $M_{Ca(OH)_2}$ is the molar mass of portlandite.

Here are some comments about the figures appearing in (8.12) from (AFGC 2007):

- The coefficient 0.418 is the stoichiometric w/c ratio for the complete hydration of C_3S (Powers 1961). This means that (w/c)/0.418 corresponds to the ultimate hydration degree if the water content is less than the stoichiometry (w/c<0.418) and inf(1, (w/c)/0.418) to the final hydration degree in any case.
- The coefficient 0.422 is the proportion of portlandite formed per unit weight of C_3S which has been hydrated, assuming that 1 mole of reacted C_3S generates 1.3 mole of portlandite (Ollivier 2008). Indeed $0.422=1.3M_{Ca(OH)2}/M_{C3S}$ with the C_3S molar mass M_{C3S}=228g.mol^{-1}.

- The coefficient 0.617 represents the weight of portlandite consumed at about 28 days by the pozzolanic reaction (reaction rate close to 0.5).

Recalling the value of the molar mass of portlandite $M_{Ca(OH)_2} = 74 g.mol^{-1}$, (8.12) rewrites

$$n^0_{Ca(OH)_2} = \sup(0\,;\, c \times f_{C_3S} \times \inf(1,(w/c)/0.418) \times 5.69 - s \times 8.33) \qquad (8.13)$$

According to (AFGC 2007), the use of the estimate (8.12) should be restricted to CEM I cement. Moreover (8.12) relies on the hypothesis that C_3S would be the only anhydrous phase leading to portlandite, disregarding then other anhydrous phases such as C_2S, C_3A or C_4AF. Of course more sophisticated hydration models such as that proposed in (Thiery 2005b) could be exploited but it requires much more parameters and the resolution of a nonlinear equation system.

Typical values of the parameters needed by the model and description of a methodology for validation

The implementation of the model for concrete carbonation requires identifying a certain number of physical parameters for which typical values or ranges are provided in this section.

First of all, it is clear that the validation concerns the evolution of the depth of carbonation front $X_c(t)$ since the thickness of the concrete cover appearing in the performance indicator (8.1) is assumed to be known. This depth of carbonation is actually measured by destructive tests on core samples by means of a coloured indicator such as phenolphthalein for which the pH transition from pink to colourless is about 9 (RILEM Draft Recommendation, CPC-18 1984, CEN Report 2003, EN 14630 2007). If the carbonation front of a piece of structure is measured at different ages, then it is possible to estimate the factor *K* in (1) on a subset of the first available ages and check the validity of the ulterior evolution $X_c(t) = K\sqrt{t}$. Nevertheless, in any case and in particular if only one age of measurement is available, a model such as the one described in the previous section can be used to estimate *K*.

Among the parameters needed for the model, some concern the formulation of concrete and others concern the environmental data. The following table based on data from (AFGC 2007) proposes some classical formulations used in experiments.

Table 8.2: Examples of concrete formulations

Concrete	1	2	3	5	5
R_{mean} at 28 days [Mpa]	22	40	50	55	75
Cement mass / m^3 of concrete [$kg.m^{-3}$] *c*		300	353	410	461
Cement density [$kg.m^{-3}$] ρ_c	3100	3100	3100	3100	3100
w/c	0.84	0.62	0.49	0.48	0.32
Aggregate mass / m^3 of concrete [$kg.m^{-3}$] *g*	1906	1898	1936	1743	1833
Aggregate density [$kg.m^{-3}$] ρ_g	2600	2600	2900	2600	2050

Concrete porosity after carbonation ϕ^c	13.9%	10.9%	10.9%	9.6%	9.6%
$n^0_{Ca(OH)_2}$ from (8.15) assuming f_{C3S}=60% and s=0 kg.m^{-3} [mol.m^{-3}]	787	1026	1208	1403	1195
Relative humidity	75%	75%	75%	75%	75%
Cement porosity after carbonation ϕ^c_p	52%	39%	36%	29%	39%
D_{CO2} [m^2.s^{-1}]	2.4 10^{-8}	1.4 10^{-8}	1.3 10^{-8}	0.8 10^{-8}	1.4 10^{-8}

The formulations presented in Table 8.2 do not incorporate mineral additions consuming portlandite such as silica fumes or pozzolanic mineral addition appearing in (8.12). Typical values of the latter can range from 0 to 50kg per m^3 of concrete.

Typical values of the ratio of C_3S within the cement f_{C3S} needed to calculate $n^0_{Ca(OH)_2}$ in (8.12) range between 60% and 65% (Vichot 2008).

In absence of any indication about the concrete content, (AFGC 2007) suggests the values of $n^0_{Ca(OH)_2}$ presented in Table 8.3.

Table 8.3: Classes and limit values of $Ca(OH)_2$ content

Potential durability with regard to reinforcement corrosion	Very low	Low	Moderate	High	Very high
$Ca(OH)_2$ content (mass % relative to the cement) i.e. $n^0_{Ca(OH)_2} M_{Ca(OH)_2} / c$	<10	10-13	13-20	22-25	≥25

Environmental data are also required to calculate (8.6) and (8.2): the relative humidity *RH* and the concentration of carbon dioxide in the outside air $[CO_2]^0$.

A classification of the relative humidity *RH* into three classes is proposed:

- Dry: *RH*<65% (typically 50%)
- Moderate Humidity: 65%<*RH*<80%
- Humid, seldom dry: RH>80%

In normal conditions, $[CO_2]^0$ can be taken as 0.013mol.m^{-3}, corresponding to an environment containing 0.03% in volume of CO_2 at 20°C. Nevertheless (AFGC 2007) mentions that the volume fraction of CO_2 can be as high as 0.1%, which corresponds to 0.043mol.m^{-3}.

Especially in the case of large uncertainty with regard to some parameters, it is important not only to collect them but also to get some indications about the margins of error in order to

calculate an interval of penetration depth evolution. When data are missing, extreme values proposed in this section could be used. Actual data of penetration depth measured from sample cores can then be compared to the bounds of the interval at the corresponding time.

Possible reasons for discrepancies between the model and actual data

Comparisons between the model of Papadakis proposed in D2.3 and results obtained in laboratory following an accelerated carbonation test as well as results obtained in-situ during four years are presented in (AFGC 2007). Two types of concrete have been considered: a very porous one (C20, *w/c*=0.84) and a less porous one (C50, *w/c*=0.48). Whereas the model overestimates the depths of carbonation in laboratory, it is not the case with in-situ data. Indeed the model tends to underestimate the depths of carbonation for the more porous concrete and overestimate them for the less porous one (see (AFGC 2007) for more details). This example illustrates the difficulty to reach a reliable prediction of the carbonation depth from a simplified model relying on strong hypotheses and a limited set of parameters and involved chemo-physical phenomena. Many possible reasons can explain the discrepancies between the model and actual in-situ data:

- The effect of wetting-drying cycles is omitted in the model although an increase of the relative humidity could severely impede the propagation of the carbonation front.
- The effect of variation of the CO_2 concentration at the boundary is not considered either.
- The model does not take into account the variations of the microstructure during carbonation leading to a decrease of the porosity and a modification of the pore size distribution. It does not either take into account the release of water from hydrates subjected to carbonation, which increases the water saturation degree and reduces the space left for gas transfer. Neglecting these effects could make the model overestimate the front depth.
- The use of the simplified form of (8.2) assuming that only the carbonation of portlandite is responsible for the pH decrease may be too conservative, i.e. it also tends to overestimate the front depth whereas other hydrates may also play a role.
- The reliability of the expression (8.3) of the diffusion coefficient might be questioned. Indeed this expression has been obtained in (Papadakis 1991b) from data concerning three types of concrete of rather high porosity (*w/c*>0.5). There is no evidence that it still applies as such for less porous concretes.
- The expression (8.3) is very sensitive to the porosity and the relative humidity, so any uncertainty concerning those parameters may have a non-negligible influence on the diffusion.
- The hypothesis highlighted in (Papadakis 1991b) according to which the tortuosity induced by aggregates is exactly compensated by the presence of a very diffusive interfacial zone around the aggregate is questionable. Although this hypothesis is qualitatively acceptable, it is far from obvious that those effects are exactly opposite. Furthermore, the latter are expected to be very dependent of the concrete composition, introducing then another source of uncertainty in the model.
- The calculation of the initial portlandite content from (8.12) or (8.13) is based on restrictive assumptions. It assumes that only the C_3S hydration reaction produces portlandite although it is well known that other hydrates also play a role.

An alternative model

Because of the limitations of the previous model, it could be interesting to focus on an alternative, namely that given in *fib* Bulletin 34 for service life modelling. That model is based on extensive studies covered by the two research projects DuraCrete and DARTS. Further information about these projects is available in (Duracrete 2000), (DARTS 2004a) and (DARTS 2004b). The model has been prepared for probabilistic calculations of the carbonation depth as a number of the input parameters are given in terms of a distribution function with a mean value and a standard deviation.

The model for carbonation depth as function of time proposed in *fib* Bulletin 34 writes

$$X_c(t) = K\sqrt{t} \quad \text{with} \quad K = \sqrt{2\, k_e\, k_c\, (k_t\, R_{ACC,0}^{-1} + \varepsilon_t)\, C_S}\; W(t) \qquad (8.14)$$

where k_e [-] is the environmental function, k_c [-] is the execution transfer parameter, k_t is a regression parameter, $R_{ACC,0}^{-1}$ is the inverse effective carbonation resistance of concrete, ε_t is the error term, C_S is the CO_2-concentration and *W(t)* is the weather function. Determination of these input parameters is beyond the scope of this document, and guidance can be found in *fib* Bulletin 34 for service life modelling for their determination.

Performance profile for de-passivation due to chloride ion ingress

Chloride induced corrosion is a problem concerning most reinforced concrete structures subjected to seawater or de-icing salts. Even though it may not be the major cause of corrosion in railway concrete tunnels, de-passivation due to chloride ion ingress is still considered in this chapter because of potential local problems (proximity of seawater, presence of de-icing salts coming from overpassing roads…) or possible applications to other infrastructures such as railway bridges.

The aggressive action of chloride ions in contact with the steel rebars is different from that of carbon dioxide. Whereas the latter induces a pH decrease and a rather uniform production of corrosion, chloride ions are not consumed in the oxidation-reduction between steel and oxygen but play the role of catalyst and induce localised corrosion (pits). Two types of chlorides can be found in concrete: the free chlorides in ionic form in the interstitial solution and the chlorides bound to the solid phase (adsorbed or chemically linked in the cement matrix). Only the free ones play a role in the de-passivation process since they can reach the steel rebars. Chlorides present in concrete may have been introduced during the mixing or may have penetrated from outside. The motion of chloride ions in concrete is controlled either by diffusion within the liquid phase (requiring then a high saturation degree) or by capillary absorption and convection in the case of wetting-drying cycles.

Review of the models and comments on their validity

A large number of models of chloride ion front propagation are reviewed in (AFGC 2007). These models are classified according to several characteristics such as their principles of elaboration, their inputs and outputs, their advantages and disadvantages and the computer methods. Moreover the models are separated into two categories: empirical models relying on analytical or numerical solutions of Fick's second law or physical models based on a more or less complete resolution of chemo-physical equations including ion transport and interactions. Of course the latter seem out of reach for our purpose of simplicity. Among the

former, the model proposed in D2.3 allows to write the chloride front depth $X_d(t)$ under the form derived from the solution of the second Fick's law:

$$X_d(t) = 2\sqrt{D^{app}}\,\mathrm{erf}^{-1}\left(\frac{C_o - C^{crit}}{C_o - C_i}\right)\sqrt{t} \qquad (8.15)$$

where

- C_i is the initial free chloride concentration
- C_o is the chloride concentration at the boundary
- C^{crit} is the critical free chloride concentration reached at the depth $X_d(t)$
- D^{app} is the apparent chloride ion diffusion coefficient

The apparent diffusion coefficient depends on the effective diffusion coefficient D^{eff} (itself depending on the intrinsic chloride diffusion coefficient in water, the porosity, the saturation degree and the tortuosity of the concrete microstructure), the porosity ϕ, the bulk density of concrete in dry state ρ as well as the slope of the chloride-matrix interaction isotherm $\partial m_b / \partial C$ relating the mass of bound chlorides per unit mass of dry solid m_b to the free chloride concentration :

$$D^{app} = \frac{D^{eff}}{\phi + \rho\dfrac{\partial m_b}{\partial C}} \qquad (8.16)$$

The expression (8.15) relies on the following limitations:

- The model is one-dimensional. The penetration of chloride ions from two non-parallel boundary planes cannot be taken into account in this model.
- The initial content of chloride ion is uniform.
- The apparent diffusion coefficient is uniform and constant. This means that the effects of ageing or chemical interactions on the microstructure and consequently on the diffusive properties are not taken into account. Spatial heterogeneities are not taken into account either.
- The previous limitations implicitly assume that the effective diffusion coefficient, the porosity as well as the slope of the chloride-matrix interaction isotherm are considered as uniform and constant, although experimental results have shown that the relationship $m_b(C)$ is highly nonlinear for small values of C.
- The wetting-drying cycles are disregarded: the chloride concentration at the boundary C_o is constant and the effects on the diffusion properties are not taken into account.
- The acceleration of the ingress of the chloride ions due to interactions between the flow of OH^- and Cl^- is neglected.

These limitations could be overcome using numerical resolutions but are out of scope in the present work. Moreover they would need parameters which may remain difficult to collect. However, a modified form of (8.15) can be built from (AFGC 2007) and (*fib* bull. 34), taking advantage of results from DuraCrete and DARTS projects:

$$X_d(t) = \Delta x + 2\sqrt{D^{app}(t)}\,\mathrm{erf}^{-1}\left(\frac{C_{\Delta x} - C^{crit}}{C_{\Delta x} - C_i}\right)\sqrt{t} \qquad (8.17)$$

and

$$D^{app}(t) = D_{ns(mig)}\left(\frac{t_0}{t}\right)^a \exp\left(b_e\left(\frac{1}{T^{ref}} - \frac{1}{T}\right)\right) \qquad (8.18)$$

The expressions (8.17)-(8.18) deserve some comments.

The diffusion properties in the liquid phase are very sensitive to the saturation degree and therefore should decrease near the boundary (non-uniform diffusion coefficient) or vary during wetting-drying cycles (non-constant diffusion coefficient). Moreover such cycles modify the penetration of chloride ions by creating a convection zone near the surface. Consequently, the expression cannot really apply in this case. Two methods are proposed in (AFGC 2007): the first one consists in considering C_o as a fictitious equivalent chloride concentration at the boundary (greater than the real one) and the second one also presented in (*fib* bull. 34) consists in shifting the boundary condition to a depth Δx, which corresponds to (8.17) where $C_{\Delta x}$ denotes the value of the concentration at depth Δx.

$D_{ns(mig)}$ corresponds to the apparent diffusion coefficient at the reference time t_0 and temperature T^{ref} obtained by a migration test in non-steady-state conditions on a core sample in laboratory ((AFGC 2007) citing (Tang 1992) and (Tang 1996)).

The time dependence $(t/t_o)^a$ reflects the decrease of the diffusion coefficient due to changes in the microstructure (in relationship with the ageing behaviour of concrete).

The exponential term in (8.18) corresponds to the Arrhenius law allowing to take into account the influence of temperature. Indeed, laboratory experiments are performed at a temperature (293K) which can be very different from that of the structure.

The parameters $D_{ns(mig)}$, a and b_e involved in (8.17) and (8.18) are expected to depend on the cement composition and possibly supplementary cementing materials as well as actual exposure conditions. Some typical values of $D_{ns(mig)}$, a and b_e will be proposed in the next section.

If no laboratory test can be performed, an empirical analytical constant expression of D^{app} is proposed in (Vu 2000) citing (Papadakis 1996):

$$D^{app} = 0.15 D_{H2O}\left(\frac{1+\frac{w\rho_c}{c\rho_w}}{1+\frac{w\rho_c}{c\rho_w}+\frac{g\rho_c}{c\rho_g}}\right)\left(\frac{\frac{w\rho_c}{c\rho_w}-0.85}{1+\frac{w\rho_c}{c\rho_w}}\right)^3 \quad \text{with } D_{H2O} = 1.6\,10^{-9}\,m^2 s^{-1} \qquad (8.19)$$

The expression (8.19) takes into account neither time nor temperature or cement composition dependence and should *a priori* be used only to estimate an order of magnitude of D^{app} when no laboratory tests, providing $D_{ns(mig)}$ and allowing to use (8.18), are available. Nevertheless calculations from (8.19) will be compared to typical values of $D_{ns(mig)}$ in the next section.

It is interesting here to note that the influence of aggregate in the estimated chloride diffusion coefficient (8.19) is different from the estimated carbon dioxide diffusion coefficient. Indeed unlike (8.6), (8.19) shows a decrease when the aggregate content increases, which means that the latter actually play the role of obstacle against chloride ingress through an increase of the tortuosity. The possible diffusive path created by ITZ is not invoked here by the author contrarily to the case of carbon dioxide. A possible reason could be that the characteristic length of pores within the ITZ is greater than in the cement paste and consequently, in the non-saturated case, ITZ pores are filled more likely with gas than with water and therefore play a role in gaseous diffusion and not in liquid diffusion.

In simple models such as (8.15) or (8.17), interactions between ionic flows implying an increase of the diffusion coefficient with respect to the chloride ion concentration are often neglected. A modification of the diffusion coefficient is proposed in (AFGC 2007). It consists in multiplying the expression (8.18) by a factor α:

$$\alpha = 1 + \frac{1}{4C_o} \quad (C_o \text{ in mol.l}^{-1}) \qquad (8.20)$$

However this correction seems valid only for constant boundary conditions C_o.

Typical values of the parameters needed by the model and description of a methodology for validation

One major difference between carbonation and chloride ingress relies on the fact that in the first case the criterion of depassivation is rather well known whereas it seems less obvious in the second case. Indeed on the one hand carbonation-induced depassivation is due to the consumption of hydrates (principally portlandite) by CO_2 leading to a decrease of pH. Simple models such as the one proposed in the previous section are based on the assumption of instantaneous chemical reactions compared to the diffusion time and the criterion of depassivation corresponds to the complete acid-base reaction between hydrates and CO_2. On the other hand it is well recognized that the presence of chloride ions facilitates the depassivation process but the value of the critical chloride content remains an open question.

In (Angst 2009), a wide review of papers dealing with the critical chloride content is proposed. First this article indicates that, whereas the chloride content threshold can naturally be defined as the criterion of de-passivation, another more practical definition of this threshold is related to visible or acceptable deterioration of the structure, leading then to a higher value. (Angst 2009) also notes that the threshold can be expressed in two different manners: either by the free chloride content diffusing through water or by the total chloride content including both free and bound (adsorbed at the solid-fluid interface) ions. The latter manner (free and bound ions) is easier to identify by means of lab experiments whereas only free chloride ions are assumed to play a chemical role in the de-passivation of steel interface. The review of multiple sources in (Angst 2009) shows that the thresholds scatter over more than two orders of magnitude when expressed in terms of total chloride content and three orders of magnitude when expressed as a ratio between free chloride and hydroxyl concentrations. The authors explain those large scatterings by very different experimental techniques but also by chemo-physical factors which can be difficult to quantify: nature of steel and steel-concrete interface, pH value of the pore solution, electrochemical potential of the steel. However, the initiation criterion proposed by (Hausmann 1967) remains the most currently used especially in models:

$$\frac{C}{[OH^-]} \geq 0.6 \text{ i.e. } C^{crit} = 0.6 \times 10^{-14+pH} \qquad (8.21)$$

This criterion allows to take into account couplings with carbonation inducing a pH decrease. As often mentioned in the literature (AFGC 2004), for a non-carbonated concrete, the critical value (8.21) corresponds to a chloride mass concentration of approximately 0.4% relative to the cement mass.

The determination of the apparent diffusion coefficient needed in models is not an easy task. This parameter strongly depends on the microstructure (and thus on the cement content and concrete formulation). In the case of non-saturated conditions, it also depends on the water saturation since chloride diffusion occurs in the liquid phase. The best way to identify the diffusion coefficient for a given concrete is probably to resort to laboratory tests on samples (migration tests in non-steady-state conditions according to (AFGC 2007) citing (Tang 1992) and (Tang 1996)). It can also be identified from chloride profiles even in the case of wetting-drying cycles (de Cássia Silva 2004). Nevertheless, using chloride profiles to identify parameters may not be the best solution here as profiles should rather be used for a posteriori validations.

When no relevant results from laboratory tests can be obtained, some typical values of cement paste migration coefficient can be found in (*fib* bull. 34) for four cement types and six *w/c* values. Table 8.4 and Figure 8.4 present those results and the corresponding values of the empirical formula (8.19).

Table 8.4: Chloride apparent coefficients ($x10^{-12} m^2 s^{-1}$) of cement

[pastes from Papadakis' model (8.19) and chloride migration coefficients from samples from fib bull. 34 at 28 days and 20°C. The equivalent water cement ratio w/ceq takes into account the effect of fly ash (FA) or silica fume (SF) with their respective k-value (efficiency factor). The considered contents were: 22 wt.-% cement; SF: 5 wt.-%cement.]

w/c_{eq}	0.35	0.4	0.45	0.5	0.55	0.6
ρ_c	3.1	3.1	3.1	3.1	3.1	3.1
Papadakis model (8.22)	0.34	1.27	2.83	4.96	7.58	10.57
CEM I 42.5 R	-	8.9	10	15.8	19.7	25
CEM I 42.5 R + FA (k=0,5)	-	5.6	6.9	9	10.9	14.9
CEM I 42.5 R + SF (k=2,0)	4.4	4.8	-	-	5.3	-
CEM III/B 42.5	_-	1.4	1.9	2.8	3	3.4

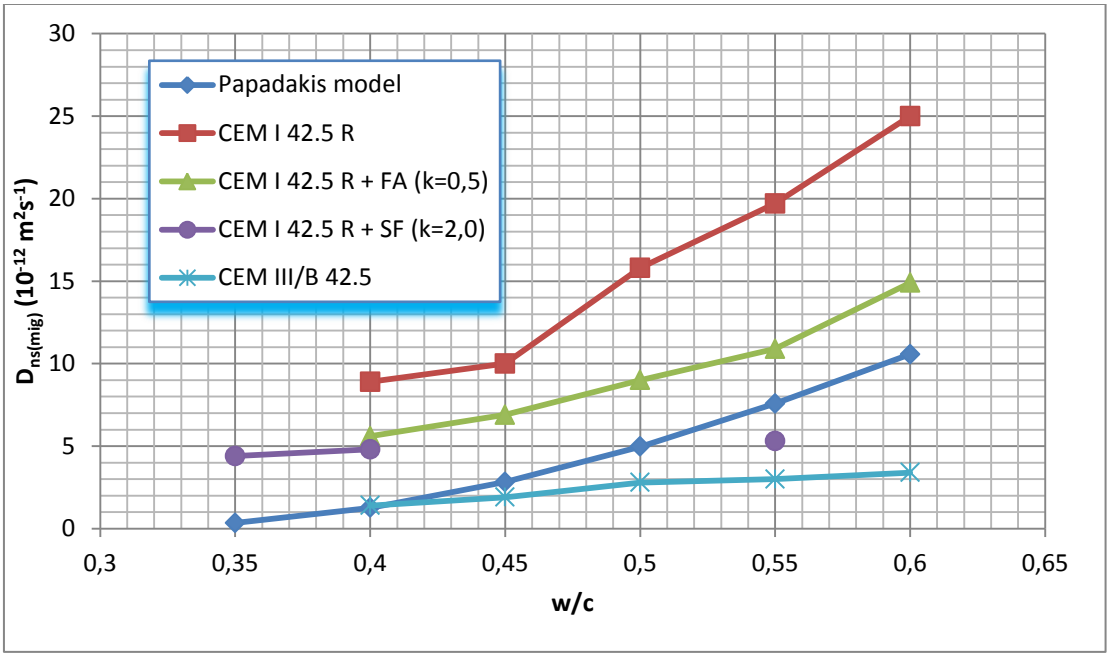

Figure 8-4: Chloride migration coefficients

[from Table 4 values *i.e. from samples (at t=28 days and T=20°C) and Papadakis' model]*

It is clear from (8.18) that the experimental chloride migration coefficients obtained at 28 days and 20°C correspond to diffusion apparent coefficients at these specific time and temperature conditions. As can be seen in Figure 8.4, the empirical formula (8.19) labeled as Papadakis' model provides values within the same order of magnitude as experimental chloride migration coefficients. Nevertheless the significant differences between experimental data obtained with various cement compositions cannot be accounted for by Papadakis' model since the latter does not depend on the cement composition. Hence, the values calculated for D^{app} with (8.19) should be interpreted with caution considering the limits of this model.

Besides, it is also possible to take advantage of classes of chloride apparent diffusion coefficient defined in (AFGC 2007) as presented in Table 8.5

Table 8.5: Classes and limit values of D^{app}

Potential durability	Very low	Low	Moderate	High	Very high
D^{app} ($x10^{-12}m^2s^{-1}$)	>50	10-50	5-10	1-5	<1

The time-dependence in (8.18) relies on the parameter *a* which is constant for a specific concrete (depending on mix composition). Values for *a* for all varieties of concrete are not well established but preliminary works cited in (Bioubakhsh 2011) give values in the range of 0.2 to 0.3 for normal Portland cement mixtures and higher values between 0.5 and 0.7 to fly ash and slag concrete. These results are relatively consistent with those proposed in (*fib* bull. 34) where *a* is assumed to follow a beta-distribution of lower bound 0 and upper bound 1 and the mean and standard deviation values shown in Table 8.6.

Table 8.6: Classes and limit values of a

Concrete	Mean value	Standard deviation
Portland cement concrete CEM I; 0.4≤*w/c*≤0.6	0.30	0.12
Portland fly ash cement concrete f≥0.20 z; k=0.5; 0.4≤w/c_{eq}≤0.62	0.60	0.15
Blast furnace slag cement concrete CEM III/B; 0.4≤*w/c*≤0.6	0.45	0.20

The evolution of the factor $(t_0/t)^a$ with time can be visualized with different values of the exponent *a* in Figure 8.5.

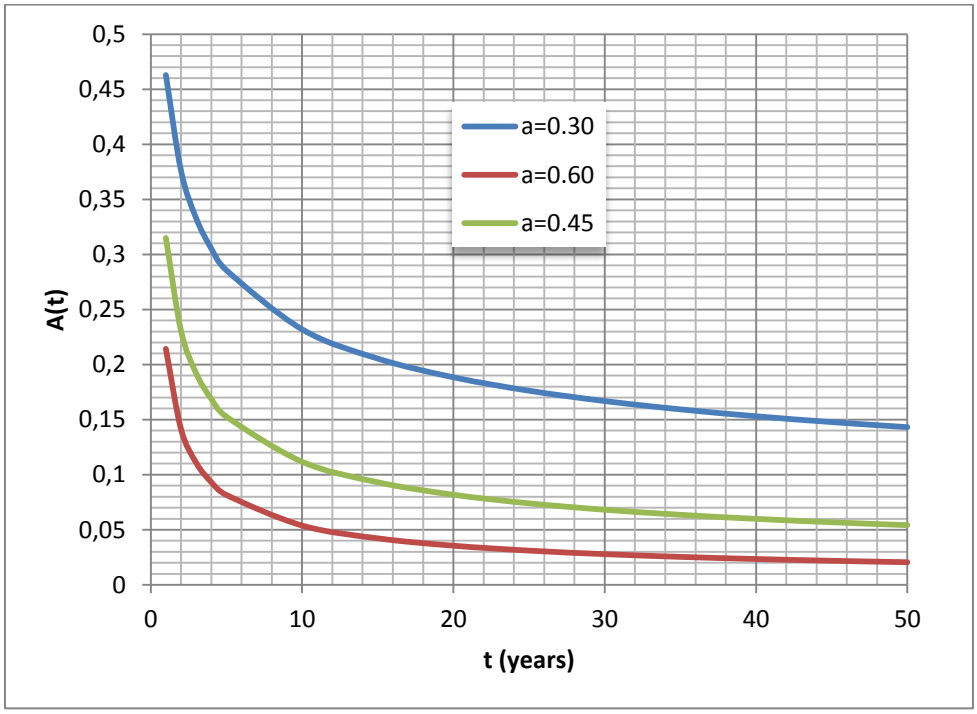

Figure 8-5: Time dependent factor of the chloride diffusion coefficient $(t_0/t)^a$

(with t0=28days)

The temperature-dependence in (8.18) relies on the Arrhenius equation where b_e is the Arrhenius constant, T^{ref} is the reference temperature (equal to 293K in laboratory conditions) and *T* is the temperature in K. Typical values of b_e can be found in (Bioubakhsh 2011) citing (Lin 1993) and are reported in Table 8.7.

Table 8.7: Values for the Arrhenius constant b_e

w/c ratio	0.4	0.5	0.6
b_e (K)	5016	5359	3830

Those values are consistent with that of 4800K suggested in (AFGC 2007) and the normal distribution of mean value 4800K and standard deviation 700K provided in (*fib* bull. 34).

The value used as boundary condition C_o or $C_{\Delta x}$ are difficult to estimate except in the case of a submerged marine environment which is not a priori our case (although the methodology could be applied to railway bridge piers for example). A methodology is proposed in (*fib* bull. 34) to take into account the effect of de-icing salt but it could be hard to apply in practice because of the difficulty to gather parameters. Hence, depending on the type of environment values suggested in (AFGC 2007) ranging from 10 to 100g.l^{-1}, i.e. 0.28 to 2.8mol.l^{-1}, could be used.

The shift abscissa Δx is also difficult to estimate. (*fib* bull. 34) suggests that it follows a beta-distribution of parameters depending on the exposure conditions:

- Mean value=8.9mm, standard deviation=5.6mm, lower bound=0, upper bound=50mm for splash conditions
- Constant value=0 for submerged marine structures, for leakage due to seawater and constant ground water level, for spray conditions
- Parameters not provided (and thus to determine) for leakage due to varying groundwater level and for tidal conditions.

Once all parameters needed by the model are gathered or estimated, the validation phase can start. Because of the large uncertainty concerning the critical chloride content responsible for corrosion initiation, it should probably be preferable to validate the model on chloride level profiles rather than on the penetration depth relying on a questionable choice of threshold. This method is then different from that regarding carbonation for which the penetration depth characterized by a pH drop is investigated.

The expression of the chloride profile consistent with (8.17) can be written

$$C(x,t) = C_{\Delta x} + (C_i - C_{\Delta x})\,\mathrm{erf}\left(\frac{x-\Delta x}{2\sqrt{D^{app}(t)t}}\right) \qquad (8.22)$$

possibly using the correction factor (8.20) for the diffusion coefficient if boundary conditions are constant.

Comparisons with (8.22) require to perform lab experiments providing free chloride content at different depth and possibly different times. Experimental procedures can be found in (Arya 1900) or (Chaussadent 1999). The discrepancy between the model and experimental curves can eventually by analyzed.

Performance profile for the corrosion propagation phase

According to Tuutti' scheme (see D2.3), the propagation period follows the initiation and starts with the production of rust. Different performance criteria and associated models have been described in D2.3 depending on the predicted effect of rust expansion. Those criteria are very briefly recalled in this section focussing on the limitations of models and then on typical values that can be used in models.

Review of the models and comments on their validity

Model of rust production and structural failure

First of all, the models are based on a simplified description of the corrosion mechanism involving the following redox equations:

$$Fe \rightarrow Fe^{z+} + ze^{-} \text{ with } z=2 \text{ or } 3 \qquad (8.23)$$

$$2e^{-} + H_2O + \frac{1}{2}0_2 \rightarrow 2OH^{-} \qquad (8.24)$$

Actually Fe^{2+} is first created and is combined with OH^- produced in (8.24) to form the ferrous hydroxide $Fe(OH)_2$, itself undergoing another oxidation step leading to ferric hydroxide $Fe(OH)_3$ a main component of rust in which the oxidation state of iron is 3. This hypothesis leads to neglect other minor components of rust.

Introducing the corrosion current density j_{cor} (Amperes per unit surface of steel rebar) at the steel-concrete interface and invoking Faraday's law, the local rate of loss of steel thickness writes:

$$\dot{e}(t) = \frac{M_s}{\rho_s zF} j_{cor}(t) \qquad (8.25)$$

where M_s, ρ_s and F respectively denote the steel molar mass (55.85g.mol^{-1}), the steel density (7874kg.m^{-3}) and Faraday's constant (96485C.mol^{-1}). The numerical value of (8.25) often evoked by authors is $\dot{e} = 0.0116 j_{cor}$ if $\dot{e}$ is in mm/year and j_{cor} in µA/cm^2 corresponding to z=2. The fact that z=2 is considered by several authors in Faraday's law, whereas the final oxidation state of iron in rust is rather 3, could be explained by a kinetics argument. Indeed the measurement of the corrosion current is practically carried out by the polarization method (RILEM 2004) based on the ratio between small variations of the steel potential around the equilibrium (potential E_{cor}) and the related difference between anodic and cathodic currents. As the first concerned oxidation reaction of Fe is that leading to Fe^{2+}, the measured corrosion current corresponds to this reaction.

Accordingly, the rates of reacted steel mass and produced rust mass ($Fe(OH)_3$) per unit surface of steel rebar respectively write:

$$\dot{\mu}_s(t) = \frac{M_s}{zF} j_{cor}(t) \text{ and } \dot{\mu}_r(t) = \frac{M_r}{zF} j_{cor}(t) \qquad (8.26)$$

where M_r is the rust molar mass (106.87g.mol^{-1}).

Once again, it is worth highlighting that the expressions (8.25) and (8.26) are local (i.e. depend on the position on the rebar). However, the corrosion current density is practically measured by means of the polarization method (RILEM 2004) under the assumption of a uniform corrosion occurring over a known exposed metallic area. Consequently, the volume

of reacted steel by time unit is straightforwardly calculated by multiplying (8.25) by this area. Similarly, the rates of reacted steel mass and produced rust mass are obtained by multiplying (8.26) by this area. Besides measurement uncertainties, the corrosion current density provided by the polarization method may be questionable due to possible errors concerning the area of the metallic surface subjected to corrosion and the assumption of uniform corrosion despite recommendations in (RILEM 2004).

All the models presented in D2.3 concerning deterioration due to rust production require the knowledge of the mass or volume of produced rust at each time. As recalled in (8.26) the latter is directly related to the corrosion current. However, the evolution of the corrosion current with time remains a difficult issue since it depends on

- the kinetics of corrosion controlled either by the electrochemical reaction or by the oxygen diffusion if the latter is too low,
- the presence of corrosion products tending to impede the diffusion process,
- the presence of cracks (due to external causes such as mechanical loading or the expansion of corrosion products) tending to increase the penetration of aggressive agents and oxygen and the transport of corrosion products far from the rebar.

All these factors influencing in a positive or negative way the corrosion current are obviously coupled and a complete resolution would require a heavy numerical computation. An example of structural numerical computation taking into account a corrosion rate controlled by the amount of oxygen and the effects of corrosion products and cracks is proposed in (Millard 2012). Such a methodology relying on a finite-element resolution can hardly be exploited in our case, recalling our need for simple analytical expressions. Therefore, it is suggested to consider that the corrosion current density belongs to the input data, either chosen in provided classes (see next section) or obtained by in-situ measurements. However, (Vu 2000) proposes an empirical expression of the corrosion current density in an environment of relative humidity 75% at 20°C:

$$j_{cor}(t) = j_{cor}(1)\,0.85\,t^{-0.29} \text{ with } j_{cor}(1) = \frac{37.8(1-w/c)^{-1.64}}{c_p} \qquad (8.27)$$

which suggests allowing a general expression of the form (8.28) to take into account a time dependence from the knowledge of j_{cor} at a given time T_o

$$j_{cor}(t) = At^{-\eta} = j_{cor}(T_0)\left(\frac{t}{T_0}\right)^{-\eta} \qquad (8.28)$$

where η=0.29 in the case of (8.27) and η=0 for a constant density and A is a constant depending on the concrete content. Collecting in-situ data of corrosion current density during a given period of time could obviously help optimizing the parameters A and η.

Integrating (8.25) between the time to depassivation T_{dep} and the current time t and using (8.28) allows to derive the expression of the reduction of rebar radius in the case of a uniform corrosion

$$e(t) = \frac{M_s}{\rho_s zF} j_{cor}(T_{dep}) \frac{T_{dep}}{1-\eta} \left(\left(\frac{t}{T_{dep}} \right)^{1-\eta} - 1 \right) \quad (8.29)$$

If η=0 (constant density), (8.29) simply becomes

$$e(t) = \frac{M_s}{\rho_s zF} j_{cor}\left(t - T_{dep}\right) \quad (8.30)$$

Eventually the area of the steel cross-section which has disappeared by uniform corrosion can be obtained at any time by

$$A_{unif}(e(t)) = \pi \left(\left(\frac{d_b}{2} \right)^2 - \left(\frac{d_b}{2} - e(t) \right)^2 \right) \quad (8.31)$$

where d_b is the initial rebar diameter

When the corrosion is actually not uniform, the measured value of the polarization resistance is related to an average corrosion current density (RILEM 2004) and a corresponding average rate of loss of steel thickness thanks to (8.25). Nevertheless, it is of interest to relate the maximal expected pit depth P_{max} to the average reduction of rebar radius e from (8.25) in order to be able to estimate the reduction of steel section in the critical zones. Several authors (Gonzalez 1995, RILEM 2004) define this relationship by means of the ratio

$$R = \frac{P_{\max}}{e} \quad (8.32)$$

Typical values of R will be provided in the next section. A geometrical model allowing to relate the area of loss steel due to pits $A_{pit}(P_{max})$ is proposed in (Stewart 2009) and recalled in the previous deliverables and herebelow.

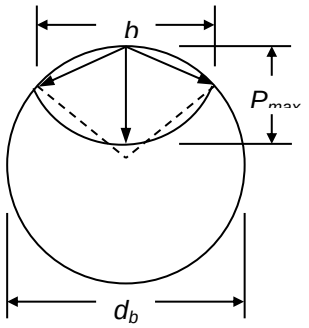

Figure 8-6: Pit configuration

(Stewart 2009)

$$A_{pit}(P_{\max}) = \begin{cases} \frac{1}{2}\theta_1\left(\frac{d_b}{2}\right)^2 - b\frac{d_b}{2} + \frac{1}{2}\theta_2 P_{\max}^2 & \text{if} \quad P_{\max} \le \frac{d_b}{\sqrt{2}} \\ A_{stnom} - \frac{1}{2}\theta_1\left(\frac{d_b}{2}\right)^2 - b\frac{d_b}{2} + \frac{1}{2}\theta_2 P_{\max}^2 & \text{if} \quad \frac{d_b}{\sqrt{2}} < P_{\max} \le d_b \\ A_{stnom} & \text{if} \quad P_{\max} = d_b \end{cases} \quad (8.33)$$

with

$$A_{stnom} = \pi\left(\frac{d_b}{2}\right)^2 \quad (8.34)$$

$$b = 2P_{\max}\sqrt{1-\left(\frac{P_{\max}}{d_b}\right)^2} \quad (8.35)$$

$$\theta_1 = 2\arcsin\left(\frac{b}{d_b}\right) \quad ; \quad \theta_2 = 2\arcsin\left(\frac{b}{2P_{\max}}\right) \quad (8.36)$$

It has been reported in D2.3 that the pit configuration and the geometrical expressions (8.33) - (8.36) could be exploited to estimate the volume or mass of reacted steel. This was actually a mistake due to misunderstanding of the referenced paper. Indeed, the creation of pits results from the random process of creation of electrochemical macrocells (see references in (Cao 2013)) and the model leading to the calculation of the area pit (8.33) only allows to estimate the maximal reduction of steel section due to pits and not the overall amount of reacted steel relying on the notion of average corrosion current density as explained a few lines above.

To summarize, both models of rebar cross-section reduction (uniform or pitting corrosion) start with the knowledge of the corrosion current density evolving with time (for example (8.28)). Eventually, the (maximum) rebar cross-section reduction $A_{loss}(t)$ is related to the (average) reduction of rebar radius by means of (8.31) in the case of a uniform corrosion and (8.33) together with (8.32) in the case of a pitting corrosion. The expression of the (average) reduction of rebar radius is finally exploited (for example (8.29) or (8.30)).

Although it occurs after crack initiation and propagation (see next paragraph), the failure due to rebar cross-section reduction is recalled here because it relies only on the rust production model and not a priori to failures of the concrete cover in this very simple model. Of course the presence of cracks and the nature of the zone neighbouring the rebar have an influence on the corrosion kinetics but as mentioned above, the latter are taken into account in an empirical way through a given evolution of the corrosion current density.

In D2.3, the performance indicator related to structural failure relies only on cross-section reduction. A correction should be made to the expression proposed in D2.3. Indeed the latter is valid only for uniform corrosion. Moreover the final calculation is based upon the assumption that the total corrosion current by unit length of rebar writes $\pi d_b j_{cor}$, which means that it neglects the diameter variations. Nevertheless, this result might not significantly differ from that obtained by means of (8.31) since a reduction of 10% of the rebar cross-

section is associated to a reduction of about 2.5% of the diameter. Finally $P_{stfail}(t)$ should rather be written, with respect to the conventional threshold defined as the fraction λ of the sound area, in the form

$$P_{stfail}(t) = 1 - \frac{A_{loss}(t)}{\lambda A_{stnom}} = 1 - \frac{A_{loss}(t)}{\lambda \pi \left(\frac{d_b}{2}\right)^2}$$

$$\text{with } A_{loss}(t) = \begin{cases} A_{unif}(e(t)) & \text{for a uniform corrosion} \\ A_{pit}(R\,e(t)) & \text{for a pitting corrosion} \end{cases} \qquad (8.37)$$

The corresponding time of structural failure is such that $P_{stfail}(T_{stfail})=0$. In the case of a uniform corrosion, T_{stfail} writes

$$T_{stfail} = T_{dep}\left(1 + \frac{d_b}{2}\frac{\rho_s z F}{M_s j_{cor}(T_{dep})}\frac{1-\eta}{T_{dep}}\left(1-\sqrt{1-\lambda}\right)\right)^{\frac{1}{1-\eta}} \approx T_{dep}\left(1 + \frac{d_b}{4}\frac{\rho_s z F}{M_s j_{cor}(T_{dep})}\frac{1-\eta}{T_{dep}}\lambda\right)^{\frac{1}{1-\eta}} \qquad (8.38)$$

where the approximation of the right hand side corresponds to a small value of λ (i.e. the rebar diameter variation is neglected) retrieving then the result provided in D2.3.

If the corrosion current density j_{cor} is constant (η=0), (8.38) becomes:

$$T_{stfail} = T_{dep} + \frac{d_b}{2}\frac{\rho_s z F}{M_s j_{cor}}\left(1-\sqrt{1-\lambda}\right) \approx T_{dep} + \frac{d_b}{4}\frac{\rho_s z F}{M_s j_{cor}}\lambda \qquad (8.39)$$

Models of crack initiation and propagation

In the propagation stage corrosion products, taking up more volume than the virgin steel, are formed. The first corrosion products may precipitate into a porous zone around the reinforcement and this does not lead to a built-up of pressure inside the concrete. Once this porous zone is filled with corrosion products, the continuous formation of the latter results in a pressure-generation inside the concrete and eventually, if the corrosion process continues, the formation of a crack in the concrete cover due to orthoradial tensile stress. This might lead to spalling of the concrete cover at a later stage if the corrosion process continues.

Before recalling the major results of D2.3 models concerning crack initiation and propagation, it is worth underlining here that the latter are valid under the assumption of uniform corrosion. Moreover the crack initiation and crack opening due to rust production is expected to occur for a small value of reacted steel cross-section with respect to the initial one, which allows us to consider that the rebar diameter remains very close to d_b.

In the modelling of corrosion-induced cracking and spalling, the concrete domain is modelled as a thick-walled cylinder with thickness c_p (thickness of concrete cover) as shown in Figure 8.7.

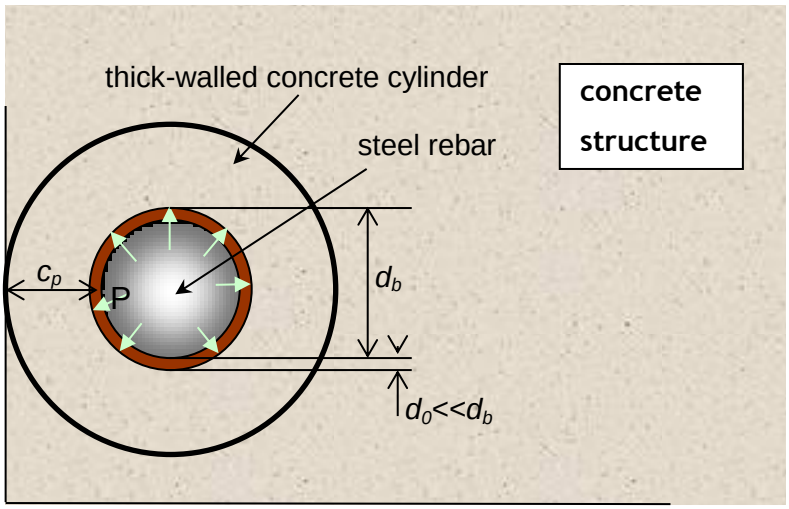

Figure 8-7: Model of concrete expansion due to corrosion

(Thoft-Christensen 2000)

In Figure 8.7 d_b is the diameter of the reinforcement bar (rebar) and d_0 is the thickness of the porous zone around the reinforcement. The pressure caused by the transformation of steel to corrosion products is calculated from (8.40).

$$P = \frac{E}{a(1+\nu)\left((1-\nu)\frac{a^2+b^2}{b^2-a^2}+\nu\right)} d_s \qquad (8.40)$$

where P is the pressure generated inside the concrete, E and ν are Young's modulus and Poisson's ratio of the concrete, a is the internal radius ($a = d_b/2$, the porous zone is neglected since $d_0 << d_b$), b is the external radius ($b = a + c_p$), and d_s is the radial expansion of the thick-walled cylinder. The relationship (40) is obtained thanks to the resolution of an elastic hollow cylinder subjected to an internal pressure and an external traction-free boundary under the assumption of plane strain.

Radial cracking occurs when the maximum tensile stress exceeds the tensile strength of the concrete. This corresponds to the radial expansion of the thick-walled cylinder calculated from (8.41).

$$d_s^{crack} = \frac{a(1+\nu)\left((1-\nu)+\nu\frac{b^2-a^2}{a^2+b^2}\right)}{E} f_t \qquad (8.41)$$

In (8.41) d_s^{crack} is the radial expansion of the thick-walled cylinder required to form a crack in the cover and f_t is the tensile strength of the concrete. The stress field solution to the problem of the hollow sphere fulfilling the criterion of radial cracking can therefore be considered as a candidate field in the approach from inside of the yield design theory (Salençon 2013). Consequently the estimate (8.41) of the radial expansion criterion is a lower bound of the actual strength criterion, leading to a conservative reasoning.

The mass of dissolved steel m_s^{crack} and produced rust m_r^{crack} per unit length of rebar required to reach the cracking criterion are obtained by considering that the produced rust occupy the initial porous zone and the shell defined by the radial expansion (8.41)

$$\frac{m_r^{crack}}{M_r} = \frac{m_s^{crack}}{M_s} = \frac{\pi d_b (d_0 + d_s^{crack})}{\frac{M_r}{\rho_r} - \frac{M_s}{\rho_s}} \qquad (8.42)$$

M_r and M_s are the molar masses of the corrosion products and the steel, respectively, and ρ_r and ρ_s are the densities of the corrosion products and the steel respectively..

Eventually the performance indicator is built by comparing the mass of dissolved steel to the threshold (8.42) taking advantage of (8.29) and the assumption of uniform corrosion.

$$P_{crack}(t) = 1 - \frac{m_s(t)}{m_s^{crack}} = 1 - \frac{\frac{M_r}{\rho_r} - \frac{M_s}{\rho_s}}{zF(d_0 + d_s^{crack})} j_{cor}(T_{dep}) \frac{T_{dep}}{1-\eta} \left(\left(\frac{t}{T_{dep}} \right)^{1-\eta} - 1 \right) \qquad (8.43)$$

The corresponding time to cracking is such that $P_{crack}(T_{crack})=0$ and writes

$$T_{crack} = T_{dep} \left(1 + \frac{zF(d_0 + d_s^{crack})}{\frac{M_r}{\rho_r} - \frac{M_s}{\rho_s}} \frac{1-\eta}{T_{dep} j_{cor}(T_{dep})} \right)^{\frac{1}{1-\eta}} \qquad (8.44)$$

In the case of a constant corrosion current density j_{cor} (η=0), (8.43) and (8.44) respectively become

$$P_{crack}(t) = 1 - \frac{m_s(t)}{m_s^{crack}} = 1 - \frac{\frac{M_r}{\rho_r} - \frac{M_s}{\rho_s}}{zF(d_0 + d_s^{crack})} j_{cor}(t - T_{dep}) \qquad (8.45)$$

and

$$T_{crack} = T_{dep} + \frac{zF(d_0 + d_s^{crack})}{j_{cor} \left(\frac{M_r}{\rho_r} - \frac{M_s}{\rho_s} \right)} \qquad (8.46)$$

After the onset of cracking, the crack propagates until reaching the external boundary. It becomes then interesting to follow the opening noted *w(t)* and define thresholds in order to build new performance indicators. A first threshold w_{SLS} corresponds to the service limit state

and a second one w_{sp} to a criterion of concrete spalling. Values are proposed in the next subsection. The performance indicators write

$$P_{SLS}(t) = 1 - \frac{w(t)}{w_{SLS}} \text{ and } P_{sp}(t) = 1 - \frac{w(t)}{w_{sp}} \qquad (8.47)$$

A model to estimate *w(t)* is proposed in D2.3 citing (Thoft-Christensen 2000). It consists in considering that the volume occupied by the open crack is equal to the volume of produced rust, under the assumption of uniform corrosion and using (8.28) with T_0=T_{crack}:

$$w(t) = \frac{\left(\frac{M_r}{\rho_r} - \frac{M_s}{\rho_s}\right)\frac{\pi d_b}{zF}\frac{j_{cor}(T_{crack})}{1-\eta}T_{crack}\left(\left(\frac{t}{T_{crack}}\right)^{1-\eta} - 1\right)}{\frac{1}{2}\left(1 + \frac{d_b/2}{d_b/2 + c_p}\right)c_p} \qquad (8.48)$$

Finally the times to reach the service limit state or spalling threshold are obtained by considering a null performance (8.47) and using (8.48):

$$T_\alpha = T_{crack}\left(1 + \frac{\frac{1}{2}\left(1 + \frac{d_b/2}{d_b/2 + c_p}\right)c_p w_\alpha}{\left(\frac{M_r}{\rho_r} - \frac{M_s}{\rho_s}\right)\frac{\pi d_b}{zF}\frac{T_{crack}\, j_{cor}(T_{crack})}{1-\eta}}\right)^{\frac{1}{1-\eta}} \text{ with } \alpha \equiv \text{"SLS" or "sp"} \qquad (8.49)$$

In the case of a constant corrosion current density j_{cor} (η=0), (8.48) and (8.49) respectively become:

$$w(t) = \frac{\left(\frac{M_r}{\rho_r} - \frac{M_s}{\rho_s}\right)\frac{\pi d_b}{zF}\, j_{cor}(t - T_{crack})}{\frac{1}{2}\left(1 + \frac{d_b/2}{d_b/2 + c_p}\right)c_p} \qquad (8.50)$$

and

$$T_\alpha = T_{crack} + \frac{\frac{1}{2}\left(1 + \frac{d_b/2}{d_b/2 + c_p}\right)c_p w_\alpha}{\left(\frac{M_r}{\rho_r} - \frac{M_s}{\rho_s}\right)\frac{\pi d_b}{zF}\, j_{cor}} \text{ with } \alpha \equiv \text{"SLS" or "sp"} \qquad (8.51)$$

Typical values of the parameters needed by the models

Faraday's constant is 96485C.mol^{-1}. The molar masses and densities of steel and rust can be found in Table 8.8.

Table 8.8: Values for rust production

Steel molar mass M_s	Rust molar mass M_r	Steel density ρ_s	Steel density ρ_r
55.85g.mol^{-1}	106.87g.mol^{-1}	7874kg.m^{-3}	3600kg.m^{-3}

Table 8.9 presents the classes of corrosion depending on the corrosion level as defined in (RILEM 2004).

Table 8.9: Classes of corrosion current from

(RILEM 2004)

Corrosion level	negligible	low	moderate	high
j_{cor} (µA/cm^2)	≤0.1	0.1-0.5	0.5-1	>1
$\dot{e}$ (mm/year)	≤0.001	0.001-0.005	0.005-0.010	>0.010

The conservative limit of the ratio P_{max}/e between the maximal expected pit depth P_{max} and the average loss of thickness e recommended in (Gonzalez 1995) is 10, which corresponds to the case of very localized pits. A range between 3 and 10 is however proposed in (RILEM 2004) invoking several references.

The values for crack opening corresponding to the criteria of service limit state according to EUROCODE 2 and concrete spalling according to (Val 2003) are recalled in Table 8.10.

Table 8.10: Threshold values for crack opening

Service limit state w_{SLS}	Concrete spalling w_{sp}
0.3mm	1mm

Availability of data in France

According to (AFGC 2003), the French railway network owner (RFF) counted in 2003 more than 1500 tunnels of a total length of 600km. Among them, 90% correspond to lined tunnels and among this subset, only 10% are concrete lined tunnels, the rest consisting of masonry tunnels. Moreover very few tunnel concrete linings contain steel reinforcement and performance variations are not monitored.

Concerning French concrete lined road tunnels, none of them contain steel reinforcement except maybe very locally, in parts potentially submitted to tractions, but not sufficient data to allow the implementation of deterioration models have been collected.

Searching data characterizing any corrosion-induced deterioration of French tunnels has revealed unsuccessful. It actually seems that collecting the data required by concrete tunnel performance models is not an easy task for the following reasons:

1. The majority of tunnels are lined with masonry.
2. Among concrete lined tunnels, very few are reinforced.
3. Models are based on quantitative indicators, many of them requiring destructive tests and laboratory experiments, which are expensive and thus very rarely performed except possibly on much degraded structures. Hence few data exist about the initiation phase.
4. Data may be confidential: infrastructure managers are more inclined to perform additional unusual measurements on the most deteriorated structures and might be reluctant to communicate the results.
5. The set of data may be incomplete so the validation may not be reliable because of an unrepresentative sampling or because missing parameters could be adjusted in order to match real outputs.

8.3.3 Case studies and validation

Introduction

Aim

The aim of this chapter is to present field-validated performance profiles for concrete tunnels. The performance profiles have been determined using the methodologies presented in D2.3, Time-variant Performance Profiles for Life-Cycle Cost and Life-Cycle Analysis, (ML D2.3), for carbonation-induced and chloride-induced corrosion. Field data from Danish structures have been used for the validation presented in the following.

Scope

The scope of the work presented herein is to provide a comparison between a predicted performance profile for a concrete tunnel and an actual performance profile based on field data. The performance models presented in D2.3, (ML D2.3) as well as the previous section cover reinforcement corrosion (see Figure 8.8).

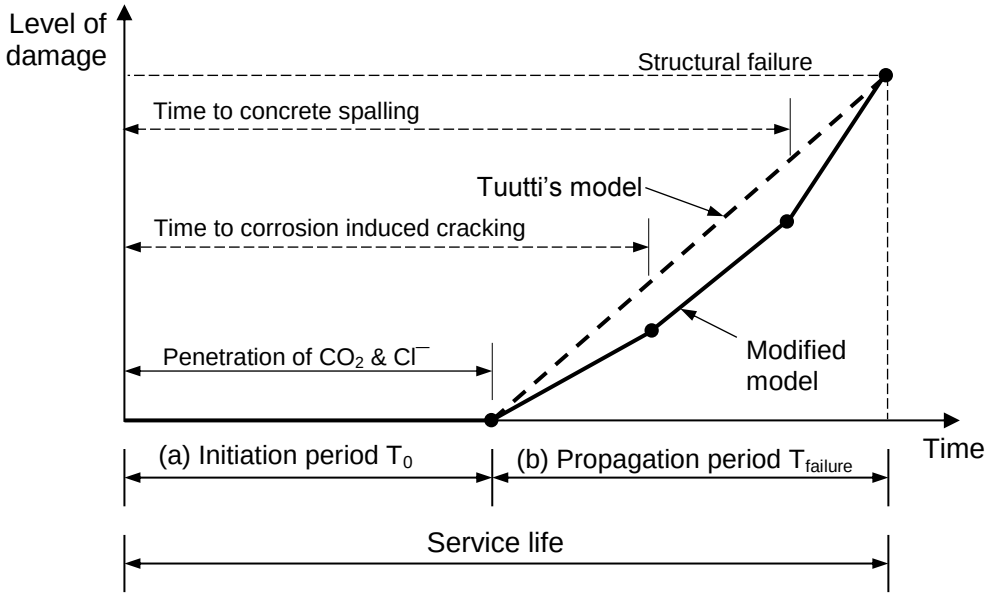

Figure 8-8: Service-life models of a corroding RC structure

[(D2.2 citing Otieno 2011): (a) Initiation and (b) propagation stages]

As illustrated in Figure 8.8 corrosion of reinforcement can be divided into two stages, i.e. initiation and propagation. During the initiation stage, de-passivating substances penetrate the concrete cover, and when a detrimental concentration is reached at the level of the reinforcement the physical (actual) corrosion process is initiated, i.e. the propagation stage.

The models for carbonation-induced and chloride-induced corrosion presented in D2.3, (ML D2.3) and section 8.2 of this report cover both stages (initiation and propagation). The performance profiles presented in this section concern both stages for carbonation-induced corrosion whereas only initiation of chloride-induced corrosion is considered. It is to be noted that only the initiation stages for the two deterioration mechanisms are validated with field data as data related to the propagation stage are not available from Danish projects (Danish practice is to only consider the initiation stage as part of the service life).

Carbonation-induced corrosion

This section concerns the performance profile with regard to carbonation-induced corrosion of concrete tunnels. Reinforcement embedded in sound concrete is electrochemically passive as the high pH of the concrete (pH~13) leads to the formation of a protective passive layer at the surface of the reinforcement. Carbonation of the concrete cover is caused by ingress of CO_2 which results in a reduction of the pH. As the carbonation-front reaches the level of the reinforcement, i.e. the concrete cover is carbonated, the passive layer at the surface of the reinforcement is broken down and the end of the initiation stage is reached. Subsequently, active corrosion (the propagation stage) may be initiated if the right conditions are present, e.g. oxygen and moisture availability. Corrosion products formed take up more volume than the steel consumed, and consequently an internal pressure is created in the reinforced concrete. As the corrosion process continues this pressure build-up leads to cracking and eventually spalling of the concrete cover if no precautions are taken to reduce/eliminate the corrosion process.

Description of models

Among those presented in D2.3 (ML D2.3) and section 8.2 of the present document, the models/methodologies used to determine the performance profile of concrete tunnels with regard to carbonation-induced corrosion, i.e. the initiation stage and the propagation stage, are briefly summarised in the following sections. Further information about the models/methodologies is provided in D2.3 (ML D2.3) and in section 8.2.

Initiation stage (MAINLINE model)

The carbonation-depth is determined from the analytically-based equation $X_c(t) = K\sqrt{t}$ already presented in (8.1).

The parameter *K* depends on the concrete composition (w/c ratio, content and type of binder, exposure conditions, etc. and can be determined in different ways, see e.g. D2.3, (ML D2.3). In this section, *K* is determined from the simplified version of (8.2) in section 8.2.2.

As input for that equation, the apparent initial concentration of $Ca(OH)_2$ is used. This value is calculated from (8.12) in section 8.2.2. The effective diffusion of CO_2 in the carbonated concrete D_{CO_2} is approximated from (8.3). The porosity of the carbonated paste which is used for the calculations of D_{CO_2} is related to the porosity of the carbonated concrete, using (8.4). For these simplified calculations, the porosity of the carbonated concrete is calculated from (8.5). Experimental data behind the formulas relate to cement paste and mortars with w/c-ratios between 0.5 and 0.8.

Propagation stage (MAINLINE model)

The case studies presented hereafter take advantage of a subset of the models proposed in D2.3, (ML D2.3). Only the necessary equations for cracking and spalling of the concrete cover are briefly mentioned in the following.

The radial expansion of the thick-walled cylinder d_s^{crack} reached at crack initiation is provided by (8.41). It allows then to calculate the time T_{crack} to reach the cracking state defined in (8.46) according to assumptions on the corrosion rate (corrosion current density assumed here uniform along the rebar surface and constant) using Faraday's law.

According to D2.3 (ML D2.3) the formation of a crack with a predefined crack width at the concrete surface can be seen as a serviceability limit state. The time T_{SLS} to form a crack of such a width assuming uniform corrosion and constant corrosion current density can be calculated from (8.51).

Alternative model for carbonation (fib approach)

An alternative method to the model presented in the sections above for estimating the carbonation depth is given in *fib* Bulletin 34 for service life modelling (fib 2006). That model is briefly described at the end of Section 8.2.2 and given in (8.14) of that section.

Case studies

Data from two case studies (field data) has been used for validation of the performance profile for carbonation-induced corrosion. A description of the two cases, viz.

Boulevardtunnelen (railway tunnel in Copenhagen) and Frederikssundsvejstunnelen (road tunnel in Copenhagen), incl. the availability of data is provided in the following.

Boulevardtunnelen

Boulevardtunnelen is a road-carrying railway concrete tunnel in Copenhagen. The tunnel was constructed in 1912. During maintenance and repair works in 2008 a number of cores were extracted from the outside (road-side) and the inside (railway tunnel wall) of the structure. Data on the carbonation-depth is available from 18 cores. Moreover, the w/c ratio of the concrete has been approximated from thin-sections of a limited number of the extracted cores. The available field data is, with permission of the owner (Rail Net Denmark) reproduced in Table 8.11. Data from top slab corresponds to measurements of carbonation depth below waterproofing membrane (bitumen), and therefore results are not representing normal exposure to air.

Table 8.11: Field data from Boulevardtunnelen

Core no.	Min. X_c [mm]	Max. X_c [mm]	w/c [-]	Comments
2	2	4		Top slab
3	14			Top slab
4	4			Top slab
5	3	4		Top slab
6	3	4		Top slab
7	3			Top slab
8	6	8		Top slab
9	4	7	0.50-0.60	Top slab
11	1	20		Wall
12	0	3		Wall
13	10	20		Wall
14	0	3		Wall
15	10	20	> 0.60	Wall
17	2	3		Wall
21	3	12	0.40-0.45	Wall w/c: variations in the range 0.35-0.55 were observed
22	1	10		Wall
23	3	10		Wall

The thickness of the concrete cover is only known from one wall (120 mm). Thus, the validation of the performance profile presented in the following only concerns the carbonation-depth. Pictures and drawings of the tunnel are enclosed in Section 8.3.4.

Frederikssundsvejstunnelen

Frederikssundsvejtunnelen is a road tunnel in Copenhagen. The tunnel was opened for traffic in 1969, and cores were extracted during an inspection in 1999. Data on the carbonation depth from four cores is available. Though the tunnel carries road traffic and not railway traffic it is suggested to use measurements of the carbonation depth for validation of the performance profiles within MAINLINE, as measurements from a road tunnel are considered representative also for a railway tunnel.

Table 8.12: Field data from Frederikssundsvejstunnelen

Core no.	Min. X_c [mm]	Max. X_c [mm]	w/c [-]	Comments
I	1	3	0.40-0.45	w/c: variations in the range 0.35-0.55 were observed
IV	3	9	0.40-0.45	w/c: variations in the range 0.35-0.60 were observed
1	0	1	0.50	w/c: variations in the range 0.40-0.55 were observed
2	0	1	0.50	w/c: variations in the range 0.40-0.60 were observed

The concrete cover thickness was measured for cores no. 1 & 2 (74mm and 64mm, respectively). Due to the limited availability of data concerning the concrete cover thickness the validation of the performance profile presented in the following is limited to the carbonation-depth. A picture of the tunnel is given in Section 8.3.4.

Modelling-input and assumptions

Boulevardtunnelen

The input used for the model is based on field data if available, see Table 8.11, and assumptions considering Danish practice and conditions. The input parameters used for simulation of the carbonation depth in Boulevardtunnelen are given in Table 8.13.

Table 8.13: Input data for modelling of carbonation in Boulevardtunnelen

Symbol	Value	Reference
$[CO_2]^0$ [mol/m³]	0.013 – 0.018	D2.3 (ML D2.3) and *fib* Bulletin 34 (fib 2006)
c [kg/m³]	300 – 350	Based on experience with Danish practice
f_{C_3S} [-]	0.50	Danish practice (assumed to some extent)
w/c [-]	0.35 – 0.60	Table 8.11
s [kg/m³]	0	Based on experience with Danish practice
$M_{Ca(OH)_2}$ [kg/mol]	0.074	D2.3 (ML D2.3)
RH [-]	0.75 – 0.84	http://www.copenhagen.climatemps.com/humidity.php
g/c [-]	5.14	D2.3 (ML D2.3)

Symbol	Value	Reference
$[CO_2]^0$ [mol/m³]	0.013 – 0.018	D2.3 (ML D2.3) and *fib* Bulletin 34 (fib 2006)
ρ_c/ρ_g [-]	1.2	D2.3 (ML D2.3)
ρ_c/ρ_w [-]	3.1	Based on values in D2.3 (ML D2.3)
$\square^c$ [-]	0.10 – 0.20	Assumed

This yields the following K-values calculated as a min, average and max value:

$K_{min} = 4.1 \cdot 10^{-7}\ m/\sqrt{s}$

$K_{avg} = 7.4 \cdot 10^{-7}\ m/\sqrt{s}$

$K_{max} = 1.2 \cdot 10^{-6}\ m/\sqrt{s}$

Frederikssundsvejstunnelen

Input data for the modelling of the carbonation-depth in Frederikssundsvejstunnelen is based on field data if available, see Table 8.12, and assumptions considering Danish practice/conditions. The input parameters are given in Table 8.14.

Table 8.14: Input data for modelling of carbonation in Frederikssundsvejstunnelen

Symbol	Value	Reference
$[CO_2]^0$ [mol/m³]	0.013 – 0.018	D2.3 (ML D2.3)
c [kg/m³]	300 – 350	Based on experience with Danish practice
f_{C_3S} [-]	0.50	Danish practice (assumed to some extent)
w/c [-]	0.35 – 0.55	Table 8.12
s [kg/m³]	0	Based on experience with Danish practice
$M_{Ca(OH)_2}$ [kg/mol]	0.074	D2.3 (ML D2.3)
RH [-]	0.74 – 0.84	http://www.copenhagen.climatemps.com/humidity.php
g/c [-]	5.14	D2.3 (ML D2.3)
ρ_g/ρ_w [-]	2.6	D2.3 (ML D2.3)
ρ_c/ρ_w [-]	3.1	Based on experience with Danish practice
$\square^c$ [-]	0.10 – 0.20	Assumed

The K-value is calculated as a min, average and max value:

$K_{min} = 4.1 \cdot 10^{-7}\ m/\sqrt{s}$

$K_{avg} = 7.1 \cdot 10^{-7}\ m/\sqrt{s}$

$K_{max} = 1.1 \cdot 10^{-6}\ m/\sqrt{s}$

Fib model for carbonation

The *fib* model for carbonation requires different input parameters than the MAINLINE model. The input parameters used for calculation of *K* and modelling of the carbonation depth with the *fib* model are given in Table 8.15.

Table 8.15: Input data for modelling carbonation depth with fib model

(Applicable for both case studies)

Symbol	Value	Reference
k_e [-]	$6 \cdot 10^{-5}$-0.146	*fib* Bulletin 34 (fib 2006) and based on http://www.copenhagen.climatemps.com/humidity.php
k_c [-]	0.456	*fib* Bulletin 34 (fib 2006) and assumptions on curing time
k_t [-]	1.25	*fib* Bulletin 34 (fib 2006)
$R_{ACC,0}^{-1}$ [(mm²/years)/(kg/m³)]	978.3-4228.6	*fib* Bulletin 34 (fib 2006) and field data
ε_t [(mm²/years)/(kg/m³)]	315.5	*fib* Bulletin 34 (fib 2006)
C_S [kg/m³]	0.00057 – 0.00082	D2.3 (ML D2.3) and *fib* Bulletin 34 (fib 2006)
W(t)	1	*fib* Bulletin 34 (fib 2006) and assumptions on exposure

Applying the values given in Table 8.5 in Eq. (8.14), a minimum, an average, and a maximum value of K is calculated.

$K_{min} = 0.0128\ mm/\sqrt{year}$
$K_{avg} = 0.092\ mm/\sqrt{year}$
$K_{max} = 0.25\ mm/\sqrt{year}$

Results

The results presented in this section include:

- Field data from the case studies presented in Section 8.3.2,
- Carbonation over time; K-value calculated using MAINLINE approach,
- Carbonation over time; K-value calculated using fib approach, and
- Calculation of time-to-cracking and time-to-service-limit-state.

Though the *fib* model can be used for probabilistic calculations only calculations based on the mean value of the input parameters are presented here. Note: time-to-cracking and time-to-SLS cannot be validated with field data as such data are not available.

In addition to the two models presented, i.e. the MAINLINE model and the *fib* model, the 'real' K-value has also been estimated from the actually measured data.

Boulevardtunnelen – Carbonation over time

The results comprise the simulated carbonation-depth as function of time. The simulated carbonation depth over time is shown in Figures 8.9 and 8.10 for the walls and top slab of Boulevardtunnelen, respectively along with the field data.

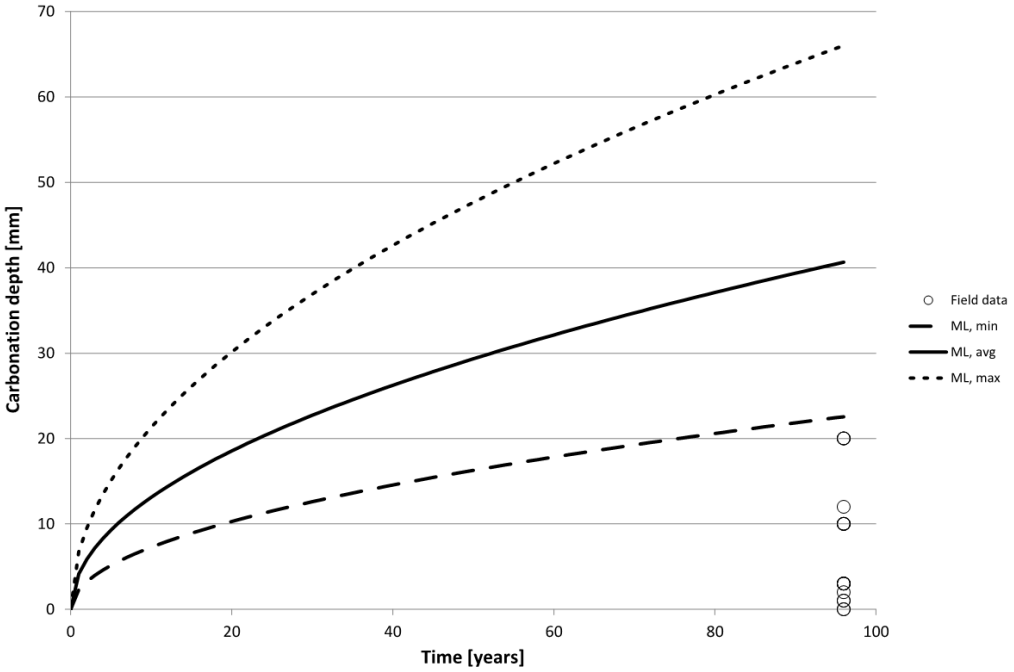

Figure 8-9: Carbonation depth of walls in Boulevardtunnelen

(as function of time, MAINLINE (ML) model and field data)

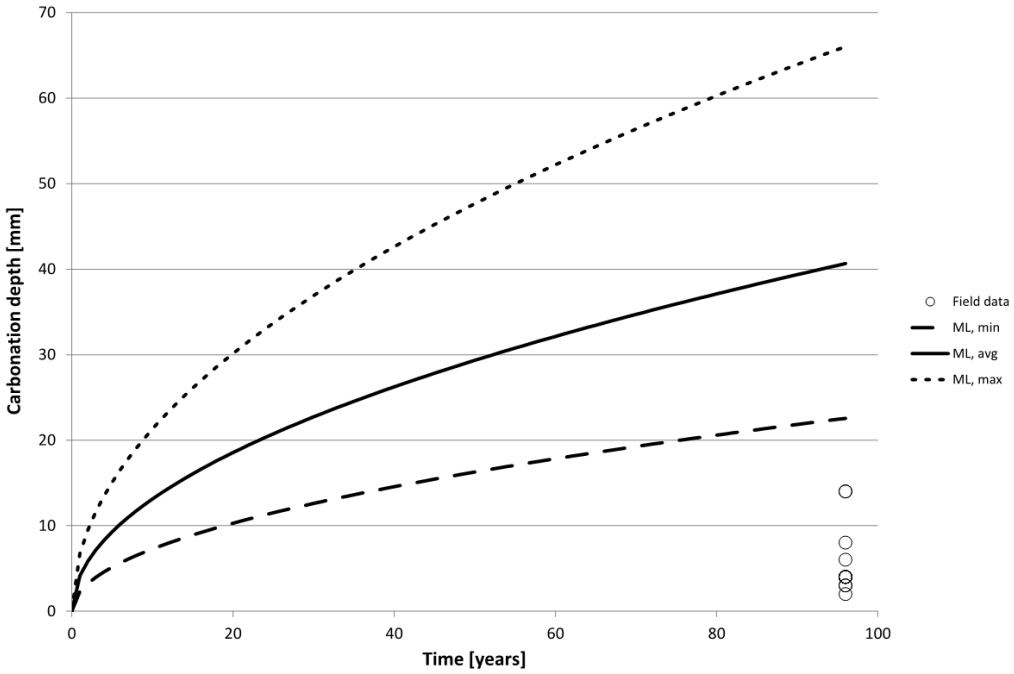

Figure 8-10: Carbonation depth of top slab in Boulevardtunnelen

(as function of time, MAINLINE (ML) model and field data)

Calculation of the carbonation depth based on the *fib* modelling approach is shown in Figures 8.11 and 8.12 for the walls and slab, respectively.

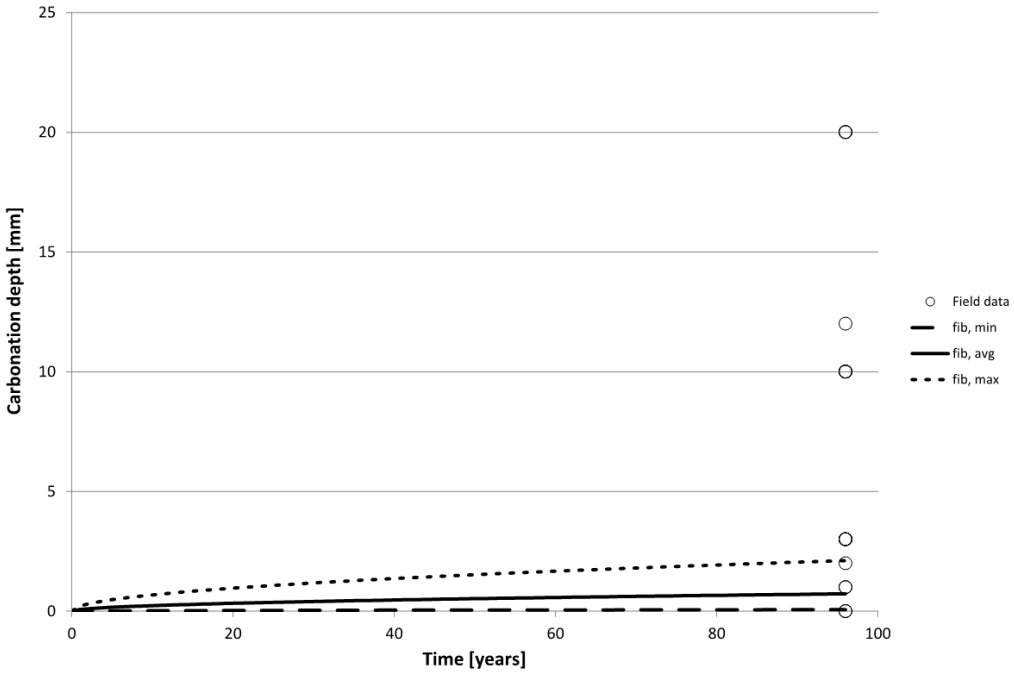

Figure 8-11: Carbonation depth of walls in Boulevardtunnelen

(as function of time, fib-model and field data)

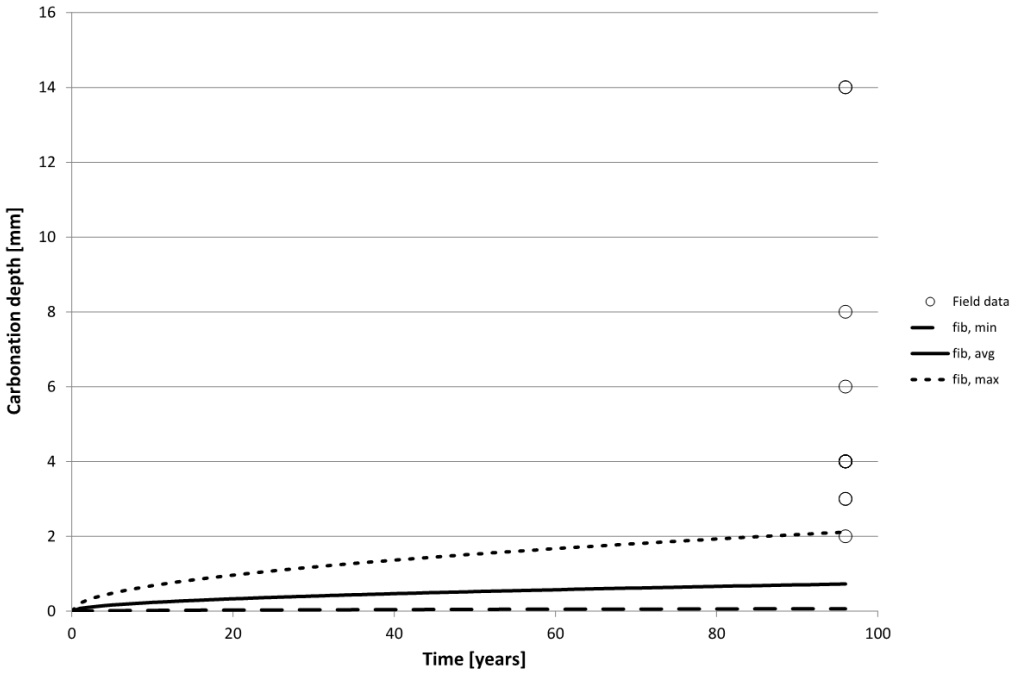

Figure 8-12: Carbonation depth of top slab in Boulevardtunnelen

(as function of time, fib-model and field data)

Finally results from calculation of the carbonation depth in the walls and the top slab as function of time using inverse analysis, are shown in Figure 8.13 and Figure 8.14, respectively. For the walls, the average carbonation depth is 7.3 mm and the standard deviation is 7.0 mm. For the top slab, the average carbonation depth is 5.7 mm and the standard deviation is 4.0 mm.

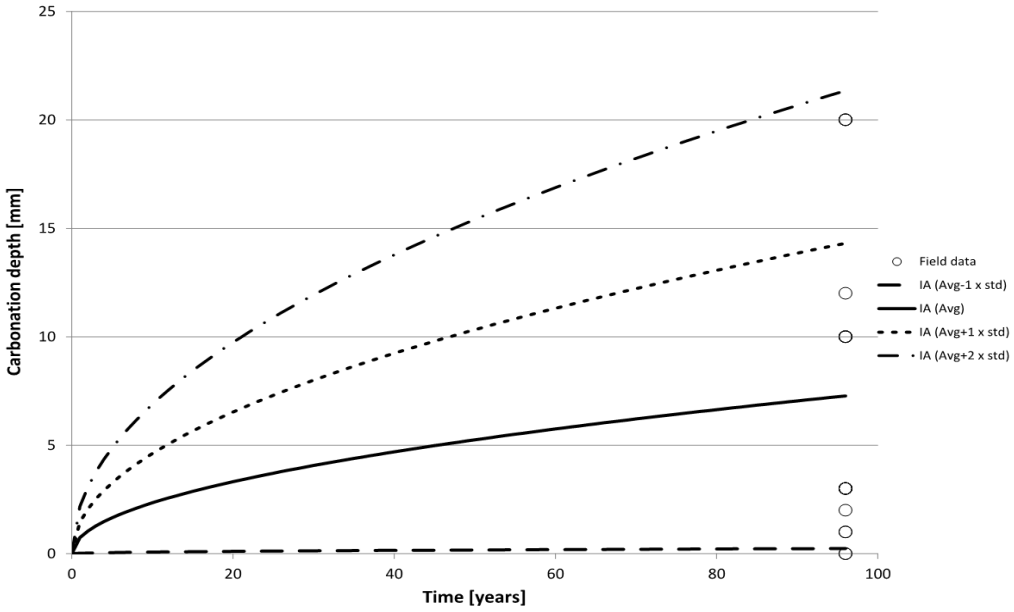

Figure 8-13: Carbonation depth of walls in Boulevardtunnelen

(as function of time, inverse analysis and field data)

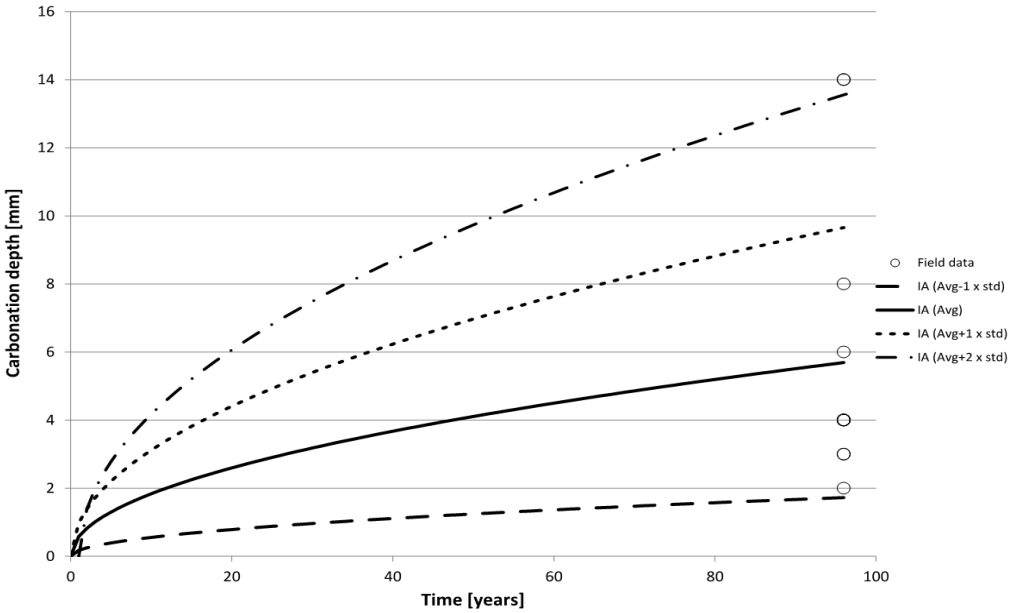

Figure 8-14: Carbonation depth of top slab in Boulevardtunnelen

(as function of time, inverse analysis and field data)

Frederikssundsvejstunnelen – Carbonation over time

The carbonation depth as function of time using the MAINLINE modelling approach for Frederikssundsvejstunnelen is shown in Figure 8.15 along with field data.

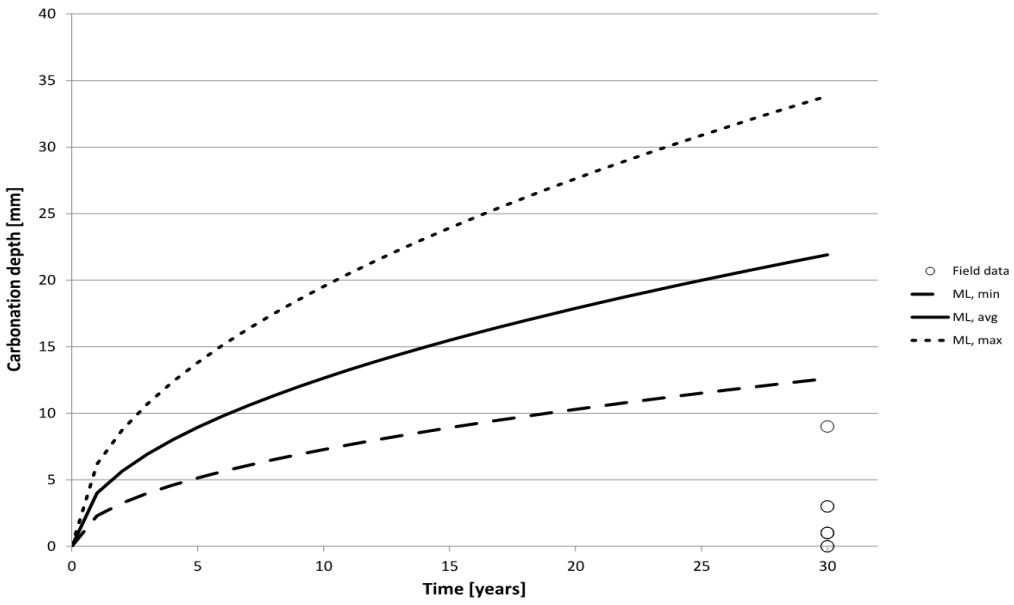

Figure 8-15: Carbonation depth in Frederikssundsvejstunnelen

(as function of time, MAINLINE (ML) model and field data)

The results of the carbonation depth as function of time using the *fib* approach are shown in Figure 8.16 together with field data from Frederikssundsvejstunnelen

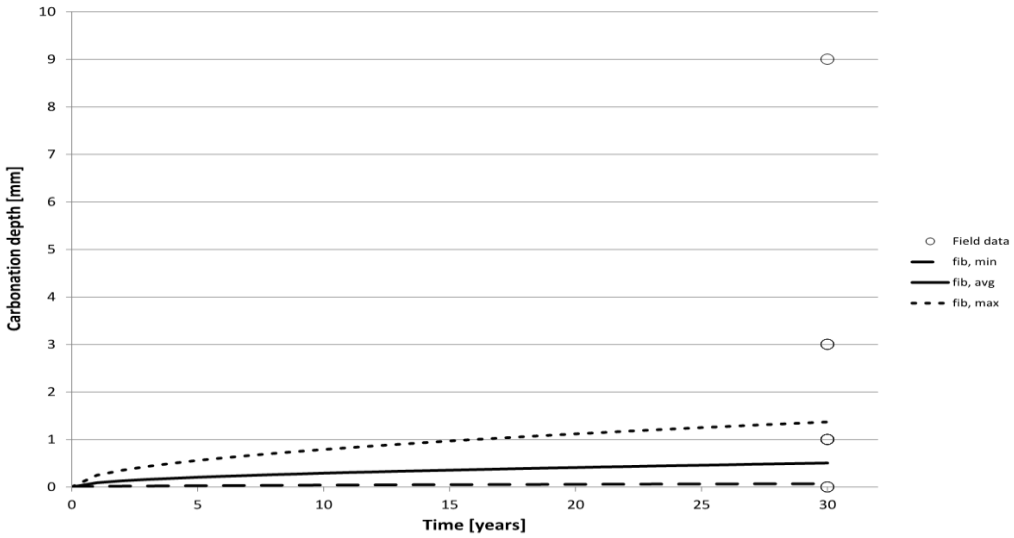

Figure 8-16: Carbonation depth in Frederikssundsvejstunnelen

(as function of time, fib-model and field data)

The K-value has been estimated from the field data from Frederikssundsvejstunnelen and the calculated carbonation depth as function of time is shown in Figure 8.17. The average carbonation depth from these measurements is 2.3 mm and the standard deviation is 3.0 mm.

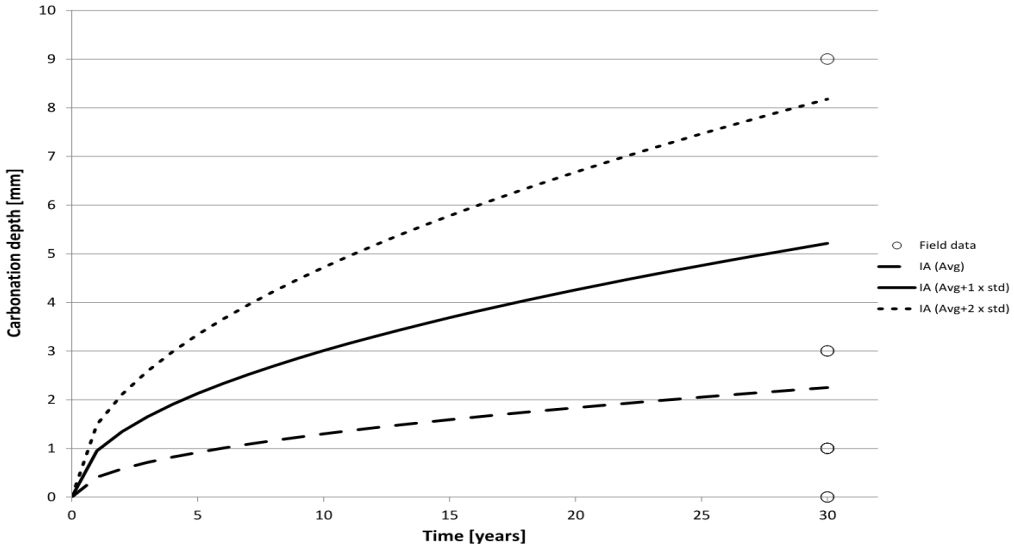

Figure 8-17: Carbonation depth in Frederikssundsvejstunnelen

(as function of time, inverse analysis and field data)

Time-to-cracking and time-to-SLS

Time-to-cracking and time-to-SLS have been calculated assuming the properties given in Table 8.16. It is assumed that the corrosion products are formed uniformly at the reinforcement circumference, and that the corrosion current is constant. Note: The properties given in Table 8.16 do not refer to the case studies presented above, but have been assumed based on values given in D2.3, (ML D2.3).

Table 8.16: Input data for modelling of time-to-cracking and time to reach the serviceability limit state

Symbol	Value	Reference
c_p [mm]	50	Assumed
d_b [mm]	20	Assumed
d_0 [µm]	12.5	D2.3, (ML D2.3)
E [GPa]	11.5	Assumed (ML D2.3)
f_t [MPa]	2.4	Assumed (ML D2.3)
v [-]	0.2	Assumed (ML D2.3)
z [-]	3	Assumed (ML D2.3)
i_{cor} [A/m²]	0.01	(ML D2.3)
w [mm]	0.3	(ML D2.3)

The time-to-depassivation is calculated assuming similar properties of the concrete as for Frederikssundsvejstunnelen, Table 8.14. The calculated time-to-depassivation, time-to-cracking and time-to-SLS are given in Table 8.17.

Table 8.17: Calculated values of T_{dep}, T_{crack}, and T_{SLS}

Time stage	Value [years]
T_{dep}	65.5
T_{crack}	66.1
T_{SLS}	71.8

Danish practice

A general observation from Danish tunnels (and large infrastructural objects in general, e.g. bridges) is that carbonation is of secondary concern when considering durability of the structures. Furthermore, use of high performance concretes, i.e. w/c ≤ 0.4-0.45 as used in modern concrete structures results in limited carbonation of the concrete cover, with only few millimetres of carbonation after exposure for several years. It is, however, noted that the number of tunnels (railway as well as road) in Denmark is limited and thus the basis for evaluating the MAINLINE model/methodology with Danish data is sparse. In general the availability of field-data from reinforced concrete tunnels is limited, not only in Denmark but also in e.g. France, cf. Section 8.2.5. Further, it was only possible to obtain field data from Danish structures under the time restraints of the present project.

Discussion

This section contains a discussion of the results obtained using the MAINLINE model which is compared to results achieved using the *fib* model and inverse analysis of the actual field data.

It is seen from Figures 8.9, 8.10 and 8.15 that the model for determination of the carbonation depth as proposed for the MAINLINE LCAT tends to overestimate the carbonation-depth compared to actual field observations. This may be explained from the fact that a number of input parameters for the model have been assumed, e.g. binder type and content, RH, the porosity of the carbonated concrete, etc.

Calculated values of the K-value using the MAINLINE model and the *fib* model are given in Table 8.18 along with the values from the inverse analysis. All values are given in mm/year^0.5

Table 8.18: Estimated values of K using ML model, fib model and inverse analysis of data

		MAINLINE model	*fib* model	Inverse analysis
Boulevardtunnelen – walls	K_{min}	2.3	0.0128	-
	K_{avg}	4.2	0.092	0.58
	K_{max}	6.7	0.25	-
Boulevardtunnelen – top slab	K_{min}	2.3	0.0128	-
	K_{avg}	4.2	0.092	0.74
	K_{max}	6.7	0.25	-
Frederikssundsvejstunnelen	K_{min}	2.3	0.0128	-
	K_{avg}	4.0	0.092	0.41
	K_{max}	6.2	0.25	-

It is seen from Table 8.18 that the calculated K-value differs with order of magnitude depending on the calculation method (model) used. Consequently, as can be concluded from the graphs showing carbonation depth as function of time, the predicted carbonation depth varies significantly depending on the calculation method used.

As seen from Table 8.17, the extra time required to reach another limit state than de-passivation, i.e. cracking and SLS (w = 0.2 mm) is very limited. Thus the actual benefit of considering these limit states during the design phase is limited. It is, however, noted that within the model this time is inverse proportional to the corrosion current density, i.e. the lower corrosion current, the longer time-to-cracking and time-to-SLS.

It is recommended that a possible LCAT contains a list of reasonable values for these parameters. Alternatively, a range of K-values for various values of *w/c*, *s*, and *RH* may be implemented in the tool.

Chloride-induced corrosion

This section concerns the performance profile for chloride-induced corrosion of concrete tunnels. Chlorides penetrating the concrete cover may lead to reinforcement corrosion when the chloride concentration at the level of the reinforcement exceeds the so-called chloride threshold of the reinforcement.

Description of model

The chloride concentration at the distance x from the concrete surface at time t can, as described in D2.3 (ML D2.3), be determined from (8.22) in which the shift abscissa Δx is taken as 0, $C_{\Delta x}$ is C_o i.e. the chloride concentration at the concrete surface and the apparent chloride diffusion coefficient D^{app} is assumed constant. It is recalled that C_o is assumed constant throughout time and C_i is uniform throughout the concrete volume. The apparent chloride diffusion coefficient may be determined in several ways as stated in D2.3 (ML D2.3) and recalled in section 8.2. However, due to a general lack of knowledge on the concrete composition and the exposure conditions, the simplified relationship proposed in (8.19) is used in the following.

Case studies

The performance profile for chloride-induced corrosion has been validated from the following case studies:

- Storebæltstunnelen (railway tunnel, submerged),
- Boulevardtunnelen (railway tunnel in Copenhagen), and
- Farøbroerne (coastal bridge in Denmark).

The performance profile will only be validated with regard to the chloride concentration profile in the concrete, as it is not possible to validate the value of the actual performance indicator. Data from Boulevardtunnelen is for concrete covered by a membrane, which has protected the concrete to chloride exposure (and ingress) and therefore data for validation of the performance profile of the concrete is not available. This case study has, however, been included to show the possible beneficial impact of a membrane on chloride ingress in concrete structures. Finally, data from a coastal bridge has been included in the case studies. The reasoning for this is that the availability of field data from tunnels with regard to chloride ingress is very limited. Since the mechanism of chloride ingress as described by the MAINLINE model, i.e. the model is based on Fick's 2nd law, it is not calibrated for a specific type of structure and consequently data from a bridge may also be used for validation of the model.

Modelling-input and assumptions

Storebæltstunnelen

Input used for modelling of chloride ingress in Storebæltstunnelen is shown in Table 8.19.

The measurements used for the model-validation have been taken from the part of the bored tunnel located more than 60 m below the sea level.

Table 8.19: Input values for calculation of chloride ingress in Storebæltstunnelen

Symbol	Value	Reference
D_{H20} [m²/s]	$1.6 \cdot 10^{-9}$	D2.3 (ML D2.3)
w/c [-] [1)]	0.33	Data from owner

Symbol	Value	Reference
D_{H20} [m²/s]	$1.6 \cdot 10^{-9}$	D2.3 (ML D2.3)
ρ_c/ρ_w [-]	3.08	Based on experience with Danish practice
g/c [-]	5.74	Based on data from IM and assumptions
ρ_c/ρ_g [-]	1.14	Based on experience with Danish practice
C_0 [wt.-%/wt. con.]	0.9	Assumed
C_i [wt.-%/wt. con]	0.0	Assumed
[1)] Cementitious materials consist of cement (315 kg/m³), fly ash (41 kg/m³) and micro silica (21 kg/m³).		

Applying (8.19) yields $D^{app} = 3.18 \cdot 10^{-14}$ m²/s.

Farøbroen

Input used for the modelling of chloride ingress in Farøbroen is shown in Table 8.20.

Table 8.20: Input values for calculation of chloride ingress in Farøbroen

Symbol	Value	Reference
D_{H20} [m²/s]	$1.6 \cdot 10^{-9}$	D2.3 (ML D2.3)
w/c [-] [1)]	0.38	Data from IM
ρ_c/ρ_w [-]	3.1	Based on experience with Danish practice
g/c [-]	4.94	Data from IM
ρ_c/ρ_g [-]	1.15	Based on experience with Danish practice
C_0 [wt.-%/wt. con.]	Case-dependent	Data from IM
C_i [wt.-%/wt. con]	0	Data from IM
[1)] Cementitious materials consist of cement (340 kg/m³) and fly ash (40 kg/m³).		

Applying (8.19) yields $D^{app} = 2.13 \cdot 10^{-13}$ m²/s.

The value of C_0 used for the calculated chloride profiles are given in the next section as it varies for each core.

Results

Storebæltstunnelen

Data from two measurements of the chloride content in the bored tunnel is shown in Figure 8.18. The age of the concrete at time of coring is approx. 7 years. Input for the calculated chloride profiles is given in Table 8.21.

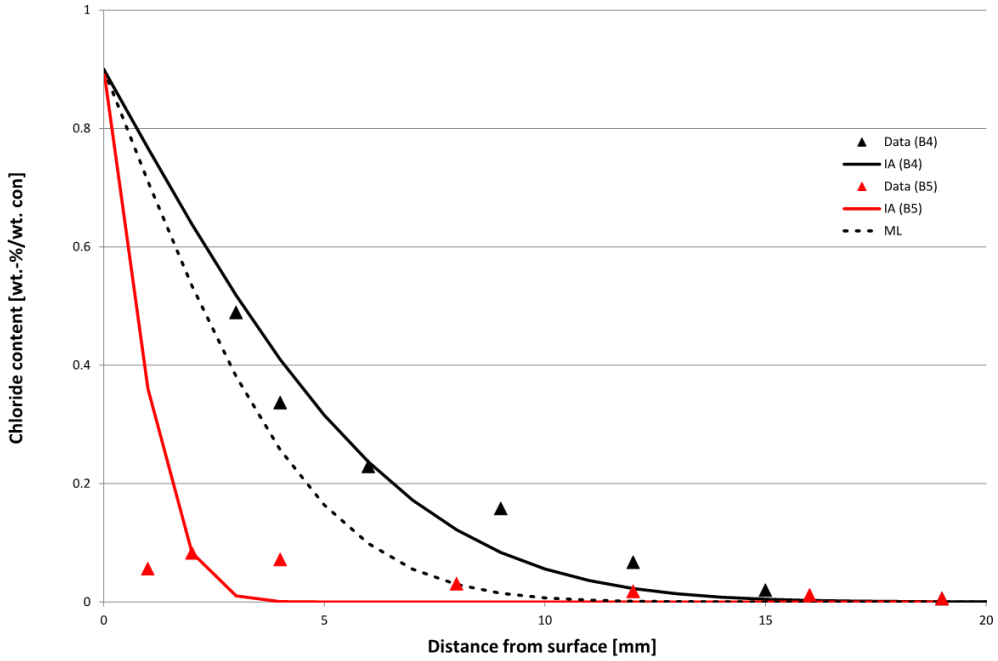

Figure 8-18: Measured chloride content at various depths

[from surface at t = 7 years in Storebæltstunnelen, and calculated chloride profiles inverse analysis (IA) and MAINLINE model (ML)]

Table 8.21: Input parameters for calculation of chloride profiles for Storebæltstunnelen

Core no.	Method	C_0 [wt.-%/wt.-% con]	C_i [wt.-%/wt.-% con]	D^{app} [x 10^{-13} m²/s]]
B4	IA	0.9	0	0.65
	ML			0.32
B5	IA			0.03
	ML			0.32

Note; the chloride concentration at the surface has been estimated from IA of core B4. This value has been used for all calculated chloride profiles.

Boulevardtunnelen

As mentioned in Section 8.3.3 modelling of the chloride profile has not been performed for Boulevardtunnelen. The cores taken from this tunnel were taken from the top surface of the tunnel, which is protected by a membrane, bituminous overlay for the overpassing traffic. The chloride content was measured in 8 cores to a depth of 50 mm from the surface. The maximum chloride content measured was 0.03 wt.-%/wt.-% of concrete.

Farøbroen

Results from Farøbroen comprise data from investigations of the chloride profile at various times and subsequent calculation of the chloride diffusion coefficient, using inverse analysis. Data measured in the splash zone of a pillar at various time steps is shown in Figures 8.19 – 8.21. Moreover, the chloride profile calculated by the use of results from the inverse analysis

(IA) and the calculated chloride profiles using the MAINLINE (ML) approach for determination of the chloride diffusion coefficient, are given in the figures. For these calculation it is assumed, based on the data, that the initial chloride concentration C_i = 0.0% and the chloride concentration at the surface as determined from the inverse analysis has also been used for the ML-calculations. The same scale has been used for all figures to ease comparison. Input for the calculations is given in Table 8.22.

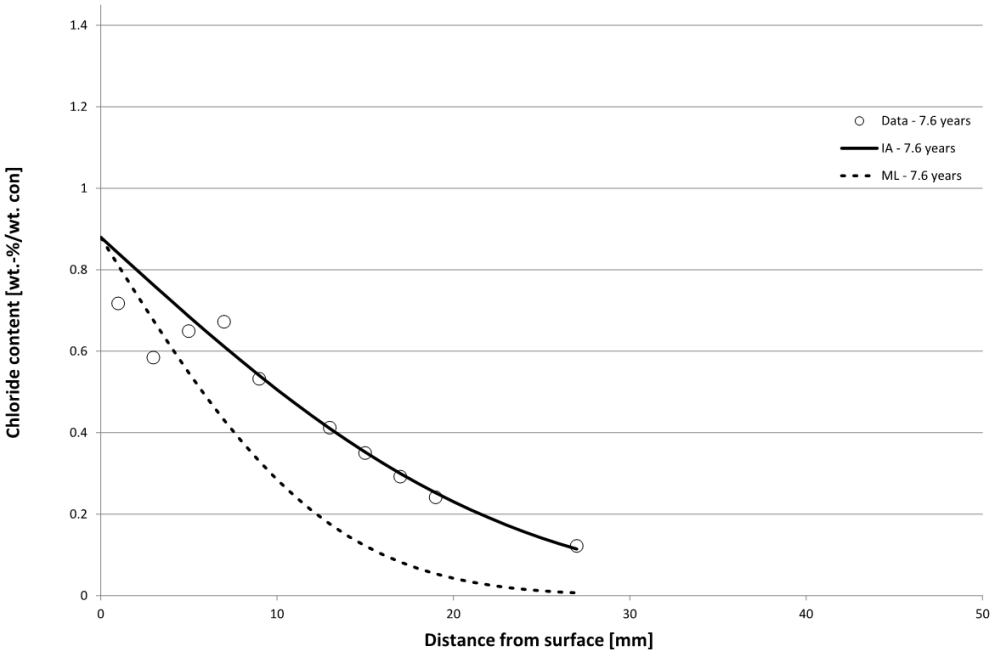

Figure 8-19: Measured chloride content at various depths from surface

[at t = 7.6 years at Farøbroen, and calculated chloride profiles inverse analysis (IA) and MAINLINE model (ML)]

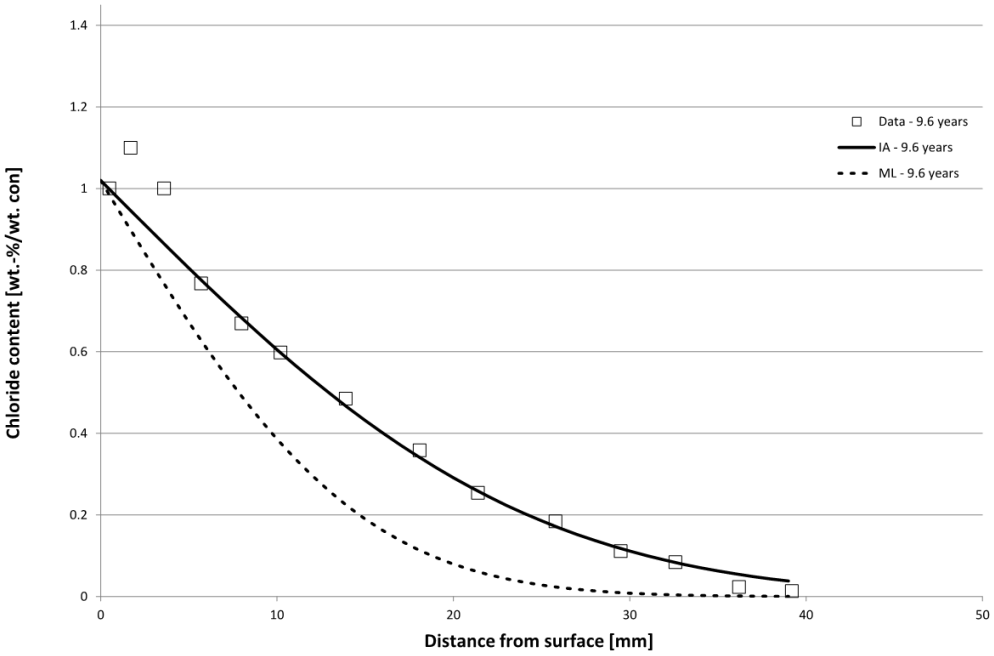

Figure 8-20: Measured chloride content at various depths from surface

[at t = 9.6 years at Farøbroen, and calculated chloride profiles inverse analysis (IA) and MAINLINE model (ML)]

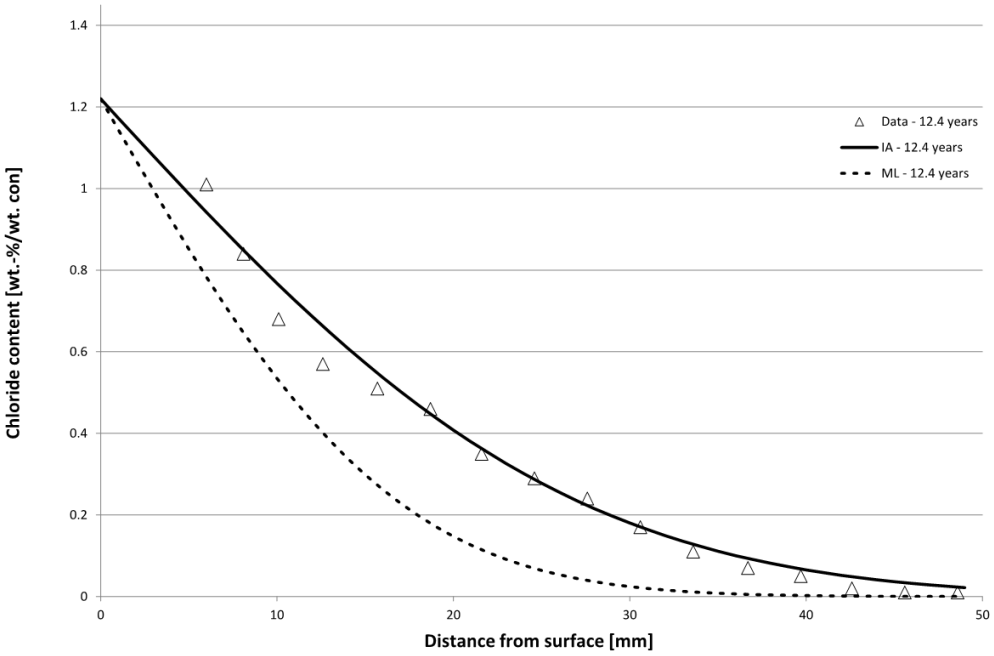

Figure 8-21: Measured chloride content at various depths from surface

[at t = 12.4 years at Farøbroen, and calculated chloride profiles inverse analysis (IA) and MAINLINE model (ML)]

Table 8.22: Input parameters for calculation of chloride profiles for Farøbroen

Time [years]	Method	C_0 [wt.-%/wt.-% con]	C_i [wt.-%/wt.-% con]	D^{app} [x 10^{-13} m²/s]]
7.6	IA	0.88	0	6.60
	ML			2.13
9.6	IA	1.02		5.80
	ML			2.13
12.4	IA	1.22		5.50
	ML			2.13

Apart from the data shown in Figures 8.19 – 8.21 a number of similar measurements have been made. The calculated chloride diffusion coefficients from all investigations are shown in Table 8.23 along with assumptions made on the initial chloride content used for these inverse analyses.

Table 8.23: Data from core-drilling at various times and locations at Farøbroen

Location	Age [years]	Core no.	D^{app} [x 10^{-13}m²/s]	C_0 [wt.-%/wt. con]	C_i [wt.-%/wt. con]
+0.4	7.6	1A	6.60	0.88	0.00
+0.35	9.6	2A	5.80	1.02	-
+0.35	9.6	3A	6.60	1.06	-
+0.35	9.6	4A	6.70	0.96	-
+0.35	9.6	5A	5.30	1.38	-
+0.35	12.4	6A	5.50	1.22	0.00
+0.35	12.4	7A	3.80	1.38	0.00
+0.35	12.4	8A	5.50	1.11	0.00
+0.35	15.4	9A	7.10	1.00	0.00
+0.35	15.4	10A	4.61	1.39	0.00
+0.35	15.4	11A	6.77	0.78	0.00
+0.35	15.4	12A	7.15	0.66	0.00
+0.35	15.4	13A	7.09	0.80	0.00
-1.3	10.7	1B	6.00	-	-
-1.5	10.7	2B	8.10	-	-
-0.9	10.7	3B	8.80	-	-
-1.3	22.4	4B	6.03	1.05	0.009
-1.5	22.4	5B	7.76	0.65	0.012
+0.65	15.4	1C	4.08	1.15	0.00

Location	Age [years]	Core no.	D^{app} [x 10^{-13}m²/s]	C_0 [wt.-%/wt. con]	C_i [wt.-%/wt. con]
+0.65	15.4	2C	3.43	0.82	0.00
+0.65	15.4	3C	5.12	0.77	0.00
+0.93	19.6	4C	3.82	0.81	0.00
+0.88	19.6	5C	3.59	0.96	0.00
+0.83	19.6	6C	3.04	0.88	0.00
+1.5	19.6	7C	4.35	0.48	0.00
+1.5	19.6	8C	3.62	0.49	0.00
+1.52	19.6	9C	3.24	0.35	0.00
+0.74	21.1	10C	3.19	1.24	0.00
+0.67	21.1	11C	3.80	1.13	0.00
+0.73	21.1	12C	3.45	1.15	0.00

Cells marked with "-" indicate data is unavailable.

Cores with the same letter in Table 8.23, e.g. 1A & 2A, are from the same structural element.

Discussion

The results from the validation of the MAINLINE model for chloride-ingress are discussed in the following sections. This outlines a comparison of the chloride profiles calculated from inverse analysis of data and the MAINLINE model. Moreover, a more general discussion of the MAINLINE model is presented.

Storebæltstunnelen

As can be seen from Figure 8.18, the chloride ingress in Storebæltstunnelen is very limited after seven years of exposure. Moreover, it is seen that there is a substantial difference between the chloride ingress at the two locations where cores have been taken. It is, however, not possible, based on the available data to identify the cause of this discrepancy.

Additionally, it is seen from Table 8.21 that the chloride diffusion coefficients calculated from the factual data, i.e. inverse analysis, are approx. twice as high or one tenth of the value calculated using the MAINLINE approach (8.19). For one of the cores (core B4), this leads to a minor underestimation of the chloride ingress, whereas the overestimation for the other core (core B5) is more pronounced, in particular at the surface of the concrete. It is to be noted that for core B5, a better correlation with the MAINLINE model can be achieved if the value of the chloride surface concentration is changed. However, such analysis is beyond the scope of this document.

Farøbroen

Results from measurements of the chloride profile in the splash zone of a pillar at various time steps and the calculated chloride profiles are shown in Figure 8.19 – 8.21. Comparisons of the chloride diffusion coefficient calculated by inverse analysis and the MAINLINE approach see Table 8.22, show that the value calculated by the MAINLINE approach is approx. 3 times smaller than the actual value calculated from inverse analysis. The inverse

analysis of the measured data also shows that the chloride diffusion coefficient slightly decreases over time. This might be referred to as ageing of the material.

By comparing the chloride diffusion coefficients calculated from all available field data, see Table 8.23, with the chloride diffusion coefficient calculated from the MAINLINE model it is seen that the MAINLINE approach underestimates the chloride diffusion coefficient approx. in the range 1.5-3 times. Consequently, applying the MAINLINE model to calculate the chloride ingress in this structure will lead to underestimations of the actual chloride ingress and thereby an overestimation of the time-to-de-passivation of the reinforcement.

General discussions

The MAINLINE approach for calculating the chloride diffusion coefficient by (8.19) underestimates (for most of the measurements covered by the two case studies described above) the value of the chloride diffusion coefficient compared to the actual value. However, it is emphasized that the model appears to be applicable as a first approximation for determining the chloride diffusion coefficient as the approach provides, in most cases, a value in the right order of magnitude.

A slight decrease in the chloride diffusion coefficient over time was observed for data from Farøbroen (Table 8.21) and this might be due to ageing of the material. The model for chloride ingress investigated herein does not consider ageing of the material, which might be considered if the method should be refined. Moreover, the difference between the chloride binding capacity and ageing of different types of binders is not covered by the MAINLINE approach for calculating D^{app}.

Danish practice

The experience with chloride-induced corrosion of reinforced concrete tunnels in Denmark is limited, mainly due to the fact that the number of Danish railway tunnels is limited. However, in general, chloride-induced corrosion of railway tunnels in Denmark is not an issue as seen from the case studies presented.

Storebæltstunnelen is a relatively new structure, constructed with high-performance concrete, and the chloride ingress is very limited after seven years. For Boulevard tunnelen, the main source of chlorides is de-icing salt at its top surface where the road is located. This surface is protected by, among others, a membrane which hinders the ingress of chlorides into the tunnel concrete. It is noted that such protective membranes also degrade and age, e.g. are effective for a time range normally shorter than the service life of the concrete, and therefore may need replacement from time to time.

Conclusions

This chapter covers case studies on deterioration models for concrete tunnels regarding carbonation and chloride ingress as proposed in D2.3 (ML D2.3). The case studies are based on data from Danish infrastructure. The case studies mainly concern data from tunnels. However, as the number of tunnels in Denmark is limited the availability of data is sparse. Moreover, assumptions have been made regarding e.g. the concrete composition, the actual exposure etc. Consequently, comparisons between the models based on the actual data should be interpreted very carefully.

The MAINLINE approach for prediction of carbonation of concrete seems to overestimate the actual carbonation depth. Another model, i.e. the *fib* model, was used for comparison purposes. This model seem to underestimate the actual carbonation depth.

As the MAINLINE model overestimates the carbonation depth it provides a conservative estimate on the remaining time-to-de-passivation of the reinforcement. The MAINLINE approach might, however, be more appropriate in a dry and warm climate where the carbonation depth is expected to be higher than in the climate (cold with high RH) of the case studies.

It is suggested that a possible LCAT may contain tabulated values of the *K*-value e.g. for different binder types, binder contents, RH etc. based on the experience of the infrastructure managers, to increase its user friendliness. This suggestion is based on the fact that a number of input parameters for the MAINLINE model as well as for the *fib* model may be difficult to assess for existing concrete structures. Drilling of cores for measuring the actual carbonation depth is an alternative which delivers correct data for use in possible LCAT models.

Based on the two case studies regarding chloride ingress in concrete it may be concluded that the approach proposed in the MAINLINE project for calculating the chloride diffusion coefficient is suitable as a first approximation, e.g. when little data on the concrete composition, binder type etc. is available.

For existing structures it might be beneficial to drill cores for determination of the chloride diffusion coefficient for a more accurate prediction of the remaining time-to-de-passivation of the reinforcement. It is recommended for a possible LCAT to prepare a list of representative values of the chloride diffusion coefficient to be used for this type of calculations.

Corrosion propagation is not considered in the case studies since data is not available (it is Danish practice only to consider the initiation stage). It is suggested to identify field data covering the propagation stage with regard to carbonation and chloride-induced corrosion to validate this part of the proposed models.

8.3.4 Case studies further information

Boulevardtunnelen

Boulevardtunnelen is a road-carrying railway concrete tunnel in Copenhagen. The tunnel was constructed in 1912. During maintenance and repair works in 2008 a number of cores were extracted from the outside (road-side) and the inside (railway tunnel) of the structure. Data from these field observations will be used for validation of performance profiles, i.e. estimates of the time-to-corrosion-initiation.

A collection of pictures of the tunnel and a cross section of the tunnel are provided below.

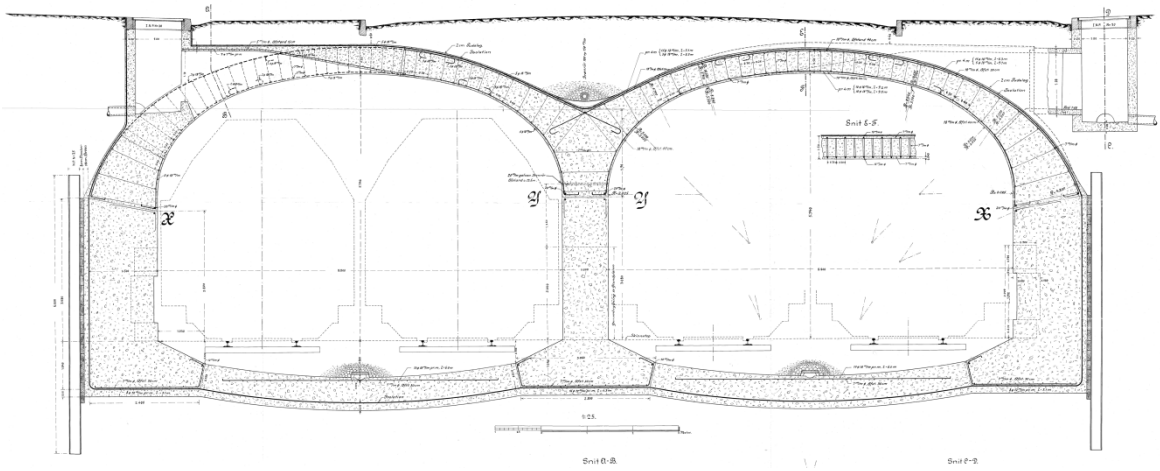

Frederikssundsvejtunnelen

Frederikssundsvejtunnelen is a road tunnel in Copenhagen. The tunnel is approx. 370 m long, 27 m wide and was opened for traffic in 1969.

Though the tunnel carries road traffic and not railway traffic it is suggested to use measurements of the carbonation depth for validation of the performance profiles within the MAINLINE, as measurements from a road tunnel might also be representative for a railway tunnel.

A pictures of the tunnel (from outside) is provided below.

Great Belt Tunnel

The Great Belt Tunnel has an approx. length of 7.7 km and was opened in 1997. The Great Belt Tunnel consists of a bored tunnel and a cut & cover tunnel. Cross passages are located per 250 m in the bored tunnel.

Data from field observations of chloride ingress (outside surface subject to sea water) will be used for validation of the performance profiles. Additional measurements of the carbonation depth may be available for estimates of the time-to-corrosion-initiation due to carbonation.

An illustrative sketch of the cross section of the bored tunnel is provided below. The internal diameter of the bored tunnel is approx. 7.5 m and the thickness of the segmental lining is 400 mm.

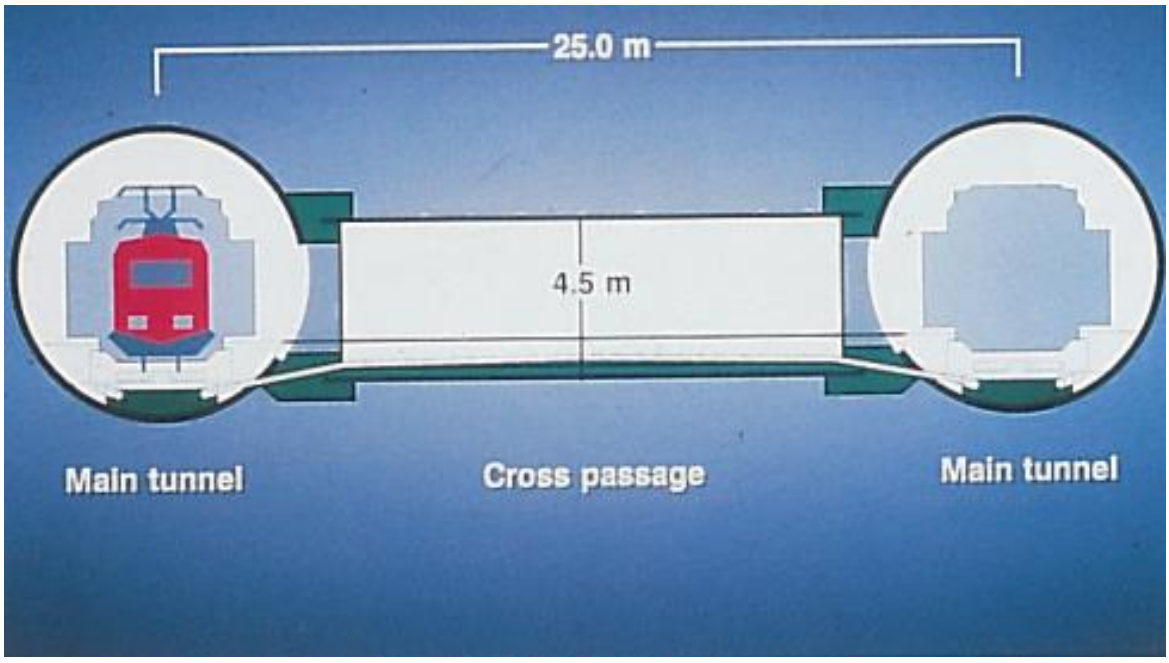

The cross sections of cut & cover tunnel and of the bored tunnel at the cross passages are shown in the figure below.

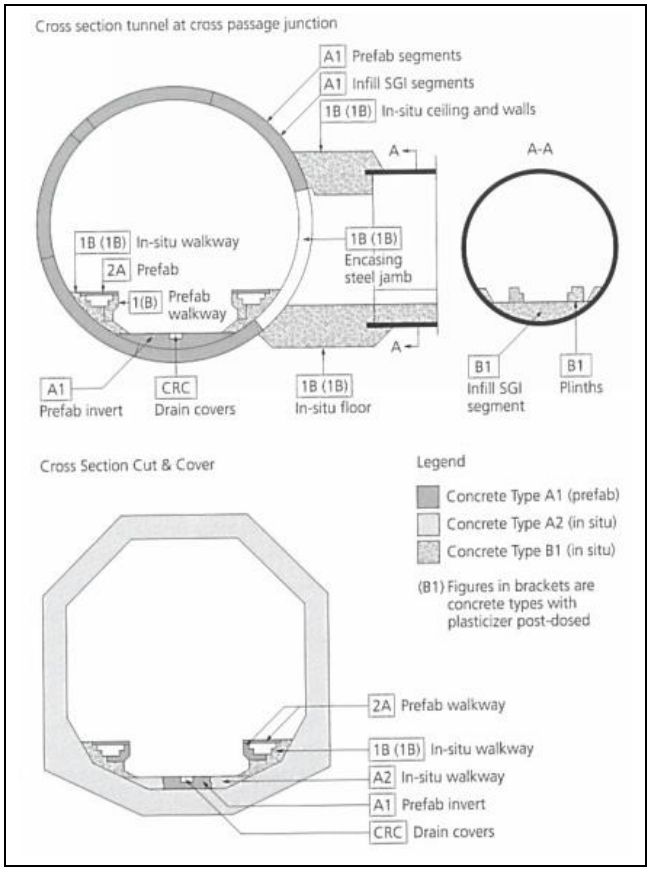

8.3.5 References

[1] AFGC (2003), "Application des notions de fiabilité à la gestion des ouvrages existants", In French

[2] AFGC (2007), "Concrete design for a given structure service life, Durability management with regard to reinforcement corrosion and alkali-silica reaction, State of the art and Guide for the implementation of a predictive performance approach based upon durability indicators"

[3] Angst U, Vennesland O (2009), "Critical chloride content in reinforced concrete – State of the art", In: Alexander et al. editors. Concrete Repair, Rehabilitation and Retrofitting II. Taylor & Francis Group, London.

[4] Arya C, Newman JB, (1990), “An assessment of four methods of determining the free chloride content of concrete”, Materials and Structures, 23(5):319-330

[5] Bakker RFM (1994), "Model to calculate the rate of carbonation in concrete under different climatic conditions", Report by the CEMIJ bv Laboratorium, Netherlands.

[6] Bioubakhsh S, (2011), "The penetration of chloride in concrete subject to wetting and drying: measurement and modelling", Doctoral thesis, UCL (University College London)

[7] Cao C, Cheung MMS, Chan BYB, (2013), “Modelling of interaction between corrosion-induced concrete cover crack and steel corrosion rate”, Corrosion Science, 69:97-109

[8] CEN Report (2003), "Testing hardened concrete - Determination of the depth of carbonation",

[9] Chaussadent T, Arliguie G, (1999), "AFREM test procedures concerning chlorides in concrete : Extraction and titration methods", Materials and Structures, 32:230-234

[10] de Cássia Silva R, (2004) "Contribution à l’analyse probabiliste de la performance des ponts en béton armé", PhD thesis ENPC (in French)

[11] DARTS, (2004a), Durable and Reliable Tunnel Structures: Deterioration Modelling, European Commission, Growths 2000, Contract GIRD-CT-2000-00467, Project GrDI-25633

[12] DARTS, (2004b), Durable and Reliable Tunnel Structures: Data, European Commission, Growths 2000, Contract GIRD-CT-2000-00467, Project GrDI-25633

[13] Dormieux L, Jeannin L, Sanahuja J (2010), "Effective Hydraulic and Mechanical Properties of Heterogeneous Media with Interfaces", In " Multiscale Methods in Computational Mechanics. Progress and Accomplishments" Eds de Borst R, Ramm E, Springer

[14] Dormieux L, Kondo D, Ulm JF, (2006), "Microporomechanics". John Wiley & Sons Inc.

[15] Duracrete, (2000), Probabilistic Performance Based Durability Design of Concrete Structures: Statistical Quantification of the Variables in the Limit State Functions. Report No.: BE 95-1347.

[16] EN 14630 (2007), Products and systems for the protection and repair of concrete structures - Test methods - Determination of carbonation depth in hardened concrete by the phenolphthalein method,

[17] fib bulletin 34 (2006) “Model Code for Service Life Design”

[18] Garboczi EJ, Bentz DP, (1997), "Analytical Formulas for Interfacial Transition Zone Properties", Adv. Cem. Based. Mater., 6, 99-108

[19] Gonzalez JA, Andrade C, Alonso C, Feliu S, (1995), “Comparison of rates of general corrosion and maximum pitting penetration on concrete embedded steel reinforcement”, Cement Conc Res, 25(2):257–264,

[20] Hausmann DA, (1967), "Steel corrosion in concrete: how does it occur?", Material Protection, 4(11): 19-23

[21] Lin S H, (1993) “Chloride diffusion in porous concrete under conditions of variable temperature” Heat & Mass Transfer (Warme- und Stoffuibertragung), 28, 411-415

[22] ML D2.2, MAINLINE Deliverable 2.2, Degradation and intervention modelling techniques, http://www.mainline-project.eu/Results,7.html

[23] ML D2.3, MAINLINE Deliverable 2.3, Time-variant Performance Profiles for Life-Cycle Cost and Life-Cycle Analysis, http://www.mainline-project.eu/Results,7.html

[24] Millard A, L’Hostis V (2012), “Modelling the effects of steel corrosion in concrete, induced by carbon dioxide penetration”, Eur. J. of Envir. and Civ. Eng., 16:3-4, 375-391

[25] Meshgin P, Xi Y, (2013), "Multi-scale composite models for the effective thermal conductivity of PCM-concrete", Construction and Building Materials, 48, 371–378

[26] Nguyen TQ, Baroghel-Bouny V, Dangla P, (2006a) "Approche multi-échelles pour modéliser la penetration des ions chlorure dans le béton". 24èmes Rencontres Universitaires de Génie Civil. In French.

[27] Nguyen VH, Nedjar B, Colina H, Torrenti JM, (2006b), “A separation of scales homogenization analysis for the modeling of calcium leaching in concrete”, Comput. Methods Appl. Mech. Engrg., 195, 7196–7210

[28] Nguyen VH, Colina H, Torrenti JM, Boulay C, Nedjar B, (2007), “Chemo-mechanical coupling behaviour of leached concrete Part I: Experimental results”, Nuc. Eng. And Design, 237, 2083-2089

[29] Ollivier JP, Maso JC, Bourdette B (1995), "Interfacial Transition Zone in Concrete", Adv. Cem. Based. Mater., 2[1], 30-38

[30] Papadakis VG, Vayenas CG, Fardis MN, (1991a), "Fundamental modeling and experimental investigation of concrete carbonation", Am, Concr, Inst, Mater, J,, 88(4):363-373

[31] Papadakis VG, Vayenas CG, Fardis MN, (1991b), "Physical and chemical characteristics affecting the durability of concrete", Am, Concr, Inst, Mater, J,, 88(2):186-196

[32] Papadakis VG, Vayenas CG, (1991c), "Experimental investigation and mathematical modelling of the concrete carbonation problem", Chemical Engineering Science, 46(5/6):1333-1338

[33] Papadakis VG, Roumeliotis AP, Fardis MN, Vagenas CG, (1996), “Mathematical modelling of chloride effect on concrete durability and protection measures”. In: Dhir RK, Jones MR, editors. Concrete repair, rehabilitation and protection. London (UK): E&FN Spon. p. 165-174.

[34] Powers TC, (1961), "Some aspects of the hydration of Portland cement", J. Port. Cem. Assoc. Res. Dev. Lab., 3, 47-56

[35] RILEM Draft Recommendation, CPC-18 (1984), "Measurement of hardened concrete carbonation depth, Materials and structures", 17 (102):435-440,

[36] RILEM TC 154-EMC (2004): “Electrochemical Techniques for Measuring Metallic Corrosion” Recommendations“ Test methods for on-site corrosion rate measurement of steel reinforcement in concrete by means of the polarization resistance method”, prepared by Andrade C, Alonso C, Materials and Structures, 37:623-643

[37] Salençon J. (2013) "Yield design", Wiley-ISTE. ISBN: 978-1-84821-540-5

[38] Stewart, M,G, (2009), “Mechanical behaviour of pitting corrosion of flexural and shear reinforcement and its effect on structural reliability of corroding RC beams”, Structural Safety 31(1):19-30,

[39] Sun G, Zhang Y, Sun W, Liu Z, Wang C, (2011), "Multi-scale prediction of the effective chloride diffusion coefficient of concrete", Construction and Building Materials, 25, 3820-3831.

[40] Tang L, Nilsson LO, (1992), "Rapid determination of the chloride diffusivity in concrete by applying an electrical field", ACI materials journal, 89(1):49-53.

[41] Tang L, (1996), "Electrically accelerated methods for determining chloride diffusivity in concrete - Current development", Magazine of concrete research, 48(176):173-179.

[42] Thiery M, (2005a), "Modélisation de la carbonatation atmosphérique des matériaux cimentaires, Prise en compte des effets cinétiques et des modifications microstructurales et hydriques", PhD thesis, In French,

[43] Thiery M, Platret G, Massieu E, Villain G, Baroghel-Bouny V, (2005b), "Un modèle d'hydratation pour le calcul de la teneur en portlandite des matériaux cimentaires comme donnée d'entrée des modèles de carbonatation", Journées Ouvrages d'Art du réseau des LPC, Lyon, In French

[44] Thiery M, Cremona C, Baroghel-Bouny V (2012), "Application of the reliability theory to the assessment of carbonation-induced corrosion risk of rebars", European Journal of Environmental and Civil Engineering, 16:3-4, 273-287

[45] Thoft-Christensen P, (2000), "Modelling of the Deterioration of Reinforced Concrete Structures", IFIP WG 7,5 Working Conference on Reliability and Optimization of Structural Systems, Ann Arbor, USA,

[46] Val DV et al. (2003), “Life-cycle analysis of reinforced concrete structures in marine environments”, Structural Safety, 25: 343-362.

[47] Vichot A, Ollivier JP, (2008), "La durabilité des bétons", Presses de l'Ecole Nationale des Ponts et Chaussées, 870p, In French

[48] Vu KAT., Stewart MG. (2000), "Structural reliability of concrete bridges including improved chloride-induced corrosion models", Structural Safety 22:313-33.